

---

# Modulation of Silicon's Lewis Acidity – Enhanced Reactivity through Ligand Design

---

INAUGURAL – DISSERTATION

to obtain the academic degree  
Doctor rerum naturalium (Dr. rer. nat.)

submitted to the Faculty of Mathematics,  
Engineering Sciences and Natural Sciences  
of Heidelberg University

by

Thaddäus Thorwart, M. Sc.  
b. in Aalen

**2023**



# DISSERTATION

to obtain the academic degree  
Doctor rerum naturalium (Dr. rer. nat.)

submitted to the Faculty of Mathematics,  
Engineering Sciences and Natural Sciences  
of Heidelberg University

by

Thaddäus Thorwart, M. Sc.  
b. in Aalen

Date of Defense: 14.12.2023

1<sup>st</sup> Reviewer: Prof. Dr. Lutz Greb  
2<sup>nd</sup> Reviewer: Prof. Dr. Dr. Hans-Jörg Himmel

The experimental part of this work was carried out under the supervision of *Prof. Dr. Lutz Greb* at the Institute of Inorganic Chemistry of Heidelberg University from December 2019 to September 2023. The results described here were in part obtained by *Rosa Müller* as part of her research internship in the group of *Prof. Dr. Greb* under my supervision. Additional results, which are not explicitly discussed in this work, were obtained by *Senta Kohl*, *Lotta Tölke*, and *Lukas Lehr* in the context of their bachelor theses or research internships in the group of *Prof. Dr. Greb* under my guidance.

Substantial parts of the present dissertation have already been published in scientific articles and presented at national and international conferences.

### **Poster Presentations:**

- I. *Pushing the Limits of Lewis Acidity: Towards a Soluble Neutral Silicon(IV) Lewis Superacid.*  
13<sup>th</sup> CaRLa Winter School, Heidelberg, Germany, **2020**.
  
- II. *Tuning Silicon's Lewis Acidity – From Structural Insights to Enhanced Reactivity.*  
10<sup>th</sup> European Silicon Days, Montpellier, France, **2023**.

### **Talks:**

- I. *Pushing the Limits of Lewis Acidity.*  
Skilizium, Engelberg, Switzerland, **2020**.
  
- II. *Tuning Silicon's Lewis Acidity – From Structural Insights to Enhanced Reactivity.*  
Skilizium, Andermatt/Hospental, Switzerland, **2023**.

## Publications:

- I. *Lewis Superacids.*  
T. Thorwart and L. Greb, *Encyclopedia of Inorganic and Bioinorganic Chemistry*, **2021**, DOI: 10.1002/9781119951438.eibc2758.
- II. *Bis(pertrifluoromethylcatecholato)silane: Extreme Lewis Acidity Broadens the Catalytic Portfolio of Silicon.*  
T. Thorwart, D. Roth, L. Greb, *Chem. Eur. J.* **2021**, *27*, 10422-10427, DOI: 10.1002/chem.202101138.
- III. *Bis(perfluoropinacolato)silane: A Neutral Silane Lewis Superacid Activates Si–F Bonds.*  
F. S. Tschernuth, T. Thorwart, L. Greb, F. Hanusch, S. Inoue, *Angew. Chem. Int. Ed.* **2021**, *60*, 25799-25803, DOI: 10.1002/anie.202110980.
- IV. *The Structure of Bis(catecholato)silanes: Phase Adaptation by Dynamic Covalent Chemistry of the Si–O Bond.*  
D. Hartmann, T. Thorwart, R. Müller, J. Thusek, J. Schwabedissen, A. Mix, J. Lamm, B. Neumann, N. W. Mitzel, and L. Greb, *J. Am. Chem. Soc.* **2021**, *143*, 18784–18793, DOI: 10.1021/jacs.1c09746.
- V. *Dihydrogen Activation with a Neutral, Intermolecular Silicon(IV)-Amine Frustrated Lewis Pair.*  
T. Thorwart, D. Hartmann, L. Greb, *Chem. Eur. J.* **2022**, *28*, e202202273, DOI: 10.1002/chem.202202273.
- VI. *Silicon Catalyzed C–O Bond Ring Closing Metathesis of Polyethers.*  
N. Ansmann, T. Thorwart, L. Greb, *Angew. Chem. Int. Ed.* **2022**, *61*, e202210132, DOI: 10.1002/anie.202210132.
- VII. *Bis(amidophenolato)phosphonium: Si–H Hydride Abstraction and Phosphorus-Ligand Cooperative Activation of C–C Multiple Bonds.*  
D. Roth, T. Thorwart, C. Douglas, L. Greb, *Chem. Eur. J.* **2023**, *29*, e202203024, DOI: 10.1002/chem.202203024.
- VIII. *Redox-Active Lewis Pairs Yield Diradicaloids and Enable Modular Control of the Diradical Character.*  
R. Maskey, T. Thorwart, S. Ebel, A. Jovic, D. Hartmann, L. Greb, *Chem. Eur. J.* **2023**, *29*, e202300269, DOI: 10.1002/chem.202300269.
- IX. *Reversible C–H bond silylation with a neutral silicon Lewis acid.*  
T. Thorwart, L. Greb, *Chem. Sci.* **2023**, *14*, 11237-11242, DOI: 10.1039/d3sc03488g.

Additional manuscripts on results described in chapters 3.1 and 3.3.3 are currently in preparation in joint work with *Prof. Dr. L. Greb*.

All rights to adapt the above publications were obtained through RightsLink®.



**Für meine Eltern.**



# ABSTRACT

---

The use of silicon compounds in challenging molecular transformations usually requires their activation by more reactive species, or a preceding transformation in reactive cationic or low-valent states. Only in the second half of the past decade, bis(perhalocatecholato)silanes (**1<sup>X</sup>**, X = F, Cl, Br) were reported as the first silane Lewis superacids – incorporating silicon in a neutral form and its natural oxidation state. Still, this burgeoning substance class suffers from drawbacks attributed to required donor-coordination, self-aggregation, poor solubility, or labile substituents. The present contribution describes strategies toward a *second-generation* of neutral silicon Lewis superacids exhibiting improved properties and an enhanced reactivity.

First, a heuristic structure-effect relation between steric modification of the ligand and the final composition of the silicon species is derived by means of suitable model systems. The found relation is applied in the rational design of electron-withdrawing ligands, ultimately resulting in the new representatives bis(tetra(trifluoromethyl)catecholato)silane (**1<sup>CF<sub>3</sub></sup>**) and bis(nonafluoro-N-phenyl-*ortho*-amidophenolato)silane (**2**). Both show an increased reactivity in comparison to their structural predecessors **1<sup>X</sup>**, with no indication on the detrimental self-aggregation.

Computations and experiments underlined that **1<sup>CF<sub>3</sub></sup>** ranks among the strongest neutral Lewis acids currently accessible in the condensed phase. It thus enabled catalytic transformations that have never been mediated by a neutral silane. In cooperative action with 1,2,2,6,6-pentamethylpiperidine (pmp), the enhanced properties of **2** allowed the isolation of a hydridosilicate directly synthesized from H<sub>2</sub> for the first time. This singularity provoked a first examination on the role of a tetrahedrally coordinated Lewis acid in the H<sub>2</sub> cleavage as hallmark FLP reaction. Moreover, spontaneous, FLP type C–H silylations with **2**/pmp leading to anionic silicates are described, which are reversible upon addition of a silaphilic donor. The thermodynamic stability of the silicates incited the assignment of an activation attribute as merely context dependent. Tangentially, a protocol for a catalytic C–C bond formation between N-heterocycles and acrylonitrile was derived.

Overall, this work documents the guided evolution of the advancement of neutral, silicon Lewis superacids, now with an extended reactivity portfolio including more challenging bond activations. The here presented findings contribute to the fundamental understanding of the molecular chemistry of silicon – the second most abundant element in the earth’s crust.



# KURZZUSAMMENFASSUNG

---

Die Verwendung von Verbindungen des Siliziums in anspruchsvollen molekularen Umwandlungen erfordert in der Regel eine aktivierte Form durch eine vorhergehende Umwandlung in reaktive kationische oder nieder-valente Zustände. Erst im vergangenen Jahrzehnt wurden Bis(perhalogenocatecholato)silane ( $\mathbf{1}^X$ ,  $X = F, Cl, Br$ ) als erste Silan-basierte Lewis-Supersäuren vorgestellt, die Silizium in neutraler Form und in seiner natürlichen Oxidationsstufe enthalten. Dennoch ergeben sich für diese aufstrebende Substanzklasse noch Limitierungen, die zurückzuführen sind auf erforderliche Donor-Koordination, Selbstaggregation, schlechte Löslichkeit oder labile Substituenten. Die vorliegende Arbeit beschreibt Strategien für eine *zweite Generation* von neutralen Silizium-Lewis-Supersäuren, die verbesserte Eigenschaften und eine erhöhte Reaktivität aufweisen.

Zunächst wird anhand geeigneter Modellsysteme eine heuristische Struktur-Wirkungs-Beziehung zwischen sterischer Modifikation am Liganden und der endgültigen Zusammensetzung der resultierenden Siliziumspezies abgeleitet. Anhand dieses Prinzips werden gezielt elektronenziehende Liganden synthetisiert, welche schließlich zu den neuen Vertretern Bis(tetra(trifluormethyl)catecholato)silan ( $\mathbf{1}^{CF_3}$ ) und Bis(nonafluoro-N-phenyl-*ortho*-amidophenolato)silan ( $\mathbf{2}$ ) führen. Beide weisen eine erhöhte Reaktivität im Vergleich zu ihren strukturellen Vorgängern  $\mathbf{1}^X$  auf, ohne Hinweise auf eine nachteilige Selbstaggregation.

Durch Berechnungen und Experimente konnte gezeigt werden, dass  $\mathbf{1}^{CF_3}$  zu den stärksten neutralen Lewis-Säuren gehört. Dadurch konnten katalytische Umwandlungen ermöglicht werden, die vorher noch nie durch ein neutrales Silan vermittelt wurden. In Kooperation mit 1,2,2,6,6-Pentamethylpiperidin (pmp) ermöglichten die verbesserten Eigenschaften von  $\mathbf{2}$  zum ersten Mal die Isolierung eines Hydridosilikats ausgehend von einer direkten Reaktion mit  $H_2$ . Diese Einzigartigkeit führte zu einer ersten Untersuchung der Rolle einer tetraedrisch koordinierten Lewis-Säure bei der  $H_2$ -Spaltung als emblematische FLP-Reaktion. Darüber hinaus werden spontane FLP C–H-Silylierungen mit  $\mathbf{2}$ /pmp beschrieben, die zu anionischen Silikaten führen, und mittels silaphilem Donor umgekehrt werden können. Durch die thermodynamische Stabilität der Silikate wurde eine kontextabhängige Einordnung der Bezeichnung *Aktivierung* angestoßen. In Anlehnung dazu konnte eine Vorschrift für eine katalytische C–C-Bindungsbildung zwischen N-Heterocyclen und Acrylnitril abgeleitet werden.

Insgesamt dokumentiert diese Arbeit die gelenkte Weiterentwicklung der neutralen Silizium-Lewis-Supersäuren, die nun über ein erweitertes Reaktivitätsportfolio inklusive anspruchsvolleren Bindungsaktivierungen verfügen. Die hier vorgestellten Ergebnisse tragen zum grundlegenden Verständnis der Molekularchemie von Silizium bei – dem zweithäufigsten Element in der Erdkruste.



# TABLE OF CONTENTS

<b>1</b>	<b>State of the Art.....</b>	<b>1</b>
1.1	Introduction.....	2
1.2	Lewis Acids (and Bases) .....	3
1.3	Lewis Acidity and Lewis Pair Formation.....	4
1.4	Classification and Scaling Methods.....	6
1.5	Lewis Superacids .....	12
1.6	Frustrated Lewis Pairs (FLPs).....	13
1.7	The Lewis Acidity of Neutral Silicon(IV) Compounds.....	15
1.8	The Chemistry of Bis(catecholato)silanes .....	19
<b>2</b>	<b>Objective.....</b>	<b>29</b>
<b>3</b>	<b>Results and Discussion .....</b>	<b>31</b>
3.1	New Insights from Bis(alkylcatecholato)silanes .....	32
3.2	Bis(per(trifluoromethyl)catecholato)silane .....	40
3.3	Bis(nonafluoro-N-phenyl- <i>ortho</i> -amidophenolato)silane.....	57
<b>4</b>	<b>Conclusion.....</b>	<b>95</b>
<b>5</b>	<b>Experimental and Computational Details.....</b>	<b>99</b>
5.1	General Information for Experiments .....	100
5.2	Syntheses, Reactivity Experiments, and Catalysis.....	106
5.3	Computational Details.....	166
<b>6</b>	<b>References.....</b>	<b>171</b>
<b>7</b>	<b>Appendix.....</b>	<b>I</b>
7.1	List of Abbreviations.....	I
7.2	List of Symbols and Constants.....	IV
7.3	Computational Data Tables and Figures .....	V

7.4	Cyclic Voltammetry Experiments.....	XV
7.5	pK <sub>a</sub> -Comparison for pmp and CH Substrates .....	XV
7.6	Crystallographic Data.....	XVI
	<b>Danksagung.....</b>	<b>XXVII</b>
	<b>Eidesstattliche Versicherung .....</b>	<b>XXIX</b>

# 1

## STATE OF THE ART

---

<b>1.1</b>	<b>Introduction .....</b>	<b>2</b>
<b>1.2</b>	<b>Lewis Acids (and Bases).....</b>	<b>3</b>
<b>1.3</b>	<b>Lewis Acidity and Lewis Pair Formation .....</b>	<b>4</b>
<b>1.4</b>	<b>Classification and Scaling Methods .....</b>	<b>6</b>
1.4.1	Spectroscopic Encryption – NMR and IR Approaches .....	7
1.4.2	Anion and Donor Affinities .....	9
<b>1.5</b>	<b>Lewis Superacids .....</b>	<b>12</b>
<b>1.6</b>	<b>Frustrated Lewis Pairs (FLPs).....</b>	<b>13</b>
<b>1.7</b>	<b>The Lewis Acidity of Neutral Silicon(IV) Compounds.....</b>	<b>15</b>
<b>1.8</b>	<b>The Chemistry of Bis(catecholato)silanes.....</b>	<b>19</b>
1.8.1	Structural Aspects of Bis(catecholato)silanes .....	21
1.8.2	Redox Chemistry .....	23
1.8.3	Bis(perhalocatecholato)silanes as Potent Lewis Acids.....	25

## 1.1 Introduction

Bond activations encompass the breaking and making of chemical bonds and represent the underlying phenomena for applied catalysis – processes which make up 80% of industrial reactions.<sup>1</sup> Traditionally, transition metals are predestined catalysts for mild transformations owed to their beneficial electronic structure. Drawbacks pertain to their high cost, toxicity, and relatively low abundance. In addition to orbital-controlled reactivity, a variety of laboratory and industrial processes require Lewis acids as rather brute reaction mediators.<sup>2,3</sup> The application of very strong transition metal based Lewis acids is limited, as their use comes along with specialized equipment, side reactivity, and toxicity.<sup>4</sup> As alternatives, the class of main group Lewis acids is continuously growing. Only in 2006, seminal work was presented by the utilization of a frustrated Lewis pair (FLP) for the first metal-free, reversible dihydrogen activation – a reaction *hitherto* only observed for transition metals.<sup>5</sup> Subsequent progress on the concepts of FLPs and element-ligand-cooperativity (ELC) further provoked intense research on novel p-block Lewis acids – with improvements regarding strength, functionality, handleability, availability of the underlying element, and toxicity. In the course, only in the past decade the first neutral silane<sup>a</sup> Lewis superacid (stronger than  $\text{SbF}_5$ ) was reported.<sup>6</sup> Silicon is the second most abundant element in the earth's crust. Yet, in its natural oxidation state *IV* (mostly as oxide) silicon is assigned with a fairly unreactive character, as it lacks typical donor or acceptor orbitals. Thus, for an enhancement of its Lewis acidity a modulation of substituents toward catecholato derivatives was required. The newly developed silicon Lewis superacids represent a steppingstone and allowed substantial reactivity advancement and prototypical activation processes. Despite this progress, there is much room for improvements in the young field. Major limitations are found in required donor stabilization, self-aggregation, or instability through labile substituents, which prevent activations of more challenging substrates by the silicon species.

This chapter will give a background on Lewis acids and their classification before briefly discussing the principles of FLPs. Ultimately, a brief survey on the Lewis acidity of silicon and a detailed view on the chemistry of bis(catecholato)silanes will

---

<sup>a</sup> In the context of this work the term *silane* is used for tetracoordinated, neutral silicon species, even when all hydrogens from the formal reference species  $\text{SiH}_4$  are substituted.

be given. The work described in the upcoming chapters will then present strategies for a further reactivity boost, to demonstrate the potential of neutral silicon *IV* species in bond activation processes.

## 1.2 Lewis Acids (and Bases)

The term acid and thus the history of the principal concept of acids and bases dates back to the 18<sup>th</sup> century, to an initial approach by *ROUELLE* in 1754.<sup>7,8</sup> The concept was continuously developed, and in the beginning of the 20<sup>th</sup> century, definitions from *BRØNSTED*,<sup>9</sup> *LOWRY*,<sup>10</sup> and *LEWIS* were presented.<sup>11,12</sup> Interestingly, those more modern concepts complement each other and were continuously generalized toward a more inclusive theory of bonding. Today Brønsted(-Lowry) and Lewis acidity are almost exclusively applied and still exist parallelly, as they are usually used in different contexts. While Brønsted acidity is referenced to protons, and is still dominantly used in this context, the generalized concept of *GILBERT N. LEWIS* is not limited to a reference element and also applied for compounds without acidic hydrogens. According to *LEWIS*, an acid is defined as electron-pair acceptor, whereas a base is an electron-pair donor. Lewis acids are broadly used in all kinds of chemistry, both on industrial and laboratory scale, ranging from materials science over organic chemistry and drug discovery to biological research.<sup>2,3,13-17</sup> Given the inherent general nature of *LEWIS*' definition, a variety of Lewis acids exists. This wide range paired with the various applications unambiguously results in the question on which Lewis acid to apply for which purpose. This know-how is considered crucial,<sup>18</sup> but at the same time the success of a Lewis acid mediated reaction is reported to frequently correlate with its strength.<sup>19</sup> This short line of thought immediately gives rise to the question on what strength is in a Lewis acidic sense. To give a small glimpse on this in the complex nature of Lewis acidity the following paragraphs will briefly discuss Lewis acidity and the scaling of such.

### 1.3 Lewis Acidity and Lewis Pair Formation

Lewis acidity according to the IUPAC recommendation is defined as “*the thermodynamic tendency of a substrate to act as a Lewis acid.*”<sup>20</sup> Therefore, from a selection of Lewis acids the strongest is the one with the highest affinity toward a Lewis base. Yet, an immediate dilemma arises from this definition, as the choice of the base is arbitrary. A simple classification would be true when the same affinities or at least the same trend for different Lewis bases would be present. Yet, the ‘*chemical intuition*’ that a pronounced discrepancy is found when varying Lewis acid or Lewis base from an initial adduct is backed by experience.<sup>21,22</sup> Consequently, the second part of the IUPAC definition is regarded to this: “*Comparative measures of [Lewis acidity] are provided by the equilibrium constants for Lewis adduct formation of a series of Lewis acids with a common reference Lewis base*”; overall disclosing a simple one-dimensional scale for Lewis acidity as not realizable. Indeed, the interaction between a Lewis acid and a Lewis base is influenced by a complex interplay of synergistic and antagonistic attractive and repulsive forces, which are reliant on the characteristics of both bonding partners (Figure 1a). Several schemes have been employed to elucidate the varying affinities that specific Lewis acids exhibit towards certain bases. Prominent examples are *PEARSON*’s principle of hard and soft acids and bases (HSAB)<sup>23</sup> or *DRAGO*’s ECW parameters.<sup>24,25</sup>

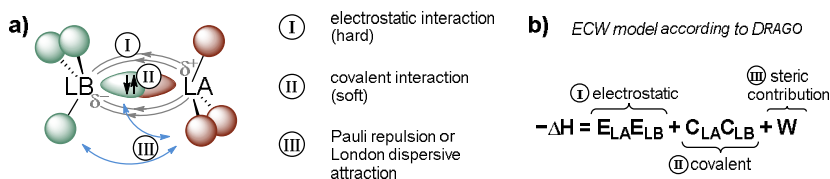


Figure 1. a) Schematic depiction of energetic contributions during Lewis pair formation and b) an attempted quantitative deconvolution according to *DRAGO*’s ECW model.

The HSAB principle states that stable Lewis adducts are formed from either a hard acid and a hard base or a soft acid and a soft base (hard: small, weakly polarizable, soft: large, well polarizable). It gives qualitative explanation to simple observations, e.g., the stronger binding of ethers by  $\text{BF}_3$  in comparison to  $\text{BH}_3$ , but the reversed trend for thioethers.<sup>21,26</sup> The ECW model approaches a quantitative representation of the HSAB factors (Figure 1b). Large enthalpic stabilization is obtained when both

Lewis acid and base exhibit either a large electrostatic contribution E (hard-hard) or a large covalent contribution C (soft-soft). From this brief outline it is apparent that simple quantitative scaling of Lewis acidity in analogy to the  $\text{pK}_a$  values of Brønsted acids is not feasible due to the lack of a unified reference Lewis base. The same issue prevents an adaption of *KROSSING*'s medium-independent chemical potential approach.<sup>27,28</sup> This conceptual problem is shared by all the various scaling methods, seemingly making a classification of Lewis acidity meaningless. Still, theoretical, statistical, and empirical reasons indicate that it is possible to break down Lewis acidity into a manageable set of factors.<sup>29</sup> A meaningful discussion can be made for example even with one scaling method, appropriately chosen for the discussion of a given aspect or a comparison within a substance class. Further, using a second dimension as proposed by *GREB* extends the significance.<sup>4</sup> A benchmark of various donor affinities (*dimensions*) suggested correlations between them.<sup>30</sup> A deconvolution of this complexity of Lewis acidity is part of current research, trying to answer how much and what kind of data are necessary for a full description of a Lewis acid. Even though such classification cannot be drawn to date, an emphasis on different scales and what they are best describing can still be given and shall be outlined in the following paragraphs.

## 1.4 Classification and Scaling Methods

Scaling the effect of Lewis pair formation displays a long history, and a variety of methods for determining Lewis basicity were developed while Lewis acidity scales were studied less extensive.<sup>31,32</sup> With respect to rising interest in highly reactive Lewis acids, different scaling methods for Lewis acidity were evaluated, leading to a general classification of *global*, *effective*, and *intrinsic* methods (Figure 2).<sup>4</sup> *Global* methods consider the whole process of adduct formation and ultimately result in thermodynamic data. Due to experimental complexity most data are collected computationally. The *effective* class refers to an induced change upon adduct formation for a chosen method, frequently shifted spectroscopic signals. The principal idea is to measure the *effectiveness* for a given purpose (e.g., polarization of a specific bond). Such methods are advantageous as they can be easily conducted and evaluated in standard laboratories but should be carefully validated for the aimed intend (section 1.4.1). *Intrinsic* classification refers to properties of the free Lewis acids, e.g., by evaluating LUMO energies,<sup>33</sup> the global electrophilicity index (GEI),<sup>34,35</sup> chemical shielding,<sup>36</sup> or electrochemical potentials.<sup>37</sup> Structurally strongly related compounds might be evaluated, yet adduct formation is not accounted for in any way, therefore effects such as deformation or steric repulsion are completely neglected. For a more detailed discussion it shall be referred to the literature.<sup>4,38</sup>

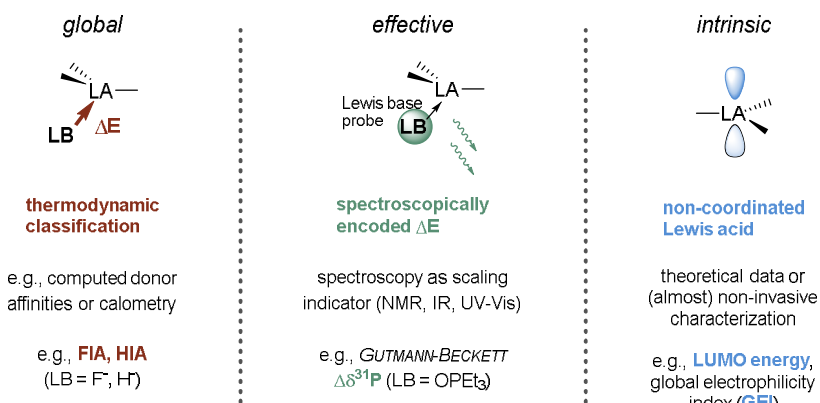


Figure 2. Schematic depiction of *global*, *effective*, and *intrinsic* Lewis acidity.

## 1.4.1 Spectroscopic Encryption – NMR and IR Approaches

### 1.4.1.1 NMR Approaches – Gutmann Beckett, Child’s and Related Methods

Two of the most commonly used methods to gauge Lewis acidity are the NMR-based *GUTMANN-BECKETT* (GB) and *CHILDS* methods. In the GB-method, the change in chemical shielding in the  $^{31}\text{P}$ -NMR signal of  $\text{Et}_3\text{PO}$  ( $\Delta\delta$ ) upon binding with a Lewis acid serves as the probe event (Figure 3a).<sup>39,40</sup> The *CHILDS* method relies on the induced shift of the H $\beta$ -proton in *trans*-crotonaldehyde upon coordination with a Lewis acid (Figure 3a).<sup>41</sup> Their popularity is easily rationalized by their practicality of simply adding commercially available probes to a solution of the compound of interest prior to NMR measurement.

Still, the conceptual problem of a single reference Lewis base can give misleading results, which can be explained by HSAB effects in first approximation. For instance, the softer donor crotonaldehyde exhibits stronger interactions with soft Lewis acids, while the rather hard donor  $\text{Et}_3\text{PO}$  shows the opposite behavior. This inconsistency is illustrated in the Lewis acidity series  $\text{B}(\text{C}_6\text{F}_5)_3$  -  $\text{B}(\text{C}_6\text{F}_5)_2(\text{OC}_6\text{F}_5)$  -  $\text{B}(\text{C}_6\text{F}_5)(\text{OC}_6\text{F}_5)_2$  -  $\text{B}(\text{OC}_6\text{F}_5)_3$ , which is represented in the opposite sense by the two methods.<sup>42,43</sup> Consequently, comparing Lewis acid classes becomes problematic and can even be meaningless. Additionally, as suggested by the series of  $\text{B}(\text{C}_6\text{F}_5)_n(\text{C}_6\text{Cl}_5)_{3-n}$ , steric effects might play a role, as increasing  $n$  leads to a decrease in Lewis acidity according to GB and *CHILDS* scaling.<sup>37,44</sup> On the contrary, computational analysis and cyclic voltammetry measurements underline that the boron atom is more electron deficient when substituting  $\text{C}_6\text{F}_5$ - with  $\text{C}_6\text{Cl}_5$ -moieties.

Other probes have been developed, e.g., using phosphine sulfide/selenide probes with respect to softer donors (*LICHTENBERG*, Figure 3a),<sup>45</sup> chelating phosphine oxides for bidentate Lewis acids (*FRANZ*, Figure 3a),<sup>46</sup> or 4-fluorobenzonitrile as weak donor that allows concurrent examination of the  $^1J_{\text{CF}}$  coupling constant as well as the  $^{19}\text{F}$  NMR shift (*MÜLLER*, Figure 3a).<sup>47</sup> They certainly exhibit advantages for tailored applications, yet they ultimately suffer from the same limitations.

One yet undiscussed but important aspect is the relation of the encrypted spectroscopic data and the thermodynamic binding tendency that corresponds to the IUPAC definition. A distinction between strength and effect was analyzed by means

of the GB method.<sup>38</sup> Important conclusions were drawn, including the finding of non-linear connection between *global* thermodynamic data and *effective* NMR shift change, disclosing the non-comparability of the general methodologies. The aimed *effective* probing event is also not sufficiently reflected, as the shift is mostly accounted for by a change in paramagnetic NMR shielding and does not correlate with the natural atomic charge at phosphorus. It is further shown that the required deformation of acid/base fragments is not considered in *effective* probing but only in *global* data. Consequently, the spectroscopic encryption correlates with the interaction energy of the deformed acid/base fragments (Figure 3b). This information enlightens some discrepancies among certain Lewis acidity scales. For instance, when comparing bis(catecholato)silane and  $B(C_6F_5)_3$ : despite being the *globally* weaker Lewis acid, bis(catecholato)silane shows a larger observed  $\Delta\delta(^{31}P) = 33$  ppm compared to the highly reactive  $B(C_6F_5)_3$  ( $\Delta\delta(^{31}P) = 27$  ppm).<sup>48</sup>  $AlEt_3$  exhibits significant *global* Lewis acidity due to its low deformation energy, making it a potent Lewis acid but only shows moderate *effective* Lewis acidity in the GB method ( $\Delta\delta(^{31}P) = 15.9$  ppm).<sup>49</sup> On the other hand, the tetrahedral Lewis acid  $SiCl_4$  is a robust *effective* Lewis acid ( $\Delta\delta(^{31}P) = 25.1$  ppm),<sup>38</sup> yet it displays weak *global* Lewis acidity because of considerable deformation energy.

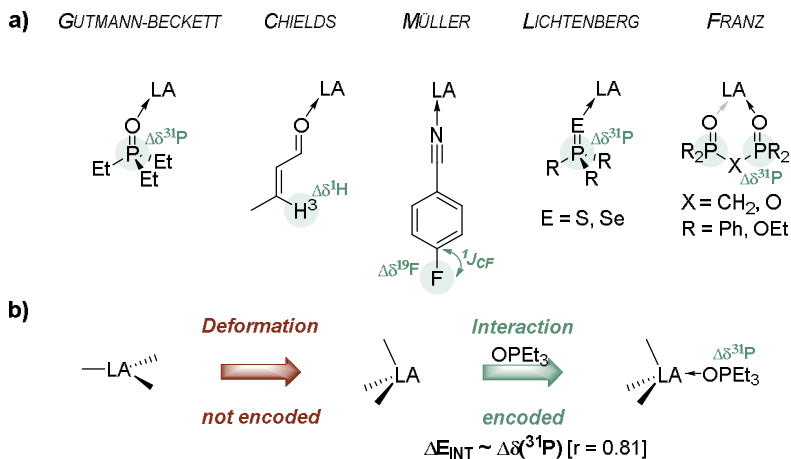


Figure 3. a) Overview of the NMR-spectroscopic probes used to gauge the *effective* Lewis acidity of a compound. b) Schematic depiction of the correlation of the interaction energy of the deformed fragments ( $E_{INT}$ ) and the resulting probe shift ( $\Delta\delta(^{31}P)$ ) in the *GUTMANN-BECKETT* method.

### 1.4.1.2 IR Approaches

As for the NMR based methods, the coordination of an IR-active probe to a Lewis acid with subsequent evaluation of a characteristic mode promises high practicality. The exposed CN stretching mode of nitriles is ideally suited to survey a shift of the mode caused by weakening of the bond upon coordination to a Lewis acid, and unsurprisingly, acetonitrile ( $\text{CH}_3\text{CN}$ ) was applied as vibrational probe early on.<sup>50-52</sup> Occurring problems regarding the interfering of the Fermi resonance of  $\nu(\text{CN})$  with the  $\text{CH}_3$  deformation can be avoided when utilizing  $\text{CD}_3\text{CN}$ .<sup>53,54</sup> With the latter as reference Lewis base, reasonable assignment of the Lewis acidity of boron trihalides was achieved, as judged by the relative difference of frequencies  $\Delta\nu(\text{CN})$ .<sup>53</sup> However, cross-class comparison revealed a huge discrepancy, evident from a significantly lower shift upon coordination to  $\text{SbF}_5$  in comparison to the boron adducts.<sup>55,56</sup> In similarity to the nitrile, the CO stretching mode was evaluated, aiming to identify solution-state structures of transition metal carbonyl complexes.<sup>57</sup> This approach was not primarily intended for quantifying Lewis acidity, its main purpose was to serve as an assisting tool for identifying intermediates. As such, IR probing of Lewis bases upon coordination is a powerful tool. Further, it can be a decisive methodology (and often the only possibility) for indications on Lewis acidity in the solid-state.<sup>58-61</sup>

### 1.4.2 Anion and Donor Affinities

Determining the enthalpic stabilization of a Lewis pair formation serves scaling in a thermodynamic manner and is thus closely oriented toward the IUPAC definition. Historically, the fluoride ion affinity (FIA) steadily took shape as measure for Lewis acids and today is still the most popular affinity in this context. The FIA is defined as the negative binding enthalpy of the fluoride ion with a Lewis acid (usually in the gas phase). Choosing fluoride as reference Lewis base for a scaling method offers several advantages: it is strongly nucleophilic and therefore binds with virtually all Lewis acids. In addition, due its small size steric factors are reduced to a minimum (although they might occur in rare cases<sup>62</sup>), and it is poorly polarizable, thus accounting for low second-order interactions such as dispersion, charge transfer, or  $\pi$ -back-bonding. FIA values were determined experimentally, using ion cyclotron resonance spectroscopy<sup>63-67</sup> or *BORN-FAJANS-HABER* cycles.<sup>68-73</sup> However, systematic errors caused by the choice of reference points,<sup>74</sup> low accuracy, and laborious set-ups

are apparent limitations for the experiments, especially in comparison to the simple protocols for spectroscopic probing.

Strikingly, today’s computational methodologies allow meaningful derived values for thermodynamic data on molecular systems,<sup>75</sup> avoiding the elaborate experimental techniques. A variety of FIAs was computed, e.g., for scaling the Lewis acidity of small species,<sup>74,76,77</sup> or to evaluate the stability of weakly coordinating anions (WCAs).<sup>69</sup> Due to difficulties of the computation of free fluoride when using methodologies that do not take full electron correlation into account, those FIAs were obtained (pseudo-)isodesmically. Indeed, a more recent benchmark study exposes the use of a suitable (pseudo-)isodesmic reference system as crucial, as direct computation can cause tremendous errors exceeding 100 kJ mol<sup>-1</sup>.<sup>78</sup> In the course, a self-consistent set of 190 FIAs was derived, for which an estimated accuracy of 5 kJ mol<sup>-1</sup> is reported, condensing the scattered landscape of computational methods for the FIA calculations into applicable candidates. Further, with a suitable protocol for solvation correction, an important point is addressed. Most FIAs are calculated as gas phase values, leading to an overestimation of the reactivity of cations as well as neutral species and an underestimation of the one of anions in the condensed phase. Therefore, when considering reactivities in the condensed phase, FIAs of species of different charge should be carefully discussed, ideally under consideration of solvation effects. Overall, the FIA is a robust and well-established method for scaling Lewis acidity. Still, the difficulty originating from a fixed reference Lewis base remains, making it primarily an exact measure for ‘*fluorophilicity*’. In a more general sense, due to the hard nature of the fluoride it might further serve as gauge of hard Lewis acidity.

To tackle the one-dimensionality, the consideration of the hydride ion affinity (HIA) was proposed with respect to softer characteristics.<sup>4</sup> The hydride as soft Lewis base is easily polarizable while steric and second-order effects are in analogy to the fluoride expected to be kept at a minimum. In follow-up work, a comprehensive study on hydride, chloride, and methide ion affinities as well as the neutral base affinities of ammonia and water was presented.<sup>30</sup> Interestingly, correlation trends between the affinity scales could be tied, emphasizing the thought of a limited number of shared principal components defining a – yet hypothetical – unified Lewis acidity. As, among other reasons, such parameters might not only be limited to simple affinities, this enigma is far out of scope for the current work. Still, to reflect the multifaceted

properties of a Lewis acid a more dimensional view always leads to a complete picture (Figure 4). Hereby the displayed affinities should be largely independent from each other. For the current work mostly FIA and HIA are used for the assessment of Lewis acidity as they are 1) reliably derived computationally with minimum distorting effects, and 2) judged to reflect the classical hard and soft features of the HSAB concept, which is still viably used for explanation and prediction of reactivity. Surely this two-dimensional approach does not reflect all properties, therefore further computational analysis and experimental probing will be applied when appropriate and within the described limitations of the methods.

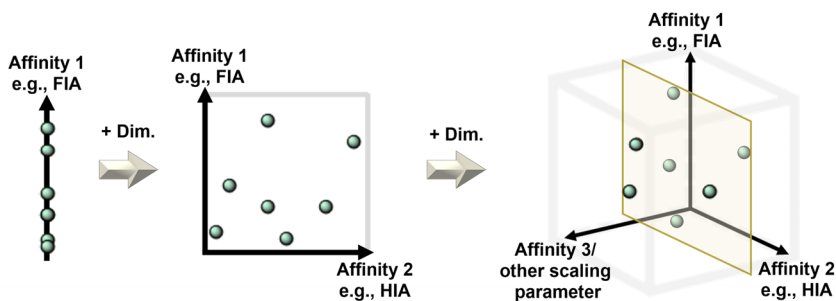


Figure 4. Schematic scatter-plot depiction for the visualization of one, two, and three parameters of Lewis acidity scales (displayed as dimensions (Dim.)).

## 1.5 Lewis Superacids

Superacids were introduced to account for the special properties of very strong Brønsted acids.<sup>79</sup> With increasingly isolable Lewis acids exhibiting outstanding reactivity, a definition for a superclass of Lewis acids appeared reasonable. The term Lewis acid was furnished with a super attribute on multiple occasions,<sup>16,80-87</sup> but without a clear definition such assignments seem arbitrary. A conclusive definition was given by *OLAH*, who defined Lewis superacids as stronger than anhydrous aluminum trichloride, yet lacking a reference Lewis base.<sup>88</sup> *KROSSING* and coworkers gave a more specific definition with antimony pentafluoride as benchmark,<sup>89</sup> and suggested fluoride as reference Lewis base.

*“Molecular Lewis acids, which are stronger than monomeric SbF<sub>5</sub> in the gas phase, are Lewis Superacids.”*

As outlined in the previous chapter, fluoride is commonly accepted as reference Lewis base. Lewis superacidity is therefore predominantly defined in a rather hard sense. Tris(pentafluorophenyl)borane (B(C<sub>6</sub>F<sub>5</sub>)<sub>3</sub>, BCF) ranks among the most used and most reactive Lewis acids for various applications,<sup>90-92</sup> yet it exhibits moderate fluorophilicity and its reactivity is predominantly orbital-controlled. With regard to this, soft Lewis superacidity was defined using B(C<sub>6</sub>F<sub>5</sub>)<sub>3</sub> as benchmark, and the overall definition of a super class extended.<sup>4</sup> For reasons discussed in section 1.4.2, FIA and HIA are recommended as gauging values.

*“Molecular Lewis acids that exceed the FIA of SbF<sub>5</sub> in the gas phase are Lewis superacids. Molecular Lewis acids that exceed the HIA of B(C<sub>6</sub>F<sub>5</sub>)<sub>3</sub> in the gas phase are soft Lewis superacids.”*

A cautious note shall be given, as according to this definition some carbocations classify as Lewis superacids, even though they were synthesized through fluoride abstraction utilizing SbF<sub>5</sub> – strongly opposing, even inverting the meaning of the classification. This is of course caused by the comparison of a cationic species with a neutral one (cmp. section 1.4.2). Technically, as the definition-medium is the gas phase, such compounds are Lewis superacidic. Yet, as the class is intended to reflect the extraordinary properties of its participants such assignment is rather unpractical for the use of a synthetic chemist working with condensed matter. In analogy,

reactivity of Brønsted superacids might seem media-dependent merely relative.<sup>93,94</sup> Therefore, throughout this work, Lewis superacidity will be assigned upon combined consideration of computation – with respect to the accuracy of the used methods, and experiment, in an aim to accordingly reflect the overall reactivity in the condensed matter.

## 1.6 Frustrated Lewis Pairs (FLPs)

The term Frustrated Lewis Pair (FLP) was coined in 2007, referring to “*systems in which steric demands preclude [...] classical [Lewis] donor–acceptor interactions.*”<sup>95</sup> A decade later, the original definition was refined and FLP reactivity referred to a kinetic phenomenon,<sup>96</sup> as over the years several examples for Lewis pairs with initial dative bonding were discovered that still displayed FLP reactivity.<sup>97,98</sup> The initial principle was reasoned by remaining ambiphilic reactivity and a small HOMO-LUMO-gap through steric repulsion (Figure 5a). Historically, a non-classical Lewis adduct was already observed by *BROWN* and coworkers in 1942,<sup>99</sup> followed by further ‘*anomalies*’ reported by *WITTIG*, and *TOCHTERMANN* – the latter reporting an *antagonistic pair* (“Antagonistenpaar”).<sup>100,101</sup> In 2006, *STEPHAN* and coworkers, reportedly working on the synthesis of an anionic phosphine ligand precursor,<sup>102</sup> discovered the intramolecular non-classical Lewis pair  $\text{Mes}_2\text{P}(\text{C}_6\text{F}_4)\text{B}(\text{C}_6\text{F}_5)_2$  – incorporating a boron Lewis acid and a phosphorus Lewis base.<sup>5</sup> Strikingly, this FLP was shown to reversibly activate dihydrogen, stating the first ever report of a reversible, metal-free dihydrogen activation (Figure 5b). This impactful contribution pioneered the research on FLPs and put them in a scientific focus, breaking the dogma of the time that (transition) metals are a requirement for dihydrogen splitting. Soon an example for an intermolecular system followed.<sup>103,104</sup> Importantly, it was shown in this course that apart from steric preclusion, a cumulative Lewis acid/base strength is crucial for the heterolytic dihydrogen cleavage. As the reactivity itself was continuously substantiated and its scope extended, the mechanistic proceeding came more into focus. *PAPAI* and coworkers emphasized synergistic molecular orbital interactions of the Lewis base ( $\sigma$  with the antibonding orbital of dihydrogen ( $\sigma^*(\text{H}_2)$ ) and the Lewis acid with the bonding orbital ( $\sigma(\text{H}_2)$ ) (electron transfer model).<sup>105,106</sup> Shortly after, *GRIMME* and coworkers presented an electric field approach, that reasons the cleavage by the strong polarization that the substrate undergoes upon

intercalation in the FLPs cavity.<sup>107</sup> Both theories disclose the importance of non-covalent interactions resulting in a preorganized intermediate, often referred to as precomplex, frustrated complex, or encounter complex.<sup>b</sup> Further experimental and theoretical research followed, continuously strengthening the understanding of this reactivity. Soon N-heterocyclic carbenes (NHCs)<sup>108,109</sup> and amines<sup>110-113</sup> extended phosphines as suitable Lewis bases for the H<sub>2</sub> activation (Figure 5c). The use of cleaving molecular hydrogen was further demonstrated in catalytic transfer reactions,<sup>114</sup> for example, to reduce substrates like imines,<sup>115</sup> enamines,<sup>116</sup> or olefins.<sup>117</sup>

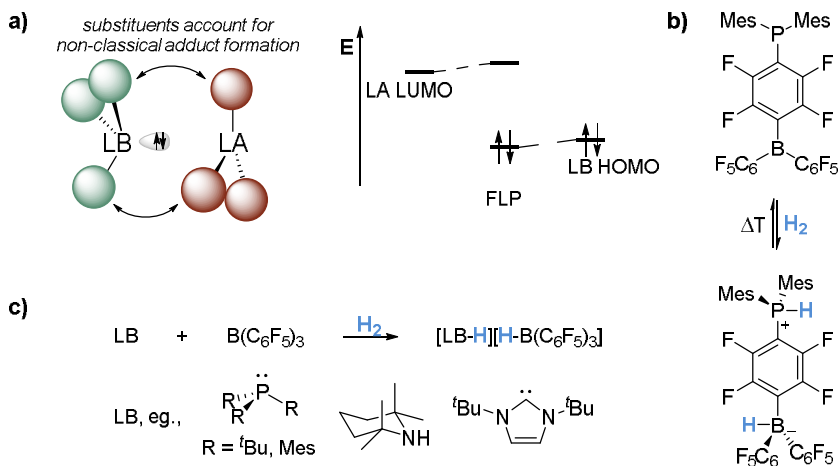


Figure 5. a) Illustration of an FLP and simplified depiction of a frontier orbital scheme. b) Pioneering example for metal-free, reversible dihydrogen activation by an FLP. c) Intermolecular FLP examples with different Lewis bases.

Up to this day the dihydrogen cleavage represents the hallmark FLP reaction and gained most interest. Still, meanwhile the diversity of FLP chemistry has expanded since its origin in 2006 to include reactions with more small molecules,<sup>102</sup> for instance, N<sub>2</sub>O,<sup>118,119</sup> NO,<sup>120,121</sup> CO<sub>2</sub>,<sup>122,123</sup> CO,<sup>124</sup> SO<sub>2</sub>,<sup>125,126</sup> olefins,<sup>127</sup> disulfides,<sup>128</sup> terminal alkynes,<sup>129</sup> or lactones.<sup>130</sup> Soft boranes proved especially useful for FLP reactivity and where thus frequently applied, yet, in the progress, more Lewis acids across the p-block were utilized.<sup>131</sup> Besides boranes, valence-*isoelectronic* species are especially

<sup>b</sup> A more detailed view on the FLP type, heterolytic cleavage of dihydrogen will be discussed in chapter 3.3.3.

reactive in the dihydrogen cleavage as original FLP reaction, for instance,  $\text{Al}(\text{C}_6\text{F}_5)_3$ ,<sup>132</sup> silylium ions,<sup>133-136</sup> or carbocations.<sup>137-139</sup> Noteworthy, the concept also transferred to transition metal Lewis acids.<sup>140-142</sup> The now established research field in all its depth and breadth was covered in a row of comprehensive reviews.<sup>114,143-148</sup> It is still bringing forth continuous development and foreshadows novel reactivities.<sup>149</sup>

## 1.7 The Lewis Acidity of Neutral Silicon(IV) Compounds

Silicon in its common oxidation state *IV* is in contrast to traditional Lewis acids not hypovalent, making it less prone to act as an electron pair acceptor – the key characteristic of Lewis acids. Naturally, it occurs mostly as  $\text{SiO}_2$  or in silicates, which represent the majority of structural motifs in the earth's crust.<sup>150</sup> In those compounds silicon is referred to as rather unreactive,<sup>151</sup> as it lacks typical acceptor orbitals. Substituting the silicon center with halogens leads to an increase in Lewis acidity, and  $\text{SiCl}_4$  is the common silicon-based Lewis acid of choice in chemical modifications. Its popularity is owed to a large extent to a remarkable concept: the Lewis base activation – meaning reactivity enhancement of a (silicon) Lewis acid and net-transfer of electron density through coordination of a donor.<sup>152-158</sup> Another strategy for an increase in reactivity of silanes is the use of ring-strain.<sup>159-164</sup> Both concepts, the transient Lewis base activation as well as the use of strained silacycles enabled potent protocols for organic transformations. These examples nicely indicate that some form of preorganization of the silicon center is beneficial regarding the species' Lewis acidity. Alongside the structural effects, more electronegative substituents have been installed at silicon, following an intuitive way of creating electron deficiency. A common structural motif is  $\text{Me}_3\text{SiX}$ , where X represents different leaving groups. Such systems were diversely applied for various catalytic applications.<sup>165</sup> The activity can be fine-tuned by modifying X, an approach which lead to the emergence of "high-performance Lewis acids."<sup>87,166,167</sup> Notably,  $\text{Me}_3\text{Si}(\text{TTP})$  (TTP = tetratriflato propenyl) displays an FIA of  $494 \text{ kJ mol}^{-1}$  and is therefore nearly reaching the threshold of Lewis superacids.<sup>167</sup> Still, it is crucial to recognize that virtually all Lewis bases induce cleavage of the Si–X bond. The compounds can thus be seen as stabilized surrogates for silylium ions, and the Lewis acidity represents the one of the silylium ion minus the dissociation enthalpy of the Si–X bond.<sup>168-170</sup> Silylium ions, in contrast to neutral silanes, range among the most Lewis acidic species.<sup>171-173</sup>

Pentafluorophenyl<sup>174,175</sup> ( $C_6F_5$ ) or pentafluoroethyl<sup>176,177</sup> ( $C_2F_5$ ) silanes exhibit an increased Lewis acidity. However, a quick comparison of the ion affinities shows that such silanes are by far not reaching the Lewis acidity of the respective boranes ( $FIA^{78}/HIA^{30} = Si(C_6F_5)_4: 336/339; Si(C_2F_5)_4: 430/409; B(C_6F_5)_3: 448/484; B(C_2F_5)_3: 581/624$ ).

In 2015 bis(perfluorocatecholato)silane (**1F**) was presented as highly Lewis acidic, neutral species ( $FIA^{178} = 490 \text{ kJ mol}^{-1}$ , cmp. section 1.8.3).<sup>48</sup> Interestingly, already the halogen-free, well-known parent compound bis(catecholato)silane displays significant Lewis acidity ( $FIA^{178} = 391 \text{ kJ mol}^{-1}$ ). In fact, the FIA is higher than for tetrahalosilanes ( $FIA^{78} = 310\text{-}352 \text{ kJ mol}^{-1}$ ). This phenomenon is related to the ring-strain and the lowered deformation energy of this compound class (cmp.  $FIA(Si(OPh)_4)^{178} = 302 \text{ kJ mol}^{-1}$ ).<sup>179</sup> This was early noticed in the course of a study on organo-silicates of bis(catecholato)silanes, stating that the compressive strain found in the tetrahedral form is essentially absent in the hypervalent state due to smaller silicon valence bond angles (approx.  $90^\circ$ ).<sup>180</sup> This effect was noticed for more systems, e.g., for *MARTIN*'s spiro-silane,<sup>181</sup> and even more pronounced for the corresponding spirogermane by *DENMARK*.<sup>182</sup> Ultimately, this was assigned with the term 'strain-release Lewis acidity' (Figure 6a).<sup>183</sup>

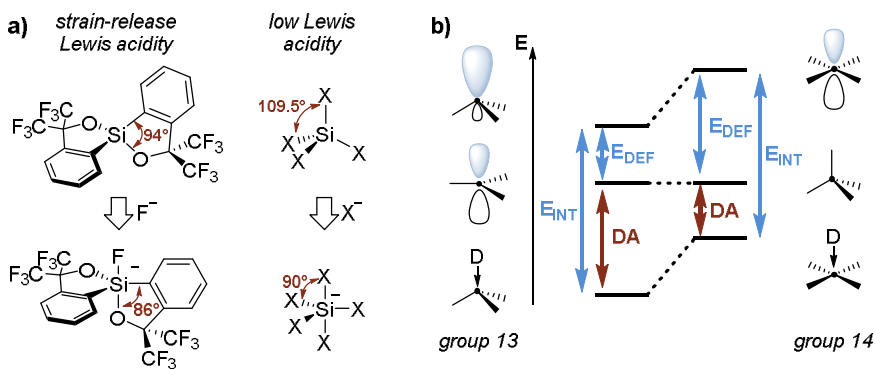


Figure 6. Deformation effects on Lewis acidity. a) Comparative illustration of strain-release Lewis acidity and b) schematic depiction of the deformation effect on the *global* Lewis acidity of group 13 and group 14 compounds.  $E_{INT}$  – Interaction energy of the deformed fragments,  $E_{DEF}$  – required energy for preorganization,  $DA$  – donor affinity.

In a more general context, it was observed that the energy that is required for preorganization of a Lewis acid into its final fragment structure in the adduct diminishes the overall donor affinity (DA) (Figure 6b).<sup>184-186</sup> This effect is also exploited in the previously mentioned strained silacycles and Lewis base activation systems. Extreme examples for this were presented in seminal work for a trigonal borane and a square-planar silane,<sup>187,188</sup> resulting in an enormous reactivity enhancement.

Apart from structural effects, the stability of the formed Lewis adducts further relies on the interaction between the deformed Lewis acid and Lewis base. The hypervalency of silicon originates from the ability to form 3-center-4-electron bonds (Figure 7a).<sup>189</sup> Previous assumptions of the involvement of d-orbitals turned out as not realistic.<sup>190</sup> Following the simple scheme, the non-bonding molecular orbital of the interaction is located on the ligands, therefore more electronegative substituents stabilize the hypervalent structures, and consequently they preferably occupy the hypervalent positions and display higher Si–L bond lengths (Figure 7b).<sup>191-193</sup>

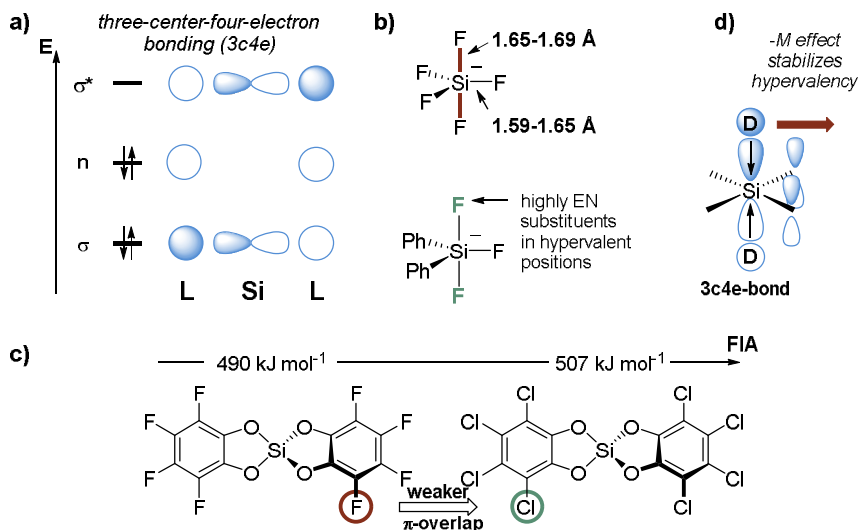


Figure 7. Thermodynamic effects on the Lewis acidity of silanes. a) Schematic depiction of the three-center-four-electron bonding in silanes, b) structural variances in hypervalent silicates, c) simplified illustration of the mesomeric effect in hypervalent silanes, and d) an example for Lewis acidity enhancement through weaker  $\pi$ -overlap.

Interestingly, when exchanging the fluorine atoms in bis(perfluorocatecholato)silane through chlorines, the Lewis acidity is boosted even further, which brought forth the first neutral silicon Lewis superacid (Figure 7c).<sup>6</sup> This at first counterintuitive trend, that opposes the electronegativity trend of the halides, is reasoned by the weaker  $\pi$ -overlap (Figure 7d) and results in an energetic stabilization with the bonding molecular orbital. Accordingly, the perbromo derivative stated a record holder for neutral silicon Lewis acids.<sup>178</sup> Of note, for more electropositive phosphorous the effect is reversed and the inductive withdrawing holds stronger than the mesomeric one.<sup>179,194</sup> Other highly Lewis (super)acidic silanes were recently presented. Triflate substituents in  $\text{SiOTf}_4$  are strongly electronegative and also  $\pi$ -acidic.<sup>195</sup> Bis(perfluoropinacolato)silane ( $\text{Si}(\text{pinF})_2$ ) exhibits the chelating and strain-characteristics of catecholates,<sup>196</sup> paired with sufficient electronegativity and resembles the mesomeric withdrawing effect with a negative hyperconjugation caused by the  $\text{CF}_3$  groups.<sup>197</sup>

## 1.8 The Chemistry of Bis(catecholato)silanes

Catechol, first isolated by *H. REINSCH* in 1839,<sup>198</sup> holds a special relationship with silicon. Already in 1920, *ROSENHEIM* demonstrated that fine powdered silica can be depolymerized using catechol under basic conditions to obtain the tris(catecholato)silicate dianion.<sup>199</sup> This reactivity was more recently exploited for the one-pot synthesis of an organosilane directly from SiO<sub>2</sub> without halogenated intermediates.<sup>200</sup> Moreover, as a result of this interplay, biogenic and natural catechols are of importance for the distribution of silicon in the geo- and biosphere.<sup>201-209</sup> After *ROSENHEIM's* discovery, reports on the neutral bis(catecholato)silane followed in the upcoming decades, using different synthetic routes.<sup>210-213</sup> Today, a modular synthesis for various derivatives is established (Figure 8).

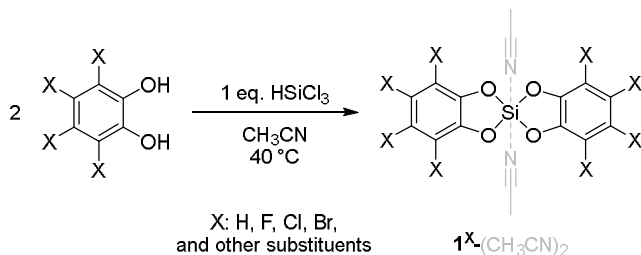


Figure 8. Modular synthesis of various bis(catecholato)silane derivatives.

Early examples for hypercoordinated silicon species were presented through mono- and dianionic catecholato-silicates.<sup>180,214-216</sup> In addition, a neutral donor acceptor interaction with pyridine as base underpinned the Lewis acidity of this system.<sup>217</sup> Owing to this ability, the silicon catecholate structural motif serves as a versatile platform for various types of chemistry. The transient hydrosilicate [H-1<sup>H</sup>]<sup>-</sup> represents a powerful reducing agent (Figure 9a),<sup>218</sup> organosilicates [R-1<sup>H</sup>]<sup>-</sup> are applied as precursors for the generation of radicals through photoredoxchemistry (Figure 9b),<sup>219-224</sup> or as trans-metalation reagents (Figure 9c).<sup>225-227</sup> The redox active nature enabled further the isolation of a neutral triplet diradical silane as a powerful oxidation agent (cmp. section 1.8.2).<sup>228</sup> Moreover, their straightforward synthesis made catecholato silicates ideally suited as building blocks for the first silicon-organic

frameworks (Figure 9d).<sup>229,230</sup> Ultimately, in the past decade, haloderivatives of the bis(catecholato)silane were discovered as potent Lewis acids (cmp. section 1.8.3).

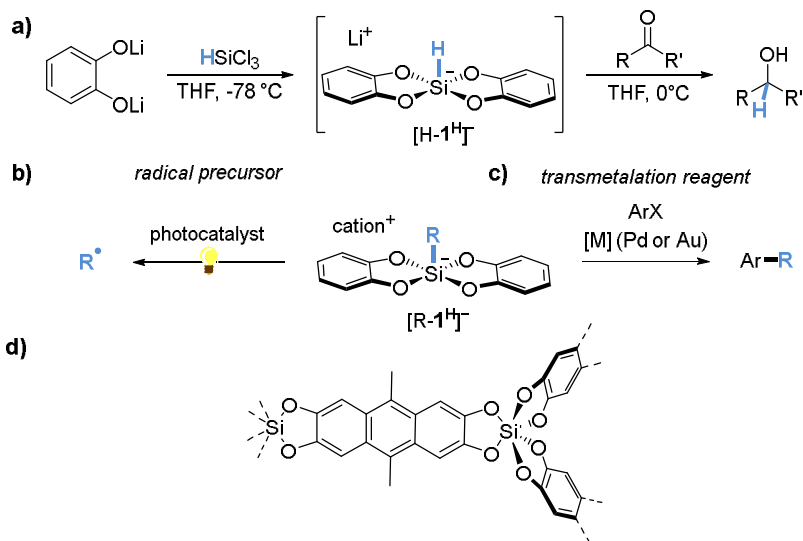


Figure 9. Applications of bis(catecholato)silicates and derivatives. a) Putative, *in situ* generated hydrosilicate for the reduction of carbonyls. Organic silicates a) for the generation of radicals and b) as transmetalation reagents. d) A silicate based covalent organic framework.

While the donor adducts and silicates of the substance class are frequently applied and well understood, less knowledge was gathered on the donor-free parent compound. The clarification of its structural nature went over decades and shall be briefly summarized in the next section. Afterwards, the redox-active role of catechol in conjunction with silicon will be enlightened before giving a brief discussion on Lewis acids based on the silicon catecholato structural motif.

### 1.8.1 Structural Aspects of Bis(catecholato)silanes

The molecular structure of  $\mathbf{1}^{\text{H}}$  was subject to a lively discourse in literature in the past decades.<sup>231</sup> In 1979 it was postulated that the central  $\text{SiO}_4$  unit in  $\mathbf{1}^{\text{H}}$  is square planar rather than tetrahedral.<sup>232</sup> This claim was based on crystallographic data, yet not on a full structure solution but on space group assignment. In contrast, Hartree-Fock calculations revealed the tetrahedral arrangement of  $\mathbf{1}^{\text{H}}$  as a global energy minimum, the square-planar configuration was however observed to possess only marginally higher energy – leaving the possibility for the proposed unconventional solid-state structure and emphasizing once more the low deformation energy of the substance class.<sup>233</sup> In opposition to the planar silicon hypothesis, *DUNITZ* instead postulated that the crystallographically analyzed substance likely was catechol that originated from hydrolysis of the target compound.<sup>234,235</sup> While other spiro-tetraoxosilanes were confirmed to exhibit a (distorted) tetrahedral ground-structure,<sup>236,237</sup> the significance for the structure of  $\mathbf{1}^{\text{H}}$  remained limited due to significant differences in bite angle (reduced ring-strain) and electronic structure.

Overall, a poorly soluble colorless solid was the common report for the appearance of bis(catecholato)silane with discrepancies on its exact composition. Notably, already in an early study oligomeric forms were proposed,<sup>212</sup> and upon sublimation a linear polymeric structure was suggested.<sup>238</sup> A monomeric motif in the shape of well-defined donor-acceptor complexes could always be formed from powders of undefined, amorphous ' $\mathbf{1}^{\text{H}}$ ' through reactions with suitable Lewis bases.<sup>239-242</sup> The structural riddle was solved several years later, nicely summarizing and concluding on the whole discourse.<sup>231</sup> In combined consideration of NMR, IR, gas phase electron diffraction (GED), matrix isolation, and scXRD the work comprehensively investigated the structural composition of  $\mathbf{1}^{\text{H}}$ .<sup>c</sup> It discloses that donor-free  $\mathbf{1}^{\text{H}}$  is monomeric and tetrahedral in the gas phase or trapped at 4 K in a neon-matrix. In the condensed phase,  $\mathbf{1}^{\text{H}}$  immediately oligomerizes concentration- and temperature-dependent with surprisingly low barriers for a non-catalyzed  $\sigma$ -Si-O-bond metathesis ( $\Delta G^\ddagger < 110 \text{ kJ mol}^{-1}$ ). Various oligomerization patterns were considered and computationally studied (Figure 10a). In the solid state, a computational preference and

---

<sup>c</sup> A part of the results described in chapter 3.1.1 of this work contributed to this report. The primary aimed deconvolution of the structure of  $\mathbf{1}^{\text{H}}$  was assisted by the here described investigation of the effect of substitution.

crystallographic proof for a macrocyclic ring consisting of 10 units ( $[1^{\text{H}}]_{10}$ ) was found (Figure 10b).

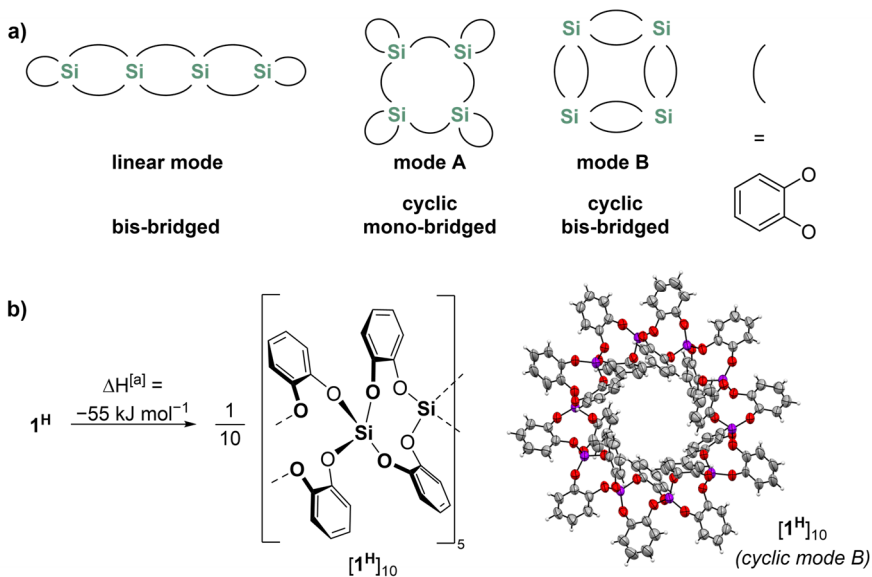


Figure 10.  $\sigma$ -Si-O bond metathesis and dynamic covalent chemistry of bis(catecholato)silane ( $1^{\text{H}}$ ). a) Possible binding modes for oligomers of  $1^{\text{H}}$ . b) Reaction scheme for the formation of  $[1^{\text{H}}]_{10}$  and scXRD derived structure (ellipsoids shown at 50% probability). [a] PW6B95-D3(BJ)/def2-TZVPP//HF-3c level of theory.<sup>231</sup>

Overall, these findings enlighten the discourse on the structure of this compound and further pave the way for follow-up work. For instance, it foreshadows applications in material science and might enlighten the unique role of biogenic catechols in our geosphere. In the context of this work more importantly, it satisfactorily explains the poor solubility of the halogenated derivatives as strong Lewis acids  $1^{\text{X}}$  ( $X = \text{F}, \text{Cl}, \text{Br}$ ) and affects their reactivity, as will be discussed in section 1.8.3.

### 1.8.2 Redox Chemistry

The catechol motif represents a redox-active ligand which can adopt three different oxidation states: the fully reduced, dianionic catecholato state, the monoanionic semiquinonate state and the fully oxidized *ortho*-quinone form (Figure 11a). Irrespective of the redox state, the system is termed dioxolene (diox). Its redox properties were largely studied in conjunction with transition metals,<sup>243-245</sup> but also intensively investigated with p-block elements.<sup>246</sup> While in the tetrahedral, uncoordinated form the redox-properties of the ligand are hardly exploited for silicon compounds, valence tautomerism comes into reach for related *ortho*-amidophenolate species with the heavier tetrel analogs Ge and especially Sn, which exhibit more stable low-valent forms.<sup>247</sup>

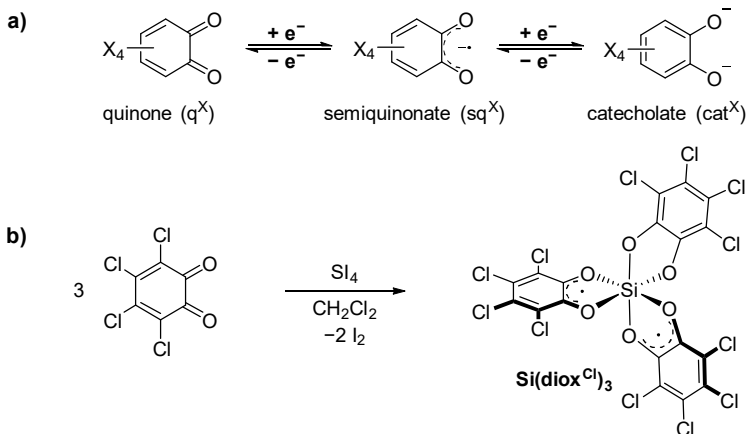


Figure 11. a) Redox states of *ortho*-dioxolene ligands. b) Synthesis of a neutral, triplet diradical based on silicon.

Paramagnetic forms of the silicon analogs were observed in hypervalent species since the second half of the 20<sup>th</sup> century. For instance, addition of different alkali semiquinonate salts to bis(3,6-di-*tert*-butyl-catecholato)silane (**1**<sup>3,6-*t*Bu</sup>) resulted in monoanionic radical species of the proposed form [**1**<sup>3,6-*t*Bu</sup>( $sq^X$ )]<sup>•-</sup>.<sup>248</sup> Other work on silicon containing free radicals included neutral monoradicals of the form [**1**<sup>3,6-*t*Bu</sup>-X]<sup>•</sup> (X = Cl, Br, I, RO).<sup>249</sup> Further, putative neutral tris(dioxolene)silane Si(diox<sup>X</sup>)<sub>3</sub> derivatives<sup>248-250</sup> and trifluorosilyl *ortho*-semiquinonate complexes<sup>251</sup> were reported.

This early work nicely demonstrates the synthetic approach toward such paramagnetic species, thereby drawing conclusions on solvation and conformation effects. However, it mainly focuses on EPR analytics, and a more comprehensive characterization is lacking, preventing conclusions on the exact structure and electronic composition of the described species. Only in 2019, the putative structures of the diradicals were confirmed for the perchlorinated derivative  $\text{Si}(\text{diox}^{\text{Cl}})_3$  (more specific:  $\text{Si}(\text{sq}^{\text{Cl}})_2(\text{cat}^{\text{Cl}})$ ).<sup>228</sup> Reaction of perchloro-*ortho*-quinone with  $\text{SiI}_4$  in non-donor solvents resulted in the formation of the stable, neutral triplet diradical (Figure 11b). Strikingly, this doubly oxidized form of the well-known dianion states the first example of two semiquinonates connected by a non-metal. Interestingly, when using acetonitrile as solvent the corresponding Lewis acid as bis-acetonitrile adduct  $\mathbf{1}^{\text{Cl}}(\text{CH}_3\text{CN})_2$  was obtained. Besides stating another route to the Lewis superacid, this also nicely demonstrates the relation between the former and the diradical and suggests a role as an intermediate. Furthermore, it exemplifies the high reactivity of the Lewis acid: binding of the quinone  $\text{q}^{\text{Cl}}$  to  $\mathbf{1}^{\text{Cl}}$  boosts the potential by 1.2 V, stating a remarkable redox amplification. This was exploited in follow-up work, in which the ability for catalytic applications was demonstrated and further the redox-series completed by isolating the mono-radical form  $[\text{Si}(\text{sq}^{\text{Cl}})(\text{cat}^{\text{Cl}})_2]^{\bullet-}$ .<sup>252</sup>

### 1.8.3 Bis(perhalocatecholato)silanes as Potent Lewis Acids

Apart from their redox-activity, catecholates are ideally suited for enhancing the Lewis acidity of p-block elements. They reduce the deformation energy and release strain upon adduct formation. The primary coordinating oxygen atoms exhibit sufficient electronegativity, and the chelating aromatic system can be substituted to induce a tremendous mesomeric withdrawing effect (cmp. section 1.7).<sup>179</sup> The latter also counteracts possible oxidation of the catechol. This way highly Lewis acidic silanes were enabled, including the first neutral silicon Lewis superacids. Various derivatives can be prepared in large quantities using a modular synthetic procedure (Figure 8). The ease of preparation and stability of the structural motif was noticed by *TILLEY* and coworkers, who equipped the parent compound with fluorine substituents and presented the pioneering bis(perfluorocatecholato)silane (**1<sup>F</sup>**).<sup>48</sup> Strikingly, **1<sup>F</sup>** was the first example of a neutral silicon species that catalyzes the hydrosilylation of aldehydes (Figure 12a). Probing according to *GUTMANN-BECKETT* and the isolation of an amide adduct further underpinned its Lewis acidic potential. In follow-up work, it was shown that more  $\pi$ -acidic perchlorocatecholato substituents further increase the Lewis acidity. The corresponding bis(perchlorocatecholato)silane (**1<sup>Cl</sup>**) exhibits a calculated FIA higher than  $\text{SbF}_5$ .<sup>6</sup> Indeed, its bis-acetonitrile-adduct is able to abstract a fluoride from  $\text{SbF}_6^-$ . The Lewis superacid, which was the first based on a neutral silicon(IV) center, was further able to catalyze a hydrodefluorination reaction, representing an early application of this extreme fluorophilicity. The logical follow-up derivative bis(perbromocatecholato)silane (**1<sup>Br</sup>**) consistently extended the row, displaying a larger *effective* and *global* Lewis acidity as well as a higher catalytic activity in the hydrodefluorination.<sup>178</sup> **1<sup>Cl</sup>** was subsequently used in FLP reactivity for  $\text{CO}_2$  capture with amines (Figure 12b),<sup>253</sup> or in conjunction with heteroleptic donors for carbonyl binding (Figure 12c) and ammonia-dehydrocoupling.<sup>254</sup> It further served as binding platform for weak anionic donors, allowing the investigation of model intermediates in Lewis base activation processes.<sup>255</sup>

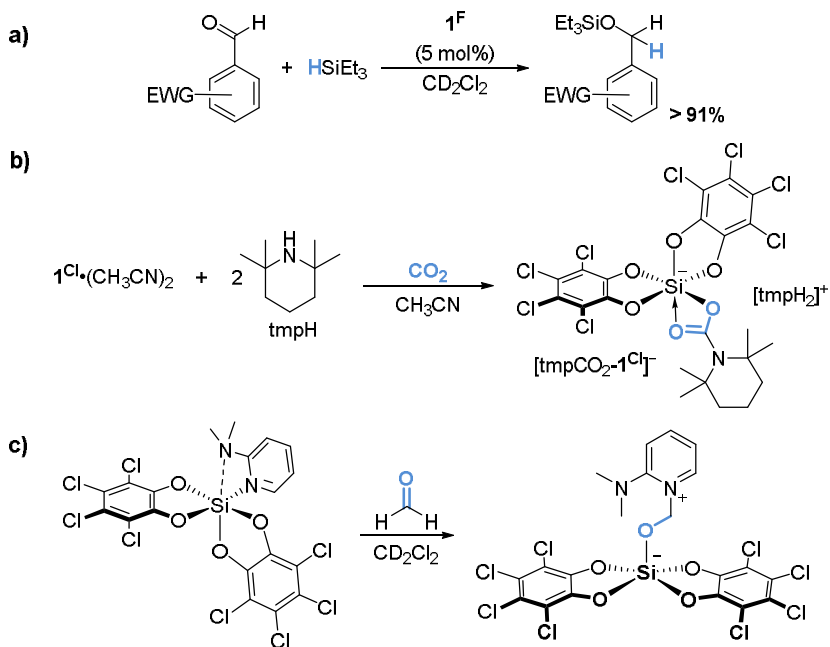


Figure 12. a) Bis(perfluorocatecholato)silane (**1<sup>F</sup>**) catalyzed hydrosilylation of aldehydes. FLP type b)  $\text{CO}_2$  and c) formaldehyde fixation incorporating bis(perchlorocatecholato)silane (**1<sup>Cl</sup>**) as Lewis acid.

However, limitations of the reactive species remain, as they are reported to be practically insoluble in non-donor solvents in their free form, and similarly their respective surrogates as acetonitrile or sulfolane adducts were observed to suffer from the same shortcoming. For example, the **1<sup>X</sup>**- $(\text{CH}_3\text{CN})_2$  ( $X = \text{F}, \text{Cl}, \text{Br}$ ) species were shown to abstract chloride from  $\text{Ph}_3\text{CCl}$  in solution, but the equilibrium reached a maximum proportion of 83% (for  $X = \text{Br}$ ). Isolation of the trityl salt in the solid state was prevented in all cases.<sup>178</sup> This limits their use in reactivities with non-donor, weakly polarizable substrates, caused by the self-aggregating nature of the substance class. In this regard, putative monomeric **1<sup>F</sup>** obtained from sublimation was found to oligomerize when dissolved, shortly after resulting in poorly soluble crystals suitable for scXRD.<sup>256</sup> A ring structure consisting of 14 units was observed [**1<sup>F</sup>**]<sub>14</sub> (Figure 13a), with an analogous structural pattern to the parent compound ([**1<sup>H</sup>**]<sub>10</sub>). While this sufficiently explains the poor solubility of the substances, it also suggests a quenching

of Lewis acidity for the halogenated derivatives. For  $\mathbf{1}^{\text{F}}$ , it amounts to an endergonic change of  $14 \text{ kJ mol}^{-1}$  and an enthalpic dampening of  $81 \text{ kJ mol}^{-1}$  for the computationally found most stable oligomer.<sup>d</sup> In analogy, solid state  $^{29}\text{Si}$  MAS NMR supported the presence of a polymeric structure in donor-free  $\mathbf{1}^{\text{Cl}}$  (Figure 13b).<sup>255</sup> Comparable investigations on the structure of  $\mathbf{1}^{\text{Br}}$  are yet unknown but the basic reactivity is expected to be fairly similar.

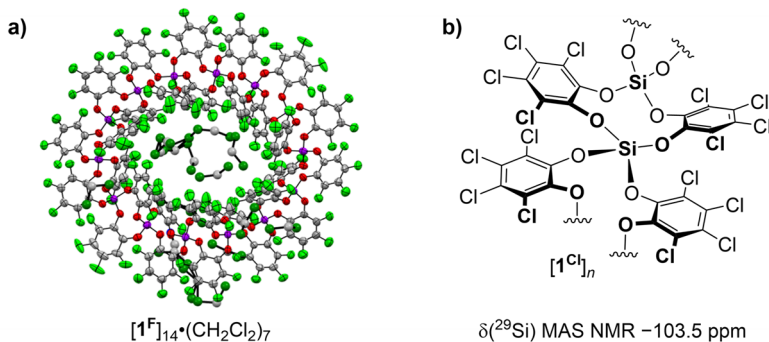


Figure 13. a) scXRD derived structure of an oligomer of  $\mathbf{1}^{\text{F}}$  (shown at 50% probability).<sup>256</sup> b) Schematic depiction of the oligomerization pattern of  $[\mathbf{1}^{\text{Cl}}]_n$  assigned after NMR spectroscopic evaluation.

Overall, while the easily accessible perhalo-derivatives  $\mathbf{1}^{\text{X}}$  established silanes into the realm of Lewis superacids, self-aggregation limits their use through an inherent quenching of the affinity paired with an essential insolubility in absence of a coordinating environment. In conjunction with (weak) donors this shortcoming was shown to be easily overcome, however, activation of less polarizable substrates is a yet unachieved challenge.

<sup>d</sup> PW6B95-D3(BJ)/def2-TZVPP//HF-3c; thermal correction at the GFN-xTB level.



# 2

## OBJECTIVE

---

The central aim of this research is the synthesis of neutral silicon species in their natural oxidation state *IV* that can be used in challenging Lewis acid catalysis or in the activation of unpolarized substrates.

To resolve current limitations of Lewis superacidic bis(perhalocatecholato)silanes **1<sup>X</sup>**, the prevention of self-aggregation by sufficient steric shielding around the reactive silicon center is hypothesized. Parallely, the preservation of electron-withdrawing properties is required to maintain the pristine Lewis acidity.

The first part of this work will focus on how sterically demanding substituents incorporated into the ligand framework influence the structure of the corresponding silane. With suitable model-systems, an empirical guideline for the development of monomeric species will be approached.

After a structure-effect relationship is established, the newly gained insights shall be applied in the development of an evolved, highly Lewis acidic bis(catecholato)silane that synergistically addresses an increased electron withdrawing effect and an augmented steric demand. From this approach, a compound with extreme Lewis acidity, a reduced oligomerization tendency, and an enhanced solubility is expected.

An alternate approach aims for a ligand modulation toward structurally related *ortho*-aminophenols. The inherently increased steric demand by an additional substituent at nitrogen is expected to be another effective method to prevent self-aggregation. While such alteration is a popular strategy for the fine-tuning of stereo-electronic properties in metal-complexes, strongly electron withdrawing derivatives of this substance class are not yet reported. Thus, a highly electron-deficient *ortho*-

## Objective

aminophenol shall be synthesized in line with the initial design principle, and subsequently installed at silicon.

Once synthesized, the newly developed silanes shall be characterized, and their reactivity probed (Figure 14). The symbiotic combination of structural design and electron deficiency promises enhanced reactivity of the envisioned silanes, including (catalytic) bond activations previously unobserved for neutral silanes. Both complementary but also contrasting aspects in comparison to archetypal Lewis (super)acids are to be expected, which shall be explored in experiment and accompanying computations. The present work intends to contribute to the fundamentals of molecular silicon chemistry, and to serve the reactivity-advancement of neutral silicon *IV* compounds which incorporate the second most abundant element of the earth's crust in its natural state.

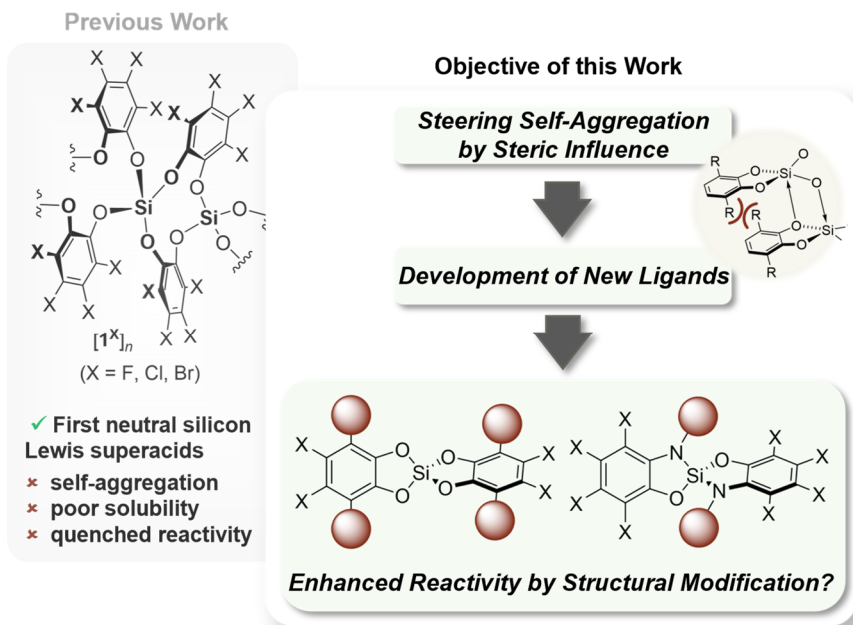


Figure 14. Schematic depiction of the objective of this work.

# 3

## RESULTS AND DISCUSSION

---

<b>3.1 New Insights from Bis(alkylcatecholato)silanes.....</b>	<b>32</b>
3.1.1 Gauging the Impact of Structural Effects on Self-Aggregation .....	32
3.1.2 Amplification of Lewis Acidity by Oxidation.....	37
<b>3.2 Bis(per(trifluoromethyl)catecholato)silane .....</b>	<b>40</b>
3.2.1 Synthesis .....	40
3.2.2 Probing the Lewis Acidity.....	44
3.2.3 Approaching Unquenched Reactivity of $1^{\text{CF}_3}$ .....	47
3.2.4 Catalysis.....	52
<b>3.3 Bis(nonafluoro-N-phenyl-<i>ortho</i>-amidophenolato)silane.....</b>	<b>57</b>
3.3.1 Synthesis and Characterization.....	57
3.3.2 Direct Synthesis of a Hydridosilicate from Dihydrogen .....	66
3.3.3 Rationalizing the FLP Activity of a Silane.....	74
3.3.4 Reversible FLP type C–H Silylation .....	84

### 3.1 New Insights from Bis(alkylcatecholato)silanes

In an aim to prevent the limitations of bis(perhalocatecholato)silanes ( $1^X - X = F, Cl, Br$ ) by tackling the underlying self-aggregation, the present chapter will deal with the investigation of the dynamic molecular behavior of bis(catecholato)silanes upon modulation of the catechol scaffold. Alkylated catecholates will serve as model systems to gauge the oligomerization process. Once a structure-effect relationship is established, a simple strategy to boost the reactivity of the model system will be discussed before the gained insights will stimulate further ligand design in the upcoming chapters.

#### 3.1.1 Gauging the Impact of Structural Effects on Self-Aggregation

As direct tool for the impediment of the self-aggregation, the installation of steric bulk seemed a promising strategy. To achieve this at the catecholate motif, the most efficient handle states substitution in *ortho*-position for a more pronounced shielding of the Lewis acidic silicon center. In an attempt to gauge this effect, alkylated catecholates were applied as model systems to allow an analysis of the oligomerization behavior. Namely, the derivatives 3,4,6-tri-*iso*-propyl-catechol ( $H_2cat^{3,4,6-iPr}$ ), 3,6-di-*tert*-butylcatechol ( $H_2cat^{3,6-tBu}$ ), and 3,5-di-cumyl-catechol (cumyl = 2-phenylpropan-2-yl,  $H_2cat^{3,5-Cm}$ ) were considered. Promisingly, substitution of less bulky catecholates with  $cat^{3,6-tBu}$  was previously shown to hinder oligomer formation of 3d metal complexes.<sup>257,258</sup>  $H_2cat^{3,4,6-iPr}$  was synthesized *via* sulfuric acid mediated alkylation of catechol with *isopropanol* (Figure 15a).<sup>259</sup>  $H_2cat^{3,6-tBu}$ , and  $H_2cat^{3,5-Cm}$  were obtained after reacting the respective alkenes (*isobutene* and  $\alpha$ -methyl-styrene) with catechol and catalytic amounts of bis(catecholato)titanium ( $Ti(cat^H)_2$ ) according to *ERSHOV's* procedure (Figure 15b and c).<sup>260,261</sup>

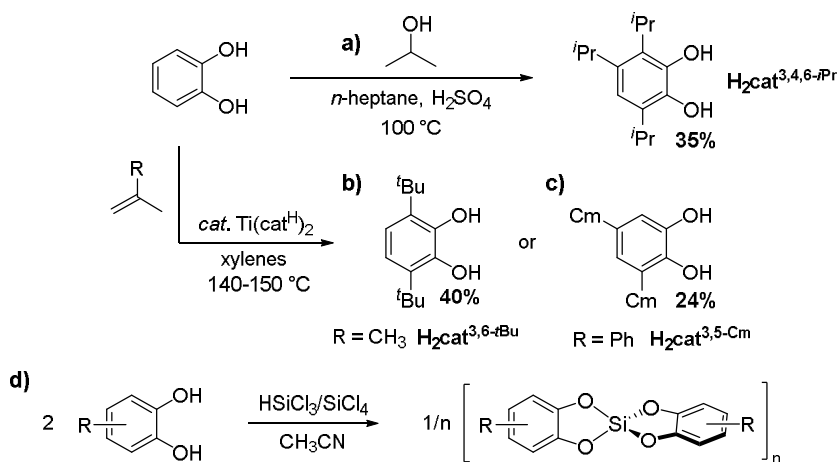


Figure 15. a)-c) Synthesis of alkylated catechol derivatives. Cm: cumyl (2-phenyl-propan-2-yl). d) Schematic depiction of the general protocol for the synthesis of bis(catecholato)silanes.

Next, the synthesis of the corresponding silanes was attempted following the modular synthetic route (Figure 15d). The three bulky derivatives were converted with  $\text{HSiCl}_3$  (or  $\text{SiCl}_4$ ) in acetonitrile, respectively. In each case a colorless precipitate was obtained. The respective solids were filtered off, all volatiles removed *in vacuo*, and the substances analyzed.<sup>e</sup> The compounds were found exceptionally soluble in dichloromethane or chloroform, not only stating the first contrast compared to the previous representatives of this substance class, but strikingly also allowing for a more profound NMR spectroscopical analysis. A first insight was given by not detecting acetonitrile signals, indeed verifying the absence of an external donor. Further, the concentrated solutions of the samples enabled meaningful  $^{29}\text{Si}$  NMR characterization in solution – a spectroscopic experiment found inconclusive for insoluble  $\mathbf{1}^{\text{X}}$  (X = H, F, Cl, Br). Through this means, first insightful conclusions regarding the structural nature of the compounds could be drawn. For  $\mathbf{1}^{3,4,6\text{-iPr}}$  and  $\mathbf{1}^{3,6\text{-tBu}}$  single signals at  $-41.2$  ppm and  $-42.9$  ppm were detected, respectively. A comparison with structurally related bis(pinacolato)silane ( $\delta(^{29}\text{Si}) = -44.4$  ppm)<sup>262</sup> gave a first shallow indication for a similar coordination environment. Further evidence for a single entity was provided by the calculation of NMR resonances for the monomeric forms

<sup>e</sup> For previous synthesis and characterizations of  $\mathbf{1}^{3,6\text{-tBu}}$  see section 1.8.2 and sources therein.

(**13,4,6-*t*Pr**:  $-38.8$  ppm, **13,6-*t*Bu**:  $-38.9$  ppm).<sup>f</sup> In contrast, calculated resonances for the corresponding dimers were in clear discrepancy to the experiment. To gain structural data in the solid state, crystallization of the compounds was approached. Unfortunately, suitable crystalline material was not yet obtained for **13,4,6-*t*Pr**. Colorless crystals, which formed upon conversion of  $\text{H}_2\text{cat}^{3,6-*t*\text{Bu}}$  with  $\text{HSi}(\text{NMe}_2)_3$ , confirmed the structure of the bis-dimethylamine adduct of **13,6-*t*Bu** (Figure 16a). For unbound **13,6-*t*Bu**, colorless crystals could be grown from a saturated chloroform solution. Even though a full refinement was prevented by poor quality of the crystal, the connectivity of **13,6-*t*Bu** and thus a monomeric form could be confirmed by scXRD analysis (Figure 50). In the case of **13,5-Cm** four  $^{29}\text{Si}$  NMR signals of different intensity were detected, overall, not pledging for a monomeric form but a diastereomeric mixture of a multinuclear entity  $[\mathbf{13,5-Cm}]_n$  ( $n > 1$ ). This was further emphasized by  $^1\text{H}$  and  $^{13}\text{C}$  NMR measurements.

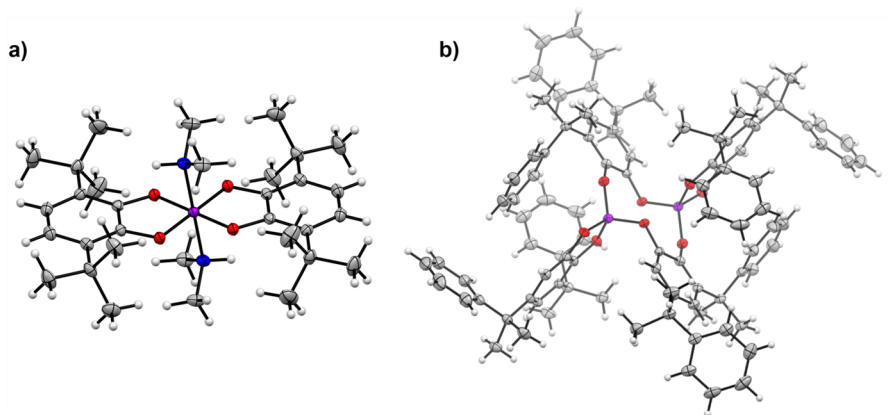


Figure 16. Molecular, scXRD derived structures of a) **13,6-*t*Bu**-( $\text{HNMe}_2$ )<sub>2</sub>, and b) dimeric  $[\mathbf{13,5-Cm}]_2$  (shown at 50% probability, solvent molecules omitted for clarity.)

Indeed, single crystals suitable for scXRD, grown from a concentrated dichloromethane solution, confirmed a dimeric product  $[\mathbf{13,5-Cm}]_2$  (Figure 16b). A calculated  $^{29}\text{Si}$  NMR shift based on the respective solid-state structure was in a fitting

<sup>f</sup> PBE0-D3(BJ)+SMD(CH<sub>2</sub>Cl<sub>2</sub>)/PBEh-3c level of theory. Details for the computation of NMR resonances are provided in section 5.3. The resonances are listed in Table A9.

range to the experimentally obtained resonances. In contrast, the calculated shift for a putative monomer was in sharp disagreement. Absence of further up-field signals ruled the possibility of higher oligomeric forms unlikely.<sup>231</sup> For a better understanding on the relation of the ligand's substituents and the structure of the silicon species, the dimerization process of the silanes **1**<sup>3,4,6-*i*Pr</sup>, **1**<sup>3,6-*t*Bu</sup>, and **1**<sup>3,5-Cm</sup> was investigated computationally.<sup>§</sup> For **1**<sup>3,4,6-*i*Pr</sup> and **1**<sup>3,6-*t*Bu</sup> the distorted tetrahedral, monomeric form was found to be thermodynamically favored in comparison to their respective dimers [**1**<sup>R</sup>]<sub>2</sub>, matching the experimental observations. Similarly, in line with the spectroscopic data, the cumyl substituted derivative **1**<sup>3,5-Cm</sup> was predicted to dimerize.

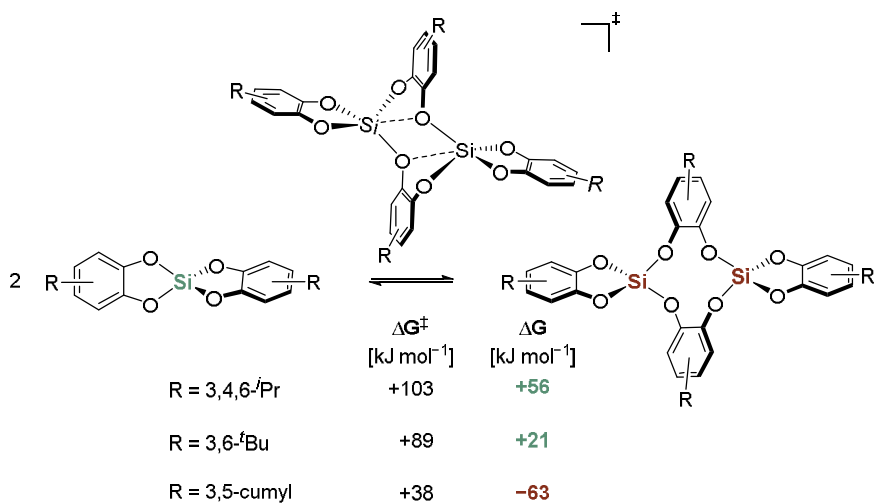


Figure 17. Schematic depiction of the dimerization process and *in silico* derived energies. DSD-BLYP-D3(BJ)/def2-QZVPP+SMD(CH<sub>2</sub>Cl<sub>2</sub>)/PBEh-3c level of theory.

The combined consideration of experiment and theory indicates a necessity for the substitution of both *ortho* positions as crucial for a thermodynamic prevention of self-aggregation. Next, the kinetic of the reactions was accounted for. In similarity to the exceptionally low barriers calculated for the Si-O *sigma* bond metathesis of **1**<sup>H</sup>,<sup>231</sup> the here found  $\Delta G^\ddagger$  energies are comparably low (Figure 17). Based on these energies, no

<sup>§</sup> DSD-BLYP-D3(BJ)/def2-QZVPP+SMD(CH<sub>2</sub>Cl<sub>2</sub>)/PBEh-3c level of theory (section 5.3).

kinetic hindrance at rt is expected. The barrier for dimerization of two **1**<sup>3,5-Cm</sup> stands out as it is remarkably low, for which two possible factors can be taken into account. First, the reduced steric shielding in one of the *ortho* positions is expected to result in less Pauli repulsion in the transition state. In this context, a dimerization with similarly low barriers was predicted for structurally related **1**<sup>3,5-*t*Bu</sup>.<sup>231</sup> Second, the large substituents can induce attractive secondary interactions during the bond formation process. Importantly, the computations overall indicate that the applied strategy is in first regard a thermodynamic but not necessarily a kinetic inhibition.

Summed up, the gained insights show a relation between the steric demand of alkyl substituents on the catecholates and the nuclearity of the most stable structural entity (Figure 18). While the small scope does not allow a quantitative interpretation, this serves as a firm principle for the subsequent design of novel ligand systems.

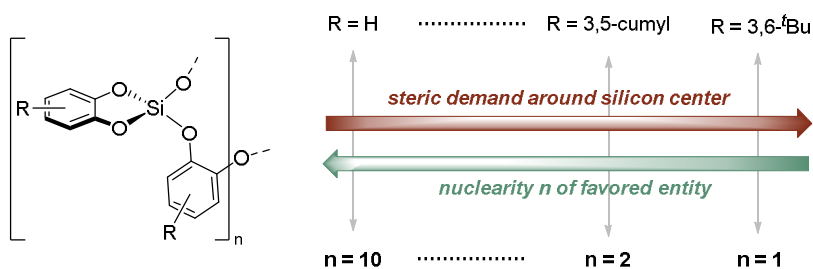


Figure 18. Schematic illustration for a relation between steric demand on the catecholates and the nuclearity of the corresponding silane entity.

### 3.1.2 Amplification of Lewis Acidity by Oxidation

The monomeric forms nicely demonstrate the principal strategy for obtaining a defined structure and an accompanying enhanced solubility upon suitable ligand modification. However, even though proofing the principle, the alkylated derivatives cannot be applied in challenging Lewis acid catalysis protocols. For such increased Lewis acidities, electron-withdrawing effects are crucial and will be addressed in the following chapters. In turn, the alkylated catecholates in the present case can be exploited in other ways. As they are rather electron-rich and exhibit a redox-active nature, a simple oxidation can be expected in contrast to other, more oxidation-resistant Lewis acidic silanes. Following this idea further, appropriate precautions were thought through for **13,6-*t*Bu**. Oxidation of **13,6-*t*Bu** results in  $\text{Si}(\text{cat}^{3,6-*t*\text{Bu}})(\text{sq}^{3,6-*t*\text{Bu}})^{\bullet+}$  ( $[\mathbf{13,6-*t*Bu}]^{\bullet+}$ ), which represents a masked silylium ion (Figure 19). Indeed, an extraordinary calculated FIA of  $784 \text{ kJ mol}^{-1}$  renders  $[\mathbf{13,6-*t*Bu}]^{\bullet+}$  a Lewis superacid.<sup>h</sup>

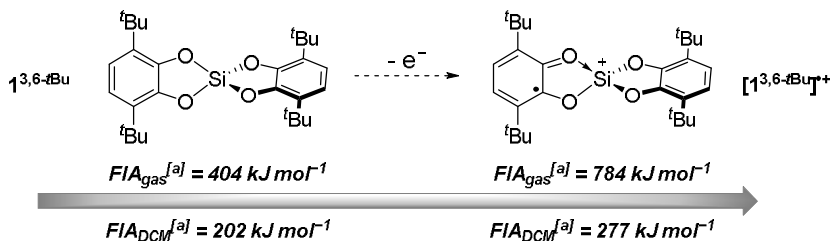


Figure 19. Schematic illustration for the strategy of Lewis acidity enhancement upon oxidation. [a] DLPNO-CCSD(T)/def2-QZVPP//PBE0-D3(BJ)/def2-TZVPP level of theory.

Thus, **13,6-*t*Bu** was reacted with various oxidation agents in dichloromethane. Cyclic voltammetry revealed an oxidation potential of 0.04 V (vs.  $\text{Fc}/\text{Fc}^+$ , Figure A3). Accordingly, ferrocenium salts did not indicate any reactivity. With  $\text{Ag}[\text{SbF}_6]$ , immediate coloration of the reaction mixture was apparent accompanied by a paramagnetic species as judged by EPR spectroscopy. Various signals in the  $^{19}\text{F}$  NMR spectrum however suggested an undefined reactivity, possibly involving ligand scrambling after initial fluoride abstraction from  $\text{SbF}_6^-$  by  $[\mathbf{13,6-*t*Bu}]^{\bullet+}$ , as previously

<sup>h</sup> Obtained at the DLPNO-CCSD(T)/def2-QZVPP//PBE0-D3(BJ)/def2-TZVPP level of theory. Solution  $FIA_{\text{DCM}} = 277 \text{ kJ mol}^{-1}$ .

reported for **1**<sup>Cl</sup>.<sup>6</sup> When using AgOTf, AgNTf<sub>2</sub>, or Ag(*o*-C<sub>6</sub>H<sub>4</sub>F<sub>2</sub>)[Al(O<sup>*i*</sup>C<sub>4</sub>F<sub>9</sub>)<sub>4</sub>] such reactivity was indeed absent. In those cases, the oxidation processes were found slowed but could be tremendously accelerated upon addition of half an equivalent of molecular iodine. Again, a deep coloration of the reaction mixtures and ultimately the obtained solids, in conjunction with an EPR active sample strongly supported the initial oxidation. Similar observations were made with the oxidation agents [N(C<sub>6</sub>H<sub>4</sub>Br)<sub>3</sub>][B(C<sub>6</sub>F<sub>5</sub>)<sub>4</sub>]<sup>263</sup> and [N(C<sub>6</sub>H<sub>4</sub>Br)<sub>3</sub>][SbCl<sub>6</sub>]. However, an isolation of the species in the crystalline state was not achieved yet, and the long-term stability of non-stabilized [**1**<sup>3,6-*t*Bu</sup>]<sup>•+</sup> is challenged by previously reported decomposition pathways for the used ligand and related *tert*-butyl-phenol derivatives under Lewis acidic or oxidative conditions.<sup>264-268</sup> Thus, it was set to make use of [**1**<sup>3,6-*t*Bu</sup>]<sup>•+</sup> through an *in situ* generation. In analogy, aryl- or alkyl-silylium ions are, owed to their high reactivity, frequently synthesized upon demand by hydride abstraction through carbocations.<sup>172,269-271</sup> The present silane offers the potential for an alternative pathway that exploits oxidation. This way the high affinity of [**1**<sup>3,6-*t*Bu</sup>]<sup>•+</sup> can be exploited when **1**<sup>3,6-*t*Bu</sup> is oxidized in the presence of a (weakly) donating substrate. To probe the proposition, the carbonyl-olefin metathesis (COM) was chosen as reaction, as its outcome is known to be critically dependent on the strength of the applied Lewis acid.<sup>272-278</sup> The respective substrate **A** (Figure 20) was dissolved in CD<sub>2</sub>Cl<sub>2</sub> and 10 mol% of **1**<sup>3,6-*t*Bu</sup> were added, and the mixture was monitored NMR spectroscopically. After one hour at rt no reactivity was observed. Subsequently, 10 mol% Ag(*o*-C<sub>6</sub>H<sub>4</sub>F<sub>2</sub>)[Al(O<sup>*i*</sup>C<sub>4</sub>F<sub>9</sub>)<sub>4</sub>] were added, resulting in an immediate reactivity apparent from a pale brown coloration of the reaction solution. Strikingly, <sup>1</sup>H NMR spectroscopy indicated acetone resonances directly after addition of the oxidant. The formation of the cyclic product **B** was found complete after 14 h (Figure 20). A control experiment that omitted the silane but utilized only the silver salt showed no apparent conversion at the same time span (for monitoring see Figure 51).

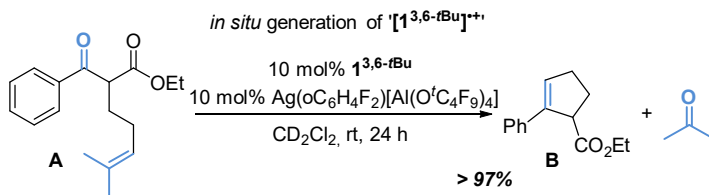


Figure 20. Intramolecular carbonyl-olefin-metathesis (COM) catalyzed by an *in situ*, oxidatively generated silylium species.

The present findings promise a valuable strategy for the generation of a Lewis superacidic species by oxidation. Further development of the conditions might result in an even more powerful protocol, for example regarding a stabilization of the active species, a lower loading of the catalyst precursors, or the utilization of a commercially available oxidant. Still, limitations can be expected in reductive catalysis, as such might result in an inhibition through reduction of the active species. Moreover, the challenging isolation of the respective radical cation prevents its use in defined bond activation experiments. In sight of this shortcomings, the synthesis of neutral, more redox-inert, silane Lewis acids is thus addressed in the upcoming chapters. Nevertheless, the present approach states a valuable alternative to existing protocols by combining two easily synthesizable and stable catalyst precursors.

## 3.2 Bis(per(trifluoromethyl)catecholato)silane

The previous results emphasized steric demand in *ortho*-positions as a key property for a composition advancement of Lewis acids based on the bis(catecholato)silane scaffold. Additionally, the substituents should be electron withdrawing to parallelly obtain high Lewis acidity. They further should be weakly nucleophilic to prevent inherent reactivity quenching by intra- or intermolecular interaction of the ligand and the Lewis acidic center. For those requirements, perfluoroalkyl substituents are ideally suited. They are expected to boost the Lewis acidity even further due to a high electronegativity and a neglectable mesomeric donation.<sup>279-281</sup> Their distinct different chemical properties render them highly popular substituents and provoked the development of multiple protocols for their installation.<sup>282-288</sup> Owing to this special role, a functionalization is highly substrate dependent and aggravatingly, most methods focus on single substitution rather than introduction of multiple CF<sub>3</sub> groups. The first part of this chapter will deal with the synthesis of a suitable ligand precursor and its subsequent installment at silicon, followed by characterization and reactivity investigations of the newly formed compound.

### 3.2.1 Synthesis

In preliminary work to this thesis, a protocol for the first synthesis of tetraiodoveratrole was presented, following tetra-trifluoromethylation, ether cleavage, and a first synthesis of the silicon motif.<sup>289</sup> This route served as a thematic starting point for the present chapter. Firstly, the synthesis of the precursor was optimized. Initially, the tetra-iodination was conducted *via* an intermediate tetra-mercuration of the parent veratrole. While this approach robustly yielded the product, the toxic nature of organomercury compounds rendered it unpractical for continuous use on a larger scale. As an alternative, HOTf induced iodination with N-iodosuccinimide (NIS) provided tetra-iodoveratrole (**ver<sup>I</sup>**) in yields up to 10 g (Figure 21a). The compound could be equipped with the trifluoromethyl groups to yield tetra(trifluoromethyl)veratrole in up to 72% yield (**ver<sup>CF<sub>3</sub></sup>**, Figure 21b),<sup>289</sup> after adaption of a related literature protocol.<sup>290</sup> Lewis acid mediated ether cleavage of **ver<sup>CF<sub>3</sub></sup>** was found unsuccessful even with BBr<sub>3</sub>. Instead, nucleophiles such as thiolates or the hydroxide anion could be applied to cleave one ether function, resulting in tetra(trifluoromethyl)guaiacol (**gua<sup>CF<sub>3</sub></sup>**). Sluggish side products and diminished yields

found in the previous synthesis could be assigned to minor base-incompatibilities of the KOH reactant and dimethylformamide (DMF) as solvent. The use of base stable dimethylacetamide (DMA) allowed for the isolation of **gua**<sup>CF<sub>3</sub></sup> in 87% yield (Figure 21c). In light of this facile ether cleavage under mild conditions and in conjunction with a the better handleability, long-term stability, and the economic advantage of saving a step, **gua**<sup>CF<sub>3</sub></sup> was used as precursor over **H<sub>2</sub>cat**<sup>CF<sub>3</sub></sup> for the attempted synthesis of bis(per(trifluoromethyl)catecholato)silane (**1**<sup>CF<sub>3</sub></sup>, Si(cat<sup>CF<sub>3</sub></sup>)<sub>2</sub>). Noteworthy, an early synthesis of the parent compound **1**<sup>H</sup> in 1943 also employed guaiacol.<sup>210</sup>

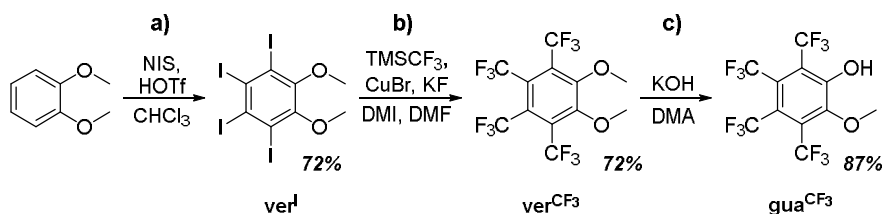


Figure 21. Cascade for the synthesis of a suitable precursor for **1**<sup>CF<sub>3</sub></sup> via a) iodination, b) trifluoromethylation, and c) nucleophilic ether cleavage.

Next, the synthesis of **1**<sup>CF<sub>3</sub></sup>·(CH<sub>3</sub>CN)<sub>2</sub> was approached according to the modular synthesis of the haloderivatives **1**<sup>X</sup>·(CH<sub>3</sub>CN)<sub>2</sub> (cmp. section 1.8, Figure 8).<sup>178</sup> Upon converting **gua**<sup>CF<sub>3</sub></sup> with half an equivalent of HSiCl<sub>3</sub> in acetonitrile, the ligand motif symmetrized and the formation of CH<sub>3</sub>Cl was apparent, as indicated by <sup>1</sup>H and <sup>19</sup>F NMR spectroscopy of aliquots.<sup>289</sup> Interestingly, no precipitation occurred, but concentrating this reaction mixture *in vacuo* led to the bis(acetonitrile)adduct **1**<sup>CF<sub>3</sub></sup>·(CH<sub>3</sub>CN)<sub>2</sub> as colorless solid, exhibiting decreased solubility in the non-donor solvent CH<sub>2</sub>Cl<sub>2</sub>.<sup>289</sup> In order to identify the intermediate, the reaction was directly monitored on an NMR scale sample in CD<sub>3</sub>CN. A continuous exchange of the atmosphere was ensured, and the reaction was found complete after 12 h. NMR examination revealed a <sup>29</sup>Si NMR signal at -90.4 ppm, advocating for a pentacoordinate silicon center. Indeed, computation of the respective resonance (-84.9 ppm) suggested the presence of the chloridosilicate [Cl-**1**<sup>CF<sub>3</sub></sup>]<sup>-</sup> (Figure 22a). A 1:1:1 triplet found in the <sup>1</sup>H NMR spectrum accounted for a nitrilium species, yet other accompanying signals rendered the nature of the cation puzzling. After addition

of one equivalent triethylamine to the fully reacted mixture, single crystals could be grown, for which scXRD verified the connectivity of the ion pair  $[\text{Et}_3\text{NH}-\text{NCCH}_3][\text{Cl}-\mathbf{1}^{\text{CF}_3}]$  (Figure 22b and Figure 52, section 5.2.5.1). Without the addition of the base, scXRD of several poor-quality crystals obtained from the reaction mixture confirmed the nature of the anion, while the cations were found to be unspecified oligomers of acetonitrile that formed under the highly Brønsted acidic conditions. When concentrated *in vacuo*, HCl was extruded resulting in the bis(acetonitrile)adduct (Figure 22c) – with the mentioned unidentified entities as impurities. Those substances turned out to be highly detrimental for further applications and accounted for a quenched reactivity.

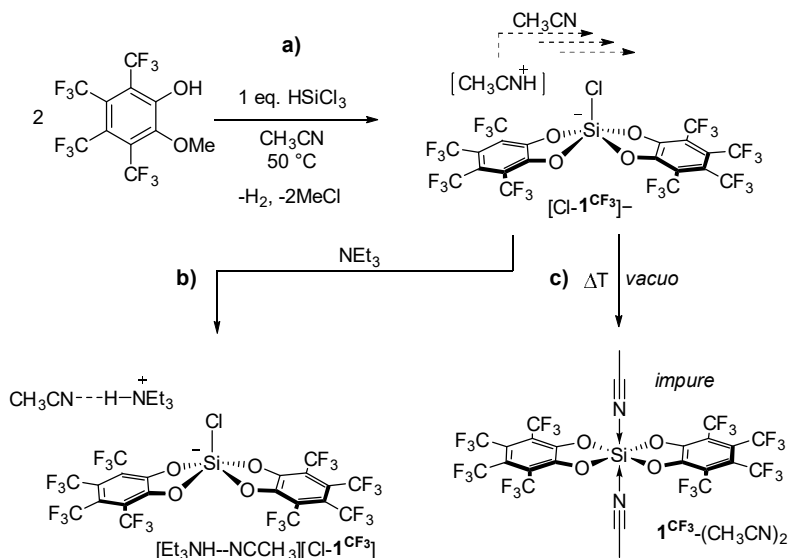


Figure 22. a) Formation of  $[\text{Cl}-\mathbf{1}^{\text{CF}_3}]^-$  in acetonitrile, b) deprotonation of the putative nitrilium ion with  $\text{NEt}_3$ , and c) formation of crude  $\mathbf{1}^{\text{CF}_3}-(\text{CH}_3\text{CN})_2$  upon extrusion of  $\text{HCl}$  *in vacuo*.

While now an alternate synthesis was required in response, these reactivities still resulted in important insights for the further proceeding. First,  $\text{gua}^{\text{CF}_3}$  is a suitable ligand precursor and can be easily demethylated with chlorosilanes. Second, the formed chlorosilicate indicates a significant chloride anion affinity of the parent compound  $\mathbf{1}^{\text{CF}_3}$  that exceeds the one of all perhaloderivatives. Given the highly

Brønsted acidic reaction medium involving nitrilium species,<sup>291</sup> the stability of the chloridosilicate hints to a highly potent corresponding Lewis acid, since acid stability of a weakly coordinating anion (WCA) and Lewis acid strength of the underlying compound are closely related.<sup>69,292</sup>

Encouraged by this, other weakly nucleophilic donors were considered. No reactivity could be observed in non-coordinating solvents such as dichloromethane or *ortho*-dichlorobenzene. Thus, a minimum donor stabilization of the solvent was ruled necessary for the successful outcome of the synthesis. Therefore, sulfolane was considered as a dipolar, aprotic solvent with a similarly low donor number (DN) (DN<sup>293</sup> = 14.8, *cmp.* DN(CH<sub>3</sub>CN)<sup>294</sup> = 14.6). It is more robust toward strong acids, strong bases, and thermal decomposition.<sup>295</sup> Heating of a sulfolane solution (+3 vol% benzene for handleability) containing two equivalents **gua**<sup>CF<sub>3</sub></sup> and HSiCl<sub>3</sub> or SiCl<sub>4</sub> to 100 °C resulted in the formation of colorless crystals in 90% yield (Figure 23). Indeed, scXRD analysis confirmed the formation of **1**<sup>CF<sub>3</sub></sup>-(sulfolane)<sub>2</sub>. The reaction could easily be scaled up, yielding >1.5 g of the product. **1**<sup>CF<sub>3</sub></sup>-(sulfolane)<sub>2</sub> thus served as good starting point for all follow-up experiments.

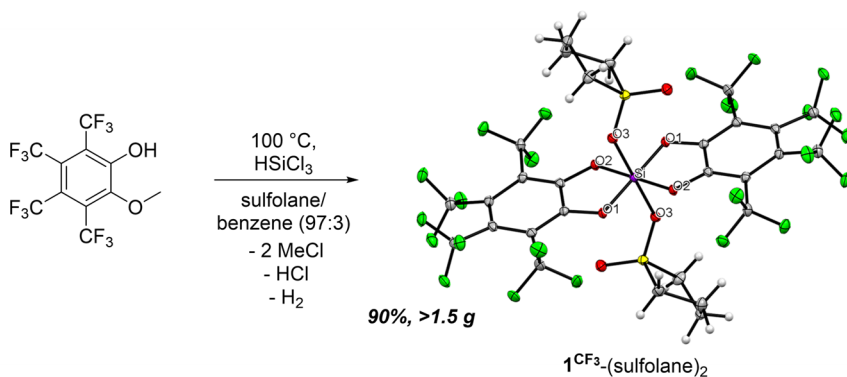


Figure 23. Synthesis of **1**<sup>CF<sub>3</sub></sup>-(sulfolane)<sub>2</sub>. **1**<sup>CF<sub>3</sub></sup>-(sulfolane)<sub>2</sub> illustrated as scXRD-derived molecular structure; co-crystallized benzene molecule was omitted for clarity. Selected bond lengths and angles: Si-O1 1.7321(10) Å, Si-O2 1.7379(10) Å, Si-O3 1.9051(11) Å; O1-Si-O2 90.10(5)°, O1-Si-O3 92.75(5)°.

### 3.2.2 Probing the Lewis Acidity

Next, experimental and theoretical probing of the newly synthesized Lewis acid was conducted. A first indication of an enhanced Lewis acidity was given by a shortened Si-OS bond length in  $\mathbf{1}^{\text{CF}_3}$ -(sulfolane) $_2$  in comparison to  $\mathbf{1}^{\text{Cl}}$ -(sulfolane) $_2$ .<sup>i</sup> To account for the *global* Lewis acidity of  $\mathbf{1}^{\text{CF}_3}$ -(sulfolane) $_2$ , FIA and HIA were computed.<sup>j</sup> Both affinities are exceptionally high, unambiguously highlighting  $\mathbf{1}^{\text{CF}_3}$  as novel record holder for neutral silicon Lewis acids. The FIA of 578 kJ mol<sup>-1</sup> not only qualifies  $\mathbf{1}^{\text{CF}_3}$  as Lewis superacid but approaches even the most fluorophilic compounds in a cross-class comparison (Figure 24). Remarkably, also the HIA (523 kJ mol<sup>-1</sup>) is exceptionally boosted, rendering  $\mathbf{1}^{\text{CF}_3}$  one of the first of two *soft* Lewis superacids.<sup>195</sup>

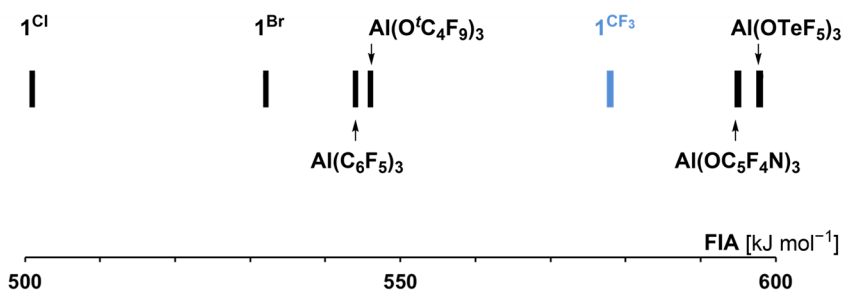


Figure 24. Comparison of computed fluoride ion affinities (FIA) of  $\mathbf{1}^{\text{CF}_3}$  and the strongest, neutral fluoride ion acceptors currently accessible (for computational details see section 5.3). FIAs shown in the plot were referenced consistently against CCSD(T)/CBS anchor points.<sup>78</sup>

Experimental evaluation of the Lewis superacidity was performed in a reaction with the  $\text{SbF}_6^-$  anion. After addition of  $[\text{PPh}_4][\text{SbF}_6]$  to a suspension of an equimolar amount of  $\mathbf{1}^{\text{CF}_3}$  in  $\text{CD}_2\text{Cl}_2$  an immediate dissolution was apparent. The fast reactivity within seconds is opposed to the longer reaction times reported for  $\mathbf{1}^{\text{Cl}}$ , and might be rationalized by an enhanced Lewis acidity, a better dissociation of the donor, and a better solubility. Isolation of a reaction product was not possible, caused by ligand scrambling or follow-up oxidation reactions, similarly observed for  $\mathbf{1}^{\text{Cl}}$ .<sup>6</sup> Immediate

<sup>i</sup> A comparison was made in sight of the close structural proximity of both candidates. An examination of bond lengths does not account for a general scaling of Lewis acidity, and reasonable comparisons should be backed by other methodologies.

<sup>j</sup> The reported ion affinities were calculated by DANIEL ROTH in the course of his master thesis at the DLPNO-CCSD(T)/aug-cc-pVQZ//PW6B95-D3(BJ)/def2-TZVPP//BP86-D3(BJ)/def2-SVP level of theory (emp. section 5.3).

NMR analysis of the reaction mixture after addition of  $\text{SbF}_6^-$  indeed revealed the presence of  $[\text{F}-\mathbf{1}^{\text{CF}_3}]^-$ , as judged by comparison with independently prepared  $[\text{N}(\text{}^n\text{Bu})_4][\text{F}-\mathbf{1}^{\text{CF}_3}]$ . The experiment thus serves as experimental gauge for the verification of the Lewis superacidity of  $\mathbf{1}^{\text{CF}_3}$ . Next, to compare the *effective* Lewis acidity within the substance class of  $\mathbf{1}^{\text{X}}$ , an evaluation according to *GUTMANN-BECKETT* was conducted. Addition of sub-stoichiometric amounts triethylphosphineoxide ( $\text{Et}_3\text{PO}$ ) to  $\mathbf{1}^{\text{CF}_3}$ -(sulfolane) $_2$  led to the formation of the mono-adduct  $\mathbf{1}^{\text{CF}_3}\text{-OPEt}_3$  (Figure 25a). The formation of the target compound was confirmed by scXRD analysis (Figure 25b). Notably, the respective mono-adducts for the perhaloderivatives  $\mathbf{1}^{\text{X}}$  could never be confirmed in the solid state. The induced  $\Delta\delta(^{31}\text{P})$  NMR shift consistently extends the observed trend for this substance class, rendering the present derivative as strongest representative (Figure 25a).

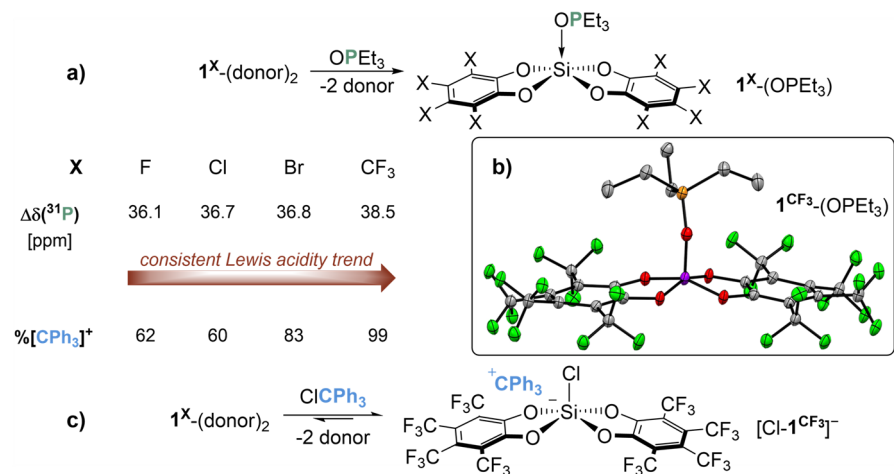


Figure 25. a) Comparative Gutmann-Beckett probing for  $\mathbf{1}^{\text{X}}$  derivatives.<sup>178</sup> b) scXRD derived molecular structure of  $\mathbf{1}^{\text{CF}_3}\text{-OPEt}_3$  (shown at 50% probability, hydrogen atoms omitted for clarity). c) Equilibrium of the chloride abstraction from trityl chloride by  $\mathbf{1}^{\text{X}}$  derivatives.  $\mathbf{1}^{\text{X}}\text{-(donor)}_2 - \text{X} = \text{F}, \text{Cl}, \text{Br}$  with donor acetonitrile,  $\text{X} = \text{CF}_3$  with donor sulfolane.

Next, the chloride affinity was approached in a qualitative experiment. Mixing  $\text{Ph}_3\text{CCl}$  and  $\mathbf{1}^{\text{CF}_3}$ -(sulfolane) $_2$  resulted in immediate dissolution of the latter and an intense yellow coloration of the solution. NMR characterization revealed quantitative formation of  $[\text{CPh}_3][\text{Cl}-\mathbf{1}^{\text{CF}_3}]$ . This states a sharp contrast to its halogenated

predecessors, for which a maximum equilibrium proportion of 83% was reached (Figure 25c). Nevertheless, solid state isolation was prevented as upon evaporation of the solvent the reaction was reversed – resulting in the initially utilized substrates in the solid state. Overall, both the chloride abstraction as well as the GB probing revealed a consistent trend of *effective* Lewis acidity, that matched the *global* order indicated by the FIA (Figure 25a/c). Finally, given the high calculated HIA of  $\mathbf{1CF}_3$ , the synthesis of the corresponding hydrosilicate  $[\text{H-}\mathbf{1CF}_3]^-$  was attempted. Following a reported general approach,<sup>296</sup>  $\mathbf{1CF}_3$ -(sulfolane)<sub>2</sub> was converted with KH and 18-crown-6 ether in  $\text{CD}_2\text{Cl}_2$ .<sup>296</sup> However, the target species  $[\text{H-}\mathbf{1CF}_3]^-$  could not be observed and gas deconvolution indicated different reactivity. Instead, scXRD analysis of poor quality crystals grown from the reaction mixture revealed the formation of  $[\text{O}(\text{Si}(\text{cat}^{\text{CF}_3})_2)_2]^{2-}$  as  $[\text{K@18c6}]^+$  salt. The elusive species could also not be detected when the hydride was added at  $-40\text{ }^\circ\text{C}$  followed by immediate NMR spectroscopic analysis.

### 3.2.3 Approaching Unquenched Reactivity of $1^{CF_3}$

Unlocking the full potential of  $1^{CF_3}$  was interesting in a twofold sense. First, the probed affinities promised a highly reactive species, and second, it would give insights on a putative self-aggregation process. Initial calculations on the self-aggregation were conducted, but convergence issues for higher oligomers ( $n > 3$ ) prevented a more comprehensive analysis of the process, even on the computationally efficient GFN2-xTB level. To account for a kinetic assertion, an investigation of the dimerization was undertaken. As for the alkylated derivatives  $1^{3,4,6-iPr}$ ,  $1^{3,6-tBu}$ , and  $1^{3,5-Cm}$  (cmp. section 3.1), the dimer formation was analyzed.<sup>k</sup> As expected, the dimer  $[1^{CF_3}]_2$  was calculated to be endergonic ( $\Delta G = +29 \text{ kJ mol}^{-1}$ ), in analogy to the species  $1^{3,4,6-iPr}$  and  $1^{3,6-tBu}$ . More interestingly, a found barrier of  $\Delta G^\ddagger = 130 \text{ kJ mol}^{-1}$  was significantly enlarged compared to the parent species  $1^H$  (Figure 26),<sup>231</sup> the alkylated derivatives (cmp. section 3.1) or  $1^F$ .<sup>256</sup> Overall, even though no thermodynamic indication for the self-aggregation behavior could be accessed, the computational considerations indicate a kinetic stabilization for monomeric  $1^{CF_3}$  at least at mild conditions – in contrast to all previous bis(catecholato)silanes.

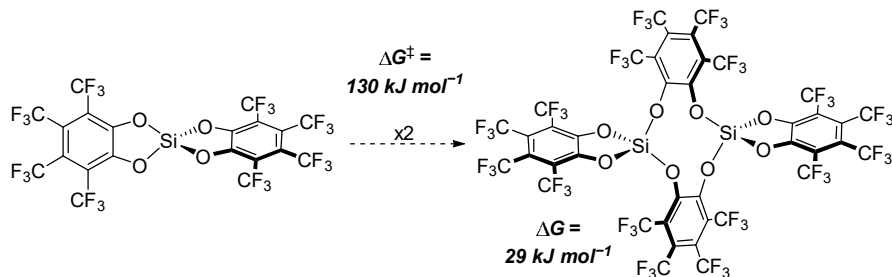


Figure 26. Computationally studied dimerization process of  $1^{CF_3}$ . Displayed energies were obtained at the DSD-BLYP-D3(BJ)/def2-QZVPP+SMD(CH<sub>2</sub>Cl<sub>2</sub>)/PBEh-3c level of theory.

Encouraged by this result, the synthesis of donor-free  $1^{CF_3}$  was approached. The use of nitrobenzene in the synthesis as even weaker coordinating solvent was attempted.<sup>32</sup> Indeed, in contrast to entirely non-donating solvents a reactivity and an accompanying coloration could be observed, however only at temperatures of 110 °C

<sup>k</sup> DSD-BLYP-D3(BJ)/def2-QZVPP+SMD(CH<sub>2</sub>Cl<sub>2</sub>)/PBEh-3c level of theory.

or higher. An aliquot of the reaction mixture was analyzed *via*  $^{19}\text{F}$  NMR spectroscopy, revealing various signals neighbored to the  $\text{CF}_3$  ligand resonances. They were accompanied by more upfield shifted fluorides with characteristic  $^{29}\text{Si}$  coupling, clearly advocating for decomposition. Next, as per the results of the initial synthesis of donor-free  $\mathbf{1}^{\text{Cl}}$ ,<sup>6</sup> formal  $\text{SiH}_4$  chemistry by the use of *OESTREICH*'s tris(cyclohexa-1,3-dien-2-yl)silane was considered.<sup>297</sup> The latter was mixed with two equivalents of  $\mathbf{gua}^{\text{CF}_3}$  and catalytic amounts  $\text{B}(\text{C}_6\text{F}_5)_3$  (5 mol%) in  $\text{CD}_2\text{Cl}_2$ , aiming for the extrusion of  $\text{H}_2$ /hydrocarbons according to a *PIERS-RUBINSZTAJN* reactivity.<sup>298,299</sup> However, the experiment did not result in the desired reactivity even after 24 h at 60 °C. Kinetic hindrance through the additional methyl group in  $\mathbf{gua}^{\text{CF}_3}$  as compared to  $\mathbf{H}_2\mathbf{cat}^{\text{Cl}}$  was taken into account. Therefore, higher boiling toluene and *ortho*-dichlorobenzene were used as solvents and the temperature gradually increased. In the primary case, no conversion could be monitored at temperatures up to 110 °C. With the more polar *ortho*-dichlorobenzene, reactivity was observed at 150 °C. The mixture adapted a red color after 24 h, which intensified tremendously after additional heating for 72 h. NMR monitoring suggested the presence of silicon bound fluorine atoms. Those observations are reminiscent to the attempted synthesis in nitrobenzene described earlier, likewise accounting for decomposition. The combined observations served as indication that the non-coordinated target system is not stable at elevated temperatures. Therefore, alternative protocols that can be conducted under milder conditions were considered. An approach found successful for the synthesis of a highly reactive silane or phosphonium(V) cations states the chloride abstraction with  $\text{Na}[\text{B}(\text{C}_6\text{F}_5)_4]$ .<sup>188,194</sup> The chloridosilicate  $[\text{PPh}_4][\text{Cl}-\mathbf{1}^{\text{CF}_3}]$  was thus synthesized and added to a suspension of  $\text{Na}[\text{B}(\text{C}_6\text{F}_5)_4]$  in  $\text{CD}_2\text{Cl}_2$ . After two hours in continuous motion the suspension ( $\text{Na}[\text{B}(\text{C}_6\text{F}_5)_4]$  initially undissolved) indicated the dissolved  $[\text{B}(\text{C}_6\text{F}_5)_4]^-$  anion by enhanced  $^{19}\text{F}$  NMR intensities, and parallelly, decreased  $\mathbf{cat}^{\text{CF}_3}$  signals. Thus, a salt metathesis to  $\text{Na}[\text{Cl}-\mathbf{1}^{\text{CF}_3}]$  and  $[\text{PPh}_4][\text{B}(\text{C}_6\text{F}_5)_4]$  was assumed. An extrusion of  $\text{NaCl}$  from the putative precipitate was attempted in benzene, *n*-pentane, and *n*-hexane, yet in all cases no  $\mathbf{1}^{\text{CF}_3}$  derived species could be observed in solution. To account for an abstraction reagent with a higher chloride ion affinity, the triethylsilylium cation was considered.  $[\text{PPh}_4][\text{Cl}-\mathbf{1}^{\text{CF}_3}]$  was added to freshly prepared  $[\text{SiEt}_3][\text{B}(\text{C}_6\text{F}_5)_4]$  in benzene. Promisingly, NMR spectroscopy revealed the formation of a symmetric species based on the  $\mathbf{cat}^{\text{CF}_3}$  ligand. In line, the expected side product  $[\text{PPh}_4][\text{B}(\text{C}_6\text{F}_5)_4]$  could be verified by scXRD of suitable crystals. Traces

of  $\text{Et}_3\text{SiF}$  were observed – leaving the possibility of decomposition of the Lewis acid under the harsh conditions. Even though an isolation was not achieved yet, the approaches by no means indicated the possibility of the formation of an insoluble oligomer, and further underlined the high reactivity of a putative, donor-free species. Still, based on these results, an isolation of the target species using the highly electrophilic reagents seemed unlikely.

Finally, a strategy was adapted from the successful isolation of donor-free bis(perchlorocatecholato)germane  $\text{Ge}(\text{cat}^{\text{Cl}})_2$ . The latter was isolated after reducing its bis-acetone-adduct with bulky 9-BBN.<sup>300</sup> To avoid side reactivities originating from the CH acidity of acetone, benzophenone was envisioned as initial coordinating donor. Formation of the respective adduct  $\mathbf{1}^{\text{CF}_3}\text{-(OCPh}_2\text{)}$  was detected by NMR spectroscopy after adding benzophenone to a suspension of  $\mathbf{1}^{\text{CF}_3}\text{-(sulfolane)}_2$  in  $\text{CH}_2\text{Cl}_2$ . Yet, separation of the released sulfolane was unsuccessful due its low volatility. The bis(sulfolane)adduct was therefore converted into the bis(acetonitrile)adduct through simple stirring in acetonitrile, followed by filtration and washing of the residue. Subsequently, excess benzophenone was added to a suspension of  $\mathbf{1}^{\text{CF}_3}\text{-(CH}_3\text{CN)}_2$  in  $\text{CH}_2\text{Cl}_2$ , the mixture stirred rigorously, and dissociated acetonitrile evaporated *in vacuo* until a complete conversion was achieved (details in section 5.2.2.7). This way a fully characterized mono-benzophenone adduct  $\mathbf{1}^{\text{CF}_3}\text{-(OCPh}_2\text{)}$  was isolated. Yellow to orange crystals suitable for scXRD were grown from a benzene solution, unambiguously confirming its molecular structure (Figure 27a). The isolated adduct not only shows excellent solubility in common organic solvents, but also serves as another example for the high Lewis acidity of the target compound, as it states – to the best of the authors knowledge – the first report of an isolated neutral Lewis adduct of a silane and a ketone. Subsequently, the reduction of the bound ketone was approached. Various boron species were formed upon addition of 9-BBN as revealed by NMR spectroscopy, accounting for unselective reactivity. Thus, less reactive silane reductants were considered, which were shown to cleanly reduce benzophenone to diphenylmethane (cmp. section 3.2.4), only revealing a virtually non-coordinating disiloxane as side product.<sup>32</sup> The only example for an unsupported, intermolecular disiloxane coordination was reported in conjunction with a cationic magnesium species.<sup>301</sup>

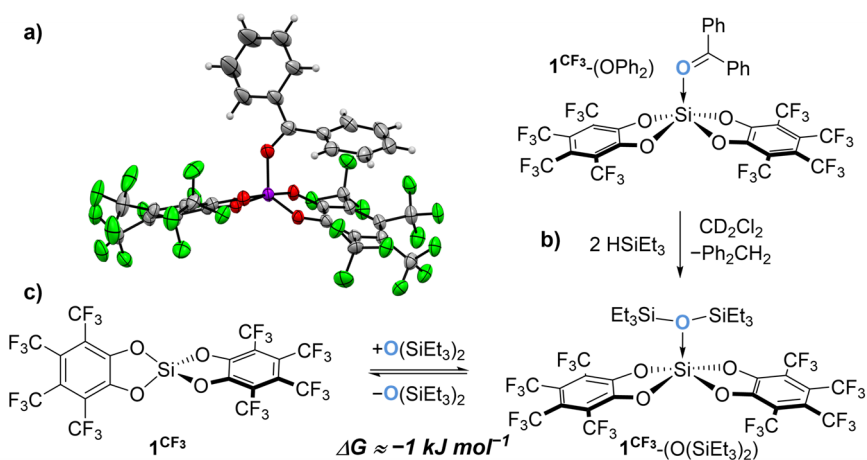


Figure 27. a) scXRD derived molecular structure of  $1^{CF_3}$ -(OCPh<sub>2</sub>) (shown at 50% probability). b) Reduction of  $1^{CF_3}$ -(OCPh<sub>2</sub>) with HSiEt<sub>3</sub>. c). Equilibrium of the adduct formation of  $1^{CF_3}$  and O(SiEt<sub>3</sub>)<sub>2</sub>.

Reaction of  $1^{CF_3}$ -(OCPh<sub>2</sub>) with two equivalents of HSiEt<sub>3</sub> in CD<sub>2</sub>Cl<sub>2</sub> resulted in the formation of diphenylmethane and the disiloxane O(SiEt<sub>3</sub>)<sub>2</sub> (Figure 27b). <sup>19</sup>F and <sup>13</sup>C NMR spectra further revealed a single symmetric *cat*<sup>CF<sub>3</sub></sup> species. However, the observed <sup>29</sup>Si NMR signal (−78.4 ppm) is in disagreement with a calculated resonance at −42.8 ppm<sup>1</sup> and also not in the expected range for a dimer or higher oligomers.<sup>231</sup> The <sup>29</sup>Si NMR signal (−21.2 ppm) for the disiloxane was found to be significantly shifted compared to its unbound form (−8.9 ppm), indicating an adduct formation. Yet, for a datively bound adduct the resonance of the Lewis acid's silicon would be expected to be more upfield shifted ( $\delta(^{29}\text{Si}_{\text{calc.}}) = -101.8 \text{ ppm}$ ). The experimental resonances are in line with an equilibrium between the separated bonding partners and their Lewis adduct (Figure 27c). Based on the calculated <sup>29</sup>Si NMR resonances of the adduct and the unbound compound  $1^{CF_3}$ , an experimentally derived value for the reaction Gibbs free energy of  $\Delta G = -1.04 \text{ kJ mol}^{-1}$  could be assessed (cmp. section 5.2.5.5). In good agreement and within the borders of chemical accuracy, computational evaluation of the adduct formation revealed a similar value of  $\Delta G_{\text{calc.}}$

<sup>1</sup> Details for the computation of NMR resonances are provided in section 5.3. The resonances are listed in Table A9.

---

= 1.18 kJ mol<sup>-1</sup>.<sup>m</sup> Still, in accordance with its high reactivity, partial self-decomposition was indicated by minor unidentified trace species in the <sup>19</sup>F NMR spectrum, even when conducted at -40 °C. The use of benzene as solvent and tri-*iso*-propylsilane as reductant minimized but could not prevent such side-reactivity. It is noteworthy that even in the case of the more sterically hindered disiloxane O(Si<sup>t</sup>Pr<sub>3</sub>)<sub>2</sub>, a <sup>29</sup>Si NMR resonance of -80.1 ppm likewise accounted for an equilibrating system.

Overall, even though the isolation of a donor-free species in the solid state was unsuccessful, the findings were promising in a dual perspective. First, an interaction with even the poorly donating disiloxanes underlines the Lewis acidity of **1**<sup>CF<sub>3</sub></sup>. Secondly, *in situ* reduction of **1**<sup>CF<sub>3</sub></sup>-(OCPh<sub>2</sub>) can be utilized to unlock almost unquenched reactivity. This way **1**<sup>CF<sub>3</sub></sup> can be unleashed in reactivities requiring the absence of sulfolane donors. Of note, similarly Lewis superacidic species like the alanes Al(OTeF<sub>5</sub>)<sub>3</sub> or Al(OC<sub>5</sub>F<sub>4</sub>N)<sub>3</sub> require weak stabilization through aggregation or donors alike.<sup>302,303</sup>

---

<sup>m</sup> DSD-BLYP-D3(BJ)/def2-QZVPP+SMD(CH<sub>2</sub>Cl<sub>2</sub>)/PBEh-3c level of theory. The Gibbs free energy was reevaluated under consideration of conformation (cmp. section 5.3) and therefore results in a more precise value compared to previously published data, , which is still in good qualitative agreement.

### 3.2.4 Catalysis

Encouraged by the significant affinities demonstrated in the previous reactions, catalytic applications were investigated using the bis-sulfolane-adduct as robust catalytic precursors. Previously,  $1^F-(\text{CH}_3\text{CN})_2$  was applied as a potent catalyst in the hydrosilylation of electron-deficient, aromatic benzaldehydes.<sup>48</sup> Following this example, *para*-fluorobenzaldehyde was efficiently converted with  $\text{HSiEt}_3$  by just 1 mol%  $1^{\text{CF}_3}$ -(sulfolane)<sub>2</sub> (Table 1, entry 1). However, opposed to the silyl ethers obtained from  $1^F$  catalysis, in this case highly selective formation of bis-(4-fluorobenzyl)-ether was observed (96%), resulting in hexaethyldisiloxane ( $\text{O}(\text{SiEt}_3)_2$ ) as side product. Strikingly, the same reactivity in similar selectivity and yield was observed for less activated *para*-methylbenzaldehyde, benzaldehyde, and cyclohexylcarbaldehyde (Table 1, entry 2-4). Of note, those substrates were not included in the scope of the  $1^F$  catalyzed protocol. Applying harsher conditions to *para*-fluorobenzaldehyde resulted in the fully reduced product *para*-fluorotoluene (Table 1, left), proceeding *via* the ether intermediate.

Table 1. Catalytic application of  $1^{\text{CF}_3}$ -(sulfolane)<sub>2</sub> in the reduction of aldehydes to dialkyl ethers and the reduction of *para*-fluorobenzaldehyde to *para*-fluorotoluene.

$\text{R}-\overset{\text{O}}{\parallel}{\text{C}}-\text{H} \xrightarrow[\text{CD}_2\text{Cl}_2, \text{rt, t}]{\begin{array}{c} 1^{\text{CF}_3}\text{-(sulfolane)}_2 \text{ (1 mol\%)} \\ \text{HSiEt}_3 \end{array}} \text{R}-\overset{\text{H}}{\text{C}}-\text{O}-\overset{\text{H}}{\text{C}}-\text{R}$		R	t [h]	Y [%]
		- <i>p</i> C <sub>6</sub> H <sub>4</sub> F	24	96
		- <i>p</i> C <sub>6</sub> H <sub>4</sub> CH <sub>3</sub>	24	97
		-C <sub>6</sub> H <sub>5</sub>	24	89
		-C <sub>6</sub> H <sub>11</sub>	24	71
$\text{R}-\overset{\text{CH}_3}{\text{C}} \xleftarrow[\text{100 }^\circ\text{C}]{\begin{array}{c} \text{PhSiH}_3 \\ \text{oC}_6\text{H}_4\text{Cl}_2 \end{array}} \text{R} = \begin{array}{l} \text{-}i\text{C}_6\text{H}_4\text{F} \\ \text{-}i\text{C}_6\text{H}_4\text{CH}_3 \end{array}$	66%			

Next, ketone derivatives were addressed. The use of benzophenone as a substrate resulted in a very fast reaction at rt, but neither the reductive ether formation nor hydrosilylation could be observed. Instead, the deoxygenation product diphenylmethane was detected as main product (Table 2, entry 1). In consistency, full conversion was only reached upon addition of at least two equivalents of triethylsilane. With acetophenone as substrate the reaction was found to require elevated temperatures and a change of solvent at a catalyst loading of 5 mol% (Table 2, entry 2).

Table 2. Catalytic application of  $1\text{CF}_3$ -(sulfolane) $_2$  in the hydrodeoxygenation of ketones and amides.

$1\text{CF}_3$ -(sulfolane) $_2$ (x mol%) reducing agent (r.a.) solvent, T, t				$1\text{CF}_3$ -(sulfolane) $_2$ (5 mol%) PhSiH $_3$ <i>o</i> C $_6$ H $_4$ Cl $_2$ , 100 °C, 72 h			
R	R'	x	r.a.	solvent	T [°C]	t [h]	Y [%]
-C $_6$ H $_5$		2	HSiEt $_3$	CD $_2$ Cl $_2$	25	0.5	99
-C $_6$ H $_5$	-CH $_3$	5	PhSiH $_3$	<i>o</i> C $_6$ H $_4$ Cl $_2$	100	72	80
-C $_6$ H $_5$	-N $^i$ Pr $_2$	5	PhSiH $_3$	<i>tol-d8</i>	100	48	95

Reduction of aliphatic cyclohexanone resulted in cyclohexene through deoxygenative alkene formation, for which likewise an increased temperature was necessary (Table 2, top right). Adapted conditions further allowed for the reduction of an amide to an amine (Table 2, entry 3), and the restoration of phosphines from respective phosphine oxides (Table 3), the latter being an important process that is performed on an industrial, multi-ton scale every year.<sup>304</sup>

Table 3. Catalytic application of  $1\text{CF}_3$ -(sulfolane) $_2$  in the deoxygenation of phosphine oxides.

$1\text{CF}_3$ -(sulfolane) $_2$ (5 mol%) PhSiH $_3$ toluene- <i>d8</i> , 100 °C, t		R	t	Y
		-C $_6$ H $_5$	48	91
		-C $_2$ H $_5$	48	96

To account for the high Lewis acidity of  $1\text{CF}_3$ , a carbonyl-olefin-metathesis (COM) reaction was attempted next. COM is critically influenced by the strength of the applied Lewis acid and previously was restricted to metal halide catalysts.<sup>272-278</sup> Strikingly, upon addition of 5 mol%  $1\text{CF}_3$ -(sulfolane) $_2$ , a solution of substrate **A** was found to be cleanly converted into the cyclization product **B** (Figure 28). This result seemed promising, as it not only accounted for the applicability of  $1\text{CF}_3$  in non-reductive catalysis, but also resembled the first example of a neutral silane catalyst in COM.

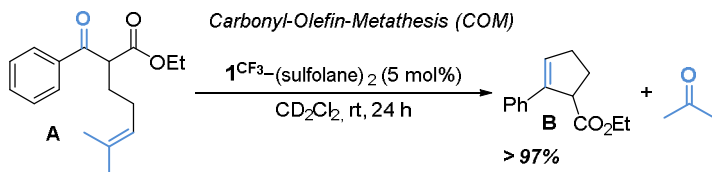


Figure 28. Catalytic application of  $1^{CF_3}$ -(sulfolane) $_2$  in the intramolecular carbonyl-olefin metathesis.

In light of this portfolio of novel reactivities at low catalyst loadings, a comparison to  $1^{Cl}$  and  $1^{CF_3}$ -(OCPH $_2$ ) was drawn. Therefore, the respective catalytic species was tested in the reduction of *para*-fluorobenzaldehyde, *para*-methylbenzaldehyde, and benzophenone under reductive conditions (Table 4). The yields were determined after 24 h, respectively.

Table 4. Comparison of catalytic activity of  $1^{CF_3}$ -(donor) $_n$  and  $1^{Cl}$ -(donor) $_2$  in the reductive alkyl ether formation and the deoxygenation of benzophenone (product P). General conditions: 150  $\mu$ mol substrate, [a] 1 mol% catalyst and 225  $\mu$ mol HSiEt $_3$  or [b] 2 mol% catalyst and 450  $\mu$ mol HSiEt $_3$  in 0.5 mL CD $_2$ Cl $_2$ ; reaction time 24 h, respectively. C: conversion, P1: yield of the dialkyl ether product, P2: yield of the carbonyl hydrosilylation product, P: yield of the hydrodeoxygenation product.

	<b>P1</b>			<b>P2</b>			<b>P</b>					
Catalyst/ Substrate	$1^{CF_3}$ -(sulfolane) $_2$			$1^{Cl}$ -(sulfolane) $_2$			$1^{Cl}$ -(CH $_3$ CN) $_2$			$1^{CF_3}$ -(OCPH $_2$ )		
	C	P1	P2	C	P1	P2	C	P1	P2	C	P1	P2
<i>p</i> C $_7$ H $_7$ CHO <sup>[a]</sup>	98%	97%	<0.5%	31%	27%	3%	7%	6%	<0.5%	98%	97%	<0.5%
<i>p</i> FC $_6$ H $_4$ CHO <sup>[a]</sup>	>99%	96%	3%	26%	10%	16%	11%	5%	5%	82%	80%	2%
<i>p</i> Ph $_2$ CO <sup>[b]</sup>	>99%	99% (P)		25%	24% (P)		16%	16% (P)		78%	77% (P)	

Using  $1^{Cl}$ -(CH $_3$ CN) $_2$  as catalytic species resulted in a clearly reduced activity and selectivity, as both hydrosilylation- and ether-product were observed (Table 4, col. 3). The use of  $1^{Cl}$ -(sulfolane) $_2$  rendered sulfolane donors as superior for the activity, as increased conversion rates compared to the bis-acetonitrile adduct could be observed (Table 4, col. 2). However, the overall activity is still inferior in comparison to  $1^{CF_3}$ -(sulfolane) $_2$ . On the whole,  $1^{CF_3}$ -(sulfolane) $_2$  shows significantly enhanced activity and selectivity for the reductive ether formation (Table 4, col. 1), whereas the product composition for the  $1^{Cl}$  catalyzed reactions is rather unselective (Table 4, col. 2/3). A possible explanation for the high selectivity in the ether-reduction

might be given through a preferred *cisoid* conformation, as observed for  $1\text{CF}_3\text{-(OPEt)}_2$  in solution and solid state (cmp. section 3.2.2). A respective configuration in the case of cyclohexanecarbaldehyde was further indicated through  $^{19}\text{F}$  NMR spectroscopy. A *cis* coordination accounts for a higher substrate activation, as the electron withdrawing catecholate coordination is located *trans* to the carbonyl. Further, a pre-organizational effect for an intramolecular ether formation seems likely due to the steric proximity of both substrate molecules.

Next, the performance of  $1\text{CF}_3\text{-(OCPh}_2\text{)}$  was probed, as it serves as precursor for unlocking an almost unquenched reactivity under reductive conditions (cmp. section 3.2.3). Surprisingly, over the course of 24 h it showed for all substrates lower convergences in comparison to the bis(sulfolane)adduct – even in the deoxygenation of benzophenone itself. A more detailed monitoring over time for the reduction of the aldehydes was undertaken (Figure 29), indicating a pronounced starting rate of the  $1\text{CF}_3\text{-(OCPh}_2\text{)}$  catalyzed reactions (green curve). In the further course, the curve shows a substantial flattening.

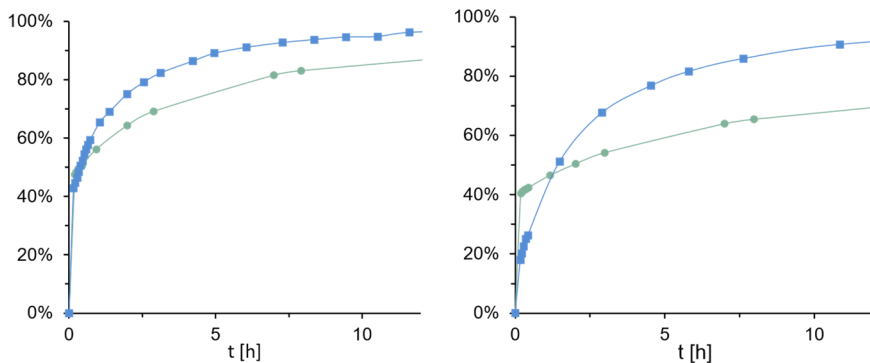


Figure 29. A comparison of the activity of  $1\text{CF}_3\text{-(sulfolane)}_2$  and  $1\text{CF}_3\text{-(OCPh}_2\text{)}$  in the catalytic, reductive ether formation from benzaldehydes and triethylsilane. The plots show the yields for the respective bisbenzylether product *versus* the time.

At first glance this might be rationalized with partial self-decomposition, resulting in a lower effective catalyst loading. However, it might also indicate an active role of an external donor that accounts for pre-organization or electric-field effects. Nevertheless,

in sight of a lower efficiency, other encountered reactivities were not reevaluated with the  $\mathbf{1}^{\text{CF}_3}\text{-(OCPh}_2\text{)}$  catalyst.

Overall, the results described in this chapter serve as pioneering example that a modulation of the catecholate scaffold enables a regulation of steric and electronic characteristics of the corresponding silane Lewis acid – while preserving their capacity to navigate complex, high-energy reaction pathways. The high FIA that approaches even established aluminum Lewis superacids further serves as manifest for the Lewis acidity of neutral silicon compounds – which were assigned with only moderate Lewis acidity up to 7 years ago.  $\mathbf{1}^{\text{CF}_3}$  was found to catalyze the deoxygenation of ketones, amides, and phosphine oxides. Moreover, it is an active catalyst in a carbonyl-olefin-metathesis. It thus broadened the spectrum of catalytic reactions achievable with neutral silanes.

### 3.3 Bis(nonafluoro-N-phenyl-*ortho*-amidophenolato)silane

With  $1^{CF_3}$ , a new derivative emerged from the previous shortcomings of its substance class  $1^X$ , yet a defined use of unquenched  $1^{CF_3}$  walks along with an elaborate set-up. Moreover, no indications for the stability of the corresponding hydridosilicate could be acquired. To allow for softer mediations involving hydride species, the synthesis of a well handleable silane and its hydridosilicate will be addressed in the present chapter.

#### 3.3.1 Synthesis and Characterization

Apart from the introduction of steric bulk through *ortho*-substitution in catecholates, an intuitive way for derivatization states the use of related *ortho*-amidophenolates. This way a similar electronic environment is maintained while parallelly accounting for more steric shielding around the reactive silicon center. Proofing the design principle, such an approach was used to exemplary show the contrasting monomeric nature of bis(amidophenolato)silanes in comparison to the oligomeric catecholates.<sup>231</sup> More generally, the substitution of catechols with *ortho*-aminophenols states a popular method to fine-tune stereo-electronic properties in metal complexes, even though their use *hitherto* focused on the exploitation of redox-reactivity and non-innocent behavior.<sup>245</sup> The synthesis of silicon Lewis superacids based on this ligand class would require strongly electron-deficient representatives, which are, to the best of the authors knowledge, not reported.

Therefore, at first the synthesis of a suitable derivative was approached. To account for an adequate ligand design, preliminary calculations regarding the effect of substitution on the FIA of bis(*ortho*-amidophenolato)silane derivatives were considered (Figure 30).<sup>n</sup> A change of the substituent  $X$  from fluoride (F) to chloride (Cl) or bromide (Br) in the backbone resulted in fairly similar FIAs for the respective silanes. In contrast, for catecholate derivatives the  $\pi$ -acidity had a more dominating influence.<sup>178</sup> Based on these data, a higher contribution from inductive withdrawing and a less dominant mesomeric effect on the Lewis acidity for the *ortho*-

---

<sup>n</sup> The discussed data were taken from research results generated by *J. LEITNER* in the course of his master studies under the supervision of *L. GREB* (2019). The affinities were obtained at the PW6B95-D3(BJ)/def2-TZVPP//BP86/def2-SVP level of theory and are in part illustrated in Figure 30.

amidophenolate representatives can be assumed. From a synthetic point of view, a fluorinated compound was preferred as it is more stable under highly electrophilic conditions, given the inertness of  $C(sp^2)-F$  bonds in comparison to the heavier halogens. Thus, it was set out to synthesize nonafluoro-N-phenyl-*ortho*-aminophenol ( $\mathbf{am}^F\mathbf{ph}^F\mathbf{H}_2$ ) as corresponding precursor for the projected silane (Figure 30,  $X = F$ ,  $R = -C_6F_5$ , marked with an arrow), combining electron-deficiency and robustness.

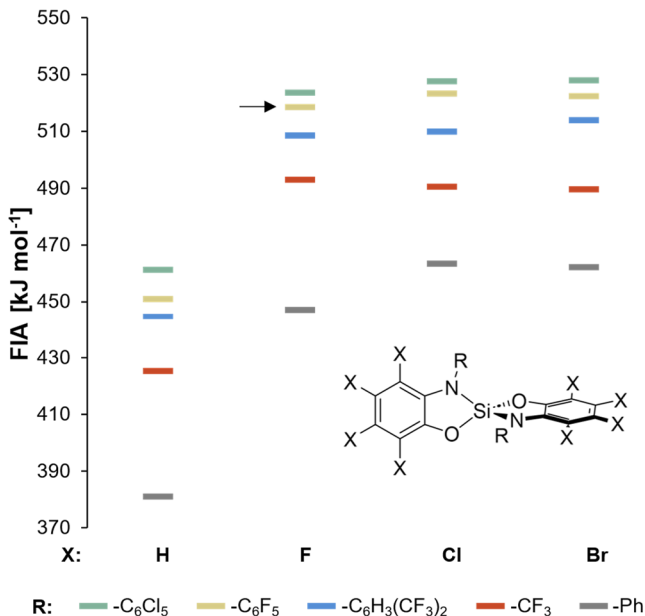


Figure 30. Illustration of *in-silico* screened FIA data (PW6B95-D3(BJ)/def2-TZVPP//BP86/def2-SVP level of theory) for various bis(*ortho*-amidophenolato)silane derivatives.<sup>11</sup>

In consideration of the rich nucleophilic addition chemistry of fluorinated arenes, a first attempt was taken utilizing hexafluorobenzene ( $C_6F_6$ ). *In situ* lithiated ethanolamine was considered as an intramolecular handle that would allow specific *ortho*-substitution (Figure 31a). Heating one equivalent ethanolamine with two equivalents hexafluorobenzene and three equivalents of LiHMDS as weakly nucleophilic base in THF indeed resulted in the formation of the alkyl ether protected intermediate ( $\mathbf{am}^F\mathbf{ph}^F\mathbf{C}_2\mathbf{H}_4$ ). However, the compound could only be isolated in 17%

yield. A change in concentration or equivalents did not result in significant yield enhancement. Still, subsequent conversion with *in situ* generated  $\text{AlI}_3$  resulted in the formation of  $\text{am}^{\text{F}}\text{ph}^{\text{F}}\text{H}_2$ , as judged by GCMS monitoring (Figure 31b). In spite of the poor efficiency and the low obtained quantities, the results were encouraging to modify the protocols to result an overall higher yielding synthesis. As an alternative, a two-step route was probed. Literature-known bis(perfluorophenyl)amine ( $\text{HN}(\text{C}_6\text{F}_5)_2$ ) served as an intermediate and could be readily synthesized on a multi-gram scale in high yields (Figure 31c).<sup>305</sup> From here, the next step involved lithiation followed by conversion with propylene oxide, yielding the benzoxazine motif ( $\text{am}^{\text{F}}\text{ph}^{\text{F}}\text{C}_3\text{H}_6$ ) in 80% yield (Figure 31d). Ultimately, the alkylated *ortho*-amidophenolate species was converted with  $\text{AlI}_3$  at elevated temperatures in *n*-hexane or toluene, to obtain the ether-cleaved *ortho*-aminophenol  $\text{am}^{\text{F}}\text{ph}^{\text{F}}\text{H}_2$  (Figure 31e, > 5 g scale).

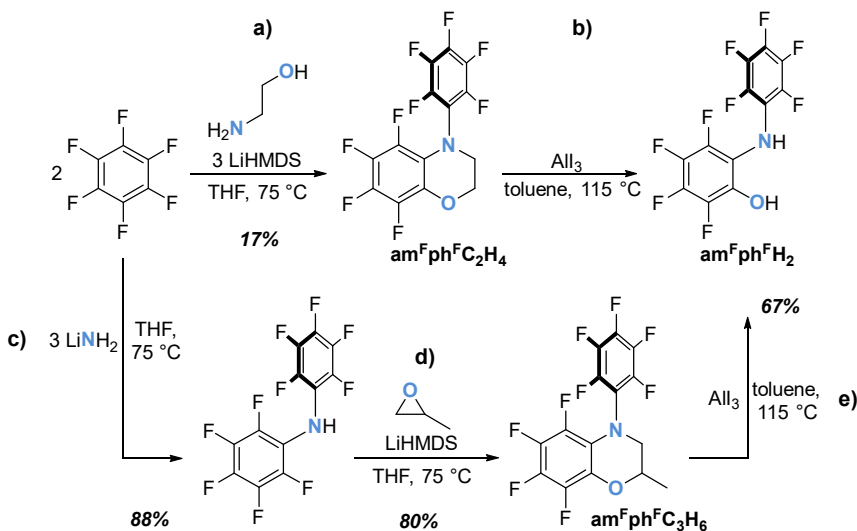


Figure 31. a-e) Schematic depiction of the approached synthetic routes for nonafluoro-N-phenyl-*ortho*-aminophenol ( $\text{am}^{\text{F}}\text{ph}^{\text{F}}\text{H}_2$ ).

Subsequently, the synthesis of the silane species was approached. A sharp contrast to the modular synthesis of bis(catecholato)silanes was found, as a reaction with  $\text{HSiCl}_3$  or  $\text{SiCl}_4$  in acetonitrile was not apparent at rt, and even at elevated temperatures

tremendously slowed. The halosilane remained largely unconverted even after several days at elevated temperatures. Application of other halogenated precursors  $\text{SiBr}_4$  and  $\text{SiI}_4$  could not tackle the slowed reactivity. Thus, employment of bases was approached next. Whereas catechols and halo-/alkoxysilanes were found to form *tris*(catecholato)silicates under basic conditions,<sup>199,200,229,252</sup> a representative of a bis(*ortho*-amidophenolato)silane could be synthesized in the presence of amines.<sup>231</sup> The ligand was reacted with  $\text{SiX}_4$  ( $X = \text{Cl}, \text{Br}, \text{I}$ ) in benzene using stoichiometric amounts of  $\text{NEt}_3$  or DBU for deprotonation. The compounds readily reacted, resulting in the respective penta-coordinated halo-silicates as indicated by  $^{29}\text{Si}$  NMR spectroscopy. However, preliminary methods for halide-abstraction from the silicates involving common alkali salts were found unsuccessful. Stronger bases were not considered, as upon lithiation of the ligand partial decomposition into a putative perfluorinated phenoxazine was observed.

Another strategy involved the commercially available silane precursor  $\text{HSi}(\text{NMe}_2)_3$  bearing basic amido substituents. A fast conversion with the acidic  $\text{am}^{\text{F}}\text{ph}^{\text{F}}\text{H}_2$  ligand resulted in the formation of the dimethylamine adduct **2**-( $\text{HNMe}_2$ ) at rt (Figure 32a). Of note, similar reactivity using  $\text{Si}(\text{OEt})_4$  could not be observed, suggesting an instability of **2** against alcohols.<sup>o</sup> Exploration of reactivities or catalysis appeared futile as the amine coordinates strongly and does not fulfill a labile stabilization role as sulfolane or acetonitrile (cmp. section 3.2).

For the synthesis of a more reactive species,  $\text{HNTf}_2$  was added to a solution of **2**-( $\text{HNMe}_2$ ) in  $\text{C}_6\text{D}_6$ , in an aim to protonate the amine. After heating the mixture to 80 °C, the formation of a varied silicon species was observed in the  $^{29}\text{Si}$  NMR spectrum. Evaporation of the solvent *in vacuo* and subsequent extraction with *n*-pentane allowed the isolation of **2**, as apparent from NMR spectroscopy. A  $^{29}\text{Si}$  NMR resonance of  $-40.6$  ppm pledged for the absence of donors and a (distorted) tetrahedral coordination sphere, as gauged through comparison with related structures.<sup>231</sup> Moreover, the shift is in excellent agreement with the computed value of  $-41.6$  ppm.<sup>p</sup> Elemental analysis and mass spectrometry further substantiated the

---

<sup>o</sup> This was later verified, as formation of  $\text{Si}(\text{OMe})_4$  and  $\text{am}^{\text{F}}\text{ph}^{\text{F}}\text{H}_2$  was observed when **2** was dissolved in MeOH.

<sup>p</sup> Details for the computation of NMR resonances are provided in section 5.3. The resonances are listed in Table A9.

formation of **2**. Ultimately, single crystals grown from a saturated  $\text{CH}_2\text{Cl}_2$  solution confirmed the distorted tetrahedral nature of the compound (Figure 32b). When carried out on larger scales, the formation of the target compound was observed in significantly reduced yield and purity. Variation of the solvent to dichloromethane, toluene, or *n*-heptane did also not resolve the encountered shortcomings. As possible reason for the hindered reactivity, weak adduct formation with the  $\text{NTf}_2^-$  anion was considered, which in consequence would mean adduct formation at ambient conditions but separated species at elevated temperatures – which were found necessary for the formation of **2**. Therefore, the reaction conditions were modified and a solution of  $\text{HNTf}_2$  was added dropwise to a toluene solution of **2**-( $\text{HNMe}_2$ ) at  $85^\circ\text{C}$ . After complete reaction the mixture was cautiously concentrated at elevated temperatures and extracted with *n*-pentane or *n*-hexane. This procedure allowed the reliable synthesis of **2** on gram-scale in good yields (77%). Strikingly, the compound was found excellently soluble in common organic non-donor solvents.

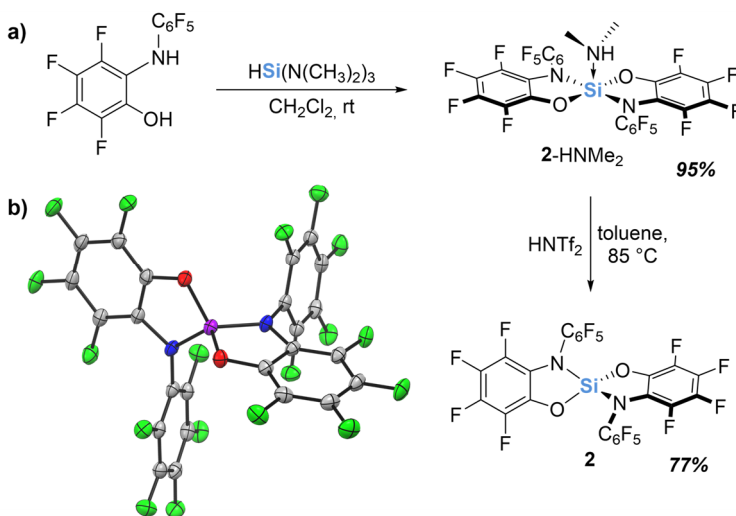


Figure 32. a) Reaction scheme for the synthesis of bis(nonafluoro-N-phenyl-ortho-amidophenolato)silane (**2**) via **2**-( $\text{HNMe}_2$ ). b) Molecular structure of **2** (shown at 50% probability, co-crystallized  $\text{CH}_2\text{Cl}_2$  molecule was omitted for clarity; selected bond lengths and angles:  $\text{Si}-\text{O}/\text{Si}-\text{O}' = 1.6465(13)$  Å,  $\text{Si}-\text{N} = 1.7138(15)$  Å,  $\text{Si}-\text{N}' = 1.7138(16)$  Å,  $\text{O}-\text{Si}-\text{O} = 118.44(10)^\circ$ ,  $\text{N}-\text{Si}-\text{N} = 119.73(11)^\circ$ ).

Encouraged by these prerequisites, the Lewis acidity was assessed in theory and experiment. The calculation of the FIA ( $494 \text{ kJ mol}^{-1}$ )<sup>q</sup> suggested a Lewis acidity in a range between monomeric **1**<sup>Cl</sup> and **1**<sup>F</sup>. For the present species, this value reflects the reactivity more viably as it comes without an effective dampening through oligomerization processes. Given the harder nature of silanes, the HIA (449)<sup>q</sup> is inherently less pronounced as the FIA but still renders **2** as strong hydride acceptor. Next, the *effective* Lewis acidity was approached *via* the Gutmann-Beckett method. The probe signal was shifted by  $\Delta^{31}\text{P} = 33 \text{ ppm}$ , firmly within the bounds of the catecholato derivatives.<sup>178</sup> A quantitative evaluation was judged to be not expedient due to the different steric and electronic composition.<sup>38</sup> When **2** was converted with trityl chloride quantitative formation toward the trityl salt  $[\text{CPh}_3][\text{Cl-2}]$  was indicated by NMR spectroscopy. Remarkably, the use of **2** in complete absence of donors allowed the isolation of the intensely yellow colored solid  $[\text{CPh}_3][\text{Cl-2}]$ . This finding contrasts the behavior of the bis(catecholato)silanes, for which evaporation of the solvent caused the reverse reaction, ultimately resulting in the respective weak donor adducts and trityl chloride.<sup>178</sup> The calculated FIA suggested a comparable value to  $\text{SbF}_5$  within the borders of *chemical accuracy*, thus an experimental hint on Lewis superacidity was approached. Reacting **2** with  $[\text{PPh}_4][\text{SbF}_6]$  in  $\text{CD}_2\text{Cl}_2$  led to an immediate reaction and a deep blue coloration of the sample within seconds. Direct NMR spectroscopic analysis revealed multiple  $^{19}\text{F}$  signals, likely associated with the strong oxidation potential of  $\text{SbF}_5$  paired with the redox-active nature of the aminophenol, or possible ligand scrambling.<sup>6</sup> Even though a defined reaction product could not be monitored, the reactivity clearly suggests an initial fluoride abstraction, followed by vivid follow-up reactions with  $\text{SbF}_5$ . **2** can thus be classified a Lewis superacid.

In light of the confirmedly high fluorophilicity, the cleavage of inert C–F bonds (approx.  $D_e = 500\text{--}550 \text{ kJ mol}^{-1}$ )<sup>306</sup> was probed next. In conjunction with suitable Lewis bases, the cleavage of a C–F bond in fluorobenzene (PhF) and  $\alpha,\alpha,\alpha$ -trifluorotoluene (PhCF<sub>3</sub>) was attempted. The N-heterocyclic carbene (NHC) 1,3-di-*tert*-butyl-1,3-imidazol-2-ylidene (NHC<sup>tBu</sup>) was added to a solution of **2** and PhF in benzene and the mixture heated to  $120 \text{ }^\circ\text{C}$  for 18 h.  $^{19}\text{F}$  NMR spectroscopy indicated the formation of the fluoridosilicate  $[\text{F-2}]^-$ . Poor quality crystals formed upon gas

---

<sup>q</sup> DLPNO-CCSD(T)/aug-cc-pVQZ//PBE0-D3(BJ)/def2-TZVPP level of theory.

diffusion of *n*-pentane into the reaction mixture and suggested the formation of [NHC<sup>Bu</sup>H][F-**2**]. Even though this reactivity more likely represents an aryne formation initiated by deprotonation rather than a cooperative bond activation, it underlines the high potential of **2** as fluoride acceptor. Exposition of PhCF<sub>3</sub> to a combination of **2** and the sterically demanding amine 1,2,2,6,6-pentamethylpiperidine (pmp) resulted in the formation of the iminium salt [tmp=CH<sub>2</sub>][F-**2**] already at 40 °C (Figure 33b) as confirmed by NMR experiments and scXRD (cmp. section 7.6). Notably, this reactivity supports an initial (base-assisted) fluoride abstraction of **2** from PhCF<sub>3</sub>. The iminium formation can then be rationalized by hydride abstraction of the intermediately generated pmp-stabilized [PhCF<sub>2</sub>]<sup>+</sup> cation. While remarkable studies demonstrated that silylium species are able to activate and (catalytically) functionalize CF bonds,<sup>270,271,307-311</sup> the here reported synthesis of an anionic fluorido-silicate from an organic fluoride source still can be considered a novelty.

To also probe the oxophilicity of **2**, its reactivity in a cooperative CO<sub>2</sub> fixation was approached – a previously common reactivity for cationic silicon species.<sup>134,312-315</sup> In analogy to the reactivity of **1**<sup>Cl</sup>,<sup>254</sup> the formation of [tmpH<sub>2</sub>][tmpCO<sub>2</sub>-**2**] was observed when a solution of **2** and two equivalents 2,2,6,6-tetramethylpiperidine (tmpH) in CD<sub>2</sub>Cl<sub>2</sub> was exposed to 1 atm CO<sub>2</sub> (Figure 33c). The detected <sup>29</sup>Si resonance (–148.6 ppm) is not only in excellent agreement with the one for [tmpCO<sub>2</sub>-**1**<sup>Cl</sup>]<sup>–</sup> (–145.4 ppm)<sup>254</sup> and the computed value (–152.3 ppm) but also advocates for a hexacoordinated silicon center. It is worth mentioning that previously no indication for hexacoordination in adducts of **2** was found even when treated with excess halide anions. In the present case, the in comparison to silicon catecholates reduced tendency for hexacoordination is likely overcome by a strong oxo-affinity of **2** in combination with a small bite angle of the formed carbamate. Moreover, a dative interaction with the weak nitrogen donor benzyl azide was indicated by NMR spectroscopy. Interestingly, the final reaction product was found to be the benzylimine adduct (**2**-HN=CHPh, see section 7.6), which formed at rt without explicit irradiation, leaving the possibility for a Lewis acid induced nitrene formation.

Next, even though silanes are typically referred to as hard Lewis acids, the high HIA of the silane was encouraging to synthesize the corresponding hydridosilicate [H-**2**]<sup>–</sup> (Figure 33d). Indeed, upon conversion of LiAlH<sub>4</sub> with **2** in THF-*d*<sub>8</sub> the formation of a new species was apparent. A <sup>1</sup>H NMR signal at 5.76 ppm with distinct satellites

( $^1J_{H-Si} = 319$  Hz), a resonance at  $-98.2$  ppm in the  $^{29}\text{Si}$  NMR DEPT experiment along with a detected cross-interaction between the shifts in the  $^1\text{H}$ - $^{29}\text{Si}$ -HMBC NMR spectrum underlined the formation of a silicon bound hydride. Furthermore, the computed value for the  $^{29}\text{Si}$  resonance ( $-98.2$  ppm) is in excellent agreement with the experimental data. Colorless crystals suitable for scXRD could be grown after complexation of the cation with 12-crown-4 ether (12c4), ultimately confirming the formation of  $[\text{Li}@12\text{c}4][\text{H}-2]$ .

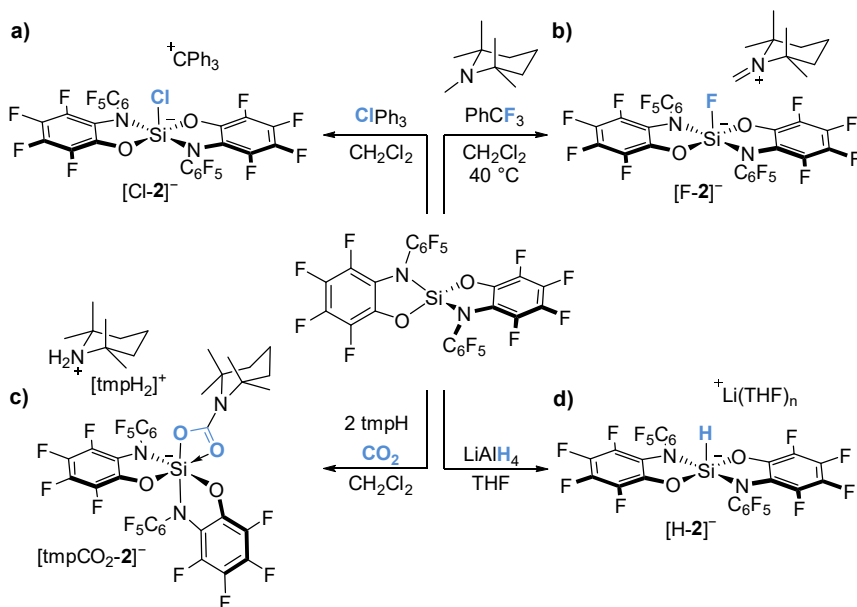


Figure 33. Experimental probing of the Lewis acidity of **2**: a) chloride abstraction from trityl chloride, b) pmp-assisted, cooperative C–F bond cleavage, c) tmpH-assisted silicon-carbamate formation by  $\text{CO}_2$  fixation, and d) synthesis of the hydrosilicate  $[\text{H}-2]^-$  from  $\text{LiAlH}_4$ .

The formation of this hydrosilicate is especially noteworthy, as for the related bis(catecholato)silanes such a motif could never be detected. The putative species  $[\text{H}-1^{\text{H}}]^-$  served as powerful reductant at low temperatures, but isolation attempts failed due to instability at rt.<sup>218</sup> For **1**<sup>Cl</sup>, decomposition into the stable weakly coordinating anion (WCA)  $[\text{Si}(\text{cat}^{\text{Cl}})_3]^{2-}$  and gaseous  $\text{SiH}_4$  was indicated upon addition of hydride donors. More generally, the analytically pure isolation of a

hypervalent silicon hydride was only reported in 1987,<sup>316</sup> and examples up to this day are still rather sparse in comparison to other main-group hydrides.

On the whole, this chapter reports a robust protocol for the gram-scale synthesis of a *second-generation*, silicon Lewis superacid that is robust, monomeric, donor-free, and readily soluble in common organic solvents. Its reactivity was gauged by theory and typical experiments, verifying a high potential. Additionally, an isolable hydrido-silicate promises to unlock reactivity previously unknown for bis(catecholato)silicates. In brief, the prerequisites for a neutral silane to activate small molecules are ideally portrayed in **2**. Accordingly, the following chapters will deal with corresponding investigations.

### 3.3.2 Direct Synthesis of a Hydridosilicate from Dihydrogen

Endowed with **2** as a readily reactive, Lewis superacidic silane, the activation of less polarizable small molecules was approached. Even though considerable progress on neutral silicon FLPs was reported, the pioneering heterolytic H<sub>2</sub> activation could hardly be mimicked. Given the achieved prerequisites, a cooperative H<sub>2</sub> cleavage utilizing **2** was envisioned which ultimately would allow the direct synthesis of a hydridosilicate from molecular dihydrogen for the first time. For an efficient strategy, an initial consideration of previously reported reactivities of silanes in this field was examined. Remarkably, MITZEL's geminal FLP (F<sub>5</sub>C<sub>2</sub>)<sub>3</sub>-Si-P<sup>t</sup>Bu<sub>2</sub> was able to scramble H<sub>2</sub> and D<sub>2</sub> to HD as only report in this regard (Figure 34a).<sup>313</sup> Yet, the endergonic nature of the reaction prevented an observation of the zwitterionic cleavage product. Therefore, the examination was extended to species valence-isoelectronic to silanes. The heavier analogue (F<sub>5</sub>C<sub>2</sub>)<sub>3</sub>-Sn-P<sup>t</sup>Bu<sub>2</sub> reacted with H<sub>2</sub> but isolation of the zwitterionic product was prevented by reductive elimination (Figure 34b).<sup>317</sup> The respective germane was found inactive toward H<sub>2</sub>.<sup>318</sup> Outstanding progress was reported by ASHLEY and coworkers on FLPs incorporating tin Lewis acids R<sub>3</sub>SnX (R = <sup>i</sup>Pr, Bn; X = OTf<sup>-</sup>/NTf<sub>2</sub><sup>-</sup>) (Figure 34c).<sup>319-321</sup> Successful FLP type H<sub>2</sub> activation resulted in catalytic applications, the findings are however of limited use for the present intend, as observed stannane reaction products (R<sub>3</sub>SnH), the dependency of X to be a good leaving group, and computationally derived mechanistic insights pledge for a stannylum characteristic reactivity.<sup>322</sup> Electrophilic phosphonium cations (EPCs) rank among the strongest Lewis acids known and are isoelectronic to neutral silanes. Surprisingly, even though an FLP incorporating the prominent EPC [(F<sub>5</sub>C<sub>6</sub>)<sub>3</sub>PF][B(C<sub>6</sub>F<sub>5</sub>)<sub>4</sub>] was shown to scramble H<sub>2</sub>/D<sub>2</sub>, and served as potent hydrogenation catalyst, the corresponding hydridophosphorane was never observed (Figure 34d).<sup>323</sup> In line, *in silico* predicted reductive elimination of HF challenged the stability of such an intermediate.<sup>324</sup> Similarly, a diphosphonium species was found reduced when exposed to H<sub>2</sub> in the presence of P<sup>t</sup>Bu<sub>3</sub>.<sup>325</sup> Summed up, a notable assortment of potent reactivities involving tetracoordinated main group Lewis acids is reported. Even though those results could not demonstrate the here aimed reactivity for the isolation of a primary reaction product, they were encouraging as the kinetic feasibility for a tetrel-modulated dihydrogen cleavage is strongly supported.

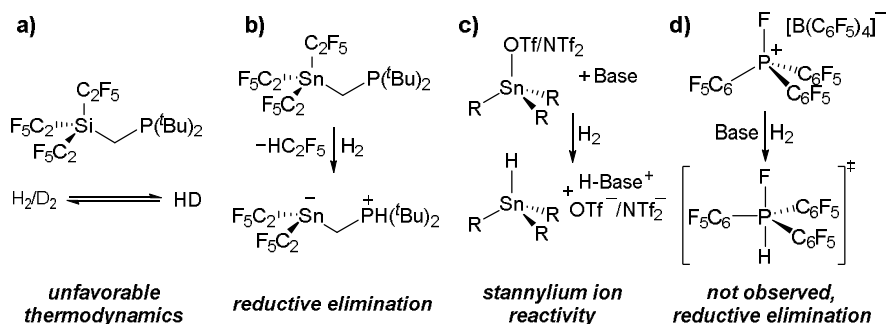


Figure 34. FLP-type  $\text{H}_2$  activation with tetrahedral Lewis acids. a) Geminal silane FLP with limited hydride ion affinity. b) Reductive elimination from a putative hydride intermediate in a geminal tin(IV) FLP. c) Tin triflates/triflimides reacting as masked stannylum ions. d) Putative, unobserved phosphorane from a hydrogenation-active P(V) based FLP.

Next, suitable Lewis bases for a cooperative activation were contemplated. To account for a suitably exergonic reaction profile, the respective Lewis bases should exhibit sufficient Brønsted basicity and steric demand. In this context, tri-*tert*-butylphosphine ( $\text{P}^t\text{Bu}_3$ ),<sup>103</sup> 1,3-di-*tert*-butyl-1,3-imidazol-2-ylidene ( $\text{NHC}^t\text{Bu}$ ),<sup>108,109</sup> 2,6-di-*tert*-butyl-pyridine (DTBP),<sup>326</sup> HÜNIG's base N,N-di-*iso*-propyl-N-ethylamine (DIPEA),<sup>112</sup> 2,2,6,6-tetramethylpiperidine (tmpH),<sup>111,112</sup> and 1,2,2,6,6-pentamethylpiperidine (pmp)<sup>111</sup> have shown to be promising candidates in borane or alane FLPs. After support through initial computations of the reaction Gibbs free energies (Table 5),<sup>r</sup> the candidates were probed in respective experiments.

Table 5. Computationally derived thermodynamic data for  $\text{H}_2$  cleavage of **2** with different Lewis bases; [a] for Lewis bases that form endergonic adducts thermodynamic data is referenced against the unbound compounds, [b] for Lewis bases with favorable adduct formation, against the adduct.<sup>r</sup>

<b>2</b> $\xrightleftharpoons{\text{Base}}$ <b>2-Base</b>		Base	$\Delta G$ [kJ mol <sup>-1</sup> ]	Base	$\Delta G$ [kJ mol <sup>-1</sup> ]
		$\text{P}^t\text{Bu}_3$ [b]	-19	DTBP [a]	-8
		$\text{NHC}^t\text{Bu}$ [b]	-86	tmp [b]	-5
		DIPEA [b]	-37	pmp [a]	-68

<sup>r</sup> DLPNO-CCSD(T)/def2-TZVPP+SMD( $\text{CH}_2\text{Cl}_2$ )/PBE0-D3(BJ)/def2-TZVPP level of theory.

To start with,  $P^tBu_3$  as ‘*typical*’ Lewis base for intermolecular FLPs was applied. Adduct formation with **2** in dichloromethane was observed in line with the calculated Gibbs free energy (Table 5). Exposing the solution to 1 atm of  $H_2$  did not result in an activation product when heated at 65 °C for 7 d. Instead, a slow side reactivity was noticed even in the absence of  $H_2$ . While not fully clarified yet, this might correspond to a nucleophilic aromatic substitution ( $S_NAr$ ), for example also observed for the FLP  $P^tBu_3/B(C_6F_5)_3$ .<sup>327</sup> As the activation was found unsuccessful, other phosphorus-bases like triarylphosphines were not attempted, given the lowered basicity in comparison to trialkylphosphines.<sup>328</sup>

Therefore, the sterically demanding  $NHC^{tBu}$  was probed next. A mixture of  $NHC^{tBu}$  with **2** in dichloromethane resulted in adduct formation as predicted by computations. However, the adduct was found to isomerize in solution without any other influence. In fact, NMR spectroscopy indicated rearrangement of the dative interaction into an *abnormal* NHC adduct (**2-<sup>a</sup>NHC<sup>tBu</sup>**, Figure 35a), in similarity to previous reports.<sup>108,109,329</sup> Consequently, dihydrogen cleavage with 1 atm  $H_2$  was found unsuccessful at ambient conditions. The analogous problem in conjunction with  $B(C_6F_5)_3$  could be tackled by application of an improved protocol, that requires cautious preparation of a cooled mixture including the unreacted Lewis pair, followed by exposition to  $H_2$ . This way, the clean formation of  $[NHC^{tBu}H][HB(C_6F_5)_3]$  (97%) was achieved before the rearrangement took place.<sup>108</sup> However, following the protocol did not allow the observation of targeted reaction products in the present case. As alternative, an abnormal adduct formation was prevented when using the 4,5-methylated  $NHC^{Dipp,Me}$  (1,3-di-*tert*-butyl-4,5-*di*-methyl-1,3-imidazol-2-ylidene). The formed adduct did not show any reactivity when exposed to  $H_2$  and was found exceptionally stable (scXRD data in section 7.6).

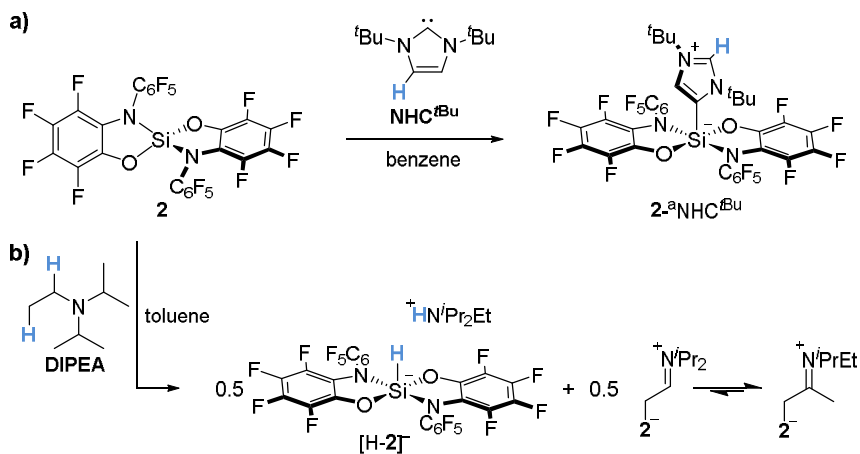


Figure 35. a) Formation of an *abnormal* adduct from **2** and NHC<sup>tBu</sup>. b) Dehydrogenative enamine formation from DIPEA by **2**.

Subsequently, a row of sterically shielded nitrogen bases was tested. A mixture of DTBP and **2** in CD<sub>2</sub>Cl<sub>2</sub> was found inactive against H<sub>2</sub> under various conditions, even though no adduct formation occurred. Similar behavior was previously attributed to an excessive frustration level, which prevents sufficient polarization and the spanning of an active cavity between the reactive centers.<sup>330</sup> As an alternative, more basic and less bulky DIPEA was probed, in expectation of an increased polarization in the active cavity. Upon addition of the amine to the Lewis acid the targeted anion [H-2]<sup>-</sup> could indeed be observed in solution, yet even in the absence of H<sub>2</sub>. Spontaneous dehydrogenative enamine formation occurred, leading to the enamine adduct <sup>t</sup>Pr<sub>2</sub>N=C<sub>2</sub>H<sub>3</sub>-**2** and the formal H<sub>2</sub> cleavage product [HN<sup>Pr</sup><sub>2</sub>Et][H-2]<sup>-</sup> (Figure 35b), as supported by theory and experiment (cmp. section 5.2.8.5). Heating the mixture in a dihydrogen atmosphere did not account for a higher proportion of the activation product. Still, the observation of the targeted salt was encouraging to attempt experiments using amines without alpha- and beta-hydrogens to prevent enamine formation. 2,2,6,6-Tetramethylpiperidine (tmpH) formed an adduct with **2** that was found inactive against H<sub>2</sub> (1 atm), even at temperatures up to 65 °C and a reaction time of 7 d. In logical consequence, the H<sub>2</sub> activation was next attempted with the trisubstituted amine 1,2,2,6,6-pentamethylpiperidine (pmp). NMR spectroscopy confirmed the absence of a dative adduct with nearly unchanged resonances in

comparison to the separated compound. Broadening of the signals suggested a non-covalent interaction common for an FLP encounter complex – the decisive intermediate in FLP type activations.<sup>331</sup> Additionally, the calculated Gibbs free energy was encouraging (Table 5), as a DFT study indicated lowered barriers for FLPs with a more exergonic reaction profile, according to the *BELL–EVANS–POLANYI* principle.<sup>332</sup> Besides this stimulating observations, the formation of the hydridosilicate [H-2]<sup>-</sup> could not be detected when exposing equimolar amounts of pmp and the silane in CD<sub>2</sub>Cl<sub>2</sub> to 1 atm H<sub>2</sub> for 7 d at rt, 40 °C, or 65 °C. In sight of no observed side reactivity, kinetic effects were assumed for the puzzling inactivity and consequently, a harsher approach was attempted. The solvent was changed to *ortho*-dichlorobenzene (*o*DCB) and the mixture heated to 115 °C under otherwise identical conditions. After 2 d, the mixture was cooled to rt and analyzed *via* NMR spectroscopy. Strikingly, 47% of the [pmpH]<sup>+</sup> cation had formed in conjunction with a distinctive hydride signal that showed characteristic <sup>29</sup>Si coupling (<sup>1</sup>J<sub>SiH</sub> = 313 Hz). Further heating marginally increased the proportion of product leading to 64% after heating for a total of 8 d (Figure 36a). The compound was separated from unreacted substrate and comprehensively analyzed. NMR characterization was found consistent, yet minor unassigned <sup>19</sup>F NMR signals pointed to partial side reactivity at the elevated temperatures. Thus, other possibilities for the tuning of the reaction kinetics were considered. Strikingly, a concentration enhancement of the Lewis base allowed the observation of reactivity already at lower temperatures. Heating of a CD<sub>2</sub>Cl<sub>2</sub> solution containing **2** and a tenfold excess pmp in a H<sub>2</sub> atmosphere (1 atm) to 65 °C resulted in the formation of 73% of the cleavage product after 7 d (Figure 36b). Crystals grown from the reaction mixture ultimately confirmed the formation of the cleavage product [pmpH][H-2] (Figure 36e). While the reaction was still rather slow in terms of FLP reactivity, the findings demonstrate a distinct concentration dependency causing a significant decrease of the lower temperature limit. Exploiting this effect even further, 100 eq. pmp were used in an otherwise identical attempt. This way, albeit slow, H<sub>2</sub> activation could be observed already at rt (13% after 20 h). As compromise between a reasonable reaction rate and mild conditions, the temperature was set to 40 °C, allowing the isolation of 71% [pmpH][H-2] in high purity after 7 d (Figure 36c). A similar accelerating effect was observed when the H<sub>2</sub> pressure was increased to 50 atm. As a result, a reasonable conversion at 60 °C was achieved when applying equimolar amounts of Lewis acid and base (Figure 36d).

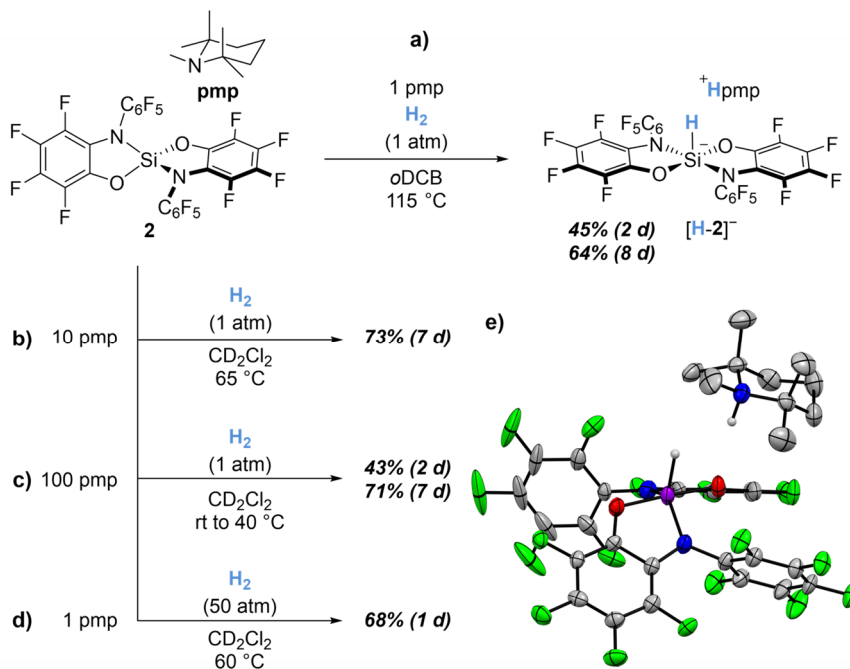


Figure 36. a)-d) Cooperative dihydrogen cleavage by **2** and pmp under various conditions. e) scXRD derived structure of the activation product [pmpH][H-2] (for details see sections 5.1.2 and 7.6, shown at 50% probability, carbon bound hydrogens omitted for clarity).

After the experiments revealed the targeted reactivity, the reaction energy profile was completed. Supporting computations revealed an accessible transition state with a barrier of  $\Delta G^\ddagger = 79 \text{ kJ mol}^{-1}$  (energy profile displayed in Figure A1).<sup>s</sup> Even when considering possible deviations through the accuracy of the computations or conformational effects, the encountered low barrier is in sharp discrepancy to the slow reactivity, especially in comparison to previously described FLP reactivities. To probe the mechanism, the origin of the proton and hydride was verified in an experiment utilizing deuterium gas and tenfold excess pmp as optimized reaction conditions. While this experiment likewise confirmed the cleavage of the heavier isotope D<sub>2</sub>, the main proportion of the deuteride was found at the pmp methyl group. This observation can be assigned to the – compared to the hydrogen cleavage – fast hydride

<sup>s</sup> DLPNO-CCSD(T)/def2-TZVPP+SMD(CH<sub>2</sub>Cl<sub>2</sub>)/PBE0-D3(BJ)/def2-TZVPP level of theory.

exchange between the silicate and pmp (in tenfold excess), likely catalyzed by **2** (Figure 37a). Still, the unexpected deuteration of the methyl group mandated a closer examination of the active species and a possible role of the iminium ion ( $[\text{tmp}=\text{CH}_2]^+$ ). Computations for a cooperative  $\text{H}_2$  activation between an intermediately formed iminium ion ( $[\text{tmp}=\text{CH}_2]^+$ ) and pmp revealed a higher kinetic barrier ( $\Delta G^\ddagger = 126 \text{ kJ mol}^{-1}$ , Figure A1) than for the FLP **2**/pmp. Still, the computed energy did not fully preclude this pathway. Thus, a control experiment was conducted. The ion pair  $[\text{tmp}=\text{CH}_2][\text{B}(\text{C}_6\text{F}_5)_4]$  was prepared and exposed in conjunction with one equivalent pmp to 1 atm  $\text{H}_2$ . NMR monitoring revealed a virtually unchanged mixture even after 5 d at 65 °C, disclosing that the iminium ion does not serve as primary active entity under the applied reaction conditions (Figure 37b).

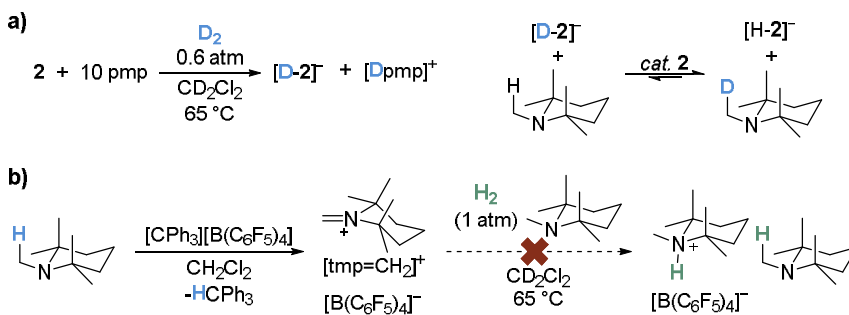


Figure 37. Mechanistic experiments for the encountered formation of  $[\text{pmpH}][\text{H-2}]$ . a)  $\text{D}_2$  cleavage by **2** and pmp and subsequent isomerization with  $\alpha$ -hydrogens in pmp. b) Synthesis of  $[\text{tmp}=\text{CH}_2][\text{B}(\text{C}_6\text{F}_5)_4]$  and failed attempt for subsequent  $\text{H}_2$  cleavage with pmp.

After the mechanistic probing experiments clearly supported the involvement of **2**, a deeper understanding of this puzzling reactivity was approached. Evidently, effects beyond the sole energetic barrier, like concentration or preorganization, which are not reflected in the static computations of an energy profile, affect the reaction outcome. To account for such effects and allow a more holistic interpretation of the observed reactivity, a profound analysis of FLP interactions was found necessary and is described in the following chapter.

Overall, the important advantages that led to the development of **2** in the first place (cmp. section 3.3.1) indeed were fruitful and enabled the first synthesis of a hydrosilicate from dihydrogen. The encountered difficulties regarding the narrow

Lewis base tolerance (side reactivity, high required strength, and steric demand) and the slow proceeding that called for extraordinary reaction conditions indicate why such reactivity previously was not observed for silanes and underline the uniqueness of the reported observation.

### 3.3.3 Rationalizing the FLP Activity of a Silane

As described in the previous chapter, the silicon/nitrogen frustrated Lewis pair (FLP) consisting of bis(nonafluoro-N-phenyl-*ortho*-amidophenolato)silane (**2**) and 1,2,2,6,6-pentamethylpiperidine (pmp) allowed the isolation of a primary reaction product from a tetrahedral Lewis acid in the heterolytic H<sub>2</sub> cleavage. In this intriguing, unprecedented observation, the calculated barrier stated an unexpected discrepancy to the observed slow proceeding of the reaction. Large excess of the amine Lewis base allowed rt reactivity, better matching the *chemical intuition* regarding temperature, but still walking along with unusually prolonged reaction times. The fundamental principles of kinetics and collision theory highlight the significance of concentration in determining reaction rates, which is often hardly considered due to a focus on activation energies. However, the distinct behavior of the system **2**/pmp in H<sub>2</sub> cleavage, particularly when compared to archetypal borane FLPs, was prompting to undertake a more comprehensive analysis on its nature. In this chapter, an initial, holistic consideration of effects on FLP reactivity will be given. Subsequently, an ensemble of structures for non-covalent associates between the FLPs **2**/pmp and P<sup>t</sup>Bu<sub>3</sub>/B(C<sub>6</sub>F<sub>5</sub>)<sub>3</sub> will be computationally analyzed, regarding thermodynamic stability, orbital interaction, deformation, and dispersion energy. The found effects will be discussed and mapped on the initial observation, ultimately providing a suitable qualitative explanation for the discrepancy to boranes in the H<sub>2</sub> activation as prototypical FLP reaction. To start with, literature insights on FLP mechanisms will be discussed.

The proceeding on how FLPs activate small molecules is largely dependent on the substrate, but of course also on the nature of the Lewis base and the Lewis acid. Typically, FLP reactions include the synergistic action of Lewis acid and Lewis base which create an ambiphilic reaction site<sup>114,145-147</sup> but other mechanisms, for example incorporating a single electron transfer (SET), can be operative.<sup>333,334</sup> In general, it is considered scientific consensus that the key reactive species in such reactions is represented by a van-der-Waals bound complex between Lewis acid and base, often referred to as *encounter complex*, *frustrated complex* or *pre-complex*.<sup>331</sup> For the emblematic H<sub>2</sub> activation by cooperative action of Lewis acid and base, two main interpretations on its proceeding exist. A detailed molecular orbital analysis supported simultaneous electron transfer from the  $\sigma(\text{H}_2)$  orbital to the vacant p-orbital of the

Lewis acid ( $\text{B}(\text{C}_6\text{F}_5)_3$ ) and from the Lewis base ( $\text{P}^t\text{Bu}_3$ ) to the antibonding  $\sigma^*(\text{H}_2)$  orbital (Figure 38a).<sup>105,106</sup> This is referred to as electron transfer (ET) model. An alternative mechanistic illustration, the electric field (EF) model, concludes that the most uphill step states the entrance of  $\text{H}_2$  into the electric field of the preorganized Lewis pair (Figure 38b).<sup>107</sup> Once in the electric field,  $\text{H}_2$  is cleaved in an almost barrierless manner.

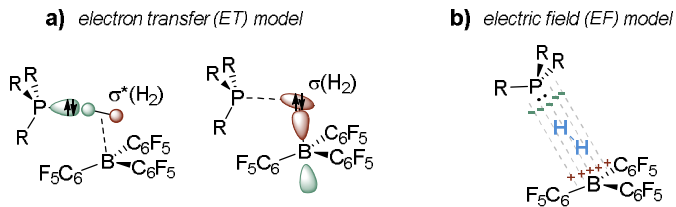


Figure 38. a-b) Schematic illustration of mechanistic interpretations on the intermolecular FLP  $\text{H}_2$  cleavage.

DFT and CI studies supported that the activation is strongly dependent on the electric field and the barrier can indeed disappear.<sup>335</sup> On the contrary, for a row of small Lewis pairs the electric field was found to be insufficiently strong for suitable polarization,<sup>336</sup> and an investigation of a set of FLP type  $\text{H}_2$  activations suggested that the main features of the cleavage process are better reflected through the electron transfer model.<sup>337</sup> While there is still some debate on the approaches, both emphasize the importance of the association between Lewis acid and Lewis base for the successful activation. Different mechanistic proceedings for early and late transition states were revealed by quantum-theoretical investigations,<sup>332,338</sup> contributing to a better understanding. Moreover, a molecular dynamics study demonstrated that they do not necessarily disagree and a combined consideration of both complements to a more holistic view.<sup>339</sup>

Through the apparent dependency on the association of the FLP, a variety of studies investigated the non-covalent interactions that drive the complex formation.<sup>107,331,340-343</sup> While NMR signals of the combined Lewis pair were often unchanged in comparison to their separated forms,<sup>103</sup> advanced techniques allowed the experimental investigation of the association.<sup>331,344-347</sup> Remarkably, even an experimental method for the determination of the concentration of the *active* encounter complex was

developed.<sup>348</sup> Theoretical analyses of the loosely bound associates were indispensable for the understanding of FLPs on a molecular level, and provided extensively valuable insights, emphasizing their reliance on secondary interactions.<sup>105,107,330,331,340-343,349-351</sup> The main contribution for their formation is represented by undirected dispersion interactions (Figure 39a, I).<sup>341</sup> Other effects contribute less to the overall stability but can affect the reactivity. In this regard, the preferred orientation in the association of the FLPs  $B(C_6F_5)_3/P^tBu_3$  and  $B(C_6F_5)_3/PMes_3$  was shown to exhibit an effect on their activity.<sup>349</sup> In the dispersion driven complexes, a higher orbital interaction (Figure 39a, II) between the reactive centers accounts for an increased proportion of the *active* conformation (Figure 39b), and consequently for a higher activity. This finding deconvolutes other previous phenomena illustratively explained with the *level of frustration*. A higher steric demand by use of 1,2,2,6,6-pentamethylpiperidine (pmp) instead of 2,2,6,6-tetramethylpiperidine led to significant rise of the lower temperature limit and a hampered activity in the cooperative  $H_2$  activation with  $B(C_6F_5)_3$ .<sup>111</sup> This is in line with the previous interpretation, as the additional substituent accounts for a lower orbital interaction between nitrogen and boron and thus effectively reduces the *active* FLP proportion. In this context, a complete inactivity was attributed to excessive frustration for the FLP  $P^tBu_3/B(Mes)_3$ .<sup>103,330</sup> Conversely, insufficient frustration leads to adduct formation by dative bonding (high orbital interaction) and accounts for quenched reactivity – representing classical adduct formation.<sup>103,111,352</sup> Along this line, the activity of a phosphorus/boron FLP was found in good correlation with a P–B distance in a range between 3.4–4.6 Å.<sup>330</sup> Of course, even when the initial geometry does not match the required prerequisites a successful activation can still be observed when an *active* formation can be energetically accessed. For instance, labile adducts enable  $H_2$  activation upon dissociation at elevated temperatures.<sup>97,98,353</sup> For a mild activation, even when exhibiting an initial *inactive* geometry, a flat potential energy surface is advantageous as the components can align without significant energetic barriers.<sup>340</sup> For this, secondary interactions between a reactive center and the substituents can be highly beneficial (Figure 39a, III). For example, attractive lone-pair- $\pi$  interactions<sup>354-356</sup> (LP- $\pi$ ) between phosphine bases and the pentafluorophenyl rings in  $B(C_6F_5)_3$  provide entropic stabilization for the corresponding FLP (Figure 39c).<sup>351</sup> In comparison, for  $BPh_3$  a much lower thermally accessible interaction volume of the FLP is reported, owed to extremely reduced LP- $\pi$  interactions. Fluorinated aryl groups are therefore

beneficial substituents beyond the sole electron withdrawing effect. Additional effects can be halogen/fluorine bonding,  $\pi$ - $\pi$  stacking, CH- $\pi$  or CH-F bonding.<sup>342</sup> Ultimately, even though boranes and alanes were shown to be virtually undeformed in associated FLPs,<sup>350</sup> deformation effects are expected to impact the reactivity of silicon FLPs (Figure 39a, IV), given the significant structural reorganization silanes undergo upon adduct formation.<sup>185,186</sup>

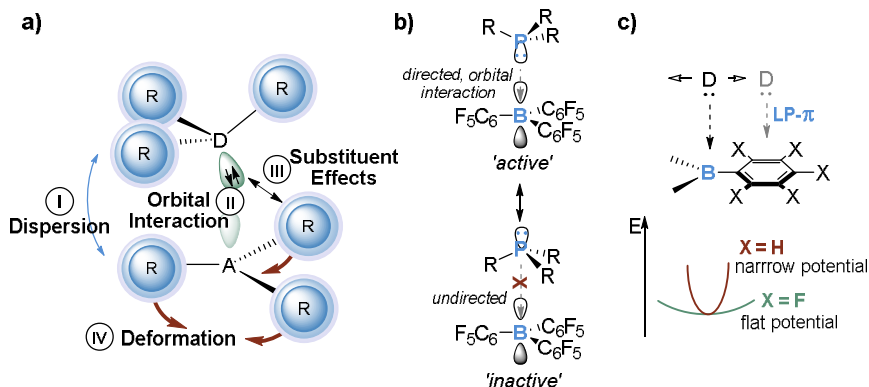


Figure 39. Schematic illustration of a) selected non-covalent interactions between Lewis pairs, b) the influence of conformation and orbital interaction for the activity of borane/phosphorus FLPs, and c) the entropic stabilization provided through a secondary lone-pair  $\pi$  (LP- $\pi$ ) interaction between a donor (D) and an aryl-substituent in B(C<sub>6</sub>F<sub>5</sub>)<sub>3</sub>/BPh<sub>3</sub>.

Guided by these insights, it was attempted to investigate such effects in the present FLP system. The significant exergonic profile for H<sub>2</sub> activation with both FLPs suggested a structural proximity of the Lewis pair assemblies and the respective transition states according to *HAMMOND's postulate*.<sup>332</sup> Thus, an ensemble of corresponding non-covalent interaction (NCI) associates was investigated computationally. The structures were optimized and thermodynamics computed.<sup>†</sup> Derivation of inter-fragment dispersions (HFLD method),<sup>357</sup> orbital interactions (ETS-NOCV),<sup>358</sup> and the deformation energies of the fragments completed the data. A detailed description of the workflow is described in section 5.3.4. This protocol was subjected to 2/pmp, resulting in 1390 structures and comparatively, to

<sup>†</sup> PW6B95-D4/def2-TZVPP+SMD(CH<sub>2</sub>Cl<sub>2</sub>)/r<sup>2</sup>SCAN-3c+CPCM(CH<sub>2</sub>Cl<sub>2</sub>) level of theory.

$P^tBu_3/B(C_6F_5)_3$  as typical intermolecular FLP, resulting in an ensemble of 695 structures.

Consistent with the previously described studies, all structures in both FLPs show stabilization by inter-fragment dispersion, with energies ranging from  $-47.2$  to  $-18.9$   $\text{kJ mol}^{-1}$  for  $P^tBu_3/B(C_6F_5)_3$  and from  $-53.3$  to  $-24.1$   $\text{kJ mol}^{-1}$  for **2**/pmp. Further, in comparison to the respective separated pairs all NCI associates are overall endergonic. As expected, orbital interactions are weakly pronounced and vary from  $-16.4$  to  $-5.7$   $\text{kJ mol}^{-1}$  for  $P^tBu_3/B(C_6F_5)_3$  and from  $-21.9$  to  $-6.2$   $\text{kJ mol}^{-1}$  for **2**/pmp. A clear discrepancy is observed for the deformation of the fragments. The silane fragment is deformed by up to  $22.2$   $\text{kJ mol}^{-1}$ , whereas  $B(C_6F_5)_3$  is for most structures virtually unaffected and reaches a maximum deformation of  $7.2$   $\text{kJ mol}^{-1}$ . To allow a better interpretation, the orbital energies, Gibbs free energies, and deformation energies were plotted three-dimensionally (Figure 40).

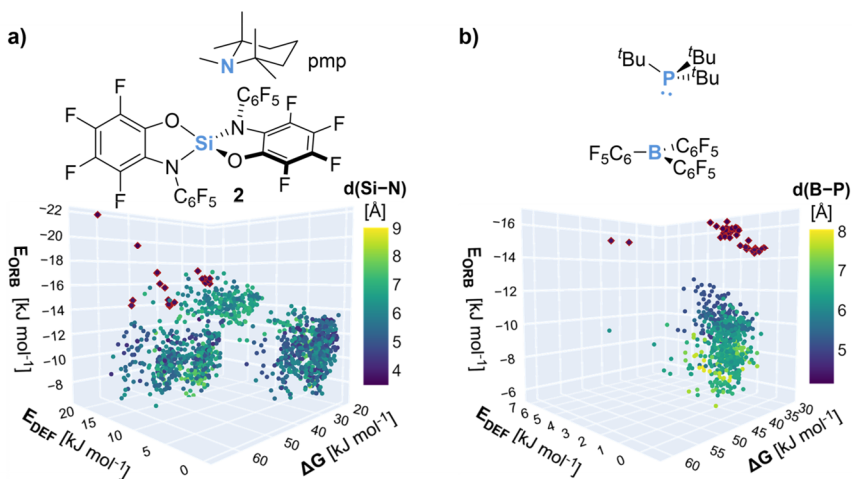


Figure 40. Depiction of scatter plots of the Gibbs free energy ( $\Delta G$ , referenced against the separated Lewis pair), the deformation energy of the Lewis acid ( $E_{DEF}$ ), the orbital energy ( $E_{ORB}$ ), and the bond length of the reactive centers (color-coded) of the geometries for the NCI ensembles of a) **2**/pmp and b)  $B(C_6F_5)_3/P^tBu_3$ . Points marked with a red diamond-shape ( $\blacklozenge$ ) refer to the *active* conformations as described in the main text.

As *active* FLP conformations are expected to exhibit higher orbital interactions, they were chosen as key property to identify the respective structures. However, the orbital interaction is not exclusively reflected by the donor-acceptor contribution (e.g., also by LP- $\pi$ ,  $\pi$ - $\pi$ , etc.). This is also apparent from the derived data when considering that reasonable orbital interactions do not necessarily walk along with shortened Si–N- or P–B-bond lengths. Therefore, two criteria were chosen for determining which structures exhibit an *active* conformation for H<sub>2</sub> activation. Structures were selected using a threshold of an orbital interaction stronger than  $-14 \text{ kJ mol}^{-1}$ , as well as a bond length shorter than  $5 \text{ \AA}$ .<sup>u</sup> The definition of the range was gauged by the interaction found between the P<sup>t</sup>Bu<sub>3</sub> and B(C<sub>6</sub>F<sub>5</sub>)<sub>3</sub> fragments in the transition state structure ( $-13.4 \text{ kJ mol}^{-1}$ ),<sup>359</sup> and the empirically derived optimal distance range for *active* intermolecular FLPs.<sup>330</sup> This resulted in 20 structures for the silane FLP and 42 structures for the borane FLP (Figure 40, resp. points are marked with a red contour, diamond shaped). The respective geometries were visually checked and found to represent the *active* FLP form,<sup>349</sup> where the lone pair of the Lewis base is directed toward the Lewis acid center. As an example, the structure with the highest orbital interaction in the **2**/pmp ensemble is shown in Figure 41a (left). In the borane FLP, the Lewis acid fragments showed neglectable deformation ( $< 3 \text{ kJ mol}^{-1}$ ) with P–B bond lengths of  $4.16\text{-}4.37 \text{ \AA}$ . In contrast, for **2**/pmp the bond distances are comparably short ( $3.49\text{-}3.89 \text{ \AA}$ ) with a pronounced deformation of **2** ( $16.8\text{-}22.2 \text{ kJ mol}^{-1}$ ). The *active* formations in the borane FLP are found to be energetically favored and the ensemble minimum structure indeed exhibits an *active* conformation (Figure 41b, left). 40 of the 42 as *active* assigned structures are more stable than any other geometry within the ensemble. Contrary, all 20 *active* **2**/pmp forms are endergonic compared to their minimum free-enthalpy structure, which is a virtually undeformed fragment of **2** stabilized by a LP- $\pi$  interaction (Figure 41a, right). Further, for **2**/pmp a mild transition to an *active* form is hindered primarily through required deformation, but also by Pauli repulsion of the O/N atoms in the primary coordination sphere of silicon (Figure 41c). Thus, the *active* conformers of **2**/pmp lack entropic stabilization through flexibility, as support through a flat potential energy surface is prevented.

---

<sup>u</sup> After the *active* structures were selected, residual conformations were checked visually to ensure a reasonable assignment.

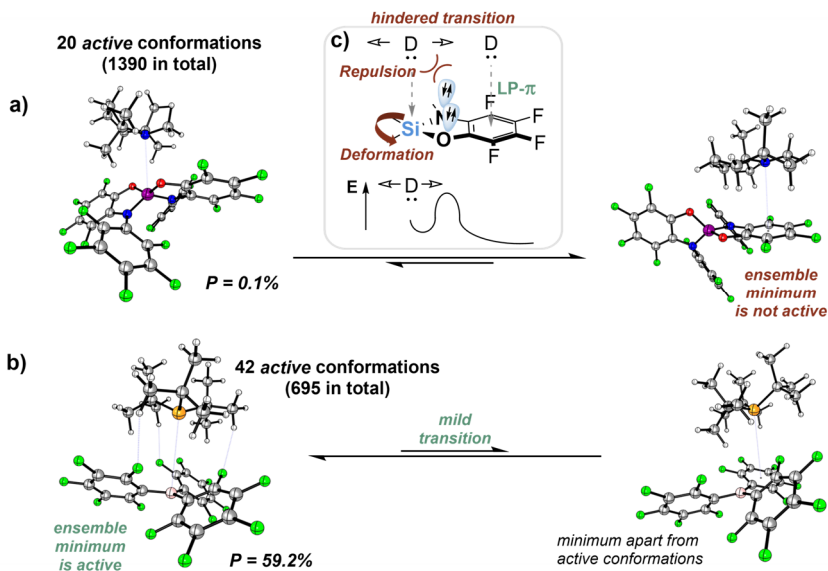


Figure 41. Depiction of an *active* FLP geometry (left), the first non-*active* minimum ensemble-structure (right) for a) **2**/pmp and b)  $P^t\text{Bu}_3/\text{B}(\text{C}_6\text{F}_5)_3$ . Boltzmann-populations referring to the sum of all *active* geometries within the ensemble are given as  $P$ . c) Schematic illustration of an impeded mild transition between the structures for **2**/pmp (middle).

It can be concluded that reasonable orbital interaction with the silane is only possible when it is considerably deformed – inherently requiring a shortened Si–N bond length. This is a strong indication that the striking balance of steric bulk and remaining interaction described earlier is even narrower for silanes than for boranes, explaining the previously observed limited choice of a suitable Lewis base (cmp. section 3.3.2). In this context, the harder nature of silanes tendentially leads to a preferred adduct formation over interaction with a softer hydride. The required balance between a strong enough bonding interaction to allow sufficient polarization (and therefore partial deformation) which is parallelly weak enough to prevent classical adduct formation is difficult to achieve.

The influence of the required preorganization of the Lewis acid is even more dominant, as it renders the *active* forms energetically less favorable, apparent from enhanced Gibbs free energies ( $\Delta G = +10.1$  to  $+42.2$  kJ mol $^{-1}$  with respect to the ensemble minimum). The impact for this effect was gauged by means of a Boltzmann population

analysis of the *active* FLP structures. Importantly, the here derived values do only refer to the investigated ensembles but do not account for any structures exhibiting larger-distance interactions, the separated fragments, or explicit solvation effects. It does therefore not reflect the real value for the proportion of *active* conformations in solution. For such it shall be referred to molecular dynamics studies which provided a reasonable value of 0.5%.<sup>360</sup> Within the calculated ensemble for  $P^tBu_3/B(C_6F_5)_3$  the 42 *active* structures are populated by 59.2% at rt. In harsh contrast and as result of their endergonic nature due to required deformation of the silane, a summed Boltzmann population of only 0.1% for the *active* conformations of **2**/pmp were derived within the NCI ensemble. The drastic population difference clearly gives qualitative support for the observed slowed proceeding of the  $H_2$  activation. To provide experimental guiding values, the FLP  $P^tBu_3/B(C_6F_5)_3$  led to 90% isolated cleavage product after exposition to 1 atm  $H_2$  for 12 h at rt,<sup>103</sup> while equimolar amounts of **2**/pmp proceeded to 64% after 8 d at 115 °C (cmp. section 3.3.2).

A more detailed kinetic prediction on the basis of the here presented static calculations is not expedient, as dynamic models emphasize the role of multi-scale motion as the predominant mechanistic aspect for reactions of  $P^tBu_3/B(C_6F_5)_3$  and similar FLPs.<sup>361-364</sup> Suitable molecular dynamics simulations are therefore highly desirable to give the present study a more quantitative dimension. Yet, various factors, such as explicit solvation correction, requirement of a suitably high computational level and a long timeframe (due to the low probability of a collision), call for a carefully designed, elaborate set-up. Respective analyses are therefore not considered in the course of this work. Nevertheless, based on previous insights, the dynamic proceeding of the FLP type  $H_2$  cleavage can be accounted for in a qualitative manner. For instance, molecular dynamics simulations suggested a two-step character for the cleavage process. First the rate-determining hydride transfer occurs, followed by the highly exergonic low-barrier protonation of the base.<sup>339</sup> Given the inherently less pronounced HIA of silanes in comparison to boranes, this might be an additional kinetic effect that is not reflected by static computations. Further, the collision of  $H_2$  with the reactive structures was not considered. The complexity of the intercalation-trajectory is emphasized by multiple dynamic studies.<sup>339,361-364</sup> To account for such influences, kinetic concepts frequently include a *pre-exponential*, *steric*, or *probability factor* to account for discrepancies of calculated and observed kinetics.<sup>365-370</sup> The *steric factor* of a reaction rises with the complexity of the underlying system, which accentuates

the slowed kinetics of the present system consisting of three reactants, which require accurate alignment parallelly to deformation. In extreme cases, a reaction can essentially be diffusion controlled, meaning that the rate is determined by the intercalation.<sup>370</sup> In this regard, valuable insights for intermolecular FLPs were revealed by detailed isothermal reaction calorimetric investigations on the cleavage of H<sub>2</sub> by P(Mes)<sub>3</sub>/B(C<sub>6</sub>F<sub>5</sub>)<sub>3</sub>. Importantly, the reaction was overall found to be well modeled by a single, termolecular reaction step.<sup>371</sup> The enthalpic barrier was found low and the reaction entropy controlled with a surprisingly low kinetic isotope effect (KIE = 1.1(1)). In good agreement with the present contribution, the authors demonstrated that for intermolecular FLPs the rate-determining step does crucially depend on the right assembling of the reaction partners into a solvent cage rather than on the energetic penalties required for the breaking and making of the respective bonds. Intramolecular FLPs show increased activity through entropic advantages and an altered kinetics (KIE(H<sub>2</sub>/D<sub>2</sub>) = 3.2 for Mes<sub>2</sub>P-C<sub>4</sub>H<sub>8</sub>-B(C<sub>6</sub>F<sub>5</sub>)<sub>2</sub>).<sup>372</sup> Still, for a row of geminal FLPs the activity was found to correlate with the interaction of Lewis acid and base centers.<sup>373</sup> The present contribution on an intermolecular silane FLP might therefore also serve in part as explanation for a slow described H/D scrambling through the geminal FLP <sup>t</sup>Bu<sub>2</sub>P-CH<sub>2</sub>-Si(C<sub>2</sub>F<sub>5</sub>)<sub>3</sub>,<sup>313</sup> for which a significant kinetic hindrance could not be substantiated by a calculated barrier of 115 kJ mol<sup>-1</sup>.<sup>374</sup>

In conclusion, in this chapter ensembles of NCI associates for the FLPs **2**/pmp and P<sup>t</sup>Bu<sub>3</sub>/B(C<sub>6</sub>F<sub>5</sub>)<sub>3</sub> were investigated computationally. Previously described phenomena on decisive FLP interactions could be mapped on the reactivity of the investigated systems. A row of factors hampers the decisive assembly of **2**/pmp into an *active* conformation, which qualitatively explains the drastically slowed rate in the reaction with H<sub>2</sub> compared to the B/P system:

- 1) The Lewis base tolerance for the silane **2** is narrow, as an interaction has to be strong enough for preorganizing the fragment but weak enough to still allow for an overall exergonic reaction.
- 2) The tetrahedral coordination sphere and the Pauli-repulsion of the primary-coordinating donor atoms of **2** hamper entropic stabilization and flexibility through secondary interactions.

- 3) Contrary to boranes, which exhibit an ideally suited vacant coordination site, the entirely undeformed silane interacts insufficiently with a Lewis base or dihydrogen.
- 4) The dominating effect is the deformation. It addresses the previous points and most importantly renders reactive alignments of the Lewis pair for a successful H<sub>2</sub> activation as less energetically accessible, and therefore improbable.

These effects emphasize why the reactive collisions are reduced when changing predetermined boranes with silanes in frustrated Lewis pairs. Future work might uncover additional factors and result in an adequate quantification. In a broader context, the pre-organizational effect through transient adduct formation exploited for silanes<sup>152-158</sup> might be transferred to the field of FLPs. Critical to this point, in the FLP type dihydrogen activation, a donor coordination according to Lewis base catalysis is not suitable. It quenches the Lewis acidity in a thermodynamic sense, and parallelly prevents a second base from spanning a sufficient polarization in an *active* orientation. In this regard, the use of more readily reactive substrates or even more Lewis acidic species such as *isoelectronic* phosphonium ions are promising extensions worth investigating.

Irrespectively, the described H<sub>2</sub> cleavage unambiguously proved the high potential of a Lewis superacidic silane that is robust and readily soluble. In contrast, the formation of an (endergonic) reactive encounter complex from Lewis acidic silanes that are insoluble, donor-stabilized, or contain labile ligands is prevented even when a sufficient HIA is ensured. Given the instability of common hydridosilicates, the previous reactivity highlights the status of **2** and serves as experimental manifestation for an unprecedented reactivity of neutral silanes. It thus provoked a profound analysis on the effects accompanying the use of a Lewis acid with a tetrahedral coordination sphere in FLP chemistry – a field dominated by boranes and valence-*isoelectronic* compounds ever since its discovery. Given the young class of Lewis superacidic tetrahedral species, those insights might pave the way for a modulation of reactivity by unlocking a whole class of Lewis acids.

### 3.3.4 Reversible FLP type C–H Silylation

The so far gained insights on the reactivity of **2** have unveiled a previously unknown phenomenon, shedding light on its immense potential but also highlighting the current limitations for a practical application. The result therefore exhibits a foundational role, serving as a vital steppingstone for further FLP reactivities. As a consecutive proposal, the formation of organic silicates was attempted. In contrast to the putative hydrido-bis(catecholato)silicates  $[\text{H-1}^{\text{X}}]^-$ , the corresponding aryl- and alkyl-silicates  $[\text{R-1}^{\text{X}}]^-$  are well-studied.<sup>375</sup> More generally, carbon-silicon functions represent important linchpins in various scientific areas. In organic chemistry they serve as strategic connecting points for the linkage of carbon-carbon or carbon-heteroatom bonds,<sup>376-378</sup> and more interdisciplinary they are of fundamental importance in biological research<sup>379-383</sup> as well as material science.<sup>384-388</sup> Several routes for the synthesis of organosilanes exist. The traditional way for silylation is the nucleophilic addition of a stoichiometrically metalated substrate to a halo-silane (Figure 42a). Owing to the importance of organosilanes, considerable progress on more atom economic direct C–H silylation protocols was made.<sup>389-391</sup> In those protocols, an activation of the silane reagent into a reactive intermediate is required, for instance, into electrophilic silylium ions (Figure 42b), transition metal activated intermediates (Figure 42c), nucleophilic silyl anions (Figure 42d), silyl radicals (Figure 42e), or through the use of designed reagents.<sup>390-392</sup> The utilization of a neutral silane for the synthesis of an organosilicate without prior activation states a yet inaccessible pathway (Figure 42f). In contrast, the formation of organic borates from Lewis acidic boranes and a Brønsted base is a viably used protocol.<sup>129,393-399</sup> In recent years, C–H functionalization came into focus as a broader research interest in FLP chemistry.<sup>400</sup> Contrary to various boron mediated protocols, common silanes are not suited for direct, spontaneous silicate formation from C–H bonds, attributed to a kinetic hindrance for the attack of an organo-nucleophile, and the lack of electrophilicity required for a thermodynamic stabilization of the silicate. With the previously demonstrated advantageous properties of **2** as excellent prerequisites, analogous reactivity was attempted. As a suitable base, 1,2,2,6,6-pentamethylpiperidine (pmp) proved viable in the previously described reactivity (cmp. section 3.3.2).

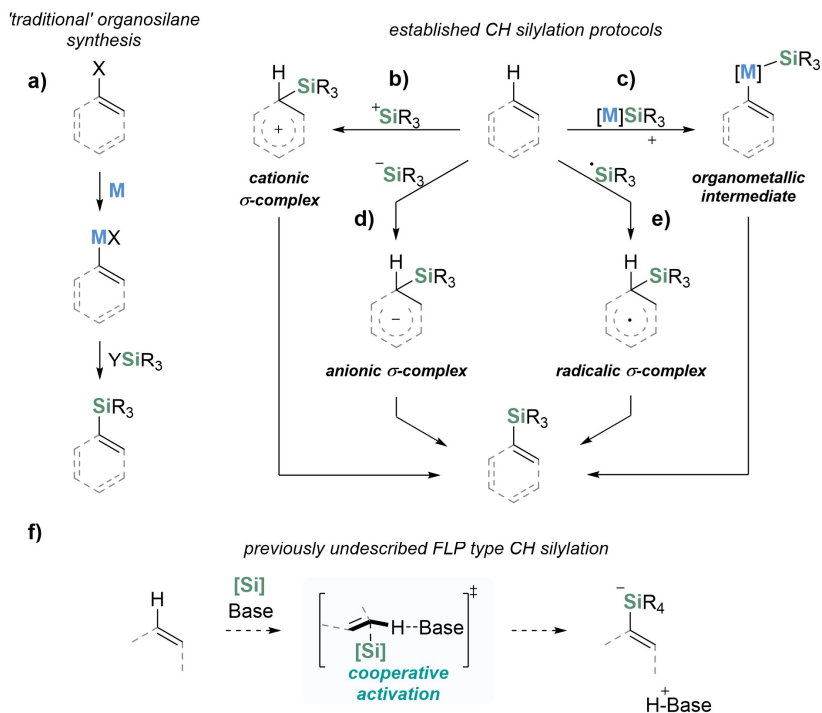


Figure 42. Schematic illustration of a) conventional silane syntheses *via* stoichiometric metalation, b)–e) silylation protocols *via* direct C–H activation,<sup>390</sup> and f) schematic illustration for a yet unreported FLP type silylation attempted in this work.

In a first experiment, N-methylindole was reacted with the FLP **2**/pmp in dichloromethane. Within one day at rt, a full conversion of the amine toward the ammonium species along with the formation of the corresponding N-methylindol-3-yl silicate [**3a**]<sup>-</sup> was observed *via* NMR spectroscopic monitoring (Figure 43a). Crystals suitable for scXRD grown by gas diffusion of *n*-pentane into the reaction mixture allowed structural classification of the formed silicate salt (Figure 43b). Related N-methylpyrrole and N-phenylpyrrole were also found to be converted to their respective silicates using the mild conditions, similarly upon cleaving the CH bond in 3-position. The hydrocarbon phenylacetylene was also cleanly converted into the terminally silylated alkyne using the same protocol. In contrast, thiophene was not activated at rt. Still, heating of the neat substrate with the FLP to 80 °C accounted

for the formation of the C2-silylated thiophene derivative. Overall, the silicates could be isolated in good to excellent yields (68-91%). Strikingly, the proceeding of the reactions did not require prior activation of the silane, extending existing silylation methods for N-heterocycles,<sup>401-404</sup> and acetylenes.<sup>405-414</sup>

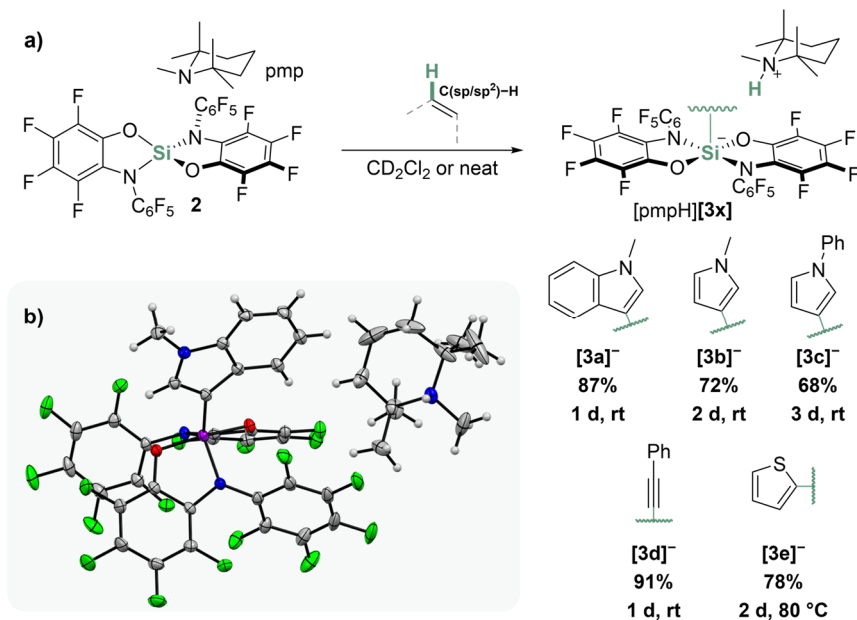


Figure 43. a) Schematic representation for the formation of silicates [pmpH][3x] from **2**, and b) scXRD-derived structure of [pmpH][3a] (ellipsoids shown at 50% probability).

Intrigued by this finding, the mechanistic pathway for the encountered reactivity was approached computationally.<sup>v</sup> In all cases, the silicate formation is accounted for by significant reaction Gibbs free energies ( $\Delta G = -53$  to  $-80$  kJ mol<sup>-1</sup>). An initial deprotonation of the substrates' C–H bond by pmp was ruled out after a comparison of respective pK<sub>a</sub> values revealed a difference of several magnitude orders (Table A10). Three different mechanistic routes were considered: 1) a *FRIEDEL-CRAFT*'s type mechanism proceeding *via* a *WHELAND* intermediate, in analogy to silylium ions,<sup>415</sup> 2) element-ligand-cooperative (ELC) bond cleavage found for *isoelectronic* phosphonium

<sup>v</sup> DLPNO-CCSD(T)/def2-TZVPP+SMD(CH<sub>2</sub>Cl<sub>2</sub>)/PBE0-D3(BJ)/def2-TZVPP level of theory.

cations,<sup>194</sup> and 3) an FLP type mechanism, as per the results of an intramolecular aminoborane FLP.<sup>399</sup> As a model system for detailed calculations N-methylpyrrole was chosen. An endergonic intermediate resembling the interaction of **2** and N-methylpyrrole was found *in silico* (Figure 44, **INT-3b**). The relatively large Si–C3 distance (2.43 Å) and the non-pyramidalized carbon ( $\alpha_{\text{H-C-Si}} = 94.5^\circ$ ,  $\Theta_{\text{H-C-C-H}} = -4.0^\circ$ ,  $10.3^\circ$ ) do not pledge for a Wheland intermediate but rather for a van-der-Waals adduct. A total of four transition states in an ELC pathway were considered, combining the two nucleophilic ligand sites (N and O) in **2** with the 2- and 3-positions in the substrate. All revealed relatively high barriers of  $>150 \text{ kJ mol}^{-1}$  and rendered an ELC pathway implausible under the mild conditions. A transition state for the FLP type C–H cleavage in 3-position revealed a suitable reaction Gibbs free energy of  $\Delta G^\ddagger = 72 \text{ kJ mol}^{-1}$ . For the C2-position a higher barrier of  $\Delta G^\ddagger = 94 \text{ kJ mol}^{-1}$  gives plausible explanation for the experimentally observed selectivity.

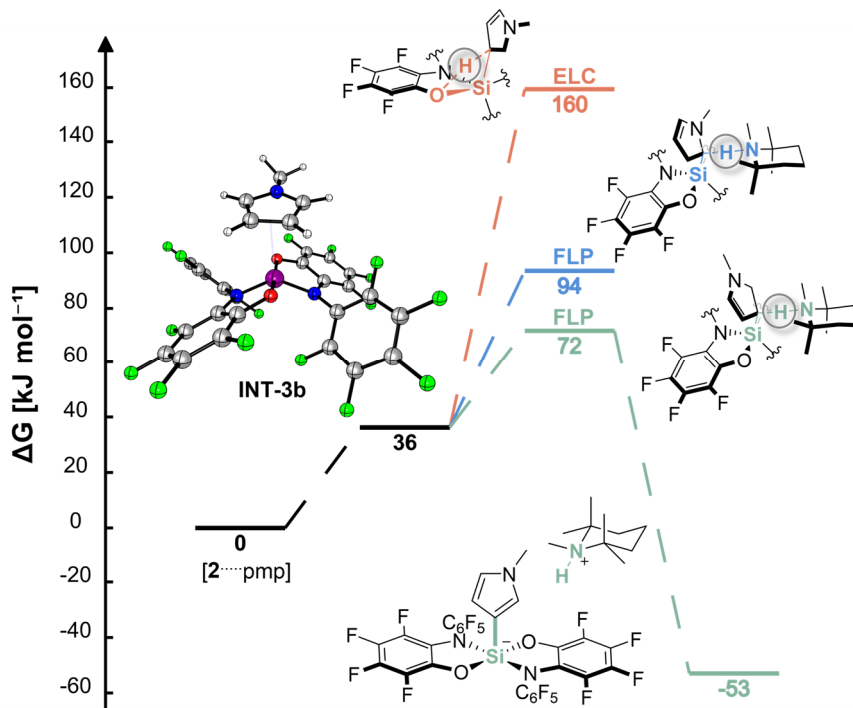


Figure 44. Different pathways for the formation of [pmpH][3b] from N-methylpyrrole, **2** and pmp (DLPNO-CCSD(T)/def2-TZVPP+SMD(CH<sub>2</sub>Cl<sub>2</sub>)/PBE0-D3(BJ)/def2-TZVPP), cmp. section 5.3 and Table A6.

The FLP mechanism was thus judged operative. Next, to rationalize their selectivity, the transition state energies for the bond cleavage of N-methylindole and thiophene were calculated. In line with the mild conditions, C3 silylation at N-methylindole revealed a barrier of  $\Delta G^\ddagger = 60 \text{ kJ mol}^{-1}$ , whereas a significantly increased value of  $\Delta G^\ddagger = 120 \text{ kJ mol}^{-1}$  gives conclusive explanation for the absence of the corresponding C2 silylation. For thiophene, a higher barrier of  $\Delta G^\ddagger = 98 \text{ kJ mol}^{-1}$  is in qualitative agreement with the required elevated temperatures. The selectivity for C2 silylation is further satisfactorily resembled by an increased energy for the transition state at C3 ( $\Delta G^\ddagger = 122 \text{ kJ mol}^{-1}$ ). Considering the reactivity displays a C–Si bond formation parallel to a C–H deprotonation, a comparison of the C2–H bonds' pK<sub>a</sub> values seemed reasonable. The acidities of thiophene = 33.0, N-methylindole = 38.1, and N-

methylpyrrole = 39.5 (in THF resp.)<sup>416</sup> suggest that the reaction kinetic is less influenced by the acidity of the bond, but rather by the nucleophilic character of the carbon. In this regard, a calculated barrier of  $\Delta G^\ddagger = 154 \text{ kJ mol}^{-1}$  for the C–H cleavage in benzene gives plausible explanation for the absence of reactivity even at elevated temperatures.

Next, experimental support for the computationally identified FLP mechanism was gathered. A first indication stated the absence of reactivity when trying to form the silicate **[3a]**<sup>−</sup> from N-methylindole, **2**, and 2,6-di-*tert*-butyl-pyridine (DTBP) as base (Figure 45a). In comparison to pmp, DTBP is more sterically demanding, likely preventing suitable polarization in the FLP's active cavity. The reactivity of FLPs is defined by weak associations (cmp. section 3.3.3),<sup>105,107</sup> which can be decisively modified upon change of the Lewis base.<sup>393</sup> In contrast, in ELC or *FRIEDEL-CRAFT*'s reactions the rate-determining step proceeds in absence of the Lewis base. Thus, less sensitivity on its nature is expected. To account for a more profound support, the kinetic isotope effect (KIE) was determined. Given the mild proceeding and the high selectivity, N-methylindole was chosen as substrate. Equimolar amounts of N-methylindole and 3-*deutero*-N-methylindole were dissolved in CD<sub>2</sub>Cl<sub>2</sub>. The exact H/D ratio was quantified *via* NMR spectroscopy before 0.5 eq. **2** and pmp were added. The reaction was monitored and after <sup>19</sup>F NMR spectroscopy indicated full conversion, the H/D ratio was again quantified (Figure 45b). From this data, a KIE of 3.5 was calculated (cmp. 5.2.11), in line with an FLP type C–H activation.<sup>399</sup>

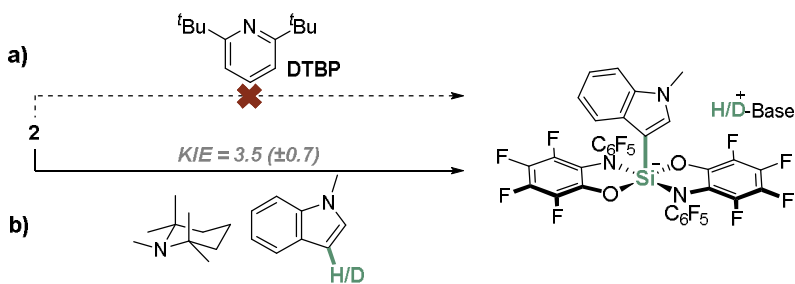


Figure 45. Mechanistic experiments for the encountered silicate formation. a) Failed formation of **[3a]**<sup>−</sup> when applying DTBP as Lewis base. b) Competition experiment between 3-*proteo*- and 3-*deutero*-N-methylindol for the determination of the kinetic isotope effect (KIE).

Even though notable progress on group 14 FLPs was reported in recent years,<sup>133-135,253,313,317,319,320,329,417,418</sup> the cleavage of C–H bonds by a neutral silane represents a novelty. To gauge the effects that enable such reactivity for **2**, a comparison with other silanes was undertaken. For SiCl<sub>4</sub> as exemplary silicon Lewis acid, a tremendous barrier of  $\Delta G^\ddagger = 181 \text{ kJ mol}^{-1}$  for the pmp-assisted activation of N-methylpyrrole ruled out a similar reactivity. In line, no activation was observed in the corresponding experiment up to a temperature of 60 °C and a reaction time of 7 d. Next, the first Lewis superacidic silane **1**<sup>Cl</sup> was probed. Indeed, similar reactivity could be observed, yet a relatively slow proceeding (56% conversion after 5 d) compared to **2** (78% after 16 h) was contradicted by a low calculated barrier ( $\Delta G^\ddagger = 63 \text{ kJ mol}^{-1}$ ). An initial reasoning is on hand by the non-monomeric structure through dynamic covalent chemistry (cmp. section 1.8.1). When considering the oligomerization energy (approx.  $\Delta G_{\text{Oligo.}} = 25 \text{ kJ mol}^{-1}$ , cmp. Table A7, Table A8, and Figure A2), a more viable barrier for the FLP [**1**<sup>Cl</sup>]<sub>n</sub>/pmp is obtained, now increased to the one of **2**/pmp ( $\Delta G^\ddagger = 88 \text{ kJ mol}^{-1}$  vs.  $\Delta G^\ddagger = 72 \text{ kJ mol}^{-1}$ ). Apart from this energetic difference, a main kinetic advantage of **2** states the excellent solubility, as concentrations were found to decisively influence reaction rates of silane FLPs (cmp. section 3.3.2). **2** is soluble right away, whereas [**1**<sup>Cl</sup>]<sub>n</sub> is only reasonably available in solution upon coordination of donors (e.g., ethers, amines).

Following on, the reactivity of the isolated products was examined. In the course, it was noticed that when handled in strong donor solvents such as DMSO, the ammonium silicate [**3a**]<sup>-</sup> decomposed partially into the putative DMSO adduct **2**-DMSO, the free amine pmp, and N-methylindole. Strikingly, addition of one equivalent 1,3-dimethylimidazolidin-2-one (DMI) to a CD<sub>2</sub>Cl<sub>2</sub> solution allowed the defined reformation of the C–H bond (Figure 46a). The at rt rather slow reactivity (31% after 48 h) could be accelerated upon heating to 60 °C (to >90% conversion after 40 h). Motivated by this finding, a transfer of a benzyl group instead of the proton was attempted. Ten equivalents of trimethyl-benzyl-ammonium chloride ([Me<sub>3</sub>NCH<sub>2</sub>Ph]Cl) were added to a solution of [pmpH][**3a**] in CH<sub>2</sub>Cl<sub>2</sub>. Still, again the reformation of the C–H bond was observed after addition of DMI and heating. Benzylation of the scaffold could also not be observed upon prior deprotonation of the ammonium cation with LiHMDS. The carbon electrophile acrylonitrile was probed next. Indeed, even in the absence of an external donor the propionitrile derivative **4a**

could be observed (Figure 46b), however in slow proceeding and low yields. The hampered reactivity was attributed to the thermodynamic stability of the silicate (Figure 44).

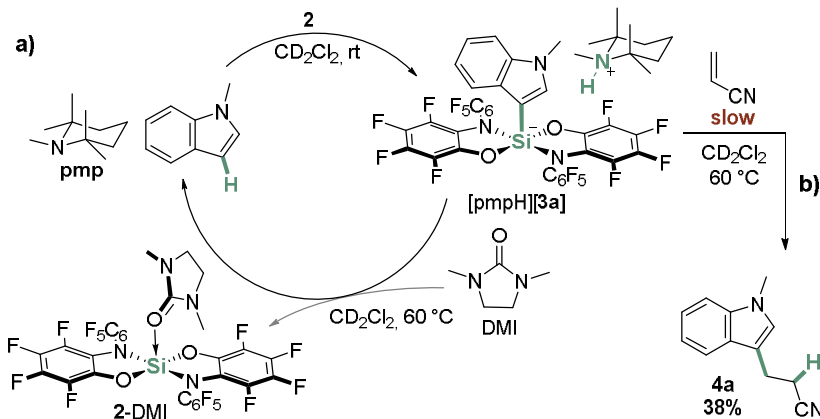


Figure 46. a) Formation of [pmpH][3a] from N-methylindole and the reverse reaction induced by DMI. b) The reaction of acrylonitrile and [pmpH][3a].

As a consecutive experiment, the reactivity was probed without a Lewis base. Remarkably, 10 mol% of **2** accounted for quantitative formation of **4a** from N-methylindole and acrylonitrile already at rt (Figure 47a). Moreover, the same conditions enabled the one- and two-fold incorporation of acrylonitrile into N-methylpyrrole to yield **4b** and **4b'** (Figure 47b). **4a** was previously synthesized *via* stoichiometric silylation of N-methylindole<sup>419</sup> and subsequent conversion with acrylonitrile under Lewis acidic conditions,<sup>420</sup> but a direct catalytic protocol for the synthesis of **4a** was not established. More generally, whereas catalytic additions of N-heterocycles to *MICHAEL*-systems are well-known for nitroolefins or acrolein derivatives,<sup>421–424</sup> less progress is reported on acrylonitriles. To the best of the authors knowledge, the only previous synthesis for **3a** states a catalytic gold(III)-protocol resulting in 52% yield.<sup>425</sup> Moreover, **4b** was *hitherto* synthesized *via* osmium catalysis in 40% yield,<sup>426</sup> and a synthesis for **4b'** was not yet reported.

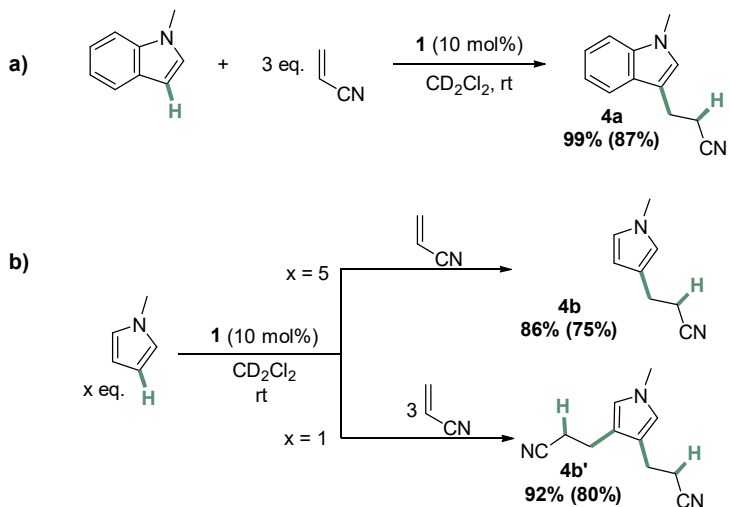


Figure 47. The **2**-catalyzed addition of a) N-methylindole and b) N-methylpyrrole to acrylonitrile. Yields were determined *via* NMR integration against cyclooctane as an internal standard, numbers in parentheses are isolated yields (cmp. section 5.2.12).

It shall be noted that, given the distinct binding tendency of this class of Lewis acids toward nitriles, an activation of the acceptor rather than the heteroarene appears as a more plausible pathway. In this regard, the organic silicate effectively is *deactivated* as it shows a reduced reactivity, even though the C–H bond cleavage certainly offers *activated* features in other pathways. Given the diverse applications of organic bis(catecholato)silicates for the generation of radicals<sup>219–224</sup> or as transmetalation reagents,<sup>225–227</sup> there is room for further development and strategic connections. Moreover, the present contribution also emphasizes that – depending on the aimed process – an apparent bond *activation* does not necessarily transfer to an enhanced reactivity. This is nicely pictured through the discrepancies observed upon conversion with acrylonitrile.

Summed up, this chapter reports on the formation of organic silicates from a neutral silane without prior activation. The mechanism was studied in experiment and theory and was shown to resemble FLP reactivity. Both the anionic reaction products as well as the cooperative mechanism were *hitherto* unobserved in this context and extend previous C–H silylation strategies. The reactivity is enabled by the high Lewis

acidity of **2** paired with its enhanced kinetic features, originating from improved properties by ligand design. Along this line, the nitrilophilicity of **2** allowed the elaboration of a catalytic C–C bond formation at N-heterocycles with acrylonitrile, a substrate that is challenging to activate with less reactive catalysts.



# 4

## CONCLUSION

Overall, this work served the evolution of neutral silicon(IV) compounds by introducing a *second-generation* of silane Lewis superacids with improved properties. Previous shortcomings of this young substance class could be resolved by rational ligand design, resulting in silanes with enhanced reactivity and handleability.

In the first part, a relation between the substitution pattern of the catecholato ligand and the structure of the corresponding silanes was investigated. The initial hypothesis that self-aggregation can be prevented by steric shielding could be confirmed, resulting in a heuristic guideline (Figure 48). Tangentially, the model experiments added an aspect to the solvation of a decades old, multifaceted structural riddle.<sup>231</sup>

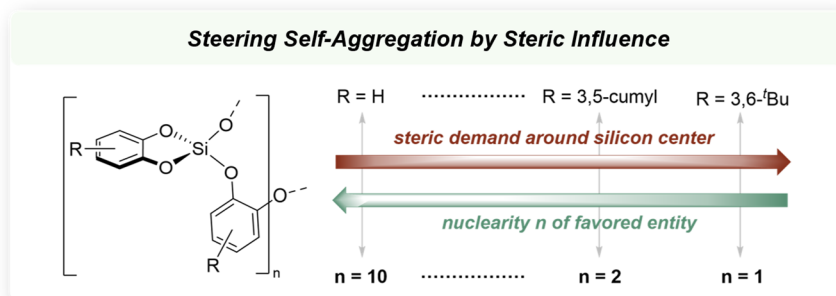


Figure 48. Conclusive illustration for the found relation between ligand substitution and the nuclearity of the corresponding silane entity.

Endowed with the principle insights, the synthesis of bis(per(trifluoromethyl)catecholato)silane  $1^{CF_3}$  was achieved.  $1^{CF_3}$  propels the advancement of Lewis acids in a two-fold sense. First, it demonstrates the feasibility

of the assumed proposition for an increase of reactivity in bis(catecholato)silanes upon combination of strong electron-deficiency and augmented steric demand. Second, it states a novel record holder for neutral silicon Lewis acids and even ranks among the most fluorophilic neutral species in a cross-class comparison. Due to its outstanding properties, it extended the catalytic portfolio of silicon species by enabling deoxygenation reactions of ketones, amides, and phosphine oxides, as well as a carbonyl-olefin-metathesis – reactions previously unprecedented for neutral silanes.

In addition, the complementary strategy for the synthesis of an unexampled, electron-withdrawing *ortho*-amidophenolato ligand was found fruitful. The rationally designed ligand allowed the isolation of the bis(nonafluoro-*N*-phenyl-*ortho*-amidophenolato)silane **2** in an unquenched monomeric and donor-free form. As proposed, **2** showed enhanced reactivity without the encountered obstacles of its predecessors. This is most remarkably underpinned by the base-assisted synthesis of a hydridosilicate directly from molecular dihydrogen. **2** is not only the first silane but more generally the only tetracoordinated Lewis acid that enabled isolation of a primary reaction product in such reactivity. The distinctiveness of the reaction, expressed through an unintuitive proceeding as well as a narrow Lewis base tolerance withheld a use as reagent or catalyst but instead provoked a foundational analysis. Accompanying computations indicated the required preorganization of **2** as dominating factor for the contrasting behavior in comparison to prevailing acceptors in FLPs. This finding is subtly resonating to the differences in reactivity between unbound and preorganized group 14 Lewis acids, exploited in Lewis base activation. In a temporal context, it is worth mentioning that the first isolation of a hydridosilicate was only achieved in 1987,<sup>316</sup> and the first non-metal dihydrogen cleavage in 2006.<sup>5</sup> In sight of this chronology, the present achievement exhibits a pioneering role in combining the two phenomena.

Beyond, the system **2**/pmp was of use in the silylation of C(sp<sup>2</sup>/sp<sup>3</sup>)–H bonds. Heterocycles could be spontaneously silylated in an FLP type fashion – a novum for silane Lewis acid/base pairs. The mechanism was fully accounted for in experiment and theory and the reaction could be reversed upon addition of a silaphilic donor. Along this line, **2** was rendered a potent Lewis acid catalyst in the C–C bond forming addition of heterocycles to acrylonitrile. In light of the prosperous chemistry of bis(catecholato)silicates, strategic connections with the found process are envisioned.

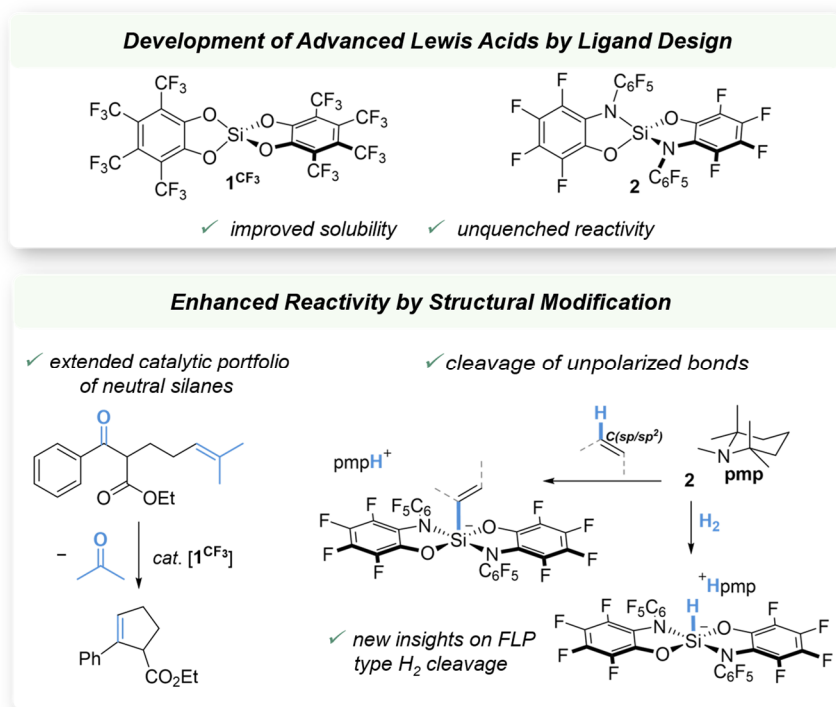


Figure 49. Conclusive illustration of the new silicon Lewis acids presented in this work and an exemplary depiction of their reactivity.

Moreover, the conducted research affected neighboring areas which were not explicitly addressed in the main text. The general progress on more Lewis acidic silanes stimulated the development of a perfluorinated silane able to activate a Si–F bond,<sup>196</sup> which was accompanied by computations in the course of this work. The distinct advantages of **2** enabled efficient C–O sigma bond metathesis and the depolymerization of polyethers.<sup>427</sup> Both electron-rich **13,4,6-*i*Pr** and electron-poor **1CF<sub>3</sub>** were valuable building blocks for a broad spectrum of modularly synthesizable diradicaloids.<sup>428</sup> Moreover, incorporation of other central elements in the here described ligands is an evident onset for further advancements. In this regard, the corresponding phosphonium cation *isoelectronic* to **2** was shown to boost the Lewis acidity of mono-cationic phosphonium species to a novel record.<sup>429</sup> First results with

the heavier germanium analog as well as the *isoelectronic* aluminate of **2** are on hand. Future directions might include a use in weakly coordinating anions (aluminates, borates, or phosphates), as extension for the diverse ligand family of catecholates and amidophenolates, or in hydrogen bond donor catalysis. Not to be overlooked, the reported silicon compounds exhibit a structural proximity regarding coordination sphere and oxidation state to silica, the most abundant mineral in the earth's crust. Within the right research focus, insights from a molecular perspective might be able to influence the rich material chemistry of silicates and *vice versa*.

In conclusion, this contribution illuminates new aspects of the burgeoning class of neutral silicon Lewis superacids. The reported findings have not only included unprecedented bond activations by a neutral silane but in a broader context serve a fundamental purpose and represent an ideal steppingstone for multifaceted advancements. Considering the abundance of silicon as underlying element and the early status of the field, further uncovering of intricacies promises an establishment of the found principles in firm applications beyond a prototypical role.

# 5

## EXPERIMENTAL AND COMPUTATIONAL DETAILS

---

<b>5.1</b>	<b>General Information for Experiments.....</b>	<b>100</b>
5.1.1	Materials and Methods.....	100
5.1.2	Analytical Methods.....	101
<b>5.2</b>	<b>Syntheses, Reactivity Experiments, and Catalysis.....</b>	<b>106</b>
<b>5.3</b>	<b>Computational Details.....</b>	<b>166</b>
5.3.1	General Remarks .....	166
5.3.2	Anion Affinities .....	167
5.3.3	Calculation of NMR Resonances.....	168
5.3.4	Workflow for the Computational Analysis of FLP Ensembles.....	168

## 5.1 General Information for Experiments

### 5.1.1 Materials and Methods

All used reagents and solvents were purchased from commercial sources. Unless otherwise noted, all manipulations were carried out under a dry nitrogen or argon atmosphere using standard Schlenk techniques, or in a glovebox (*SylaTech* type GB1950, *MBraun LABstar (MB-10-G)* or *MBraun LABmaster DP (MB-20-G)*). Reactions on preparative scale were carried out in flame-dried standard laboratory glassware under a dry argon atmosphere using Schlenk line techniques and were permanently magnetically stirred. Syringes, magnetic stirring bars, and needles were dried and/or flushed with argon prior to use. Reactions on NMR sample scale were conducted in dry *J. Young* NMR tubes and prepared in a glovebox.

Chemicals used in this work were obtained from the central dispensary of Heidelberg University, the chemical dispensary of the chemical institutes of Heidelberg University, or directly purchased from the respective suppliers: *Sigma Aldrich (Merck KGaA)*, *abcr GmbH*, *Alfa Aesar* and *Acros Organics B.V.B.A. (Thermo Fisher Scientific)*, *VWR*, *TCI Chemicals*, *Fluorochem*, *BLDpharm*. The solvents used were obtained from a solvent purification system (*MB-SPS-800*, *MBraun*). Deuterated solvents were purchased from *Deutero GmbH*, *Eurisotop* or *Sigma Aldrich (Merck KGaA)*. Solvents were degassed prior to use with at least three freeze-pump-thaw cycles and were stored in sealed *J. Young*, *Normag* or *FengTecEx* valve ampoules over activated molecular sieve (3 or 4 Å, respectively) under a dry argon atmosphere for at least 24 h prior to use. Acetonitrile and DMSO were degassed by saturation with argon. Removal of solvents *in vacuo* was performed using a *Heidolph VV2000* rotary evaporator or a Schlenk line.

Liquid reactants were degassed for at least 10 min with a constant stream of dry argon through the fluid phase and were dried by storage over activated molecular sieve (3 or 4 Å, respectively). Solid reagents were dried *in vacuo* and purified if necessary either by the application of *vacuum* and elevated temperature or by sublimation under reduced pressure at elevated temperature. N-methylindole and N-methylpyrrole were filtered over silica prior to use.

Literature-known compounds were synthesized following published procedures, which are cited. Analytical data of known compounds were compared to data of the respective reference and were found to be consistent in all cases. Novel compounds were characterized to the reported structures to the best of the authors knowledge.

General procedure for experiments with gaseous substrates on NMR scale, unless stated otherwise: the reaction mixture was prepared in a N<sub>2</sub>-Glovebox, frozen at 77 K, the vessel evacuated and then charged with 1 atm H<sub>2</sub> (additionally dried over a column of P<sub>4</sub>O<sub>10</sub>) or CO<sub>2</sub> at 77 K before sealed and cautiously thawed. The pressure was regulated with a fine valve or adjusted to ambient atmosphere *via* an overpressure-valve with a spring-loaded spherical ground joint seal.

## Software

This document was authored with *Microsoft Word* and the *Microsoft Office* program package. The chemical structures were visualized with *ChemDraw 21/22* by *PerkinElmer Informatics*. Evaluation of the spectroscopic and spectrometric data was accomplished using *OriginPro 2021b* by *OriginLab Corporation* (IR, EPR), *TopSpin 4.1.4* by *Bruker* or *MestReNova 14.2* by *MestreLab Research* (NMR) and *OpenChrom* by *Lablicate* (GCMS). For visualization of scXRD data *Mercury 4.1.3* was used.<sup>430-432</sup> *Avogadro* was used for the generation of xyz starting structures.<sup>433</sup> Computational output data were visualized using *Chemcraft*.<sup>434</sup> Reaction energy profiles were initially created with *mechaSVG*,<sup>435</sup> and customized with *Inkscape*.

## 5.1.2 Analytical Methods

### Cyclovoltammetry

Electrochemical measurements were performed with a potentiostat (*EmStat3+ Blue, PalmSens Compact Electrochemical Interfaces*) in the *SylaTech* glovebox under nitrogen atmosphere in a glass cell using a three-electrode configuration. A glassy carbon electrode with a working area of 0.07 cm<sup>2</sup>, was used as working electrode, a platinum wire as counter electrode; a silver wire served as quasi reference electrode. The program *PSTrace 5.9* was used to record all measurements. The substances were examined at room temperature with the electrolyte [PF<sub>6</sub>][N<sup>n</sup>Bu<sub>4</sub>] (*c* = 0.1 M, *V* = 5 mL) in dichloromethane at a scan rate of 50 mV/s, unless otherwise stated. The

solutions were stirred between each measurement and kept under nitrogen atmosphere throughout. As internal standard ferrocene was measured at the very end of each set of measurements.

### Electron Paramagnetic Spectroscopy (EPR)

X-band EPR measurements (9.30-9.55 GHz) were conducted on a spectrometer (*MiniScope MS400*, *magenettech*) with a modulation frequency of 100 kHz at rt.

### Elemental Analysis

The elemental analyses for the determination of C-, H- and N-content [%] were performed by the staff of the Microanalytical Laboratory of the Institutes of Chemistry at Heidelberg University on an elemental analyzer (*vario EL* or *vario MICRO cube*, *Elementar Analysensysteme GmbH*).

### Gas Chromatography Mass Spectrometry (GCMS)

Gas chromatography mass spectrometry (GCMS) experiments were conducted utilizing helium as carrier gas on **(A)** an *Agilent Technologies 6890 Series* gas chromatograph equipped with a HP-5MS-column (5% diphenylpolysiloxane, 95% dimethylpolysiloxane, 30 m x 0.25 mm x 0.25  $\mu\text{m}$ ) and an *Agilent 5973* Mass Selective Detector, or **(B)** a *Thermo Fischer Scientific Ultra Trace* gas chromatograph equipped with a *TraceGOLD TG-1701MS* column (14% cyanopropylphenyl, 86% dimethylpolysiloxane, 30 m x 0.25 mm x 0.25  $\mu\text{m}$ ) and a *Thermo Fischer Scientific ISQ Single Quadropole* Mass Selective Detector. Unless stated otherwise, the following column programs were used: **(A)** at a constant pressure of 68 kPa the initial temperature of 80 °C was held for 2 min after injection, then increased by 15 K/min to 250 °C, this temperature kept for 15 min, increased again by 20 K/min to 280 °C, held for 3 min; or **(B)** at a constant pressure of 50 kPa the initial temperature of 35 °C was held for 5 min after injection, then increased by 30 K/min to 250 °C, this temperature kept for 10 min before cooling to 150 °C at a rate of 25 K/min. Reported retention times refer to these programs.

## Mass Spectrometry

High resolution mass spectrometry (HRMS) was conducted with the electrospray ionization method (ESI), the direct analysis in real time method (DART) on a *Bruker ApexQe hybrid 9.4 T FT-ICR* or with electron impact ionization (EI) on a *JEOL JMS-700 magnetic sector*, carried out by the Mass Spectrometry Facility of the Institute of Organic Chemistry of the University of Heidelberg. HRMS ESI measurements were also conducted on a *Bruker micrOTOF II* ESI Mass Spectrometer by *C. DIENEMANN* from the group of *Prof. Dr. R. KRÄMER*. Mass spectrometry data is reported as follows: m/z ratio (relative intensity) [assigned fragment] (for HR experiments: calculated exact mass).

## Nuclear Magnetic Resonance Spectroscopy

Nuclear magnetic resonance (NMR) spectra were collected with a *Bruker BZH 200/52*, a *Bruker DPX 200*, a *Bruker Avance I 200*, a *Bruker Avance II 400*, or a *Bruker Avance III 600* spectrometer at 298 K unless otherwise noted. Measurements were in part carried out by the NMR facility of the Institutes of Inorganic or Organic Chemistry of Heidelberg University. Chemical shifts  $\delta$  are given in parts per million (ppm) relative to the tetramethylsilane resonance. Deuterated acetonitrile, dichloromethane, chloroform, tetrahydrofuran (THF), benzene, and toluene were used as solvents, and the signals of CHD<sub>2</sub>CN, CHDCl<sub>2</sub>, CHCl<sub>3</sub>, THF-*d*<sub>7</sub>, C<sub>6</sub>HD<sub>5</sub> or C<sub>6</sub>D<sub>5</sub>CD<sub>2</sub>H were used for calibration of the spectra (CD<sub>3</sub>CN: <sup>1</sup>H: 1.94, <sup>13</sup>C: 118.26 ; CD<sub>2</sub>Cl<sub>2</sub>: <sup>1</sup>H: 5.32 ppm, <sup>13</sup>C: 53.84 ppm; CDCl<sub>3</sub>: <sup>1</sup>H: 7.26 ppm, <sup>13</sup>C: 77.16 ppm; THF-*d*<sub>8</sub>: <sup>1</sup>H: 3.58 ppm, <sup>13</sup>C: 67.21 ppm; C<sub>6</sub>D<sub>6</sub>: <sup>1</sup>H: 7.16 ppm, <sup>13</sup>C: 128.06 ppm; toluene-*d*<sub>8</sub>: <sup>1</sup>H: 2.08 ppm, <sup>13</sup>C: 20.43 ppm). Spectra in *ortho*-dichlorobenzene (*o*DCB) were obtained after the addition of CD<sub>2</sub>Cl<sub>2</sub> or without lock. In the latter case the solvent signals against the tetramethylsilane resonance were determined and served as reference for calibration (<sup>1</sup>H: 7.26 (m), 7.00 (m) ppm; <sup>13</sup>C: 132.57, 130.56, 127.81).

<sup>1</sup>H and <sup>19</sup>F NMR data is reported as follows: chemical shift  $\delta$  [ppm], multiplicity (s = singlet, br = broad singlet, d = doublet, t = triplet, q = quartet, quin = quintet, sext = sextet, sept = septet, m = multiplet, and combinations; pseudo-multiplicities are reported likewise), scalar spin-spin coupling constant [Hz] as <sup>X</sup>J<sub>AB</sub> (if apparent: X = number of chemical bonds between coupled nuclei; A, B = coupled nuclei), integration value. <sup>13</sup>C, <sup>29</sup>Si and <sup>31</sup>P spectra were recorded <sup>1</sup>H-decoupled if not stated otherwise.

$^{19}\text{F}$  decoupled spectra are specified ( $\{^{19}\text{F}\}$ ).  $^{13}\text{C}$  and  $^{29}\text{Si}$  data is reported as follows: chemical shift  $\delta$  [ppm], multiplicity (if apparent), scalar spin-spin coupling constant [Hz] as  $^XJ_{AB}$ .

### Single Crystal Xray Diffraction (scXRD)

The scXRD measurements were carried out by technically instructed members of the groups *HIMMEL* and *GREB* from Heidelberg University. The structures were solved and refined by *Prof. Dr. L. GREB, Dr. D. HARTMANN, Dr. M. SCHORPP, and Q. LUO*.

For scXRD measurements, a suitable crystal was picked from the mother liquor, immersed in perfluorinated polyether oil, and fixed on top of a cryo loop. A *Bruker APEX-III CCD* diffractometer with a low-temperature unit using  $\text{Mo-K}_\alpha$  radiation, chromated by mirror optics, was used for phi- and omega- scans. Data acquisition was done at 100.0 K. A strategy for data collection was calculated with Bruker's APEX3 software. The same program was used for processing of collected data. Data reduction, scaling, and absorption corrections were done with *SAINT. SA-DABS-2016/2* was used for multi-scan absorption correction. Structures were solved with dual methods as implemented in the *ShelXT 2018* structure solution program. Structure refinement was carried out by full matrix least squares minimization on  $F^2$  using the 2018/3 version of *ShelXL*. All non-hydrogen atoms were refined anisotropically. Hydrogen atom positions were calculated geometrically and refined using a riding model. Handling of the structural data during solution and refinement was performed with the *Olex2 v1.3* graphical interface.<sup>436</sup>

Electron density attributed to solvent of crystallization ( $\text{CH}_2\text{Cl}_2$ ), which could not be modelled was removed from the structure of  $[\text{Li}@12\text{c4}][\text{H-2}]$  with the BYPASS procedure,<sup>437,438</sup> as implemented in *PLATON* (squeeze/hybrid).<sup>439</sup> Partial structure factors from the solvent masks were included in the refinement as separate contributions to  $F_{\text{calc}}$ . 54 electrons were found in a volume of  $227 \text{ \AA}^3$  in one void per unit cell. This is consistent with the presence of 0.625  $\text{CH}_2\text{Cl}_2$  per unit cell which accounts for 52 electrons per unit cell.

For data visualization, *Mercury 4.1.3* was used.<sup>430-432</sup> The thermal displacement ellipsoids are shown at the probability level of 50%.

CCDC 2070464-2070469, 2095074-2095075, 2181650-2181656, and 2279861 contain supplementary crystallographic data for some structures described in this work. These data can be obtained free of charge from the *Cambridge Crystallographic Data Centre's* and *FIZ Karlsruhe's* joint Access Service via <https://www.ccdc.cam.ac.uk/structures/>.

Crystallographic data is tabulated in section 7.6. Structures are shown at a probability of 50%, solvent molecules, hydrogen atoms, or cations are occasionally omitted for clarity.

### **Vibrational Spectroscopy**

Infrared (IR) spectra of solids and oils were obtained on a FTIR spectrometer (*Cary 630, Agilent*) equipped with a diamond ATR sampling module in the *SylaTech* GB1950 glovebox under nitrogen atmosphere. The samples were directly deposited on the diamond crystal and in case of solid samples pressed down with a stamp. Spectra were manually baseline corrected. The IR absorption bands are given in wavenumbers  $\tilde{\nu}$  [ $\text{cm}^{-1}$ ] and the signal intensities are divided into s = strong, m = medium, w = weak and sh = shoulder, relative to the strongest signal in the respective spectra.

## 5.2 Syntheses, Reactivity Experiments, and Catalysis

5.2.1 Alkylated Catechols and Respective Bis(catecholato)silanes .....	109
5.2.1.1 3,4,6-Tri- <i>iso</i> -propylcatechol ( $\text{H}_2\text{cat}^{3,4,6-i\text{Pr}}$ ).....	109
5.2.1.2 3,5-Di-cumyl-catechol.....	110
5.2.1.3 3,6-Di- <i>tert</i> -butyl-catechol ( $\text{H}_2\text{cat}^{3,6-t\text{Bu}}$ ) .....	111
5.2.1.4 Bis(3,4,6-tri- <i>iso</i> -propylcatecholato)silane ( $1^{3,4,5-i\text{Pr}}$ ) .....	112
5.2.1.5 Dimeric bis(3,5-di-cumyl-catecholato)silane [ $1^{3,5-\text{Cum}}$ ] $_2$ .....	113
5.2.1.6 $1^{3,6-t\text{Bu}}(\text{HNMe}_2)_2$ .....	113
5.2.1.7 Bis(3,6-di- <i>tert</i> -butyl-catecholato)silane ( $1^{3,6-t\text{Bu}}$ ) .....	114
5.2.2 Synthesis Route to Adducts of $1^{\text{CF}_3}$ .....	115
5.2.2.1 1,2,3,4-Tetraiodo-5,6-dimethoxy-benzene ( $\text{ver}^{\text{I}}$ ) .....	115
5.2.2.2 1,2-Dimethoxy-3,4,5,6-tetra(trifluoromethyl)benzene ( $\text{ver}^{\text{CF}_3}$ ) .....	116
5.2.2.3 2-Methoxy-3,4,5,6-tetra(trifluoromethyl)phenol ( $\text{gua}^{\text{CF}_3}$ ) .....	117
5.2.2.4 $1^{\text{CF}_3}-(\text{sulfolane})_2$ .....	118
5.2.2.5 3,4,5,6-Tetra(trifluoromethyl)catechol ( $\text{H}_2\text{cat}^{\text{CF}_3}$ ) .....	119
5.2.2.6 $[\text{N}(^n\text{Bu})_4][\text{F}-1^{\text{CF}_3}]$ .....	120
5.2.2.7 $1^{\text{CF}_3}-(\text{OCPH}_2)$ .....	121
5.2.3 Synthetic Route to 2.....	122
5.2.3.1 $\text{am}^{\text{F}}\text{phFC}_3\text{H}_6$ .....	122
5.2.3.2 $\text{am}^{\text{F}}\text{phFH}_2$ .....	123
5.2.3.3 2-HNMe $_2$ .....	124
5.2.3.4 Bis(nonafluoro-N-phenyl- <i>ortho</i> -amidophenolato)silane (2).....	125
5.2.3.5 [cation][H-2].....	126
5.2.4 Catalytic Carbonyl-Olefin-Metathesis upon Oxidation.....	128
5.2.5 Lewis Acidity Assessment and Reactivities of $1^{\text{CF}_3}$ .....	129

---

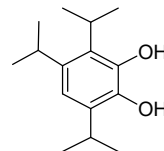
5.2.5.1	Reactivity of $\text{gua}^{\text{CF}_3}$ with $\text{HSiCl}_3$ in Acetonitrile .....	129
5.2.5.2	GB-Assessment of the Lewis Acidity .....	130
5.2.5.3	Reactivity against $[\text{PPh}_4][\text{SbF}_6]$ .....	131
5.2.5.4	Chloride-Abstraction from Trityl Chloride.....	132
5.2.5.5	Reduction of $1^{\text{CF}_3}(\text{OCPh}_2)$ .....	132
5.2.6	Catalytic Protocols incorporating $1^{\text{CF}_3}$ .....	134
5.2.6.1	Characterization Data.....	136
5.2.7	Lewis Acidity Assessment and Reactivities of 2.....	139
5.2.7.1	GB-Assessment of the Lewis Acidity .....	139
5.2.7.2	Chloride-Abstraction from Trityl Chloride.....	140
5.2.7.3	$\text{CO}_2$ Fixation.....	141
5.2.7.4	Lewis Base Cooperative Reactivity with $\text{PhCF}_3$ .....	142
5.2.8	Reactivities of 2 and Sterically Demanding Lewis Bases .....	143
5.2.8.1	Adduct Formation of 2 and $\text{P}^t\text{Bu}_3$ .....	143
5.2.8.2	Adduct Formation of 2 and $\text{tmpH}$ .....	144
5.2.8.3	Experiment with 2 and DTBP .....	144
5.2.8.4	Reactivity of 2 and $\text{NHC}^t\text{Bu}$ .....	145
5.2.8.5	Reactivity of 2 and DIPEA.....	146
5.2.9	Dihydrogen Activation Experiments with 2 $\text{pmp}$ .....	147
5.2.9.1	Characterization Data for $[\text{pmpH}][\text{H-2}]$ .....	148
5.2.9.2	Reference Experiment (1 eq. $\text{pmp}$ , 1 atm, < 65 °C).....	149
5.2.9.3	Increased Temperature (115 °C).....	149
5.2.9.4	Increased $\text{pmp}$ Concentration (10 and 100 eq.).....	149
5.2.9.5	Increased Pressure (50 atm $\text{H}_2$ ) .....	150
5.2.9.6	Cleavage of $\text{D}_2$ by 2/ $\text{pmp}$ .....	151

5.2.9.7	Probing the Activity of [tmp=CH <sub>2</sub> ] <sup>+</sup> against H <sub>2</sub> .....	152
5.2.10	C–H Silylations with 2 and pmp and related Reactivities .....	153
5.2.10.1	General Procedure (GP) for the Syntheses of [pmpH][3x] .....	153
5.2.10.2	[pmpH][3a].....	154
5.2.10.3	[pmpH][3b] .....	155
5.2.10.4	[pmpH][3c].....	156
5.2.10.5	[pmpH][3d] .....	157
5.2.10.6	[pmpH][3e].....	158
5.2.10.7	Donor Induced Reversal of the Bond Cleavage.....	159
5.2.11	KIE Determination for CH Cleavage of N-methylindole.....	160
5.2.12	Catalytic Addition of N-heterocycles to Acrylonitrile.....	162
5.2.12.1	General Procedure .....	162
5.2.12.2	3-(N-methylpyrrole-3-yl)-propionitrile (4a).....	162
5.2.12.3	3-(N-methylpyrrole-3-yl)-propionitrile (4b) .....	163
5.2.12.4	3,3'-(N-methylpyrrole-3,4-diyl)-dipropionitrile (4b').....	163
5.2.12.5	Reaction of [pmpH][3a] with Acrylonitrile.....	163
5.2.12.6	Comparison Experiments with SiCl <sub>4</sub> and 1 <sup>Cl</sup> .....	164
5.2.13	Other Syntheses.....	165
5.2.13.1	1 <sup>Cl</sup> -(sulfolane) <sub>2</sub> .....	165

## 5.2.1 Alkylated Catechols and Respective Bis(catecholato)silanes

### 5.2.1.1 3,4,6-Tri-*iso*-propylcatechol ( $\text{H}_2\text{cat}^{3,4,6-i\text{Pr}}$ )

According to a literature procedure,<sup>259</sup> a solution of catechol (2.2 g, 20.0 mmol) and *isopropanol* (4.0 eq.) in *n*-heptane (5 mL) was heated to reflux (100 °C). Concentrated sulfuric acid (4.05 eq.) was added dropwise and stirring continued for 5 h at that temperature.



The reaction mixture was diluted with ethyl acetate and the phases were separated. The combined organic phases were washed with  $\text{NaOH}_{(\text{aq})}$  (0.5 M) and water, and dried over  $\text{MgSO}_4$ . Contrary to the guiding protocol, in the present case the compound could not be purified by recrystallization from *n*-hexane. The black, viscous crude reaction product was thus purified *via* column chromatography (silica gel, petroleum ether 10:1 ethyl acetate) to yield the target compound as pale brownish oil (1.85 g, 39%), that solidified upon staying undisturbed. Colorless crystals were obtained from a saturated *n*-hexane solution at  $-40$  °C.

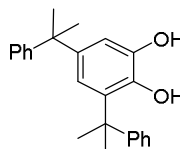
$^1\text{H-NMR}$  (200 MHz,  $\text{CDCl}_3$ )  $\delta$  6.64 (s, 1H,  $\text{C}_{\text{Ar}}\text{H}$ ), 3.37 (sept, 1H,  $\text{C}_{\text{Pr}}\text{H}$ ), 3.09 (m, 2H,  $\text{C}_{\text{Pr}}\text{H}$ ), 1.38 (d,  $J = 7.2$  Hz, 6H,  $\text{CH}(\text{CH}_3)_2$ ), 1.26 (d,  $J = 6.9$  Hz, 6H,  $\text{CH}(\text{CH}_3)_2$ ), 1.20 (d,  $J = 6.9$  Hz, 6H,  $\text{CH}(\text{CH}_3)_2$ ).

$^{13}\text{C NMR}$  (151 MHz,  $\text{CDCl}_3$ ):  $\delta$  143.0 ( $\text{C}_{\text{Ar}}\text{O}$ ), 138.8 ( $\text{C}_{\text{Ar}}$ ), 138.6 ( $\text{C}_{\text{Ar}}\text{O}$ ), 131.3 ( $\text{C}_{\text{Ar}}$ ), 129.0 ( $\text{C}_{\text{Ar}}$ ), 113.7 ( $\text{C}_{\text{Ar}}\text{H}$ ), 29.3 ( $\text{C}_{\text{Pr}}\text{H}$ ), 27.7 ( $\text{C}_{\text{Pr}}\text{H}$ ), 26.9 ( $\text{C}_{\text{Pr}}\text{H}$ ), 24.4 ( $\text{CH}_3$ ), 22.7 ( $\text{CH}_3$ ), 21.2 ( $\text{CH}_3$ ).

**GCMS EI+ (A)** 10.5 min.  $m/z$  236.2 (10%)  $[\text{M}]^+$ .

### 5.2.1.2 3,5-Di-cumyl-catechol

The literature-known<sup>261</sup> compound was obtained *via* a slightly modified procedure. Titanium catecholate (0.02 eq.) was added to a solution of catechol (1.0 g, 1.0 eq.) in xylenes (3.0 mL) and the mixture was heated to 150 °C. At this temperature  $\alpha$ -methylstyrene (2.1 eq.) was added dropwise and the reaction was stirred for 18 h at that temperature. The reaction mixture was cooled to rt and the crude reaction product was concentrated *in vacuo*, and purified *via* column chromatography (silica gel, petroleum ether 5:1 ethyl acetate), to give a pale-yellow solid (761 mg, 24%), that can be further purified through recrystallization from *n*-hexane.



Single crystals suitable for scXRD were obtained from a saturated *n*-hexane solution at -20 °C.

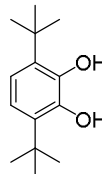
<sup>1</sup>H NMR (400 MHz, CD<sub>2</sub>Cl<sub>2</sub>)  $\delta$  = 7.43 - 7.19 (m, 10H, **H<sub>Ph</sub>**), 7.01 (d,  $J$  = 2.2 Hz, 1H, *meta*-**H<sub>cat</sub>**), 6.72 (d,  $J$  = 2.2 Hz, 1H, *ortho*-**H<sub>cat</sub>**), 5.38 (s, 1H, **O**H****), 4.28 (s, 1H, **O**H****), 1.75 (s, 6H, C(**CH<sub>3</sub>**)<sub>2</sub>), 1.67 (s, 6H, C(**CH<sub>3</sub>**)<sub>2</sub>).

<sup>13</sup>C NMR (101 MHz, CD<sub>2</sub>Cl<sub>2</sub>)  $\delta$  = 151.5, 149.1, 145.5, 143.8, 139.0, 135.8, 129.5, 128.3, 127.3, 127.1, 126.4, 125.9, 116.3, 113.1, 43.1 (C(**CH<sub>3</sub>**)<sub>2</sub>), 42.4 (C(**CH<sub>3</sub>**)<sub>2</sub>), 31.1 (C(**CH<sub>3</sub>**)), 29.7 (C(**CH<sub>3</sub>**)).

**GCMS EI+ (A)** 19.0 min.  $m/z$  346.2 (69%) [M]<sup>+</sup>, 331.2 (100%) [M - CH<sub>3</sub>]<sup>+</sup>, 253.1 (39%) [M - C<sub>6</sub>H<sub>6</sub> - CH<sub>3</sub>]<sup>+</sup>, 91.1 (24%) [PhCH<sub>2</sub>]<sup>+</sup>.

### 5.2.1.3 3,6-Di-*tert*-butyl-catechol ( $\text{H}_2\text{cat}^{3,6\text{-tBu}}$ )

The compound was prepared under guidance of literature known procedures.<sup>260,440,441</sup> Bis(catecholato)titanium (0.1 eq.) was added to a solution of catechol (2.6 g, 1.0 eq.) in toluene/xylenes (5.9 mL) in a 35 mL heavy-walled ampulla with a side valve (*FengTecEx*). The mixture was frozen in a liquid nitrogen bath and the vessel evacuated ( $10^{-2}$  mbar). *Isobutylene* (2.5 eq.) was cautiously condensed onto the frozen reaction mixture (the volume was gauged by the respective fill level which was priorly measured). The ampulla was thoroughly sealed, placed behind an additional protecting shield, and the mixture allowed to warm to rt. The mixture was then gradually heated in 20 K steps to a final temperature of 140 °C and allowed to proceed for 15 h at this temperature. The dark brown to red reaction mixture was cooled to 0 °C and the valve cautiously opened under vigorous stirring of the reaction mixture, to allow remaining gas to evaporate. The mixture was filtered over celite eluting with diethyl ether and concentrated *in vacuo*. In contrast to literature protocols, the crude residue revealed a reduced proportion of the target species. This is most likely reasoned by a reduced pressure of *isobutylene* in the present case, which could not be increased for technical reasons. Therefore, another purification protocol was found necessary. The compound was purified using column chromatography (silica gel, petroleum ether 10:1 ethyl acetate) to yield the analytically pure target compound (2.1 g, 40%). Minor pale green coloration was found reduced upon recrystallization from *n*-hexane or removed upon *vacuum* distillation (10 mbar, 140 °C).



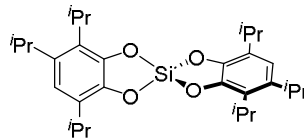
$^1\text{H NMR}$  (200 MHz,  $\text{CDCl}_3$ )  $\delta$  6.77 (s, 2H,  $\text{CH}$ ), 5.36 (s, 2H,  $\text{OH}$ ), 1.41 (s, 18H,  $\text{CH}_3$ ).

$^{13}\text{C NMR}$  (101 MHz,  $\text{CDCl}_3$ )  $\delta$  143.3 ( $\text{C}_{\text{Ar}}\text{O}$ ), 134.3 ( $\text{C}_{\text{Ar}}\text{C}_4\text{H}_9$ ), 117.6 ( $\text{C}_{\text{Ar}}\text{H}$ ), 34.1 ( $\text{C}_q(\text{CH}_3)_3$ ), 30.0 ( $\text{CH}_3$ ).

$\text{GCMS EI}^+$  (B) 12.9 min.  $m/z$  222.3  $[\text{M}]^+$  (24%), 207.4  $[\text{M} - \text{CH}_3]^+$  (100%).

**5.2.1.4 Bis(3,4,6-tri-*iso*-propylcatecholato)silane (**1**<sup>3,4,5-*iPr*</sup>)<sup>w</sup>**

Under a dry inert atmosphere 3,4,6-tri-*iso*-propylbenzene-1,2-diol (300 mg, 2.0 eq.) and trichlorosilane (1.0 eq) were dissolved in dry acetonitrile (5.0 mL) and stirred at room temperature overnight. The formed brown-pink viscous precipitate was dried under reduced pressure after decantation of the solvent and washed with acetonitrile to give the title compound as colorless pink solid (180 mg, 57%).



<sup>1</sup>H NMR (600 MHz, CD<sub>2</sub>Cl<sub>2</sub>) δ 6.80 (s, 2H, C<sub>Ar</sub>H), 3.33 (m, 2H, C<sub>Pr</sub>H), 3.19 (m, 4H, C<sub>Pr</sub>H), 1.37 (m, 12H, CH(CH<sub>3</sub>)<sub>2</sub>), 1.25 (m, 24H, CH(CH<sub>3</sub>)<sub>2</sub>).

<sup>13</sup>C NMR (100 MHz, CD<sub>2</sub>Cl<sub>2</sub>) δ 144.5, 142.0, 139.9, 131.4, 131.1, 129.4, 116.5, 116.1, 29.2, 28.4, 27.0, 24.0, 24.0, 22.1, 20.8.

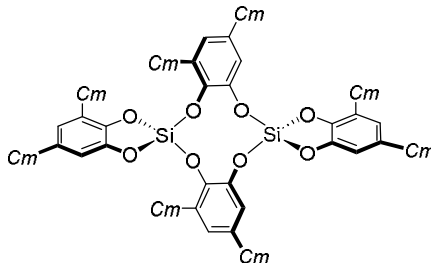
<sup>29</sup>Si NMR (79 MHz, CD<sub>2</sub>Cl<sub>2</sub>) δ -41.2.

---

<sup>w</sup> **1**<sup>3,4,6-*iPr*</sup> was first synthesized in the course of this work and subsequently compiled in cooperation with *R. MASKEY*, who optimized reaction conditions and completed the characterization of the compound.

**5.2.1.5 Dimeric bis(3,5-di-cumyl-catecholato)silane [1<sup>3,5-Cm</sup>]<sub>2</sub>**

3,5-Di-cumyl-catechol (100 mg, 4.0 eq.) was dissolved in acetonitrile (2 mL) and trichlorosilane (2.1 eq.) was added dropwise at rt. The reaction mixture was stirred for 18 h, the colorless precipitate separated from the solution and dried *in vacuo* (68 mg, 95  $\mu$ mol, 66%).



Single crystals suitable for scXRD were obtained from a saturated CH<sub>2</sub>Cl<sub>2</sub> solution at rt.

NMR spectroscopy indicated the presence of a diastereomeric mixture rather than the single isomer structure obtained from scXRD.

**<sup>1</sup>H NMR** (600 MHz, CD<sub>2</sub>Cl<sub>2</sub>, 298K)  $\delta$  = 7.36 - 6.49 (m, 12H, C<sub>Ar</sub>H), 1.73 - 1.36 (m, 12H, CH<sub>3</sub>).

**<sup>13</sup>C NMR** (151 MHz, CD<sub>2</sub>Cl<sub>2</sub>, 298K)  $\delta$  = 151.2, 151.0, 150.7, 150.6, 150.1, 149.7, 147.0, 146.6, 146.2, 145.3, 143.8, 143.0, 142.8, 142.4, 141.2, 140.9, 140.3, 140.0, 139.9, 139.8, 139.6, 139.5, 134.2, 128.3, 127.9, 127.0, 126.5, 126.4, 126.1, 125.9, 125.6, 125.5, 125.1, 122.0, 121.6, 121.4, 119.2, 118.1, 117.7, 117.2, 116.6, 116.1, 111.5, 111.2, 43.4, 43.2, 42.9, 42.9, 42.7, 42.4, 42.2, 42.0, 42.0, 31.3, 31.1, 31.0, 30.7, 30.5, 30.2, 29.8, 29.3, 28.9, 28.4, 28.0, 27.8, 27.6.

**<sup>29</sup>Si NMR** (119 MHz, CD<sub>2</sub>Cl<sub>2</sub>, 298K)  $\delta$  = -62.8, -71.2 (br), -71.7 (br), -71.9.

**5.2.1.6 1<sup>3,6-tBu</sup>-(HNMe<sub>2</sub>)<sub>2</sub>**

HSi(NMe<sub>2</sub>)<sub>3</sub> (1.0 eq.) was slowly added to a solution of 3,6-di-*tert*-butyl-catechol (22 mg, 2.1 eq.) in acetonitrile. An immediate gas deconvolution was apparent. After one hour, a colorless crystalline solid had formed (suitable for scXRD). The solid was separated from the solution and dried *in vacuo* (23 mg, 87%).

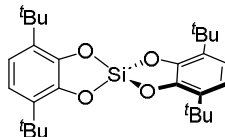
**<sup>1</sup>H NMR** (600 MHz, CDCl<sub>3</sub>) 6.67 (s, 4H, C<sub>Ar</sub>H), 2.89 (br, 2H, NH), 2.41 (s, 12H, NCH<sub>3</sub>), 1.45 (s, 36H, CH<sub>3</sub>).

**<sup>13</sup>C NMR** (151 MHz, CDCl<sub>3</sub>)  $\delta$  147.1 (C<sub>Ar</sub>O), 132.4 (C<sub>Ar</sub>C<sub>4</sub>H<sub>9</sub>), 115.4 (C<sub>Ar</sub>H), 39.7 (NCH<sub>3</sub>), 34.1 (C<sub>q</sub>(CH<sub>3</sub>)<sub>3</sub>), 30.0 (CCH<sub>3</sub>).

**<sup>29</sup>Si NMR** (119 MHz, CDCl<sub>3</sub>)  $\delta$  -142.0.

**5.2.1.7 Bis(3,6-di-*tert*-butyl-catecholato)silane (**1<sup>3,6-*t*Bu</sup>**)**

$\text{HSiCl}_3$  (1.0 eq.) was slowly added to a solution of 3,6-di-*tert*-butyl-catechol (400 mg, 2.1 eq.) in acetonitrile. The mixture was stirred at rt overnight and a continuous exchange of the inert atmosphere was ensured. The formed colorless precipitate was filtered, washed with acetonitrile, and dried *in vacuo*, to yield a colorless solid (287 mg, 71%).



$^1\text{H}$  NMR (600 MHz,  $\text{CDCl}_3$ )  $\delta$  6.90 (s, 4H,  $\text{C}_{Ar}\text{H}$ ), 1.40 (s, 36H,  $\text{C}(\text{CH}_3)_3$ ).

$^{13}\text{C}$  NMR (151 MHz,  $\text{CDCl}_3$ )  $\delta$  144.9 ( $\text{C}_{Ar}\text{O}$ ), 134.4 ( $\text{C}_{Ar}\text{C}_4\text{H}_9$ ), 119.2 ( $\text{C}_{Ar}\text{H}$ ), 34.3 ( $\text{C}_q(\text{CH}_3)_3$ ), 29.6 ( $\text{CH}_3$ ).

$^{29}\text{Si}$  NMR (119 MHz,  $\text{CDCl}_3$ )  $\delta$  -42.9.

**HRMS EI+** ( $m/z$ ) calc. for  $[\text{C}_{28}\text{H}_{40}\text{O}_4\text{Si}]^+ [\text{M}]^+$ , 468.2690, found 468.2704 (23%), deviation 2.9 ppm; calc. for  $[\text{C}_{27}\text{H}_{37}\text{O}_4\text{Si}]^+ [\text{M}-\text{CH}_3]^+$ , 453.2456, found 453.2466 (100%), deviation 2.3 ppm.

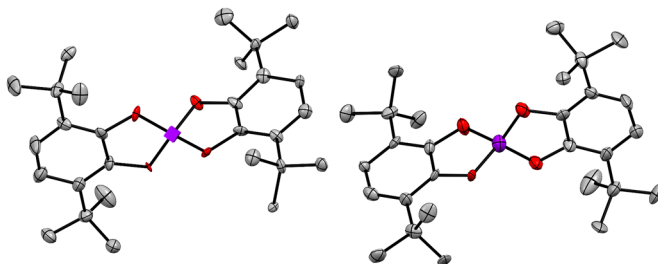
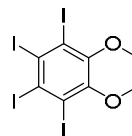


Figure 50. Molecular, scXRD derived structure of **1<sup>3,6-*t*Bu</sup>**. The structure is shown to confirm its connectivity and cannot be used for the discussion of structural data, as full refinement was prevented by poor quality of the crystals. Hydrogen atoms are omitted for clarity. Crystals were obtained from a concentrated chloroform solution.

## 5.2.2 Synthesis Route to Adducts of $1^{\text{CF}_3}$

### 5.2.2.1 1,2,3,4-Tetraiodo-5,6-dimethoxy-benzene (ver<sup>l</sup>)

N-iodosuccinimid (NIS) (4.50 eq.) was added to a solution of veratrole (3.0 g, 1.0 eq.) in chloroform (200 mL) in an argon-atmosphere and the suspension was cooled to 0 °C. At that temperature, trifluoromethanesulfonic acid (1.0 eq.) was added dropwise. The reaction mixture was warmed to 65 °C and stirred for two hours at that temperature. After cooling briefly, an additional quantity of NIS (1.50 eq.) was added, and the heating was continued for two hours. The mixture was allowed to cool to room temperature, and water was added. The phases were separated, and the organic layer was washed with aqueous  $\text{Na}_2\text{S}_2\text{O}_3$ -solution (1 M) and brine. The organic phase was dried over sodium sulfate and concentrated *in vacuo* to a volume of approx. 100 mL. 900 mL ethanol were added, the mixture kept at -20 °C for 12 h and the formed cloudy precipitate was filtered off, washed with ethanol and dried *in vacuo*, to give a bright yellow solid (10.1 g, 15.74 mmol, 72%), that yielded thin, yellow needles after recrystallization from toluene.



$^1\text{H NMR}$  (400 MHz,  $\text{CDCl}_3$ )  $\delta$  3.82 (s, 6H,  $\text{CH}_3$ ).

$^{13}\text{C NMR}$  (101 MHz,  $\text{CDCl}_3$ )  $\delta$  152.4 ( $\text{C}_q\text{O}$ ), 115.5 (*meta-C*), 108.4 (*ortho-C*), 60.5 ( $\text{OCH}_3$ ).

**HRMS DART+** ( $m/z$ ) calc. for  $[\text{M}+\text{OH}]^+$  658.6568, found 658.6555 (100%), deviation 2.0 ppm; calc. for  $[\text{M}]^+$  641.6541, found 641.6529 (42%), deviation 1.9 ppm.

**5.2.2.2 1,2-Dimethoxy-3,4,5,6-tetra(trifluoromethyl)benzene (ver<sup>CF<sub>3</sub></sup>)**

The trifluoromethylation protocol was developed in preliminary work,<sup>289</sup> adapted from a literature known synthesis.<sup>290</sup> Freshly purified copper(I) bromide<sup>442</sup> (9.0 eq.) was suspended in DMF (47 mL) and (trifluoromethyl)trimethylsilane (7.5 eq.) was added.



The mixture was cooled to  $-5\text{ }^{\circ}\text{C}$  and KF (7.5 eq.) was added in roughly three equal portions, so that the temperature rose not above  $0\text{ }^{\circ}\text{C}$ . Subsequently DMI (12 ml) was added, and the mixture stirred for 3 h at  $0\text{ }^{\circ}\text{C}$ . Then, 1,2,3,4-tetraiodo-5,6-dimethoxybenzene (5.00 g, 1.0 eq.) was added in one portion followed by another 56 mL DMI. The mixture was stirred for 30 h, then water (50 mL) and diethyl ether (200 mL) were added, and the phases separated. The organic phase was washed with water, half concentrated brine and brine, dried ( $\text{Na}_2\text{SO}_4$ ) and afterwards concentrated *in vacuo*. The residue was purified using column chromatography (silica gel, petroleum ether 19:1 ethyl acetate), to give a colorless solid (2.29 g, 72%).

Importantly, and as noted before,<sup>290</sup> yield and formation of the described product depend heavily on the purity of the applied CuBr (ideally colorless) and the content of water in solvents. The formation of the reactive copper reagent can be verified *via*  $^{19}\text{F}$  NMR spectroscopy.<sup>290</sup>

Single crystals suitable for scXRD developed from a saturated petroleum ether, ethyl acetate (19:1) solution at rt (details see section 7.6).

$^1\text{H}$  NMR (400 MHz,  $\text{CDCl}_3$ )  $\delta$  4.03 (s,  $\text{CH}_3$ ).

$^{13}\text{C}$  NMR (101 MHz,  $\text{CDCl}_3$ )  $\delta$  156.2 ( $\text{C}_q\text{O}$ ), 129.3 (q,  $^2J_{\text{CF}} = 32.8\text{ Hz}$ ,  $\text{C}_q\text{CF}_3$ ), 121.7 (q,  $^1J_{\text{CF}} = 277\text{ Hz}$ ,  $\text{CF}_3$ ), 61.9 ( $\text{OCH}_3$ ).

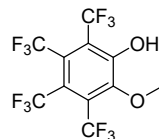
$^{19}\text{F}$  NMR (376 MHz,  $\text{CDCl}_3$ )  $\delta$   $-51.4$  (br, 12F),  $-56.7$  (m, 12F).

GCMS EI+ (A) 5.3 min.  $m/z$  410.0  $[\text{M}]^+$  (100%), 69.0  $[\text{CF}_3]^+$  (41%).

Elemental analysis calc. C 35.14%, H 1.47%; found C 35.17%, H 1.84%.

**5.2.2.3 2-Methoxy-3,4,5,6-tetra(trifluoromethyl)phenol (gua<sup>CF<sub>3</sub></sup>)**

1,2-Dimethoxy-3,4,5,6-tetra(trifluoromethyl)benzene (1.60 g, 1.0 eq.) was dissolved in dimethylacetamide (25 mL) in an argon-atmosphere. Potassium hydroxide (2.5 eq.) was added, and the mixture stirred for 18 h at room temperature. The orange solution was cooled to 0 °C and quenched through slow addition of 15 mL water and 10 mL HCl<sub>(aq.)</sub> (1 M). The colorless precipitate was filtered off, washed with water, and taken up in diethyl ether. The filtrate was extracted once with diethyl ether and the combined organic phases were washed with water, half concentrated brine, and brine, and dried over Na<sub>2</sub>SO<sub>4</sub>. The residue was purified using column chromatography (silica gel, petroleum ether 1:1 dichloromethane), to yield a colorless solid (1.35 g, 87%), which can be recrystallized from *n*-heptane.



Single crystals suitable for scXRD developed from a saturated dichloromethane solution at rt (see section 7.6).

**<sup>1</sup>H NMR** (600 MHz, CDCl<sub>3</sub>) δ 7.04 (s, 1H, **OH**), 4.08 (s, 3H, **CH<sub>3</sub>**).

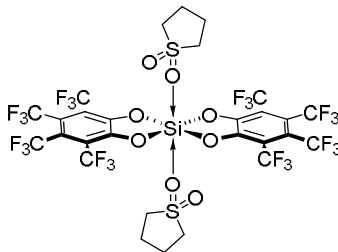
**<sup>13</sup>C NMR** (151 MHz, CDCl<sub>3</sub>) δ 152.6 (**C<sub>q</sub>OCH<sub>3</sub>**), 149.8 (**C<sub>q</sub>OH**), 128.2 (q, <sup>2</sup>J<sub>CF</sub> = 37.2 Hz, **C<sub>q</sub>CF<sub>3</sub>**), 127.1 (q, <sup>2</sup>J<sub>CF</sub> = 37.1 Hz, **C<sub>q</sub>CF<sub>3</sub>**), 123.2 (q, <sup>2</sup>J<sub>CF</sub> = 36.8 Hz, **C<sub>q</sub>CF<sub>3</sub>**), 121.9 (q, <sup>1</sup>J<sub>CF</sub> = 276 Hz, **CF<sub>3</sub>**), 121.7 (q, <sup>1</sup>J<sub>CF</sub> = 277 Hz, 2 **CF<sub>3</sub>**), 121.6 (q, <sup>1</sup>J<sub>CF</sub> = 277 Hz, **CF<sub>3</sub>**), 120.4 (q, <sup>2</sup>J<sub>CF</sub> = 34.2 Hz, **C<sub>q</sub>CF<sub>3</sub>**), 64.3 (**OCH<sub>3</sub>**).

**<sup>19</sup>F NMR** (376 MHz, CDCl<sub>3</sub>) δ -51.0 (sept, <sup>5</sup>J<sub>FF</sub> = 15.8 Hz), -51.7 (sept, <sup>5</sup>J<sub>FF</sub> = 15.8 Hz), -56.1 (q, <sup>5</sup>J<sub>FF</sub> = 16.0 Hz), -57.0 (q, <sup>5</sup>J<sub>FF</sub> = 16.0 Hz).

**GCMS EI+ (A)** 6.3 min. m/z 396.2 [M]<sup>+</sup> (68%), 356.0 [M - 2 HF]<sup>+</sup> (100%), 69.0 [CF<sub>3</sub>]<sup>+</sup> (26%).

#### 5.2.2.4 $1^{\text{CF}_3}$ -(sulfolane) $_2$

To a solution of  $\text{gua}^{\text{CF}_3}$  (1.35 g, 3.41 mmol, 2.0 eq.) in a sulfolane, benzene mixture (12 mL, 97:3 V%)  $\text{HSiCl}_3$  (195  $\mu\text{L}$ , 1.93 mmol, 1.1 eq.) was added dropwise at rt. The reaction mixture was stirred for 15 min and then heated to 100 °C for 15 h. After cooling to rt, the colorless, crystalline solid (suitable for scXRD, details see section 7) was filtered off and washed with benzene, dichloromethane, *n*-pentane and dried *in vacuo* (1.63 g, 1.58 mmol, 90%).



$^1\text{H NMR}$  (600 MHz,  $\text{CD}_2\text{Cl}_2$ )  $\delta$  3.23 (m, 8H,  $\alpha\text{-CH}_2$ ), 2.24 (m, 8H,  $\beta\text{-CH}_2$ ).

$^{13}\text{C NMR}$  (151 MHz,  $\text{CD}_2\text{Cl}_2$ )  $\delta$  52.0 ( $\alpha\text{-CH}_2$ ), 23.2 ( $\beta\text{-CH}_2$ ).

Aromatic signals not detected due to limited solubility and high fluorine content (coupling).

$^{19}\text{F NMR}$  (188 MHz,  $\text{CD}_2\text{Cl}_2$ )  $\delta$  -51.7 (m, 12F), -56.7 (m, 12F).

$^{29}\text{Si NMR}$  spectroscopy was prevented by limited solubility in common deuterated organic solvents.

**IR (ATR-FTIR)**  $\tilde{\nu}$  [ $\text{cm}^{-1}$ ] 3070 (w), 1644 (m), 1589 (m), 1462 (s), 1378 (s), 1354 (s), 1266 (s), 1148 (s), 973 (s).

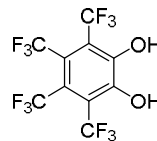
**HRMS ESI-** ( $m/z$ ) calc. for  $[\text{1}^{\text{CF}_3} + \text{OH}]^-$  818.9372, found 818.9373 (59%), deviation -0.1 ppm; calc. for  $[\text{1}^{\text{CF}_3}]_2^-$  583.9450, found 583.9449 (6%), deviation 0.2 ppm.

**Elemental analysis** calc. +0.5  $\text{CH}_2\text{Cl}_2$  C 31.96%, H 1.60%; found C 31.99%, H 1.62%.

**HRMS DART+** ( $m/z$ ) calc. for  $[\text{M} + \text{OH}]^+$  658.6568, found 658.6555 (100%), deviation 2.0 ppm; calc. for  $[\text{M}]^+$  641.6541, found 641.6529 (42%), deviation 1.9 ppm.

### 5.2.2.5 3,4,5,6-Tetra(trifluoromethyl)catechol ( $\mathbf{H}_2\text{cat}^{\text{CF}_3}$ )

Clean formation of the per(trifluoromethyl)catechol was observed upon addition of water to  $\mathbf{1}^{\text{CF}_3}$ -(sulfolane)<sub>2</sub> in  $\text{CH}_2\text{Cl}_2$ . The suspension was filtered, and sXRD analysis of suitable crystals formed from the filtrate revealed the molecular structure of  $\mathbf{H}_2\text{cat}^{\text{CF}_3}$  (see section 7.6). To obtain the compound without residues of sulfolane, donors in  $\mathbf{1}^{\text{CF}_3}$ -(sulfolane)<sub>2</sub> (30.0 mg, 1.0 eq.) were exchanged with acetonitrile in advance (as described in 5.2.2.7). Subsequent hydrolyzation (2.5 eq.) of a suspension in  $\text{CH}_2\text{Cl}_2$  (1 mL), filtration and concentration of the filtrate *in vacuo* yielded per(trifluoromethyl)catechol as colorless solid, that develops a purple shade within a day on ambient atmosphere. (17.0 mg, 44.5  $\mu\text{mol}$ , 76%).



$^1\text{H NMR}$  (400 MHz,  $\text{CD}_2\text{Cl}_2$ )  $\delta$  7.12 (s,  $\text{OH}$ ).

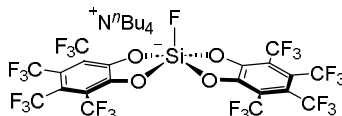
$^{13}\text{C NMR}$  (151 MHz,  $\text{CD}_2\text{Cl}_2$ )  $\delta$  147.4 ( $\text{C}_q\text{OH}$ ), 122.8 (q,  $^1J_{\text{CF}} = 276$  Hz,  $\text{CF}_3$ ), 122.3 (q,  $^1J_{\text{CF}} = 277$  Hz,  $\text{CF}_3$ ), 118.9 (q,  $^2J_{\text{CF}} = 33.2$  Hz,  $\text{CF}_3$ ).

$^{19}\text{F NMR}$  (188 MHz,  $\text{CD}_2\text{Cl}_2$ )  $\delta$  -51.8 (m, 6F), -56.2 (m, 6F).

**HRMS EI+** (m/z) calc. for  $[\text{M}]^+$  381.9858, found 381.9884 (14%), deviation -6.8 ppm; calc. for  $[\text{M} - \text{F}]^+$  362.9874, found 362.9831 (42%), deviation 11.8 ppm; calc. for  $[\text{M} - \text{CF}_3 + \text{H}]^+$  313.9984, found 313.9778 (90%), deviation 65.6 ppm.

### 5.2.2.6 [N(*n*Bu)<sub>4</sub>][F-1CF<sub>3</sub>]

1CF<sub>3</sub>-(sulfolane)<sub>2</sub> (20.0 mg, 1.0 eq.) and tetra-*n*-butylammonium difluoro-triphenylsilicate (1.0 eq.) were mixed in CH<sub>2</sub>Cl<sub>2</sub> (0.2 mL). The solid reactants dissolved immediately to give a colorless solution. Addition of *n*-pentane led to the precipitation of a colorless solid which was separated from the solution, washed once with *n*-pentane, and dried *in vacuo* (18.7 mg, 92%).



Single crystals suitable for scXRD developed from a saturated dichloromethane solution at rt confirmed the connectivity of the title species (cmp. section 7.6).

<sup>1</sup>H NMR (400 MHz, CD<sub>2</sub>Cl<sub>2</sub>) δ 3.06 (m, 2H), 1.59 (quin, <sup>3</sup>J<sub>HH</sub> = 8.2, 7.8 Hz, 2H), 1.40 (sext, <sup>3</sup>J<sub>HH</sub> = 7.3 Hz, 2H), 1.00 (t, <sup>3</sup>J<sub>HH</sub> = 7.3 Hz, 3H).

<sup>13</sup>C NMR (151 MHz, CD<sub>2</sub>Cl<sub>2</sub>) δ 152.1 (C<sub>q</sub>O), 123.1 (d, <sup>1</sup>J<sub>CF</sub> = 276 Hz, CF<sub>3</sub>), 122.9 (d, <sup>1</sup>J<sub>CF</sub> = 276 Hz, CF<sub>3</sub>), 115.0 (d, <sup>2</sup>J<sub>CF</sub> = 37.8 Hz, C<sub>q</sub>CF<sub>3</sub>), 59.0 (α-CH<sub>2</sub>), 23.7 (β-CH<sub>2</sub>), 19.6 (γ-CH<sub>2</sub>), 13.1 (CH<sub>3</sub>).

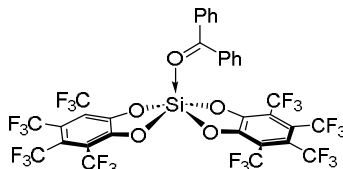
Quartets appear as doublets due to spectrometer sensitivity.

<sup>19</sup>F NMR (376 MHz, CD<sub>2</sub>Cl<sub>2</sub>) δ -51.3 (dq, J = 15.3, 7.5, 6.1 Hz, 12F), -56.7 (qd, J = 15.2, 5.3 Hz, 12F), -132.1 (<sup>1</sup>J<sub>SiF</sub> = 194 Hz, 1F).

<sup>29</sup>Si NMR (119 MHz, CD<sub>2</sub>Cl<sub>2</sub>) δ -105.0 (<sup>1</sup>J<sub>SiF</sub> = 194 Hz).

5.2.2.7  $1^{\text{CF}_3}$ -(OCPh<sub>2</sub>)

$1^{\text{CF}_3}$ -(sulfolane)<sub>2</sub> (350 mg, 1.0 eq.) was suspended in a mixture of acetonitrile and CH<sub>2</sub>Cl<sub>2</sub> (2.5 mL, 1:1) and stirred for 12 h (exchange of sulfolane donors through acetonitrile). The colorless solid was filtered off, washed with benzene, CH<sub>2</sub>Cl<sub>2</sub> and *n*-pentane and then suspended in toluene (5 mL). To the suspension benzophenone (20.0 eq.) was added and the liquid phase turned immediately yellow. The solution was stirred for 15 min and the volatiles were removed *in vacuo*. This step was repeated for a total of five times, until all components were found to be a homogeneous solution without observable solid residues. The yellow solution was then concentrated *in vacuo* and the residue washed with *n*-pentane to remove excess benzophenone, taken up in CH<sub>2</sub>Cl<sub>2</sub>, filtered, and again concentrated *in vacuo* to yield a yellow solid (215 mg, 65%). Single crystals suitable for scXRD were obtained from a concentrated benzene solution.



$^1\text{H NMR}$  (600 MHz, CD<sub>2</sub>Cl<sub>2</sub>)  $\delta$  7.83 (d,  $^3J_{\text{HH}} = 7.7$  Hz, 2H, *ortho-H*), 7.74 (t,  $^3J_{\text{HH}} = 7.5$  Hz, 1H, *para-H*), 7.55 (t,  $^3J_{\text{HH}} = 7.5$  Hz, 2H, *meta-H*).

$^{13}\text{C NMR}$  (151 MHz, CD<sub>2</sub>Cl<sub>2</sub>)  $\delta$  153.3 ( $\text{C}_q\text{OSi}$ ), 152.1 ( $\text{C}_{\text{Ar}}$ ), 137.2 ( $\text{C}_{\text{Ar}}$ ), 133.7 ( $\text{C}_{\text{Ar}}$ ), 130.6 ( $\text{C}_{\text{Ar}}$ ), 123.8 (q,  $^1J_{\text{CF}} = 278$  Hz,  $\text{CF}_3$ ), 123.5 (q,  $^1J_{\text{CF}} = 276$  Hz,  $\text{CF}_3$ ), 117.6 (q,  $^2J_{\text{CF}} = 34.7$  Hz,  $\text{C}_q\text{CF}_3$ ), 115.9 (q,  $^2J_{\text{CF}} = 33.8$  Hz,  $\text{C}_q\text{CF}_3$ ).

Carbonyl-carbon not detected.

$^{19}\text{F NMR}$  (188 MHz, CD<sub>2</sub>Cl<sub>2</sub>)  $\delta$  -51.6 (m, 12F), -56.8 (m, 12F).

$^{29}\text{Si NMR}$  (119 MHz, CD<sub>2</sub>Cl<sub>2</sub>)  $\delta$  -104.9.

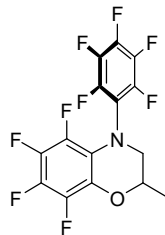
**HRMS ESI**– (m/z) calc. for  $[\text{M}-\text{C}_6\text{H}_5]^-$  892.9529, found 892.9577 (1%), deviation -8.1 ppm; calc. for  $[\text{1}^{\text{CF}_3}+\text{OCH}_3]^-$  818.9372, found 818.9370 (100%), deviation 0.2 ppm; calc. for  $[\text{1}^{\text{CF}_3}+\text{OH}]^-$  804.9216, found 804.9222 (36%), deviation -7.5 ppm.

**IR** (ATR-FTIR)  $\tilde{\nu}$  [cm<sup>-1</sup>] 2990, 1477, 1379, 1266, 1214, 1153, 1042, 969, 867.

## 5.2.3 Synthetic Route to 2

### 5.2.3.1 am<sup>F</sup>ph<sup>F</sup>C<sub>3</sub>H<sub>6</sub>

To a solution of *bis*(pentafluorophenyl)amine<sup>305</sup> (25.0 g, 1.0 eq.) in THF (350 mL) LiHMDS (1.05 eq.) was added in one portion at 0 °C. The reaction mixture was stirred for 30 min at 0 °C, propylene oxide (2.0 eq.) was added in one portion and the mixture stirred for an additional hour. The mixture was then heated to 80 °C under reflux conditions for 14 h. The crude reaction mixture was concentrated to approx. 100 mL and diethyl ether and water (150 mL each) were added, the phases separated, and the aqueous phase extracted with diethyl ether (x2). The combined organic layers were washed with water, sat. aq. K<sub>2</sub>CO<sub>3</sub> and brine and dried over MgSO<sub>4</sub>, to yield a pale-yellow oil, that solidifies upon staying. The compound was purified *via vacuum* distillation (120 °C, 10<sup>-1</sup> mbar) to yield a colorless solid (22.2 g, 80%). Colorless crystals suitable for scXRD developed from a saturated chloroform solution at ambient temperature.



<sup>1</sup>H NMR (600 MHz, CDCl<sub>3</sub>) δ 4.29 (m, 1H, **CH**), 3.50 (dd, <sup>3</sup>J<sub>HH</sub> = 13.2 Hz, J<sub>HH</sub> = 2.4 Hz, 1H, **CH<sub>2</sub>**), 3.42 (dd, <sup>3</sup>J<sub>HH</sub> = 13.3 Hz, J<sub>HH</sub> = 8.5 Hz, 1H, **CH<sub>2</sub>**), 1.45 (d, <sup>3</sup>J<sub>HH</sub> = 6.4 Hz, 3H, **CH<sub>3</sub>**).

<sup>13</sup>C NMR (151 MHz, CDCl<sub>3</sub>) δ 143.8 (d, <sup>1</sup>J<sub>CF</sub> = 249 Hz, **CF**), 139.5 (d, <sup>1</sup>J<sub>CF</sub> = 254 Hz, **CF**), 138.9 (d, <sup>1</sup>J<sub>CF</sub> = 244 Hz, **CF**), 138.0 (d, <sup>1</sup>J<sub>CF</sub> = 244 Hz, **CF**), 136.2 (d, <sup>1</sup>J<sub>CF</sub> = 244 Hz, **CF**), 135.5 (d, <sup>1</sup>J<sub>CF</sub> = 244 Hz, **CF**), 131.8 (**CO**), 121.6 (**CN**), 117.3 (**CN**), 70.8 (**CH**), 55.5 (**CH<sub>2</sub>**), 17.7 (**CH<sub>3</sub>**).

For the <sup>13</sup>C NMR spectrum a highly concentrated sample was prepared. Broadened resonances were observed, finer coupling is not listed due to limited intensity and resolution.

<sup>19</sup>F NMR (376 MHz, CDCl<sub>3</sub>) δ -148.8 (br, 2F), -157.9 (ddd, <sup>3</sup>J<sub>FF</sub> = 21.3 Hz, <sup>4</sup>J<sub>FF</sub> = 6.3, J<sub>FF</sub> = 3.3 Hz, 1F), -158.5 (t, <sup>3</sup>J<sub>FF</sub> = 21.4 Hz, 1F), -162.5 (br, 2F), -163.7 (ddd, <sup>3</sup>J<sub>FF</sub> = 21.6 Hz, <sup>4</sup>J<sub>FF</sub> = 6.3 Hz, J<sub>FF</sub> = 3.9 Hz, 1F), -168.3 (td, <sup>3</sup>J<sub>FF</sub> = 21.7, J<sub>FF</sub> = 3.4 Hz, 1F), -170.0 (td, <sup>3</sup>J<sub>FF</sub> = 21.6 Hz, J<sub>FF</sub> = 3.9 Hz, 1F).

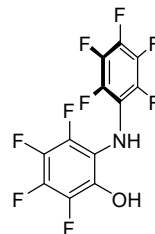
**GCMS EI+ (A)** 10.5 min. m/z 387.0 [M]<sup>+</sup> (97%).

**HRMS EI+ (m/z)** calc. for C<sub>15</sub>H<sub>6</sub>F<sub>9</sub>NO [M]<sup>+</sup>, 387.0300; found 387.0319 (100%), deviation 4.8 ppm.

**Elemental analysis** calc. C 46.53%, H 1.56%, N, 3.62%. found C 46.58%, H 2.01%, N 3.62%.

5.2.3.2 am<sup>F</sup>ph<sup>F</sup>H<sub>2</sub>

Aluminum (2.96 g, 2.5 eq.) and iodine (3.0 eq.) were refluxed in toluene (145 mL) for one hour, after which the reaction mixture turned from violet to colorless. The reaction mixture was allowed to cool to rt, and the substrate (17.0 g) was added in one portion, upon which the mixture took a violet to red tone. After stirring for 10 min at rt, the reaction was again refluxed for four hours, and reaction control by GCMS indicated full conversion. The mixture was diluted with diethyl ether (100 mL), cooled to 0 °C, then slowly quenched with 6 M HCl (aq.) (100 mL) and subsequently stirred for 30 min at 0 °C. The phases were separated, the aqueous phase extracted with diethyl ether (x2 50 mL) and the combined organic phases washed with sat. NaHSO<sub>3</sub> (aq.) (50 mL) (solution turned from a brownish tone to orange) and dried over MgSO<sub>4</sub>. The residue was dried rigorously *in vacuo* and purified *via* sublimation at 40 °C and dynamic *vacuum* (approx. 5x 10<sup>-2</sup> mbar). The off-white sublimate was recrystallized from *n*-hexane and washed with small amounts cold (0 °C) *n*-hexane, to yield the product as a colorless solid (10.2 g, 67%).<sup>x</sup>



<sup>1</sup>H NMR (400 MHz, CDCl<sub>3</sub>) δ 5.58 (br, 1H), 5.12 (br, 1H).

<sup>13</sup>C NMR (151 MHz, CDCl<sub>3</sub>) δ 143.0 (d, <sup>1</sup>J<sub>CF</sub> = 246 Hz, CF), 140.14 (d, <sup>1</sup>J<sub>CF</sub> = 245 Hz, CF), 139.2 (d, <sup>1</sup>J<sub>CF</sub> = 250 Hz, CF), 138.0 (d, <sup>1</sup>J<sub>CF</sub> = 250 Hz, CF), 137.3 (d, <sup>1</sup>J<sub>CF</sub> = 241 Hz, CF), 136.8 (d, <sup>1</sup>J<sub>CF</sub> = 250 Hz, CF), 135.8 (CO), 135.3 (d, <sup>1</sup>J<sub>CF</sub> = 246 Hz, CF), 119.3 (CN), 115.0 (CN).

For the <sup>13</sup>C NMR spectrum a highly concentrated sample was prepared. Broadened resonances were observed, finer coupling is not listed due to limited intensity and resolution.

<sup>19</sup>F NMR (376 MHz, CDCl<sub>3</sub>) δ -152.1 (dd, <sup>3</sup>J<sub>FF</sub> = 22.0 Hz, <sup>4</sup>J<sub>FF</sub> = 7.1 Hz, 1F), -155.5 (d, <sup>3</sup>J<sub>FF</sub> = 20.7 Hz, 2F), -161.1 (t, <sup>3</sup>J<sub>FF</sub> = 21.7 Hz, 1F), -163.0 (td, <sup>3</sup>J<sub>FF</sub> = 21.1 Hz, <sup>4</sup>J<sub>FF</sub> = 4.6 Hz, 2F), -164.4 (m, 2F), -168.6 (td, <sup>3</sup>J<sub>FF</sub> = 21.8 Hz, <sup>4</sup>J<sub>FF</sub> = 4.6 Hz, 1F).

GCMS EI+ (A) 10.1 min. m/z 347.0 [M]<sup>+</sup> (97%).

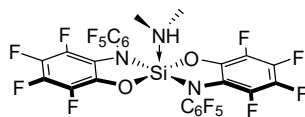
HRMS EI+ (*m/z*) calc. for [M]<sup>+</sup>, 346.9987; found 346.9987 (100%), deviation -0.15 ppm.

Elemental analysis calc. C 41.52%, H 0.58%, N, 4.03%. found C 41.76%, H 0.78%, N 4.12%.

<sup>x</sup> A minor trace (<5%) derivative with a mono-hydrodefluorinated ligand backbone stemmed from the harsh conditions. Due to hard separation of this derivative, it is subsequently observed in all following steps involving the ligand. Alternatively, the compound was obtained in purer form when using *n*-hexane instead of toluene as solvent at milder temperatures, however with significant prolonged reaction times (for AlI<sub>3</sub> formation and ether cleavage each >24 h).

### 5.2.3.3 2-HNMe<sub>2</sub><sup>y</sup>

To a solution of **am<sup>F</sup>ph<sup>F</sup>H<sub>2</sub>** (4.0 g, 2.0 eq.) in toluene (35 mL), tris(dimethylamido)silane (1.05 eq.) was added slowly in four portions at rt. The reaction mixture was heated to 100 °C for 4 h while ensuring a continuous exchange of the inert atmosphere. The solution was concentrated and dried *in vacuo*, the resulting solid suspended in *n*-pentane (15 mL) and stirred rigorously for one hour. The solid was filtered off, washed with *n*-pentane and dried *in vacuo*, yielding a colorless solid (4.2 g, 95%).<sup>z</sup>



Colorless crystals suitable for scXRD developed *via* gas diffusion of *n*-pentane to a saturated dichloromethane solution at ambient temperature.

<sup>1</sup>H NMR (400 MHz, CD<sub>2</sub>Cl<sub>2</sub>) δ 4.61 (s, 1H, **NH**), 2.88 (s, 3H, **CH<sub>3</sub>**), 2.74 (s, 3H, **CH<sub>3</sub>**).

<sup>13</sup>C NMR (151 MHz, CD<sub>2</sub>Cl<sub>2</sub>) δ 146.0 (d, <sup>1</sup>J<sub>CF</sub> = 243 Hz, **CF**), 145.5 (d, <sup>1</sup>J<sub>CF</sub> = 252 Hz, **CF**), 140.6 (d, <sup>1</sup>J<sub>CF</sub> = 256 Hz, **CF**), 137.9 (d, <sup>1</sup>J<sub>CF</sub> = 249 Hz, **CF**), 136.0 (d, <sup>1</sup>J<sub>CF</sub> = 242 Hz, **CF**), 135.9 (d, <sup>1</sup>J<sub>CF</sub> = 243 Hz, **CF**), 135.8 (d, <sup>1</sup>J<sub>CF</sub> = 240 Hz, **CF**), 135.4 (d, <sup>1</sup>J<sub>CF</sub> = 244 Hz, **CF**), 132.7 (**CO**), 121.6 (**CN**), 118.3 (**CN**), 38.8 (**CH<sub>3</sub>**), 38.2 (**CH<sub>3</sub>**).

For the <sup>13</sup>C NMR spectrum a highly concentrated sample was prepared. Reported resonances are observed as broadened signals, finer coupling is not listed due to limited intensity and resolution.

<sup>19</sup>F NMR (376 MHz, CD<sub>2</sub>Cl<sub>2</sub>) δ -146.3 (dd, <sup>3</sup>J<sub>FF</sub> = 22.9 Hz, <sup>4</sup>J<sub>FF</sub> = 5.9 Hz, 2F), -146.7 (m, 2F), -155.7 (t, <sup>3</sup>J<sub>FF</sub> = 21.4 Hz, 2F), -162.2 (t, <sup>3</sup>J<sub>FF</sub> = 19.3 Hz, 2F), -162.7 (t, <sup>3</sup>J<sub>FF</sub> = 21.2 Hz, 2F), -165.0 (m, 2F), -166.4 (m, 2F), -169.0 (td, <sup>3</sup>J<sub>FF</sub> = 21.1 Hz, <sup>4</sup>J<sub>FF</sub> = 4.8 Hz, 2F), -169.8 (td, <sup>3</sup>J<sub>FF</sub> = 21.0 Hz, <sup>4</sup>J<sub>FF</sub> = 4.9 Hz, 2F).

<sup>29</sup>Si NMR (119 MHz, CD<sub>2</sub>Cl<sub>2</sub>) δ -98.9.

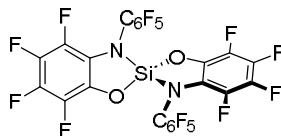
**HRMS EI+** (*m/z*) calc. for C<sub>15</sub>H<sub>6</sub>F<sub>9</sub>NO [M-HNMe<sub>2</sub>]<sup>+</sup>, 717.9436; found 717.9435 (100%), deviation -0.10 ppm.

<sup>y</sup> The germanium analog of **2-HNMe<sub>2</sub>** could be synthesized in similar fashion when Ge(NMe<sub>2</sub>)<sub>4</sub> was utilized instead of HSi(NMe<sub>2</sub>)<sub>3</sub>

<sup>z</sup> The compound was initially synthesized in CH<sub>2</sub>Cl<sub>2</sub> at rt, which required significantly prolonged reaction times at larger scales in comparison to the here described protocol.

### 5.2.3.4 Bis(nonafluoro-*N*-phenyl-*ortho*-amidophenolato)silane (2)

A solution of **2**-HNMe<sub>2</sub> (3.00 g, 1.0 eq.) in toluene (10 mL) was heated to 85 °C. At this temperature, a solution of HNTf<sub>2</sub> (1.05 eq.) in toluene (2 mL) was added dropwise over 15 min. The reaction mixture was



further stirred for three hours at 85 °C. The solvent was cautiously removed *in vacuo* at the elevated temperature. The temperature was reduced to 50 °C and *n*-hexane (10 mL) was added to the viscous residue. The mixture was rigorously stirred for 5 min and then filtered. This step was repeated two times. The combined extracts were concentrated *in vacuo* to give a colorless solid, which was taken up in CH<sub>2</sub>Cl<sub>2</sub> (approx. 2.5 mL) and recrystallized at -40 °C (repeated once) to yield a colorless, crystalline solid (2.17 g, 77%).

Colorless crystals suitable for scXRD developed from a saturated dichloromethane solution at ambient temperature.

**<sup>13</sup>C NMR** (151 MHz, CD<sub>2</sub>Cl<sub>2</sub>) δ 145.2 (d, <sup>1</sup>J<sub>CF</sub> = 253 Hz, CF), 144.9 (d, <sup>1</sup>J<sub>CF</sub> = 253 Hz, CF), 141.9 (d, <sup>1</sup>J<sub>CF</sub> = 257 Hz, CF), 138.4 (d, <sup>1</sup>J<sub>CF</sub> = 253 Hz, CF), 138.2 (d, <sup>1</sup>J<sub>CF</sub> = 251 Hz, CF), 137.9 (d, <sup>1</sup>J<sub>CF</sub> = 251 Hz, CF), 137.3 (d, <sup>1</sup>J<sub>CF</sub> = 248 Hz, CF), 137.0 (d, <sup>1</sup>J<sub>CF</sub> = 249 Hz, CF), 136.6 (d, <sup>1</sup>J<sub>CF</sub> = 249 Hz, CF), 129.6 (CO), 120.6 (CN), 111.7 (CN).

For the <sup>13</sup>C NMR spectrum a highly concentrated sample was prepared. Reported resonances are observed as broadened signals, finer coupling is not listed due to limited intensity and resolution.

**<sup>19</sup>F NMR** (376 MHz, CD<sub>2</sub>Cl<sub>2</sub>) δ -146.8 (d, <sup>3</sup>J<sub>FF</sub> = 22.7 Hz, 2F), -147.7 (m, 2F), -153.0 (t, <sup>3</sup>J<sub>FF</sub> = 21.4 Hz, 2F), -160.6 (td, <sup>3</sup>J<sub>FF</sub> = 22.0 Hz, <sup>4</sup>J<sub>FF</sub> = 4.2 Hz, 2F), -161.6 (dd, <sup>3</sup>J<sub>FF</sub> = 20.8 Hz, <sup>4</sup>J<sub>FF</sub> = 7.9 Hz, 2F), -161.8 (m, 2F), -164.8 (m, 4F), -165.9 (td, <sup>3</sup>J<sub>FF</sub> = 20.7 Hz, <sup>4</sup>J<sub>FF</sub> = 5.7 Hz, 2F).

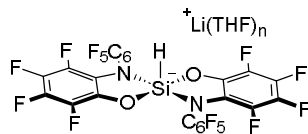
**<sup>29</sup>Si NMR** (119 MHz, CD<sub>2</sub>Cl<sub>2</sub>) δ -40.6.

**HRMS EI+** (*m/z*) calc. for C<sub>15</sub>H<sub>6</sub>F<sub>9</sub>NO [M]<sup>+</sup>, 717.9436; found 717.9467 (9%), deviation 4.23 ppm; calc. for C<sub>12</sub>H<sub>2</sub>F<sub>9</sub>NO [am<sup>F</sup>ph<sup>F</sup>H<sub>2</sub>]<sup>+</sup>, 346.9987; found 346.9994 (100%), deviation 2.02 ppm.

**Elemental analysis** calc. C 40.13%, N, 3.90%. found C 39.56%, N 4.08%.

### 5.2.3.5 [cation][H-2]

A mixture of **2** (10.0 mg) and LiAlH<sub>4</sub> (0.5 mg) was dissolved in THF-*d*8 (0.45 mL)<sup>aa</sup> and the solution analyzed *via* NMR spectroscopy, which supported the formation of the hydridosilicate anion. <sup>1</sup>H, <sup>29</sup>Si and



<sup>13</sup>C NMR experiments did not indicate any side products, the <sup>19</sup>F NMR spectrum however revealed the presence of another species based on the **am<sup>F</sup>ph<sup>F</sup>** structure motif. The target compound was formed in 79% yield based on internal NMR integration.



<sup>1</sup>H NMR (600 MHz, THF-*d*8) δ 5.76 (s, <sup>1</sup>J<sub>SiH</sub> = 319 Hz, SiH), 3.17 (s, Li-O-CD<sub>2</sub>H).

<sup>13</sup>C NMR (151 MHz, THF-*d*8) δ 67.4 (quin, -OCD<sub>2</sub>-), 25.5 (quin, -OCD<sub>2</sub>-CD<sub>2</sub>-).

Residual signals not detected due to limited concentration and intense fluorine coupling.

<sup>19</sup>F NMR (376 MHz, THF-*d*8) δ -150.9 (d, <sup>3</sup>J<sub>FF</sub> = 22.7 Hz, 4F), -170.6 (t, <sup>3</sup>J<sub>FF</sub> = 20.3 Hz, 4F), -171.2 (m, 2F), -171.7 (dt, <sup>3</sup>J<sub>FF</sub> = 21.0 Hz, <sup>4</sup>J<sub>FF</sub> = 7.6 Hz, 2F), -174.8 (dt, <sup>3</sup>J<sub>FF</sub> = 21.7 Hz, <sup>4</sup>J<sub>FF</sub> = 8.0 Hz, 2F), -182.4 (td, <sup>3</sup>J<sub>FF</sub> = 22.0 Hz, <sup>4</sup>J<sub>FF</sub> = 9.1 Hz, 2F), -183.0 (td, <sup>3</sup>J<sub>FF</sub> = 21.6 Hz, <sup>4</sup>J<sub>FF</sub> = 9.3 Hz, 2F).

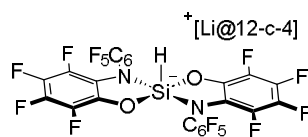
<sup>29</sup>Si NMR [<sup>29</sup>Si-IG, <sup>1</sup>H-<sup>29</sup>Si-HMBC, <sup>29</sup>Si(<sup>1</sup>H)DEPT] (119 MHz, THF-*d*8) δ -98.2.

Of note, in the course of the hydride experiments, trace amounts of [Li(OEt<sub>2</sub>)] [Et<sub>2</sub>O-Al(am<sup>F</sup>ph<sup>F</sup>)<sub>2</sub>] could be detected. When LiAlH<sub>4</sub> and **2** were reacted in Et<sub>2</sub>O, the product was precipitated with *n*-pentane. After filtration, a minor, colorless trace crystal that developed from the supernatant was apparent, for which scXRD confirmed the molecular structure of [Li(OEt<sub>2</sub>)] [Et<sub>2</sub>O-Al(am<sup>F</sup>ph<sup>F</sup>)<sub>2</sub>] (section 7.6).

<sup>aa</sup> When allowed to stay for prolonged times the reaction mixture was found to polymerize.

To isolate the target species, the reaction mixture was concentrated to 0.05 mL and the salt was precipitated with *n*-pentane. The supernatant was decanted and the residue rigorously dried *in vacuo*.

Dichloromethane (0.5 mL) was added followed by the slow addition of stoichiometric amounts of 12-crown-4 ether. The mixture was filtered, and the filtrate concentrated *in vacuo* to give a colorless solid (8.5 mg, 68%). The compound was also found to form when the crown-ether was added dropwise to a suspension of LiAlH<sub>4</sub> and **2** dissolved in CH<sub>2</sub>Cl<sub>2</sub>.



[Li@12c4][H-2]

<sup>1</sup>H NMR (600 MHz, CD<sub>2</sub>Cl<sub>2</sub>) δ 5.76 (s, <sup>1</sup>J<sub>SiH</sub> = 320 Hz, SiH), 3.64 (s, CH<sub>2</sub>).

<sup>13</sup>C NMR (151 MHz, CD<sub>2</sub>Cl<sub>2</sub>) δ 68.1 (CH<sub>2</sub>).

Residual signals not detected due to limited concentration and intense fluorine coupling.

<sup>19</sup>F NMR (376 MHz, CD<sub>2</sub>Cl<sub>2</sub>) δ -147.8 (dd, <sup>3</sup>J<sub>FF</sub> = 23.5 Hz, <sup>4</sup>J<sub>FF</sub> = 5.8 Hz, 2F), -148.9 (m, 2F), -162.0 (t, <sup>3</sup>J<sub>FF</sub> = 21.5 Hz, 2F), -166.9 (t, <sup>3</sup>J<sub>FF</sub> = 23.2 Hz, 2F), -167.1 (m, 2F), -170.2 (dt, <sup>3</sup>J<sub>FF</sub> = 21.5 Hz, <sup>4</sup>J<sub>FF</sub> = 7.5 Hz, 2F), -172.6 (dt, <sup>3</sup>J<sub>FF</sub> = 21.4 Hz, <sup>4</sup>J<sub>FF</sub> = 7.9 Hz, 2F), -175.9 (td, <sup>3</sup>J<sub>FF</sub> = 21.4 Hz, <sup>4</sup>J<sub>FF</sub> = 6.9 Hz, 2F), -177.4 (td, <sup>3</sup>J<sub>FF</sub> = 21.4 Hz, <sup>4</sup>J<sub>FF</sub> = 7.7 Hz, 2F).

<sup>29</sup>Si NMR [<sup>29</sup>Si-IG, <sup>1</sup>H-<sup>29</sup>Si-HMBC, <sup>29</sup>Si(<sup>1</sup>H)DEPT] (119 MHz, CD<sub>2</sub>Cl<sub>2</sub>) δ -96.0.

HRMS ESI<sup>-</sup> (in CH<sub>2</sub>Cl<sub>2</sub>) (*m/z*) calc. for [C<sub>24</sub>HF<sub>18</sub>N<sub>2</sub>O<sub>2</sub>Si]<sup>-</sup> [M]<sup>-</sup>, 718.9525; found 718.9525 (100%), deviation 0.01 ppm.

IR (ATR-FTIR)  $\tilde{\nu}$  [cm<sup>-1</sup>] 2913 (m, ν<sup>CH</sup>), 2871 (m, ν<sup>CH</sup>), 2151 (m, ν<sup>SiH</sup>), 1024 (δ<sup>SiH</sup>), 985 (δ<sup>SiH</sup>).

The experiment was also conducted with *proteo-ortho*-difluorobenzene (*o*DFB) as a solvent. Reactivity was only observed after addition of one equivalent 12-crown-4 ether. The mixture was stirred for 30 min and then an aliquot was evaluated *via* NMR spectroscopy, revealing the formation of the hydridosilicate species as judged by <sup>1</sup>H, <sup>29</sup>Si-HMBC, -DEPT and -IG experiments. Internal integration against the signal of 12-crown-4 protons suggested that the desired species had formed in 53% yield. The solvent was removed *in vacuo* and the residue taken up in 1 mL diethyl ether. The solution was layered with 5 mL *n*-pentane and stored at -40 °C, resulting in colorless crystals after several days, for which scXRD revealed the ion pair structure containing [H-2]<sup>-</sup> (cmp. section 5.1.2 and 7.6).

### 5.2.4 Catalytic Carbonyl-Olefin-Metathesis upon Oxidation

The metathesis substrate **A** was synthesized according to a literature procedure.<sup>443</sup> To a solution of **A** (14.3 mg, 1.0 eq.) in  $\text{CD}_2\text{Cl}_2$  (0.45 mL) was added **1**<sup>3,6-*t*Bu</sup> (0.1 eq.). Subsequently,  $\text{Ag}(\text{oC}_6\text{H}_4\text{F}_2)[\text{Al}(\text{O}^t\text{C}_4\text{F}_9)_4]$ <sup>444</sup> (0.1 eq.) was added, upon which immediate conversion was observed. After 14 h, full conversion of the starting material was observed.

Characterization data for product **B** is given in section 5.2.6.

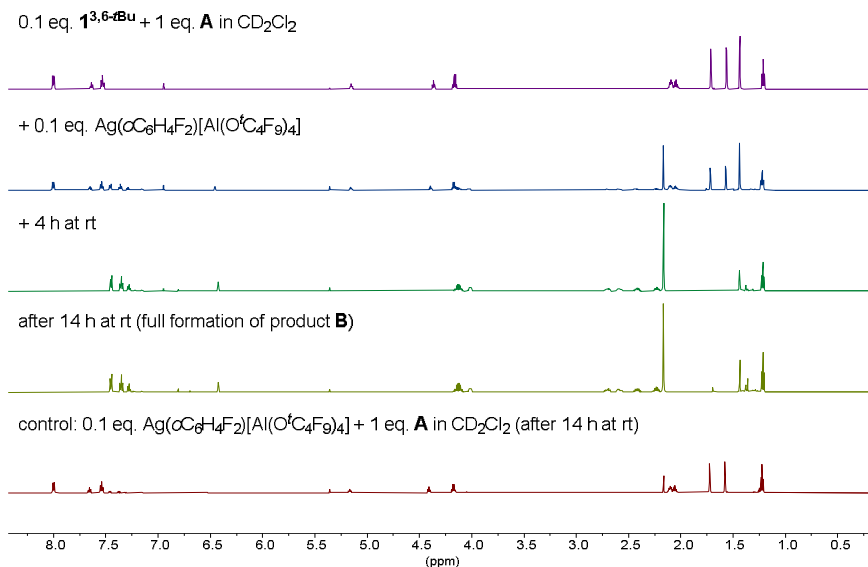


Figure 51. Stacked <sup>1</sup>H NMR spectra for the monitoring of the carbonyl-olefin-metathesis catalyzed by oxidized **1**<sup>3,6-*t*Bu</sup> (described in section 3.1.2) as well as a control experiment.

## 5.2.5 Lewis Acidity Assessment and Reactivities of $1^{\text{CF}_3}$

### 5.2.5.1 Reactivity of $\text{gua}^{\text{CF}_3}$ with $\text{HSiCl}_3$ in Acetonitrile

Synthesis of the bis-acetonitrile adduct of  $1^{\text{CF}_3}$  was attempted *via* previously described procedures for related bis(perhalocatecholato)silanes.<sup>6,178</sup> A *J. Young* type NMR tube was charged with 20 mg of  $\text{gua}^{\text{CF}_3}$  dissolved in 0.5 mL  $\text{CD}_3\text{CN}$ .  $\text{HSiCl}_3$  (0.5 eq.) was added to the solution dropwise, the reaction mixture was heated to 60 °C and monitored with  $^1\text{H}$ - and  $^{19}\text{F}$ -NMR spectroscopy. After 24 h,  $^1\text{H}$  NMR experiments revealed the formation of  $\text{CH}_3\text{Cl}$  and the decrease of the ligands OH and  $\text{OCH}_3$  signals along with a 1:1:1 triplet at 6.35 ppm.<sup>bb</sup>  $^{19}\text{F}$ -NMR spectra showed symmetrization of the trifluoromethyl groups in the catechol motif. In contrast to the halo-derivatives, no precipitation occurred.<sup>6,178</sup>  $^{29}\text{Si}$  NMR spectrum showed a sharp signal at  $-90.4$  ppm, indicating a pentacoordinated silicon species. The signal is in agreement with the calculated value of  $-84.9$  ppm for the chloridosilicate  $[\text{Cl}-1^{\text{CF}_3}]^-$  (Table A9). When the reaction mixture is concentrated to a fifth of its volume and subsequently refilled with  $\text{CH}_2\text{Cl}_2$ , crystals formed after several days for which scXRD indicated the chloridosilicate anion. The exact composition of the cation was not assignable. It proposedly originates from side reactivity of acetonitrile under the acidic conditions of the reaction mixture. After addition of one equivalent triethylamine to the reaction mixture, scXRD analysis of formed colorless crystals confirmed the nature of the ion pair  $[\text{Et}_3\text{N}-\text{H}--\text{NCCH}_3][\text{Cl}-1^{\text{CF}_3}]$  (Figure 52).

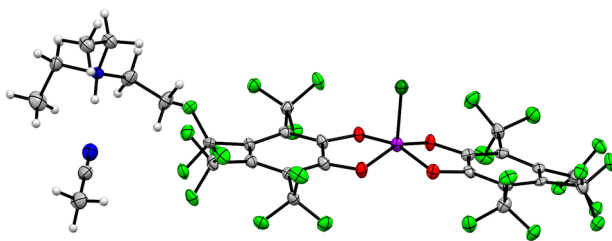
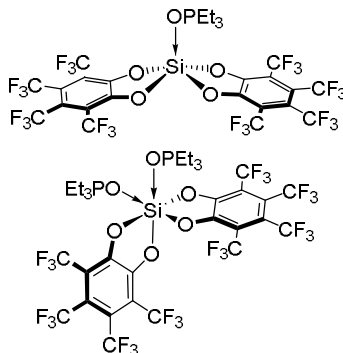


Figure 52. Molecular, scXRD derived structure of  $[\text{Et}_3\text{N}-\text{H}--\text{NCCH}_3][\text{Cl}-1^{\text{CF}_3}]$ . The structure is shown to confirm its connectivity and cannot be used for the discussion of structural data, as full refinement was prevented by poor quality of the crystals.

<sup>bb</sup> Corresponding spectra are shown in the supporting information of the respective publication, which is accessible free of charge.

### 5.2.5.2 GB-Assessment of the Lewis Acidity

To a suspension of  $1^{\text{CF}_3}$ -(sulfolane) $_2$  (20.0 mg, 1.0 eq.), triethylphosphine oxide (a. 1.0 eq.; b 2.0 eq.) was added in roughly three equal portions. The colorless solid dissolved within seconds and  $^1\text{H}$ ,  $^{19}\text{F}$ ,  $^{13}\text{C}$  and  $^{31}\text{P}$  NMR spectroscopy revealed the formation of  $1^{\text{CF}_3}$ -OPEt $_3$  (a) and *cis*- $1^{\text{CF}_3}$ -(OPEt $_3$ ) $_2$  (b) in quantitative yields according to NMR spectroscopy, respectively. Single-crystals suitable for scXRD grown gas diffusion of *n*-pentane into the reaction mixture confirmed the molecular structure of  $1^{\text{CF}_3}$ -OPEt $_3$ .



#### $1^{\text{CF}_3}$ -OPEt $_3$

$^1\text{H}$  NMR (600 MHz,  $\text{CD}_2\text{Cl}_2$ )  $\delta$  2.10 – 2.02 (dq,  $^2J_{\text{PH}}$ ,  $^3J_{\text{HH}} = 11.5, 7.7$  Hz, 6H), 1.15 (dt,  $^3J_{\text{HH}} = 7.7$  Hz, 9H).

$^{13}\text{C}$  NMR (151 MHz,  $\text{CD}_2\text{Cl}_2$ )  $\delta$  150.67 ( $\text{C}_q\text{O}$ ), 122.08 (q,  $^1J_{\text{CF}} = 275.74$  Hz,  $\text{CF}_3$ ), 115.85 (q,  $^2J_{\text{CF}} = 34.7$  Hz,  $\text{C}_q\text{CF}_3$ ), 17.00 (d,  $^1J_{\text{PC}} = 62.5$  Hz), 4.34 (d,  $^3J_{\text{PC}} = 5.2$  Hz).

$^{19}\text{F}$  NMR (376 MHz,  $\text{CD}_2\text{Cl}_2$ )  $\delta$  -51.5 (m, 12F), -56.7 (m, 12F).

$^{31}\text{P}$  NMR (243 MHz,  $\text{CD}_2\text{Cl}_2$ )  $\delta$  89.4.

#### *cis*- $1^{\text{CF}_3}$ -(OPEt $_3$ ) $_2$

$^1\text{H}$  NMR (600 MHz,  $\text{CD}_2\text{Cl}_2$ )  $\delta$  2.11 (ddq,  $J = 15.4, 12.5, 7.7$  Hz, 6H), 1.96 (ddq,  $J = 15.4, 11.8, 7.7$  Hz, 6H), 1.11 (dt,  $^3J_{\text{HH}} = 7.7$  Hz, 18H).

$^{13}\text{C}$  NMR (151 MHz,  $\text{CD}_2\text{Cl}_2$ )  $\delta$  154.4 ( $\text{C}_q\text{O}$ ), 153.9 ( $\text{C}_q\text{O}$ ), 124.6, 122.8, 122.5, 113.0, 17.2 (d,  $^1J_{\text{PC}} = 66.2$  Hz), 5.2 (d,  $^3J_{\text{PC}} = 4.9$  Hz).

$^{19}\text{F}$  NMR (376 MHz,  $\text{CD}_2\text{Cl}_2$ )  $\delta$  -50.9 (sept,  $^5J_{\text{FF}} = 14.9$  Hz, 6F), -51.3 (sept,  $^5J_{\text{FF}} = 15.5, 15.0$  Hz, 6F), -56.6 (q,  $^5J_{\text{FF}} = 14.9$  Hz, 6F), -56.6 (q,  $^5J_{\text{FF}} = 15.3$  Hz, 6F).

$^{31}\text{P}$  NMR (243 MHz,  $\text{CD}_2\text{Cl}_2$ )  $\delta$  74.7.

### 5.2.5.3 Reactivity against $[\text{PPh}_4][\text{SbF}_6]$

$1\text{CF}_3\text{-(sulfolane)}_2$  (20.0 mg, 1.0 eq.) was suspended in  $\text{CD}_2\text{Cl}_2$  (0.5 mL). Upon addition of  $[\text{PPh}_4][\text{SbF}_6]$  (1.0 eq.) at rt the colorless solid dissolved immediately. Monitoring of the reaction using  $^{19}\text{F}$  NMR spectroscopy revealed the immediate formation of the fluoridosilicate  $[\text{F-}1\text{CF}_3]^-$  and  $\text{SiF}_4$  (Figure 53).

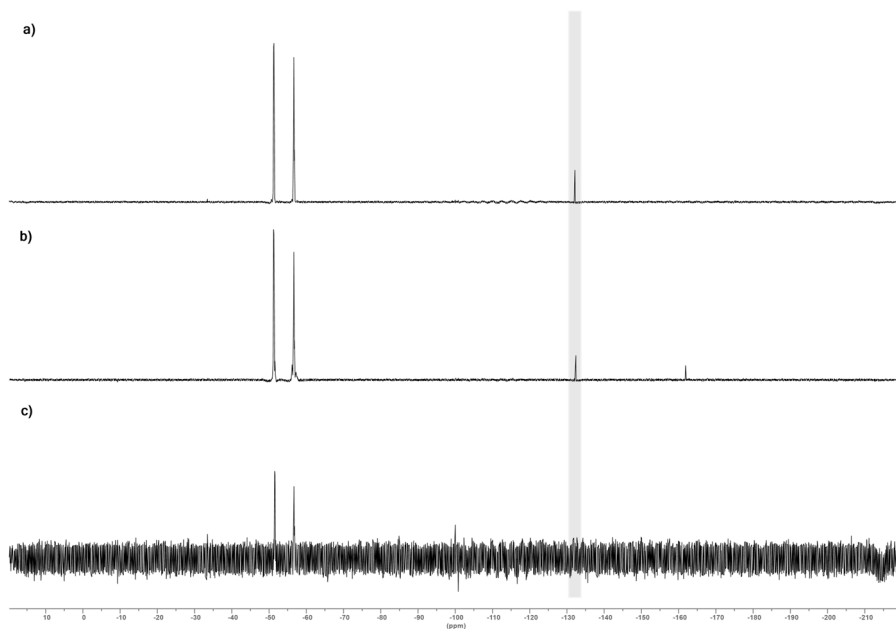


Figure 53. Stacked  $^{19}\text{F}$  NMR (188 MHz,  $\text{CD}_2\text{Cl}_2$ ) spectra of a)  $[\text{N}^t\text{Bu}]_4[\text{F-}1\text{CF}_3]$ , b) the reaction mixture of  $1\text{CF}_3\text{-(sulfolane)}_2$  and  $[\text{PPh}_4][\text{SbF}_6]$  5 min after mixing and c)  $1\text{CF}_3\text{-(sulfolane)}_2$ . The  $[\text{F-}1\text{CF}_3]$ -resonance is highlighted in grey.

#### 5.2.5.4 Chloride-Abstraction from Trityl Chloride

To a solution of trityl chloride (1.0 eq.) in  $\text{CD}_2\text{Cl}_2$ ,  $\mathbf{1}^{\text{CF}_3}$ -(sulfolane)<sub>2</sub> (25.0 mg, 1.0 eq.) was added at rt. The solution turned immediately yellow to orange, indicating the formation of the tritylium cation along with the corresponding chloridosilicate  $[\text{CPh}_3][\text{Cl-1}^{\text{CF}_3}]$ . After 24 h at rt, NMR spectroscopy revealed the absence of tritylchloride.

$[\text{CPh}_3][\text{Cl-1}^{\text{CF}_3}]$ :

$^1\text{H}$  NMR (600 MHz,  $\text{CD}_2\text{Cl}_2$ )  $\delta$  8.28 (t,  $^3J_{\text{HH}} = 7.4$  Hz, 3H, *para-H*), 7.89 (t,  $^3J_{\text{HH}} = 7.4$  Hz, 6H, *ortho-H*), 7.7 (t,  $^3J_{\text{HH}} = 7.7$  Hz, 6H, *meta-H*).

$^{13}\text{C}$  NMR (151 MHz,  $\text{CD}_2\text{Cl}_2$ )  $\delta$  211.3 (+ $\text{CPh}_3$ ), 152.1 ( $\text{C}_q\text{OSi}$ ), 144.1 ( $\text{C}_{\text{Ar}}$ -trityl), 143.1 ( $\text{C}_{\text{Ar}}$ -trityl), 140.3 ( $\text{C}_{\text{Ar}}$ -trityl), 131.1 ( $\text{C}_{\text{Ar}}$ -trityl), 122.8 (q,  $^1J_{\text{CF}} = 276$ ,  $\text{CF}_3$ ), 115.4 (q,  $^2J_{\text{CF}} = 34.0$  Hz,  $\text{C}_q\text{CF}_3$ ).

$^{19}\text{F}$  NMR (376 MHz,  $\text{CD}_2\text{Cl}_2$ )  $\delta$  -51.34 (m, 12F), -56.6 (m, 12F).

$^{29}\text{Si}$  NMR (119 MHz,  $\text{CD}_2\text{Cl}_2$ )  $\delta$  -89.7.

#### 5.2.5.5 Reduction of $\mathbf{1}^{\text{CF}_3}$ -( $\text{OCPH}_2$ )

$\mathbf{1}^{\text{CF}_3}$ -( $\text{OCPH}_2$ ) (35 mg, 1.0 eq.) was dissolved in  $\text{CH}_2\text{Cl}_2$  (1 mL) and cooled to  $-40$  °C. Triethylsilane (2.1 eq.) was added in three portions, the reaction mixture kept at  $-40$  °C for 12 h and was then allowed to warm to rt. Volatiles were removed *in vacuo*, and the residue taken up in  $\text{CD}_2\text{Cl}_2$  (0.45 mL) and transferred to a *J. Young* type NMR tube.  $^1\text{H}$  NMR of the red solution indicated quantitative formation of diphenylmethane. Parallely,  $^{19}\text{F}$  NMR spectra indicated the formation of a newly formed species assigned with two resonances of similar intensity. A  $^{13}\text{C}\{^{19}\text{F}\}$  NMR spectrum supported the formation of one species containing one **cat** $^{\text{CF}_3}$  unit. The  $^{29}\text{Si}$  NMR spectrum showed two signals at 21.2 ppm and  $-78.4$  ppm. The downfield signal assigned to the disiloxane was found to be significantly shifted to the free hexaethylidisiloxane (reference: 8.9 ppm).<sup>445</sup> In accordance, the methylene protons in the  $^1\text{H}$  NMR spectrum were also more deshielded (0.63 ppm, reference 0.56 ppm<sup>445</sup>). Additionally, the calculated  $^{29}\text{Si}$  NMR resonance for donor-free  $\mathbf{1}^{\text{CF}_3}$  ( $-42.8$  ppm, Table A9) differed from the signal found experimentally at  $-78.4$  ppm. For an adduct  $\mathbf{1}^{\text{CF}_3}$ - $\text{O}(\text{SiEt}_3)_2$ , calculated  $^{29}\text{Si}$  NMR references are 58.0 ppm (average for the two  $\text{SiEt}_3$  groups) and  $-101.8$  ppm (Table A9). From the experimental equilibrium

resonance and the computed resonances of the adduct and unbound  $\mathbf{1CF}_3$ , equilibrium proportions of 60.34%  $\mathbf{1CF}_3\text{-O}(\text{SiEt}_3)_2$  and 39.66%  $\mathbf{1CF}_3$  were assessed, which transfer to a reaction Gibbs free energy of  $\Delta G_{\text{exp}} = -1.04 \text{ kJ mol}^{-1}$  (298 K). The computed  $\Delta G_{\text{comp}} = 1.18 \text{ kJ mol}^{-1}$  is in good agreement and within the borders of *chemical accuracy* (DSD-BLYP-D3(BJ)/def2-QZVPP+SMD(CH<sub>2</sub>Cl<sub>2</sub>)/PBEh-3c level, Table A2).



$$K = e^{-\frac{\Delta G}{RT}}. \text{ Proportions [\%]: } [\mathbf{1CF}_3\text{-O}(\text{SiEt}_3)_2] = \frac{K}{1+K} \text{ and } [\mathbf{1CF}_3], [\text{O}(\text{SiEt}_3)_2] = \frac{1}{1+K}.$$

$\mathbf{1CF}_3\text{-O}(\text{SiEt}_3)_2$ :

$^1\text{H}$  NMR (600 MHz, CD<sub>2</sub>Cl<sub>2</sub>)  $\delta$  0.94 (t,  $^3J_{\text{HH}} = 8.0 \text{ Hz}$ , 18H,  $-\text{CH}_3$ ), 0.63 (q,  $^3J_{\text{HH}} = 8.0 \text{ Hz}$ , 12H,  $-\text{CH}_2-$ ).

$^{13}\text{C}\{\text{F}\}$  (126 MHz, CD<sub>2</sub>Cl<sub>2</sub>)  $\delta$  150.6 ( $C_q\text{OSi}$ ), 123.6 ( $C_q\text{CF}_3$ ), 122.5 ( $\text{CF}_3$ ), 122.0 ( $\text{CF}_3$ ), 118.5 ( $C_q\text{CF}_3$ ), 6.3 ( $-\text{CH}_3$ ), 5.9 ( $-\text{CH}_2-$ ).

$^{13}\text{C}$  (151 MHz, CD<sub>2</sub>Cl<sub>2</sub>)  $\delta$  150.6 ( $C_q\text{OSi}$ ), 123.7 (m), 122.4 (q,  $^1J_{\text{CF}} = 276 \text{ Hz}$ ,  $\text{CF}_3$ ), 121.9 (q,  $^1J_{\text{CF}} = 279 \text{ Hz}$ ,  $\text{CF}_3$ ), 118.5 (q,  $^2J_{\text{CF}} = 35.1 \text{ Hz}$ ,  $C_q\text{CF}_3$ ), 6.3 ( $-\text{CH}_3$ ), 5.9 ( $-\text{CH}_2-$ ).

$^{19}\text{F}$  NMR (188 MHz, CD<sub>2</sub>Cl<sub>2</sub>)  $\delta$   $-51.7$  (m, 12F),  $-57.2$  (m, 12F).

$^{29}\text{Si}$  NMR (119 MHz, CD<sub>2</sub>Cl<sub>2</sub>)  $\delta$  21.2,  $-78.4$ .

### 5.2.6 Catalytic Protocols incorporating $1^{\text{CF}_3}$

**General procedure for reduction catalysis.** A *J. Young* type NMR tube was charged with **x mol% catalyst**, **substrate** (150  $\mu\text{mol}$ , 1.0 eq.) and **solvent** (0.5 mL). The respective **reducing agent (r.a.)** was added and the reaction was conducted at the specified **temperature (T)** and monitored using GCMS spectrometry,  $^1\text{H}$  or  $^{31}\text{P}$  NMR spectroscopy. Mesitylene, cyclooctane (75  $\mu\text{mol}$ ) or tri-*n*-butylphosphate were added as internal standard and conversion as well as yields were determined by integration. When non-deuterated solvent was used for the reaction, 50  $\mu\text{L}$   $\text{CD}_2\text{Cl}_2$  were added prior to the final NMR measurement and the sample locked on  $\text{CD}_2\text{Cl}_2$ , to ensure sufficient resolution for yield determination by integration, if required. Exact conditions are specified in the following tables.

**Carbonyl-olefin metathesis.** The metathesis substrate A was synthesized according to a literature procedure.<sup>443</sup> To a solution of A (27.4 mg, 100  $\mu\text{mol}$ , 1 eq.) in  $\text{CD}_2\text{Cl}_2$  (0.5 mL) was added  $1^{\text{CF}_3}\text{-}(\text{sulfolane})_2$  (3.23 mg, 10.0  $\mu\text{mol}$ , 0.05 eq.) and the reaction progress monitored *via*  $^1\text{H}$  NMR. After 24 h, full conversion of the starting material was observed. After the reaction was found to be complete the mixture was analyzed by GCMS.

Table 6. Conditions for the hydrodeoxygenation of carbonyls.

Substrate	Catalyst	x	solvent	eq. r.a.	T [ $^\circ\text{C}$ ]	t [h]	Yield <sup>[a]</sup> [%]
$\text{Ph}_2\text{CO}$	$1^{\text{CF}_3}\text{-}(\text{sulfolane})_2$	2	$\text{CD}_2\text{Cl}_2$	3.0 $\text{HSiEt}_3$	25	0.5	99
$\text{PhCOCH}_3$	$1^{\text{CF}_3}\text{-}(\text{sulfolane})_2$	5	<i>o</i> DCB	3.0 $\text{PhSiH}_3$	100	72	80
$(\text{CH}_2)_5\text{CO}$	$1^{\text{CF}_3}\text{-}(\text{sulfolane})_2$	5	<i>o</i> DCB	3.0 $\text{PhSiH}_3$	100	72	61 <sup>[b]</sup>
$\text{PhCON}^i\text{Pr}_2$	$1^{\text{CF}_3}\text{-}(\text{sulfolane})_2$	5	toluene- <i>d</i> 8	3.0 $\text{PhSiH}_3$	100	48	95
$\text{Ph}_2\text{CO}$	$1^{\text{CF}_3}\text{-}(\text{Ph}_2\text{CO})$	2	$\text{CD}_2\text{Cl}_2$	3.0 $\text{HSiEt}_3$	25	24	77
$\text{Ph}_2\text{CO}$	$1^{\text{CL}}\text{-}(\text{sulfolane})_2$	2	$\text{CD}_2\text{Cl}_2$	3.0 $\text{HSiEt}_3$	25	24	24
$\text{Ph}_2\text{CO}$	$1^{\text{CL}}\text{-}(\text{CH}_3\text{CN})_2$	2	$\text{CD}_2\text{Cl}_2$	3.0 $\text{HSiEt}_3$	25	24	16

[a] yield for dihydrodeoxygenated product, [b] yield for cyclohexene, observed as main product.

Table 7. Conditions for the deoxygenation of phosphine oxides.

Substrate	Catalyst	x	solvent	eq. r.a.	T [°C]	t [h]	Yield <sup>[a]</sup> [%]
Et <sub>3</sub> PO	<b>1</b> CF <sub>3</sub> -(sulfolane) <sub>2</sub>	5	toluene- <i>d</i> 8	3.0 PhSiH <sub>3</sub>	100	48	96
Ph <sub>3</sub> PO	<b>1</b> CF <sub>3</sub> -(sulfolane) <sub>2</sub>	5	toluene- <i>d</i> 8	3.0 PhSiH <sub>3</sub>	100	48	91

[a] yield for phosphine product.

Table 8. Conditions for reduction of aldehydes.

Substrate	Catalyst	x	solvent	eq. r.a.	T [°C]	t [h]	Yield <sup>[a]</sup> [%]
PhCHO	<b>1</b> CF <sub>3</sub> -(sulfolane) <sub>2</sub>	1	CD <sub>2</sub> Cl <sub>2</sub>	1.5 HSiEt <sub>3</sub>	25	24	89
<i>p</i> FC <sub>6</sub> H <sub>4</sub> CHO	<b>1</b> CF <sub>3</sub> -(sulfolane) <sub>2</sub>	1	CD <sub>2</sub> Cl <sub>2</sub>	1.5 HSiEt <sub>3</sub>	25	24	96 (3 <sup>[b]</sup> )
<i>p</i> CH <sub>3</sub> C <sub>6</sub> H <sub>4</sub> CHO	<b>1</b> CF <sub>3</sub> -(sulfolane) <sub>2</sub>	1	CD <sub>2</sub> Cl <sub>2</sub>	1.5 HSiEt <sub>3</sub>	25	24	97 (<0.5 <sup>[b]</sup> )
C <sub>7</sub> H <sub>11</sub> CHO	<b>1</b> CF <sub>3</sub> -(sulfolane) <sub>2</sub>	1	CD <sub>2</sub> Cl <sub>2</sub>	1.5 HSiEt <sub>3</sub>	25	24	71
<i>p</i> FC <sub>6</sub> H <sub>4</sub> CHO	<b>1</b> CF <sub>3</sub> -(Ph <sub>2</sub> CO)	1	CD <sub>2</sub> Cl <sub>2</sub>	1.5 HSiEt <sub>3</sub>	25	24	80 (2 <sup>[b]</sup> )
<i>p</i> CH <sub>3</sub> C <sub>6</sub> H <sub>4</sub> CHO	<b>1</b> CF <sub>3</sub> -(Ph <sub>2</sub> CO)	1	CD <sub>2</sub> Cl <sub>2</sub>	1.5 HSiEt <sub>3</sub>	25	24	97 (<0.5 <sup>[b]</sup> )
<i>p</i> FC <sub>6</sub> H <sub>4</sub> CHO	<b>1</b> Cl-(sulfolane) <sub>2</sub>	1	CD <sub>2</sub> Cl <sub>2</sub>	1.5 HSiEt <sub>3</sub>	25	24	10 (16 <sup>[b]</sup> )
<i>p</i> CH <sub>3</sub> C <sub>6</sub> H <sub>4</sub> CHO	<b>1</b> Cl-(sulfolane) <sub>2</sub>	1	CD <sub>2</sub> Cl <sub>2</sub>	1.5 HSiEt <sub>3</sub>	25	24	27 (3 <sup>[b]</sup> )
<i>p</i> FC <sub>6</sub> H <sub>4</sub> CHO	<b>1</b> Cl-(CH <sub>3</sub> CN) <sub>2</sub>	1	CD <sub>2</sub> Cl <sub>2</sub>	1.5 HSiEt <sub>3</sub>	25	24	5 (5 <sup>[b]</sup> )
<i>p</i> CH <sub>3</sub> C <sub>6</sub> H <sub>4</sub> CHO	<b>1</b> Cl-(CH <sub>3</sub> CN) <sub>2</sub>	1	CD <sub>2</sub> Cl <sub>2</sub>	1.5 HSiEt <sub>3</sub>	25	24	6 (<0.5 <sup>[b]</sup> )
<i>p</i> FC <sub>6</sub> H <sub>4</sub> CHO	<b>1</b> CF <sub>3</sub> -(sulfolane) <sub>2</sub>	5	<i>o</i> DCB	6.0 PhSiH <sub>3</sub>	100	168	66 <sup>[c]</sup>

[a] yield for dialkyl ethers; [b] yield for hydrosilylation product – (methylene resonances in the reaction mixture at 4.70 ppm (*p*-FC<sub>6</sub>H<sub>4</sub>CH<sub>2</sub>OSiEt<sub>3</sub>, 4.69 ppm in CDCl<sub>3</sub><sup>446</sup>) and 4.69 ppm (*p*-CH<sub>3</sub>C<sub>6</sub>H<sub>4</sub>CH<sub>2</sub>OSiEt<sub>3</sub>, 4.69 ppm in CD<sub>2</sub>Cl<sub>2</sub><sup>447</sup>) were found to be consistent with literature values); [c] yield for dihydrodeoxygenation (*para*-fluorotoluene).

### 5.2.6.1 Characterization Data

#### Bisbenzyl ether

<sup>1</sup>H NMR (200 MHz, CD<sub>2</sub>Cl<sub>2</sub>) δ 7.47 - 7.24 (m, 10H), 4.58 (s, 4H).

Obtained signals matched the ones found in literature.<sup>448</sup>

**GCMS EI+ (A)** 18.0 min. *m/z* 107.0 [C<sub>6</sub>H<sub>5</sub>-CH<sub>2</sub>-O]<sup>+</sup> (15%), 91.1 [C<sub>6</sub>H<sub>5</sub>-CH<sub>3</sub>]<sup>+</sup> (100%), 91.1 [C<sub>6</sub>H<sub>5</sub>-CH<sub>2</sub>]<sup>+</sup> (81%).

#### Bis(4-fluoro)benzyl ether

<sup>1</sup>H NMR (200 MHz, CD<sub>2</sub>Cl<sub>2</sub>) δ 7.44 - 7.27 (m, 4H), 7.17 - 6.96 (m, 4H), 4.57 - 4.48 (m, 4H).

Obtained signals matched the ones found in literature.<sup>449</sup>

**GCMS EI+ (A)** 17.9 min. *m/z* 234.1 [M]<sup>+</sup> (< 0.5%), 125.0 [F-C<sub>6</sub>H<sub>4</sub>-CH<sub>2</sub>-O]<sup>+</sup> (15%), 109.1 [F-C<sub>6</sub>H<sub>4</sub>-CH<sub>2</sub>]<sup>+</sup> (100%).

#### Bis(4-methyl)benzyl ether

<sup>1</sup>H NMR (200 MHz, CD<sub>2</sub>Cl<sub>2</sub>) δ 7.27 (d, <sup>3</sup>*J*<sub>HH</sub> = 8.2 Hz, 4H), 7.18 (d, <sup>3</sup>*J*<sub>HH</sub> = 8.2 Hz, 4H), 4.51 (s, 4H), 2.37 (s, 6H).

Obtained signals matched the ones found in literature.<sup>448</sup>

**GCMS EI+ (A)** 19.2 min. *m/z* 226.1 [M]<sup>+</sup> (< 0.5%), 121.1 [CH<sub>3</sub>-C<sub>6</sub>H<sub>4</sub>-CH<sub>2</sub>-O]<sup>+</sup> (11%), 106.1 [CH<sub>3</sub>-C<sub>6</sub>H<sub>4</sub>-CH<sub>3</sub>]<sup>+</sup> (100%), 91.1 [C<sub>6</sub>H<sub>5</sub>-CH<sub>2</sub>]<sup>+</sup> (45%).

#### Bis(cyclohexyl)methyl ether

<sup>1</sup>H NMR (200 MHz, CD<sub>2</sub>Cl<sub>2</sub>) δ 3.17 (d, <sup>3</sup>*J*<sub>HH</sub> = 6.4 Hz, 4H), 1.82 - 1.60 (m, 10H), 1.63 - 1.42 (m, 2H), 1.23 (tq, 4H), 1.15 (tq, 2H), 0.09 (dq, 4H).

Obtained signals matched the ones found in literature.<sup>448</sup>

**GCMS EI+ (A)** 17.4 min. *m/z* 210.2 [M]<sup>+</sup> (1%), 97.1 [C<sub>6</sub>H<sub>11</sub>-CH<sub>2</sub>]<sup>+</sup> (100%), 81.1 [C<sub>6</sub>H<sub>9</sub>]<sup>+</sup> (31%).

#### Diphenylmethane

<sup>1</sup>H NMR (200 MHz, CD<sub>2</sub>Cl<sub>2</sub>) δ 7.42 - 7.14 (m, 10H), 4.01 (s, 2H).

Obtained signals matched the ones found in literature.<sup>450</sup>

**GCMS EI+ (A)** 16.6 min. *m/z* 168.1 [M]<sup>+</sup> (98%), 167.1 [M - H]<sup>+</sup> (100%), 91.1 [C<sub>6</sub>H<sub>5</sub>-CH<sub>2</sub>]<sup>+</sup> (17%).

**Ethylbenzene**

$^1\text{H}$  NMR (600 MHz, *o*DCB)  $\delta$  2.57 (q,  $^3J_{\text{HH}} = 7.7$  Hz, 2H), 1.18 (t,  $^3J_{\text{HH}} = 7.7$ , 3H).

Aromatic signals not resolved due to interference with solvent.

$^{13}\text{C}$  NMR (151 MHz, *o*DCB)  $\delta$  144.2, 128.5, 125.8, 29.1, 15.9.

GCMS EI+ (A) 6.5 min.  $m/z$  106.1  $[\text{M}]^+$  (35%), 91.0  $[\text{M} - \text{CH}_3]^+$  (100%), 77.0  $[\text{C}_6\text{H}_5]^+$  (7%).

The identity of the product was additionally verified through matching signals in comparison with a spectrum of the commercially obtained chemical in the same solvent system that was used throughout the reaction.

**Cyclohexene**

$^1\text{H}$  NMR (600 MHz, *o*DCB)  $\delta$  5.61 (br, 2H), 1.92 (br, 4H), 1.53 (br, 4H).

Bad resolution originating from the use of non-deuterated solvent did not allow the assignment of coupling patterns.

$^{13}\text{C}$  NMR (151 MHz, *o*DCB)  $\delta$  127.3, 25.4, 22.9.

GCMS EI+ (A) 2.9 min.  $m/z$  82.1  $[\text{M}]^+$  (44%), 67.1  $[\text{M} - \text{CH}_3]^+$  (100%), 54.1  $[\text{M} - \text{C}_2\text{H}_4]^+$  (60%).

The identity of the product was additionally verified through matching signals in comparison with a spectrum of the commercially obtained chemical in the same solvent system that was used throughout the reaction.

***p*-Fluorotoluene**

$^1\text{H}$  NMR (600 MHz, *o*DCB)  $\delta$  6.95 (m, 2H), (t,  $^3J_{\text{HH}} = 8.7$  Hz, 2H), 2.15 (s, 3H).

$^{13}\text{C}$  NMR (151 MHz, *o*DCB)  $\delta$  161.1 (d,  $^1J_{\text{CF}} = 242$  Hz), 133.5 (d,  $^4J_{\text{CF}} = 3.2$  Hz), 130.4 (d,  $^3J_{\text{CF}} = 7.7$  Hz), 114.8 (d,  $^2J_{\text{CF}} = 21.0$  Hz), 20.4.

$^{19}\text{F}$  NMR (188 MHz, *o*DCB)  $\delta$  -117.9.

The identity of the product was additionally verified through matching signals in comparison with a spectrum of the commercially obtained chemical in the same solvent system that was used throughout the reaction.

**N,N-di-*iso*-propyl-N-benzylamine**

$^1\text{H}$  NMR (200 MHz, *tol-d8*)  $\delta$  7.43 - 7.30 (m, 5H), 3.50 (s, 2H), 2.90 (sept,  $^3J_{\text{HH}} = 6.6$  Hz, 2H), 0.92 (d,  $^3J_{\text{HH}} = 6.6$  Hz, 12H).

$^1\text{H}$  NMR (200 MHz,  $\text{CDCl}_3$ )  $\delta$  7.44 - 7.27 (m, 5H), 3.20 (sept,  $^3J_{\text{HH}} = 6.6$  Hz, 2H), 1.10 (d,  $^3J_{\text{HH}} = 6.6$  Hz, 12H).

After the reaction the solvent was removed *in vacuo*, the residue washed with *n*-pentane and taken up in CDCl<sub>3</sub>, for which solution the <sup>1</sup>H NMR spectrum matched the one found in literature.<sup>451</sup>

**GCMS EI+ (A)** 15.8 min. *m/z* 191.2 [M]<sup>+</sup> (6%), 176.1 [M - CH<sub>3</sub>]<sup>+</sup> (54%), 91.0 [C<sub>6</sub>H<sub>5</sub>CH<sub>2</sub>]<sup>+</sup> (100%).

### Triethylphosphine

<sup>1</sup>H NMR (200 MHz, *tol-d8*) δ 1.32 - 1.09 (m, 6H), 1.08 - 0.80 (m, 9H).

<sup>31</sup>P NMR (81 MHz, *tol-d8*) δ -19.7 (s).

Obtained signal was found to be consistent with a literature spectrum.<sup>452</sup>

**GCMS EI+ (A)** 5.8 min. *m/z* 118.1 [M]<sup>+</sup> (55%), 90.1 [M - C<sub>2</sub>H<sub>4</sub>]<sup>+</sup> (82%), 62.0 [M - 2 C<sub>2</sub>H<sub>4</sub>]<sup>+</sup> (100%).

### Triphenylphosphine

<sup>1</sup>H NMR (200 MHz, *tol-d8*) δ 7.43 - 7.20 (m, 6H), 7.16 - 6.92 (m, 9H).

<sup>31</sup>P NMR (81 MHz, *tol-d8*) δ -5.1 (s).

**GCMS EI+ (A)** 20.9 min. *m/z* 262.1 [M]<sup>+</sup> (100%), 183.0 [M - C<sub>6</sub>H<sub>5</sub> - 2 H]<sup>+</sup> (75%), 108.0 [M - 2 C<sub>6</sub>H<sub>5</sub>]<sup>+</sup> (28%).

The identity of the product was verified through matching signals in comparison with a spectrum of the commercially obtained chemical in the same solvent.

### Hexaethyldisiloxane

<sup>1</sup>H NMR (200 MHz, CD<sub>2</sub>Cl<sub>2</sub>) δ 0.95 (t, <sup>3</sup>J<sub>HH</sub> = 7.9 Hz, 18H), 0.56 (q, <sup>3</sup>J<sub>HH</sub> = 7.9 Hz, 12H).

Obtained signals matched the ones found in literature.<sup>445</sup>

**GCMS EI+ (A)** 15.6 min. *m/z* 246.2 [M]<sup>+</sup> (< 0.5%), 217.2 [M - C<sub>2</sub>H<sub>5</sub>]<sup>+</sup> (100%).

### Ethyl 2-phenylcyclopent-2-ene-1-carboxylate (B).

<sup>1</sup>H NMR (600 MHz, CD<sub>2</sub>Cl<sub>2</sub>) δ 7.45 - 7.40 (m, 2H), 7.34 - 7.27 (m, 2H), 7.25 - 7.19 (m, 1H), 6.36 (td, *J*<sub>HH</sub> = 2.6, 1.6 Hz, 1H), 4.13 - 4.00 (m, 2H), 3.96 (m, 1H), 2.68 (m, 1H), 2.60 - 2.50 (m, 1H), 2.36 (dtd, *J*<sub>HH</sub> = 13.0, 9.2, 6.6 Hz, 1H), 2.25 - 2.15 (m, 2H), 1.15 (t, <sup>3</sup>J<sub>HH</sub> = 7.1 Hz, 3H).

Obtained shifts matched the ones found in literature.<sup>300</sup>

**GCMS EI+ (A)** 18.0 min. *m/z* 216.1 [M]<sup>+</sup> (16%), 142.1 [M - HCO<sub>2</sub>Et]<sup>+</sup> (100%).

## 5.2.7 Lewis Acidity Assessment and Reactivities of **2**

### 5.2.7.1 GB-Assessment of the Lewis Acidity

To a solution of **2** (11.1 mg, 1.0 eq.) in CD<sub>2</sub>Cl<sub>2</sub>, triethylphosphine oxide (a. 2.1 mg, 1.0 eq.; b. 4.2 mg, 2.0 eq.) was added. <sup>1</sup>H-, <sup>19</sup>F-, <sup>13</sup>C-, <sup>29</sup>Si- and <sup>31</sup>P -NMR spectroscopy revealed the immediate formation of **2**-OPEt<sub>3</sub> (a.) in near quantitative yields (based on internal integration), the *bis*-adduct **2**-(OPEt<sub>3</sub>)<sub>2</sub> was however not observed (b.). Instead, in the case of (b.) <sup>31</sup>P NMR spectroscopy indicated dynamic exchange of unbound and silicon bound OPEt<sub>3</sub> (see Figure S1). Connectivity of **2**-OPEt<sub>3</sub> was confirmed *via* scXRD of suitable crystals, that developed after gas diffusion of *n*-pentane into a saturated dichloromethane solution of the target compound over several days.

#### **2**-OPEt<sub>3</sub>

<sup>1</sup>H NMR (600 MHz, CD<sub>2</sub>Cl<sub>2</sub>) δ 2.06 (dq, <sup>2</sup>J<sub>PH</sub> = 15.2 Hz, <sup>3</sup>J<sub>HH</sub> = 7.7 Hz, 6H, **CH**<sub>2</sub>), 1.16 (dt, <sup>3</sup>J<sub>PH</sub> = 18.9 Hz, <sup>3</sup>J<sub>HH</sub> = 7.7 Hz, 9H, **CH**<sub>3</sub>).

<sup>13</sup>C NMR (151 MHz, CD<sub>2</sub>Cl<sub>2</sub>) δ 17.5 (d, <sup>1</sup>J<sub>PC</sub> = 64 Hz, **CH**<sub>2</sub>), 5.0 (d, <sup>2</sup>J<sub>PC</sub> = 4.8 Hz, **CH**<sub>3</sub>). Residual signals not detected due to limited concentration and intense fluorine coupling.

<sup>19</sup>F NMR (188 MHz, CD<sub>2</sub>Cl<sub>2</sub>) δ -148.6 (m, 4F), -159.2 (t, <sup>3</sup>J<sub>FF</sub> = 21.3 Hz, 2F), -164.9 (m, 2F), -165.6 (t, <sup>3</sup>J<sub>FF</sub> = 22.5 Hz, 2F), -168.2 (dt, <sup>3</sup>J<sub>FF</sub> = 21.4 Hz, <sup>4</sup>J<sub>FF</sub> = 7.3 Hz, 2F), -170.3 (dt, <sup>3</sup>J<sub>FF</sub> = 21.3 Hz, <sup>4</sup>J<sub>FF</sub> = 7.5 Hz, 2F), -172.8 (td, <sup>3</sup>J<sub>FF</sub> = 21.5 Hz, <sup>4</sup>J<sub>FF</sub> = 6.4 Hz, 2F), -173.7 (td, <sup>3</sup>J<sub>FF</sub> = 21.3 Hz, <sup>4</sup>J<sub>FF</sub> = 6.3 Hz, 2F).

<sup>29</sup>Si NMR (119 MHz, CD<sub>2</sub>Cl<sub>2</sub>) δ -111.0.

<sup>31</sup>P NMR (243 MHz, CD<sub>2</sub>Cl<sub>2</sub>) δ 83.3.

### 5.2.7.2 Chloride-Abstraction from Trityl Chloride

To a solution of **2** (25.0 mg, 1.0 eq.) in dichloromethane (1 mL) was added trityl chloride (1.0 eq.), upon which the solution turned immediately deep yellow. The mixture was stirred for 15 min (after which NMR spectroscopy indicated full conversion) and then concentrated *in vacuo*. The residue was suspended in 1 mL *n*-pentane and stirred rigorously for 15 min, the solid was allowed to settle and the supernatant was decanted. This step was repeated two times. The dark yellow to green solid was dried *in vacuo* (28.1 mg, 81%).

#### [CPh<sub>3</sub>][Cl-2]

<sup>1</sup>H NMR (600 MHz, CD<sub>2</sub>Cl<sub>2</sub>) δ 8.27 (t, <sup>3</sup>J<sub>HH</sub> = 7.4 Hz, 3H, *para*-H), 7.88 (t, <sup>3</sup>J<sub>HH</sub> = 7.7 Hz, 6H, *ortho*-H), 7.66 (d, <sup>3</sup>J<sub>HH</sub> = 7.6 Hz, 6H, *meta*-H).

<sup>13</sup>C NMR (151 MHz, CD<sub>2</sub>Cl<sub>2</sub>) δ 211.2 (+CPh<sub>3</sub>), 144.0 (C<sub>Ar</sub>-trityl), 143.1 (C<sub>Ar</sub>-trityl), 140.3 (C<sub>Ar</sub>-trityl), 131.0 (C<sub>Ar</sub>-trityl).

Residual signals not detected due to limited concentration and intense fluorine coupling.

<sup>19</sup>F NMR (376 MHz, CD<sub>2</sub>Cl<sub>2</sub>) δ -147.0 (dd, <sup>3</sup>J<sub>FF</sub> = 23.0 Hz, <sup>4</sup>J<sub>FF</sub> = 5.9 Hz, 2F), -148.9 (d, <sup>3</sup>J<sub>FF</sub> = 22.3 Hz, 2F), -160.9 (t, <sup>3</sup>J<sub>FF</sub> = 21.5 Hz, 2F), -166.1 (tq, <sup>3</sup>J<sub>FF</sub> = 22.3 Hz, <sup>4</sup>J<sub>FF</sub> = 3.0 Hz, 2F), -166.5 (tq, <sup>3</sup>J<sub>FF</sub> = 22.4 Hz, <sup>4</sup>J<sub>FF</sub> = 3.1 Hz, 2F), -169.6 (dt, <sup>3</sup>J<sub>FF</sub> = 21.0 Hz, <sup>4</sup>J<sub>FF</sub> = 7.5 Hz, 2F), -170.8 (dt, <sup>3</sup>J<sub>FF</sub> = 21.2 Hz, <sup>4</sup>J<sub>FF</sub> = 7.3 Hz, 2F), -174.8 (td, <sup>3</sup>J<sub>FF</sub> = 21.5 Hz, <sup>4</sup>J<sub>FF</sub> = 6.4 Hz, 2F), -175.7 (td, <sup>3</sup>J<sub>FF</sub> = 21.3 Hz, <sup>4</sup>J<sub>FF</sub> = 6.5 Hz, 2F).

<sup>29</sup>Si NMR (119 MHz, CD<sub>2</sub>Cl<sub>2</sub>) δ -98.5.

Calculated <sup>29</sup>Si resonance: -97.3 (see section Table A9 for details).

### 5.2.7.3 CO<sub>2</sub> Fixation

In a *J. Young* type NMR tube 50 mg **2** were dissolved in 0.45 mL CD<sub>2</sub>Cl<sub>2</sub>. Two equivalents tmp were added, and the mixture exposed to 1 atm CO<sub>2</sub> after removing the initial atmosphere (general remarks on gas reactions). The tube was kept in constant motion for 14 h, upon which NMR spectroscopy indicated the formation of the title compound. Obtained resonances were in good qualitative agreement with [tmpH<sub>2</sub>][tmpCO<sub>2</sub>-**1**<sup>Cl</sup>].<sup>254</sup> Precipitation with *n*-pentane in an off-white solid. Yield was not determined. In sight of the well-studied, analogous reactivity with **1**<sup>Cl</sup>, optimizations and further reactivities were not undertaken.<sup>254</sup>

**<sup>1</sup>H NMR** (600 MHz, CD<sub>2</sub>Cl<sub>2</sub>) δ 4.57 (br, 2H, N**H**<sub>2</sub>), 1.71 (m, 4H), 1.52 (m, 6H), 1.36 (m, 2H), 1.26 (br, 24H).

**<sup>13</sup>C NMR** (151 MHz, CD<sub>2</sub>Cl<sub>2</sub>) δ 56.5 (C(CH<sub>3</sub>)<sub>2</sub>), 54.4 (C(CH<sub>3</sub>)<sub>2</sub>), 41.8 (CH<sub>2</sub>), 36.7 (CH<sub>2</sub>), 29.5 (CH<sub>3</sub>), 29.1 (CH<sub>3</sub>), 17.0 (CH<sub>2</sub>), 15.8 (CH<sub>2</sub>).

**<sup>19</sup>F NMR** (565 MHz, CD<sub>2</sub>Cl<sub>2</sub>) δ -144.7 (br, 1F), -145.3 (br, 1F), -147.4 (br, 1F), -149.8 (br, 1F), -162.6 (br, 1F), -163.4 (br, 1F), -163.6 (br, 1F), -165.4 (br, 1F), -166.4 (br, 1F), -167.8 (br, 1F), -168.2 (br, 1F), -169.0 (br, 1F), -169.4 (br, 1F), -171.3 (br, 1F), -173.6 (br, 1F), -174.4 (br, 2F), -177.3 (br, 1F).

Further signals indicated the presence of various conformers, which prevented a full assignment of resonances.

**<sup>29</sup>Si NMR** (119 MHz, CD<sub>2</sub>Cl<sub>2</sub>) δ -148.6.

Calculated resonance -152.3 (see Table A9).

#### 5.2.7.4 Lewis Base Cooperative Reactivity with PhCF<sub>3</sub>

In a *J. Young* NMR tube 10 mg **2** were dissolved with equimolar amounts pmp and 1,1,1-trifluorotoluene (PhCF<sub>3</sub>) in CD<sub>2</sub>Cl<sub>2</sub>. The mixture was heated for 20 h at 40 °C, upon which NMR spectroscopy indicated the formation of the title compound. Pale orange crystals (suitable for scXRD, section 7.6) were obtained *via* gas diffusion of *n*-pentane into the reaction mixture at −40 °C. Yield was not determined.



**<sup>1</sup>H NMR** (600 MHz, CD<sub>2</sub>Cl<sub>2</sub>) δ 8.19 (s, 2H, NCH<sub>2</sub>), 1.94 (s, 6H, CH<sub>2</sub>), 1.62 (s, 12H, C(CH<sub>3</sub>)<sub>2</sub>).

**<sup>13</sup>C NMR** (151 MHz, CD<sub>2</sub>Cl<sub>2</sub>) δ 163.3 (NCH<sub>2</sub>), 71.8 (C(CH<sub>3</sub>)<sub>2</sub>), 37.2 (CH<sub>2</sub>), 30.9 (CH<sub>3</sub>), 15.4 (CH<sub>2</sub>).

**<sup>19</sup>F NMR** (376 MHz, CD<sub>2</sub>Cl<sub>2</sub>) δ −115.5 (s, 1F, SiF), −148.6 (dd, *J* = 23.5, 5.9 Hz, 2F), −148.9 (tdd, *J* = 14.1, 9.5, 5.4 Hz, 2F), −160.5 (t, *J* = 21.5 Hz, 2F), −165.9 (t, *J* = 17.7 Hz, 2F), −166.3 (t, *J* = 23.8 Hz), −169.3 (ddd, *J* = 21.2, 8.7, 6.2 Hz, 2F), −171.3 (ddd, *J* = 21.1, 8.7, 6.7 Hz, 2F), −174.5 (td, *J* = 21.3, 6.3 Hz, 2F), −175.6 (td, *J* = 21.3, 6.8 Hz, 2F).

**<sup>29</sup>Si NMR** (119 MHz, CD<sub>2</sub>Cl<sub>2</sub>) δ −109.3 (d, <sup>1</sup>*J*<sub>SiF</sub> = 191 Hz).

## 5.2.8 Reactivities of **2** and Sterically Demanding Lewis Bases

Of note, additional reactivities which are not mentioned in the main text with the sterically demanding phosphazene base  $P_1$  as well as LiHMDS in conjunction with 12-crown-4 ether were attempted. In the latter case a stable adduct formation was observed in the solid state. For the phosphazene base, a cleavage of the N-*t*Bu bond was observed.

### 5.2.8.1 Adduct Formation of **2** and $P^t\text{Bu}_3$

Upon addition of equimolar amounts of **2** and  $P^t\text{Bu}_3$  in  $\text{CD}_2\text{Cl}_2$  adduct formation was indicated by NMR spectroscopy. Slow decomposition to yet unidentified species was indicated by NMR spectroscopy. Exposition of a freshly prepared mixture of **2** and  $P^t\text{Bu}_3$  to  $\text{H}_2$  (1 atm) did not result in the observation of an  $\text{H}_2$  activation process up to temperatures of 65 °C and reaction times of 7 d, but similar decomposition was observed.

**2**- $P^t\text{Bu}_3$

$^1\text{H}$  NMR (400 MHz,  $\text{CD}_2\text{Cl}_2$ )  $\delta$  1.38 (d,  $^3J_{PH} = 11.3$  Hz).

$^{13}\text{C}$  NMR (101 MHz,  $\text{CD}_2\text{Cl}_2$ )  $\delta$  36.6, 32.0.

Residual signals not detected due to limited concentration and intense fluorine coupling.

$^{19}\text{F}$  NMR (188 MHz,  $\text{CD}_2\text{Cl}_2$ )  $\delta$  -145.5 (d,  $J = 21.2$  Hz, 2F), -147.3 (m, 2F), -154.5 (t,  $J = 21.3$  Hz, 2F), -162.0 (t,  $J = 20.8$  Hz, 2 F), -162.8 (br, 2F), -163.9 (br, 2F), -165.4 (m, 2F), -166.9 (br, 2F), -167.7 (br, 2F).

$^{31}\text{P}$  NMR (162 MHz,  $\text{CD}_2\text{Cl}_2$ )  $\delta$  56.0 (br).

No  $^{29}\text{Si}$  resonance could be detected.

### 5.2.8.2 Adduct Formation of **2** and tmpH

Upon addition of equimolar amounts of **2** and tmpH in CD<sub>2</sub>Cl<sub>2</sub> adduct formation was indicated by NMR spectroscopy. Exposition of a freshly prepared mixture of **2** and tmpH to H<sub>2</sub> (1 atm) did not result in the observation of an H<sub>2</sub> activation process up to temperatures of 65 °C and reaction times of 7 d.

**2**-tmpH

**<sup>1</sup>H NMR** (400 MHz, CD<sub>2</sub>Cl<sub>2</sub>) δ 1.67 (m, 2H), 1.43 (m, 4H), 1.19 (s, 12H).

**<sup>13</sup>C NMR** (101 MHz, CD<sub>2</sub>Cl<sub>2</sub>) δ 39.5, 30.3 (br), 17.6.

Residual signals not detected due to limited concentration and intense fluorine coupling.

**<sup>19</sup>F NMR** (376 MHz, CD<sub>2</sub>Cl<sub>2</sub>) δ -143.9 (br, 2F), -146.4 (br, 2F), -156.0 (br, 2F), -163.5 (br, 4F), -166.0 (br, 2F), -166.5 (br, 2F), -168.9 (br, 4F).

**<sup>29</sup>Si NMR** (119 MHz, CD<sub>2</sub>Cl<sub>2</sub>) δ -110.3.

### 5.2.8.3 Experiment with **2** and DTBP

Upon addition of equimolar amounts of **2** and DTBP no adduct formation was observed. H<sub>2</sub> cleavage at 1 atm H<sub>2</sub> pressure was not observed up to temperatures of 65 °C even when the mixture was heated over several days.

#### 5.2.8.4 Reactivity of **2** and NHC<sup>tBu</sup>

Upon addition of equimolar amounts 1,3-di-*tert*-butyl-1,3-imidazol-2-ylidene (NHC<sup>tBu</sup>) to a solution of **2** in C<sub>6</sub>D<sub>6</sub> immediate adduct formation was apparent. NMR spectroscopic analysis indicated the formation of the classical adduct (**2**-NHC<sup>tBu</sup>), however the slow isomerization towards the ‘abnormal’ adduct (**2**-<sup>a</sup>NHC<sup>tBu</sup>, Figure 35) was already apparent within minutes. Colorless crystals of the abnormal adduct that were suitable for scXRD developed from the reaction mixture through gas diffusion of *n*-pentane over several days at ambient temperature. The immediate exposition towards an H<sub>2</sub> atmosphere (1 atm) after preparation did not result in the observation of [H-**2**]<sup>-</sup>. The hydride species could also not be observed when utilizing a procedure that gave improved yield of the hydrogen cleavage product in conjunction with B(C<sub>6</sub>F<sub>5</sub>)<sub>3</sub>,<sup>453</sup> namely the preparation of the mixture at -196 °C, the exposition to dihydrogen (1 atm) at that temperature followed by cautious warming to -78 °C and then room temperature. Supporting calculations underpinned the proposed reactivity (Table A5).

In one of the attempts, the compound [NHC<sup>tBu</sup>H]<sub>2</sub>[Si<sub>2</sub>am<sup>F</sup>ph<sup>F</sup><sub>5</sub>] (reaction in C<sub>6</sub>D<sub>6</sub>, crystallization from CH<sub>2</sub>Cl<sub>2</sub> and *n*-pentane at -40 °C) incorporating a bridged dianion was indicated by scXRD as a trace product (for data see section 7.6).

##### **2**-NHC<sup>tBu</sup>

<sup>1</sup>H NMR (600 MHz, C<sub>6</sub>D<sub>6</sub>) δ 6.18 (s, 2H, CH), 1.14 (s, 18H, CH<sub>3</sub>).

<sup>13</sup>C NMR (151 MHz, C<sub>6</sub>D<sub>6</sub>) δ 118.0 (CH), 62.2 (C<sub>q</sub>), 31.8 (CH<sub>3</sub>).

Residual signals not detected due to limited concentration and intense fluorine coupling.

<sup>19</sup>F NMR (376 MHz, C<sub>6</sub>D<sub>6</sub>) δ -138.5 (d, <sup>3</sup>J<sub>FF</sub> = 24.6 Hz, 2F), -143.6 (m, 2F), -156.1 (t, <sup>3</sup>J<sub>FF</sub> = 22.2 Hz, 2F), -163.7 (m, 2F), -165.0 (t, <sup>3</sup>J<sub>FF</sub> = 22.2 Hz, 2F), -165.9 (m, 2F), -169.2 (dt, <sup>3</sup>J<sub>FF</sub> = 22.7 Hz, <sup>4</sup>J<sub>FF</sub> = 7.7 Hz, 2F), -169.6 (td, <sup>3</sup>J<sub>FF</sub> = 21.6 Hz, <sup>4</sup>J<sub>FF</sub> = 5.4 Hz, 2F), -170.4 (td, <sup>3</sup>J<sub>FF</sub> = 22.1 Hz, <sup>4</sup>J<sub>FF</sub> = 5.1 Hz, 2F).

<sup>29</sup>Si NMR (119 MHz, C<sub>6</sub>D<sub>6</sub>) δ -98.8.

**2-<sup>a</sup>NHC<sup>t</sup>Bu**

<sup>1</sup>H NMR (600 MHz, C<sub>6</sub>D<sub>6</sub>) δ 7.42 (s, 1H), 6.97 (s, 1H), 1.07 (s, 9H), 0.51 (s, 9H).

<sup>13</sup>C NMR (151 MHz, C<sub>6</sub>D<sub>6</sub>) δ 128.8, 127.0, 61.0 (C<sub>q</sub>), 58.4 (C<sub>q</sub>), 29.6 (CH<sub>3</sub>), 28.6 (CH<sub>3</sub>).

Residual signals not detected due to limited concentration and intense fluorine coupling.

<sup>19</sup>F NMR (188 MHz, C<sub>6</sub>D<sub>6</sub>) δ -145.9 (m, 2F), -147.5 (d, <sup>3</sup>J<sub>FF</sub> = 21.9 Hz, 2F), -157.8 (t, <sup>3</sup>J<sub>FF</sub> = 22.0 Hz, 2F), -163.7 (m, 2F), -165.6 (t, <sup>3</sup>J<sub>FF</sub> = 23.1 Hz, 2F), -166.9 (m, 2F), -170.3 (m, 2F), -171.5 (m, 4F).

<sup>29</sup>Si NMR (119 MHz, C<sub>6</sub>D<sub>6</sub>) δ -102.1.

**5.2.8.5 Reactivity of 2 and DIPEA**

To a solution of **2** in toluene-*d*<sub>8</sub> (0.5 mL) in a *J. Young* type NMR tube was added an equimolar amount of N,N'-di-*iso*-propyl-N''-ethylamine (DIPEA). NMR spectroscopic characterization revealed a mixture of various species (Figure 54), for which the presence of the hydridosilicate could be confirmed through <sup>1</sup>H-<sup>29</sup>Si-HMBC experiments and comparison to isolated [H-**2**]<sup>-</sup> species. The species were not isolated and yields not determined. Exposition of the sample to 1 atm H<sub>2</sub> and heating up to 110 °C over several days did not lead to further conversion to [H-**2**]<sup>-</sup>. Similar reactivity was observed in dichloromethane or benzene as solvent. Supporting calculations underpinned the proposed reactivity of dehydrogenative enamine formation and the subsequent reaction to an adduct (Table A5 and Table A9), that was similarly found for the reaction of B(C<sub>6</sub>F<sub>5</sub>)<sub>3</sub> and DIPEA.<sup>112</sup>

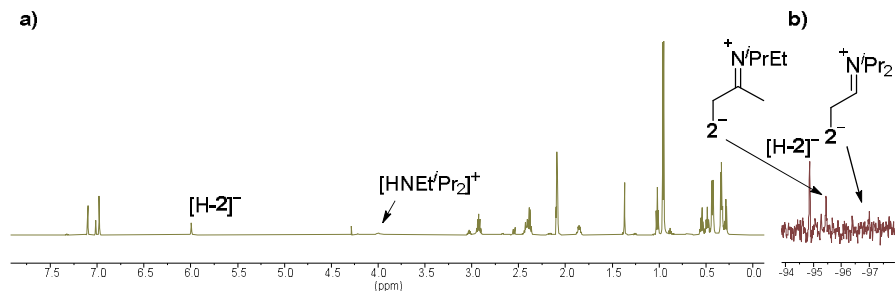


Figure 54. a) <sup>1</sup>H and b) <sup>29</sup>Si NMR spectra of the reaction mixture originating from **2** and DIPEA in toluene-*d*<sub>8</sub>.

## 5.2.9 Dihydrogen Activation Experiments with 2 pmp

**Characterization of the target species.**  $^1\text{H}$ ,  $^{13}\text{C}$ ,  $^1\text{H}/^{29}\text{Si}$  HMBC and  $^{29}\text{Si}$  NMR spectroscopic data of [pmpH][H-2] are consistent within all experiments, with the exception of the  $^1\text{H}$  NMR resonance for the N-bound proton in [pmpH] $^+$ , for which chemical shift and multiplicity (br or t) vary slightly. Assignment of defined  $^{19}\text{F}$  NMR chemical shifts to the anion in the splitting product [pmpH][H-2] was possible, well in line with the resonance for [Li@12c4][H-2] (see section 5.2.3.5), yet  $^{19}\text{F}$  NMR spectra were found to contain minor, unassigned signals. Even though a silicon bound fluorine could not be assigned NMR spectroscopically, it is within the possibilities of hydridosilicates to undergo hydride/fluoride exchange with a  $\text{C}(\text{sp}^2)\text{-F}$  bond.<sup>454</sup> Grown crystals from the reaction mixture containing [pmpH][H-2] (see also sections 5.1.2 and 7.6), suitable for scXRD, indicated a mixed crystal system that also contained a proportion of the fluoridosilicate [F-2] $^-$ . In line, a previous report on hypervalent hydridosilicates states that when synthesizing [K@18c6][(*p*-FC<sub>6</sub>H<sub>4</sub>)<sub>3</sub>SiH<sub>2</sub>] the target species is obtained as initial reaction product, yet, “*upon crystallization the compound undergoes some decomposition to release fluoride, resulting in the formation of mixed crystals of the hydride [(p-FC<sub>6</sub>H<sub>4</sub>)<sub>3</sub>SiH<sub>2</sub>] $^-$  and the fluoro/hydrido [(p-FC<sub>6</sub>H<sub>4</sub>)<sub>3</sub>Si(F)H] $^-$  anion*”.<sup>296</sup> The additional NMR spectroscopic signals of the initial reaction product might also be originating from dynamic processes of the formed hydridosilicate and the present parent compound, in related fashion to recently reported oligomerization<sup>231</sup> or ligand exchange processes<sup>178</sup> of bis(catecholato)silanes.

**Determination of conversions.** Due to the mentioned observations and as it was judged that the formation of the protonated pmp cation originates from the hydrogen cleavage reaction (underpinned by the absence of such resonances in control experiments without H<sub>2</sub>), reported conversions are based on internal integration of the pmp species (utilizing the  $\text{NCH}_3$  resonance of the cation compared to the one in free pmp; also reasoned by possibly different intensities due to slower relaxation times of [H-2] $^-$  compared to the pmp species in standard  $^1\text{H}$  NMR spectra). As this methodology arguably lacks some accuracy, the data given is intended to be understood as assessment.

### 5.2.9.1 Characterization Data for [pmpH][H-2]

**$^1\text{H}$  NMR** (600 MHz,  $\text{CD}_2\text{Cl}_2$ )  $\delta$  5.87 (s,  $^1J_{\text{SiH}} = 316$  Hz, SiH), 5.07 (t,  $^1J_{\text{NH}} = 47.8$  Hz, 1H, NH), 2.86 (d,  $J = 5.8$ , 3H, NCH<sub>3</sub>), 1.95z (m, 2H, CH<sub>2</sub>), 1.86 – 1.73 (m, 4H, CH<sub>2</sub>), 1.47 (s, 6H, C(CH<sub>3</sub>)), 1.42 (s, 6H, C(CH<sub>3</sub>)).

**$^{13}\text{C}$  NMR** [ $^{13}\text{C}$ ,  $^1\text{H}$ - $^{13}\text{C}$ -HSQC] (151 MHz,  $\text{CD}_2\text{Cl}_2$ )  $\delta$  67.4 (-C(CH<sub>3</sub>)<sub>2</sub>), 39.0 ( $\beta$ -C), 30.8 (CH<sub>3</sub>), 30.7 (NCH<sub>3</sub>), 20.1 (CH<sub>3</sub>), 15.9 ( $\gamma$ -C).

Residual signals not detected due to limited concentration and intense fluorine coupling.

Cation resonances in  $^1\text{H}$  and  $^{13}\text{C}$  spectra are in line with literature known data for [pmpH][BF<sub>4</sub>] in  $\text{CD}_2\text{Cl}_2$ .<sup>393</sup>

**$^{19}\text{F}$  NMR** (376 MHz,  $\text{CD}_2\text{Cl}_2$ )  $\delta$  -148.0 (m, 2F), -148.6 (dd,  $^3J_{\text{FF}} = 23.8$  Hz,  $^4J_{\text{FF}} = 5.3$  Hz, 2F), -161.2 (t,  $^3J_{\text{FF}} = 21.5$  Hz, 2F), -166.5 (m, 2F), -166.6 (t,  $^3J_{\text{FF}} = 23.7$  Hz, 2F), -169.5 (dt,  $^3J_{\text{FF}} = 20.9$  Hz,  $^4J_{\text{FF}} = 7.5$  Hz, 2F), -171.9 (dt,  $^3J_{\text{FF}} = 21.0$  Hz,  $^4J_{\text{FF}} = 7.7$  Hz, 2F), -175.2 (td,  $^3J_{\text{FF}} = 21.5$  Hz,  $^4J_{\text{FF}} = 6.9$  Hz, 2F), -176.2 (td,  $^3J_{\text{FF}} = 21.6$  Hz,  $^4J_{\text{FF}} = 7.4$  Hz, 2F).

**$^{29}\text{Si}$  NMR** [ $^{29}\text{Si}$ -IG,  $^1\text{H}$ - $^{29}\text{Si}$ -HMBC,  $^{29}\text{Si}$ ( $^1\text{H}$ )DEPT] (119 MHz,  $\text{CD}_2\text{Cl}_2$ )  $\delta$  -98.5.

**HRMS ESI-** (in  $\text{CH}_2\text{Cl}_2$ ) ( $m/z$ ) calc. for [C<sub>24</sub>HF<sub>18</sub>N<sub>2</sub>O<sub>2</sub>Si]<sup>-</sup> [M]<sup>-</sup>, 718.9525; found 718.9519 (100%), deviation 0.83 ppm.

**IR (ATR-FTIR)**  $\tilde{\nu}$  [ $\text{cm}^{-1}$ ] 3416 (w,  $\nu^{\text{NH}}$ ), 2957 (m,  $\nu^{\text{CH}}$ ), 2165 (m,  $\nu^{\text{SiH}}$ ), 1021 ( $\delta^{\text{SiH}}$ ), 982 ( $\delta^{\text{SiH}}$ ).

Data was collected from a spectrum, obtained from a concentrated crude reaction mixture that contained the target species.

### 5.2.9.2 Reference Experiment (1 eq. pmp, 1 atm, < 65 °C)

Equimolar amounts of **2** (13 mg) and pmp were dissolved in CD<sub>2</sub>Cl<sub>2</sub> (0.45 mL) in a *J. Young* type NMR tube. The mixture was exposed to H<sub>2</sub> (1 atm) and the reaction was monitored NMR spectroscopically over several days and at different temperatures (stepwise at rt, then 40 °C and then 65 °C, for 7 d resp.). In the whole process signals assignable to [H-**2**]<sup>-</sup> could not be detected and the substrates remained the main species.

### 5.2.9.3 Increased Temperature (115 °C)

Equimolar amounts of **2** (20 mg) and pmp were dissolved in *ortho*-dichlorobenzene (*o*DCB, 0.5 mL) in a *J. Young* type NMR tube. The mixture was exposed to H<sub>2</sub> (1 atm), heated to 115 °C and the reaction was monitored NMR spectroscopically over several days. After the reaction was allowed to proceed 7 d at the elevated temperature, the solvent was removed *in vacuo* and the colorless residue washed with *n*-pentane. After the solid was dried, it was taken up in CD<sub>2</sub>Cl<sub>2</sub> and analyzed NMR spectroscopically, confirming the formation of [pmpH][H-**2**] in <sup>1</sup>H, <sup>13</sup>C, and <sup>29</sup>Si NMR spectra.

### 5.2.9.4 Increased pmp Concentration (10 and 100 eq.)

In a *J. Young* type NMR tube **2** (15 mg) and tenfold excess pmp were dissolved in CD<sub>2</sub>Cl<sub>2</sub> (0.45 mL) and exposed to H<sub>2</sub> (1 atm). The reaction was heated to 65 °C and continuously monitored. After 7 d the conversion was estimated to be 73%. Subsequently, *n*-pentane was allowed to gas-diffuse into the reaction mixture, yielding a colorless precipitate after several days that contained crystals, for which scXRD confirmed the molecular structure of [pmpH][H-**2**] in a mixed crystal that also contained a proportion of [pmpH][F-**2**] (see sections 5.1.2 and 7.6 for crystallographic data and 5.2.6.1 for an additional comment).

In a *J. Young* type NMR tube **2** (10 mg) and 100 eq. pmp were dissolved in CD<sub>2</sub>Cl<sub>2</sub> (0.25 mL, making the solvent approximately a 1:1 mixture of pmp:CD<sub>2</sub>Cl<sub>2</sub>) and exposed to H<sub>2</sub> (1 atm). The reaction was first allowed to react at rt before it was heated to 40 °C and continuously monitored. After 7 d the conversion was estimated to be 71%. Removing the solvent *in vacuo* and washing the residue with *n*-pentane allowed the isolation of the colorless solid.

#### 5.2.9.5 Increased Pressure (50 atm H<sub>2</sub>)

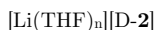
In a N<sub>2</sub>-Glovebox a standard mass vial was charged with **2**, equimolar amounts of pmp and CD<sub>2</sub>Cl<sub>2</sub> (0.3 mL). The vial was transferred into a *Man on the Moon* millireactor, which was sealed and connected to a H<sub>2</sub> supply. The pipe leading towards the reactor was freed from ambient atmosphere through standard Schlenk techniques before the reaction vessel was filled with 50 bar H<sub>2</sub>. After ensuring the sealing of the reactor, it was placed behind an additional protecting shield before heated to 60 °C in an oil bath. After 24 h the mixture was cooled to rt, the reactor transferred into a N<sub>2</sub>-Glovebox, opened carefully and the clear, colorless reaction mixture transferred in a *J. Young* type NMR tube. The vial was rinsed with 0.15 mL CD<sub>2</sub>Cl<sub>2</sub>, the tube sealed, and the crude reaction mixture analyzed *via* NMR spectroscopy (68% conversion after 24 h).

Subsequently, the mixture was layered with *n*-pentane (2.0 mL) and stored at -40 °C for several days. A colorless precipitate was apparent, among which colorless crystals suitable for scXRD were found, which confirmed the molecular structure of [pmpH][H-**2**] (cmp. section 5.2.9.4). Residual substrates were removed by washing the residue with *n*-hexane, and the colorless solid was subsequently dried *in vacuo*.

### 5.2.9.6 Cleavage of D<sub>2</sub> by **2**/pmp

For technical reasons the applied pressure of D<sub>2</sub> was limited to 0.6 bar. Tenfold excess of pmp was added to a solution of **2** in CH<sub>2</sub>Cl<sub>2</sub> and exposed to D<sub>2</sub> after evacuating the sample at 77 K. The reaction was then heated to 65 °C.

For comparison, [Li@12c4][D-**2**] was prepared in analogy to the <sup>1</sup>H species described above by employing LiAlD<sub>4</sub> (cmp. section 5.2.3.5).



<sup>2</sup>H NMR (92 MHz, CH<sub>2</sub>Cl<sub>2</sub>) δ 5.81 (s).

<sup>29</sup>Si NMR (119 MHz, CH<sub>2</sub>Cl<sub>2</sub>) δ -95.2 (t, <sup>1</sup>J<sub>SiD</sub> = 31.1 Hz).

The reaction was monitored *via* <sup>2</sup>H and <sup>29</sup>Si NMR spectroscopy. While the <sup>2</sup>H signal for [pmpD]<sup>+</sup> was clearly apparent, instead of the resonance of [D-**2**]<sup>-</sup> an increase of the -NCH<sub>2</sub>D pmp signal was found. In sight of the alpha-hydride abstraction that was found to readily occur upon reactivity of **2** and DIPEA (cmp. section 5.2.8.5). This observation is assigned to the (compared to the hydrogen cleavage) fast hydride exchange between the silicate and pmp (in tenfold excess), likely catalyzed by **2**. In accordance, the <sup>1</sup>H and <sup>29</sup>Si resonance (observed singlet instead of triplet through D-coupling) of the [H-**2**]<sup>-</sup> in the corresponding spectra was detected. In further alignment, in HRMS ESI<sup>-</sup> experiments the most intense signal was found to correspond to [H-**2**]<sup>-</sup>, but the m/z ratio assigned to [D-**2**]<sup>-</sup> was only marginally increased. The possible involvement of the iminium species as the active Lewis acid was precluded by computations and control experiments (cmp. section 5.2.9.7).

### 5.2.9.7 Probing the Activity of [tmp=CH<sub>2</sub>]<sup>+</sup> against H<sub>2</sub>

Even though the rapid abstraction of a hydride from pmp by **2**, and the subsequent deuteride addition from [D-**2**]<sup>-</sup> gives a plausible explanation, the deuteration of the methyl group in pmp in the D<sub>2</sub> experiments called for a closer examination on a possible intermediate role of the iminium ion (tmp=CH<sub>2</sub>)<sup>+</sup> in the hydrogen cleavage process. Therefore, the kinetics and thermodynamics for the FLP type cleavage of H<sub>2</sub> between the iminium ion (tmp=CH<sub>2</sub>)<sup>+</sup> and pmp (to yield [pmpH]<sup>+</sup> and pmp) were calculated (Table A5). While the thermodynamics were calculated to be favorable, the barrier was found to be higher than the one calculated for the pathway utilizing **2** and pmp. As the formation of the iminium ion from **2** and pmp is already an endergonic process, the total pay in Gibbs free energy from the substrates rises to 126 kJ mol<sup>-1</sup> (Figure A1).

To further disclose a possible active role of [tmp=CH<sub>2</sub>]<sup>+</sup> in the activation process, [tmp=CH<sub>2</sub>][B(C<sub>6</sub>F<sub>5</sub>)<sub>4</sub>] was synthesized according to a literature known procedure<sup>455</sup> (CH<sub>2</sub>Cl<sub>2</sub> was used as solvent instead of PhCF<sub>3</sub>). The ion pair was mixed with an equimolar amount of pmp in CD<sub>2</sub>Cl<sub>2</sub>, the solution exposed to H<sub>2</sub> (1 atm) and the reaction monitored <sup>1</sup>H NMR spectroscopically (see Figure S12). Allowing the mixture to proceed for 15 h at rt did not lead to any change in the <sup>1</sup>H NMR spectrum. The sample was subsequently heated to 65 °C. Even after heating for 5 d at 65 °C, no resonances assignable to [pmpH]<sup>+</sup> were detected, combined with no apparent decrease of the intensity of the cationic species.

[tmp=CH<sub>2</sub>][B(C<sub>6</sub>F<sub>5</sub>)<sub>4</sub>]

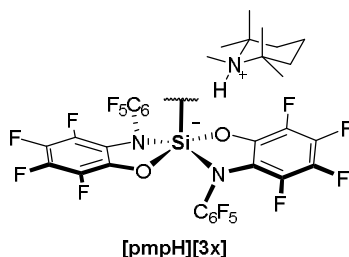
<sup>1</sup>H NMR (200 MHz, CD<sub>2</sub>Cl<sub>2</sub>) δ 8.15 (s, 2H, NCH<sub>2</sub>), 1.97 (s, 6H, CH<sub>2</sub>), 1.66 (s, 12H, C(CH<sub>3</sub>)<sub>2</sub>).

Resonances are under the consideration of minor shifting through solvent effects in line with the ones reported in literature.<sup>455</sup>

5.2.10 C–H Silylations with **2** and pmp and related Reactivities

## 5.2.10.1 General Procedure (GP) for the Syntheses of [pmpH][3x]

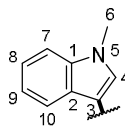
In a *J. Young* type NMR tube (NMR scale), a crimp vial, or a Schlenk-tube, **2** (1.0 eq.), substrate (1.0 eq.) and pmp (1.0 eq.) were dissolved in CD<sub>2</sub>Cl<sub>2</sub> (0.45 mL, NMR scale) or CH<sub>2</sub>Cl<sub>2</sub> (0.1 M), the vessel sealed, and the mixture allowed to react at the specified temperature. After the reaction proceeded, the mixture was concentrated *in vacuo* and the solid/viscous residue layered with benzene or toluene. The mixture was shaken and allowed to settle. The solvent was separated from the residue and the step repeated two times. The residue was dried *in vacuo*.



**Remarks on NMR characterization:** Data reported is in part taken from spectra obtained from reaction mixtures. While the NMR data is generally consistent with the isolated substances, occasionally minor variation in shift and multiplicity was found, which were neglectable for most resonances but pronounced for the *NH* <sup>1</sup>H-resonance (br or t, varying chemical shift).

## 5.2.10.2 [pmpH][3a]

GP: Reaction was kept for 24 h at rt, yielding colorless crystals (182 mg, 87%; NMR scale 16 mg, 92%) suitable for scXRD (see section 7). When conducted in toluene as solvent, direct crystallization from the reaction mixture was observed.



**<sup>1</sup>H NMR** (600 MHz, CD<sub>2</sub>Cl<sub>2</sub>) δ 7.90 (d, <sup>3</sup>J<sub>HH</sub> = 8.0 Hz, 1H, **H<sup>7</sup>**), 7.35 (s, 1H, **H<sup>4</sup>**), 7.27 (d, <sup>3</sup>J<sub>HH</sub> = 8.1 Hz, 1H, **H<sup>10</sup>**), 7.14 (t, <sup>3</sup>J<sub>HH</sub> = 7.0 Hz, 1H, **H<sup>9</sup>**), 7.01 (t, <sup>3</sup>J<sub>HH</sub> = 7.5 Hz, 1H, **H<sup>8</sup>**), 3.93 (t, <sup>4</sup>J<sub>NH</sub> = 49 Hz, 1H, **NH**), 3.73 (s, 3H, indole-N**CH<sub>3</sub>** (**H<sup>6</sup>**)), 2.61 (d, *J* = 5.8 Hz, 3H, pmp-N**CH<sub>3</sub>**), 1.84 (d, *J* = 14.8 Hz, 2H, **CH<sub>2</sub>**), 1.78 – 1.59 (m, 2H, **CH<sub>2</sub>**), 1.51 (t, *J* = 14.0 Hz, 2H, **CH<sub>2</sub>**), 1.28 (s, 6H, C(**CH<sub>3</sub>**)), 1.27 (s, 6H, C(**CH<sub>3</sub>**)).

**<sup>13</sup>C NMR** [<sup>13</sup>C, <sup>1</sup>H-<sup>13</sup>C-HSQC, <sup>1</sup>H-<sup>13</sup>C-HMBC] (151 MHz, CD<sub>2</sub>Cl<sub>2</sub>) δ 140.2 (**C<sup>4</sup>**), 138.9, 134.0, 129.3, 124.2 (**C<sup>7</sup>**), 121.0 (**C<sup>9</sup>**), 119.5 (**C<sup>8</sup>**), 111.3, 109.4 (**C<sup>10</sup>**), 67.6 (pmp C(CH<sub>3</sub>)<sub>2</sub>), 39.0 (pmp β-C), 33.1 (indole NCH<sub>3</sub>, **C<sup>6</sup>**), 31.0 (pmp CH<sub>3</sub>), 30.6 (pmp NCH<sub>3</sub>), 19.9 (pmp CH<sub>3</sub>), 15.8 (pmp γ-C).

**<sup>19</sup>F NMR** (376 MHz, CD<sub>2</sub>Cl<sub>2</sub>) δ -147.4 (dd, <sup>3</sup>J<sub>FF</sub> = 23.7, <sup>4</sup>J<sub>FF</sub> = 6.0 Hz, 2F), -148.7 (m, 2F), -162.4 (t, <sup>3</sup>J<sub>FF</sub> = 21.6 Hz, 2F), -167.1 (m, 4F), -170.3 (dt, <sup>3</sup>J<sub>FF</sub> = 21.4, <sup>4</sup>J<sub>FF</sub> = 7.7 Hz, 2F), -172.9 (dt, <sup>3</sup>J<sub>FF</sub> = 21.4, <sup>4</sup>J<sub>FF</sub> = 8.0 Hz, 2F), -176.4 (td, <sup>3</sup>J<sub>FF</sub> = 21.5, <sup>4</sup>J<sub>FF</sub> = 7.3 Hz, 2F), -177.7 (td, <sup>3</sup>J<sub>FF</sub> = 21.5, <sup>4</sup>J<sub>FF</sub> = 7.9 Hz, 2F).

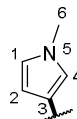
**<sup>29</sup>Si NMR** (119 MHz, CD<sub>2</sub>Cl<sub>2</sub>) δ -94.6.

**HRMS ESI<sup>-</sup>** (in CH<sub>2</sub>Cl<sub>2</sub>) (*m/z*) calc. for [C<sub>33</sub>H<sub>8</sub>F<sub>18</sub>N<sub>3</sub>O<sub>2</sub>Si]<sup>-</sup> [M]<sup>-</sup>, 848.0104; found 848.0104 (87%), deviation -0.1 ppm.

**Elemental analysis** calc. C 51.40%, H 3.01%, N, 5.58%. found C 51.09%, H 3.13%, N 5.66%.

## 5.2.10.3 [pmpH][3b]

GP: Reaction was kept for 48 h at rt, yielding a pale red, viscous oil. Upon grinding with a spatula, first a viscous solid was obtained, ultimately turning into a sticky, off-white powder (101 mg, 72%). The reaction was also found to be successful when conducted neat (xs. N-methylpyrrole), forming a pale red to brown oil directly from the reaction mixture. Minor unassigned trace impurities were detected, possibly originating from double activation or side reactivities with the fluorinated ligand, as for the related species [H-2]<sup>-cc</sup>. Extensive extraction with benzene diminished the proportion of impurity but resulted in disproportionate yield loss.



<sup>1</sup>H NMR (600 MHz, CD<sub>2</sub>Cl<sub>2</sub>) δ 6.84 (t, *J* = 1.8 Hz, 1H, **H<sup>1</sup>**), 6.60 (t, <sup>3</sup>*J*<sub>HH</sub> = 2.2 Hz, 1H, **H<sup>2</sup>**), 6.32 (t, <sup>3</sup>*J*<sub>HH</sub> = 1.9 Hz, 1H, **H<sup>4</sup>**), 4.35 (t, <sup>1</sup>*J*<sub>NH</sub> = 49 Hz, 1H, **NH**), 3.61 (s, **H<sup>6</sup>**), 2.79 (d, *J* = 5.8 Hz, 3H, pmp-N**CH<sub>3</sub>**), 1.94 (d, *J* = 14.3 Hz, 2H, **CH<sub>2</sub>**), 1.82 – 1.63 (m, 4H, **CH<sub>2</sub>**), 1.40 (s, 6H, C(**CH<sub>3</sub>**)), 1.38 (s, 6H, C(**CH<sub>3</sub>**)).

<sup>13</sup>C NMR [<sup>13</sup>C, <sup>1</sup>H-<sup>13</sup>C-HSQC, <sup>1</sup>H-<sup>13</sup>C-HMBC] (151 MHz, CD<sub>2</sub>Cl<sub>2</sub>) δ 132.0 (**C<sup>1</sup>**), 122.1 (**C<sup>2</sup>**), 119.9 (**C<sup>3</sup>**), 116.9 (**C<sup>4</sup>**), 67.6 (pmp **C(CH<sub>3</sub>)<sub>2</sub>**), 39.0 (pmp β-**C**), 36.1 (pyrrole-N**CH<sub>3</sub>** (**C<sup>6</sup>**)), 30.9 (pmp **CH<sub>3</sub>**), 30.7 (pmp N**CH<sub>3</sub>**), 20.0 (pmp **CH<sub>3</sub>**), 15.9 (pmp γ-**C**).

<sup>19</sup>F NMR (376 MHz, CD<sub>2</sub>Cl<sub>2</sub>) δ -147.0 (dd, <sup>3</sup>*J*<sub>FF</sub> = 23.6 Hz, <sup>4</sup>*J*<sub>FF</sub> = 5.8 Hz, 2F), -148.9 (m, 2F), -162.7 (t, <sup>3</sup>*J*<sub>FF</sub> = 21.5 Hz, 2F), -167.2 (t, <sup>3</sup>*J*<sub>FF</sub> = 21.7 Hz, 2F), -167.3 (m, 2F), -170.5 (dt, <sup>3</sup>*J*<sub>FF</sub> = 21.5 Hz, <sup>4</sup>*J*<sub>FF</sub> = 7.8 Hz, 2F), -173.2 (dt, <sup>3</sup>*J*<sub>FF</sub> = 21.4 Hz, <sup>4</sup>*J*<sub>FF</sub> = 8.0 Hz, 2F), -176.7 (td, <sup>3</sup>*J*<sub>FF</sub> = 21.5 Hz, <sup>4</sup>*J*<sub>FF</sub> = 7.3 Hz, 2F), -178.2 (td, <sup>3</sup>*J*<sub>FF</sub> = 21.4 Hz, <sup>4</sup>*J*<sub>FF</sub> = 8.1 Hz, 2F).

<sup>29</sup>Si NMR (119 MHz, CD<sub>2</sub>Cl<sub>2</sub>) δ -95.8.

HRMS ESI<sup>-</sup> (in CH<sub>2</sub>Cl<sub>2</sub>) (*m/z*) calc. for [C<sub>29</sub>H<sub>6</sub>F<sub>18</sub>N<sub>3</sub>O<sub>2</sub>Si]<sup>-</sup> [M]<sup>-</sup>, 797.9947; found 77.9955 (20%), deviation -1.0 ppm.

<sup>cc</sup> Of note, traces of the dianion [pmpH]<sub>2</sub>[Si<sub>2</sub>(am<sup>F</sup>ph<sup>F</sup>)<sub>5</sub>] were observed upon gas-diffusion of *n*-pentane into a solution of the title compound in CH<sub>2</sub>Cl<sub>2</sub>. While a clear proceeding of this reaction was not clarified yet, it might indicate an exchange of the carbanionic heteroaryl group and the ligand between silicates (e.g., 3 [Si(am<sup>F</sup>ph<sup>F</sup>)<sub>2</sub>-R]<sup>-</sup> → [R<sub>3</sub>Si(am<sup>F</sup>ph<sup>F</sup>)]<sup>-</sup> + [Si<sub>2</sub>(am<sup>F</sup>ph<sup>F</sup>)<sub>3</sub>]<sup>2-</sup>).

**5.2.10.4 [pmpH][3c]**

**GP** (NMR scale): Reaction was kept for 72 h at rt, yielding a pale red, viscous oil (22 mg, 68%). Upon trituration with a spatula, a viscous solid was obtained at first, ultimately turning into a sticky, off-white powder.

**<sup>1</sup>H NMR** (600 MHz, CD<sub>2</sub>Cl<sub>2</sub>) δ 7.44 – 7.37 (m, 4H, **H<sup>Ph</sup>**), 7.30 (br, 1H, **H<sup>I</sup>**), 7.21 (m, 1H, **H<sup>Ph</sup>**), 7.10 (t, <sup>3</sup>J<sub>HH</sub> = 2.4 Hz, 1H, **H<sup>2</sup>**), 6.53 (br, 1H, **H<sup>4</sup>**),

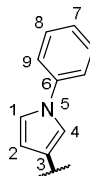
4.61 (t, <sup>1</sup>J<sub>NH</sub> = 45 Hz, 1H, **NH**), 2.81 (d, *J* = 5.5 Hz, 3H, pmp-N**CH<sub>3</sub>**), 1.94 (d, *J* = 14.5 Hz, 2H, **CH<sub>2</sub>**), 1.83 – 1.64 (m, 4H, **CH<sub>2</sub>**), 1.43 (s, 6H, C(**CH<sub>3</sub>**)), 1.38 (s, 6H, C(**CH<sub>3</sub>**)).

**<sup>13</sup>C NMR** [<sup>13</sup>C, <sup>1</sup>H-<sup>13</sup>C-HSQC, <sup>1</sup>H-<sup>13</sup>C-HMBC] (151 MHz, CD<sub>2</sub>Cl<sub>2</sub>) δ 140.7 (**C<sup>6</sup>**), 129.4 (**C<sup>Ph</sup>** (**C<sup>8</sup>**)), 127.9 (**C<sup>I</sup>**), 125.2 (**C<sup>7</sup>**), 122.1 (**C<sup>9</sup>**), 120.2 (**C<sup>Ph</sup>** (**C<sup>9</sup>**)), 119.1 (**C<sup>2</sup>**), 118.4 (**C<sup>4</sup>**), 67.8 (pmp C(CH<sub>3</sub>)<sub>2</sub>), 39.2 (pmp β-**C**), 31.2 (pmp **CH<sub>3</sub>**), 30.8 (pmp N**CH<sub>3</sub>**), 20.0 (pmp **CH<sub>3</sub>**), 15.8 (pmp γ-**C**).

**<sup>19</sup>F NMR** (376 MHz, CD<sub>2</sub>Cl<sub>2</sub>) δ -146.9 (dd, <sup>3</sup>J<sub>FF</sub> = 23.7 Hz, <sup>4</sup>J<sub>FF</sub> = 5.6 Hz, 2F), -148.9 (m, 2F), -162.6 (t, <sup>3</sup>J<sub>FF</sub> = 21.6 Hz, 2F), -167.1 (t, <sup>3</sup>J<sub>FF</sub> = 22.6 Hz, 2F), -167.3 (m, 2F), -170.4 (dt, <sup>3</sup>J<sub>FF</sub> = 21.2 Hz, <sup>4</sup>J<sub>FF</sub> = 7.8 Hz, 2F), -172.9 (dt, <sup>3</sup>J<sub>FF</sub> = 21.5 Hz, <sup>4</sup>J<sub>FF</sub> = 8.0 Hz, 2F), -176.5 (td, <sup>3</sup>J<sub>FF</sub> = 21.5 Hz, <sup>4</sup>J<sub>FF</sub> = 7.5 Hz, 2F), -178.0 (td, <sup>3</sup>J<sub>FF</sub> = 21.5 Hz, <sup>4</sup>J<sub>FF</sub> = 7.9 Hz, 2F).

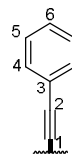
**<sup>29</sup>Si NMR** (119 MHz, CD<sub>2</sub>Cl<sub>2</sub>) δ -96.0.

**HRMS ESI-** (in CH<sub>2</sub>Cl<sub>2</sub>) (*m/z*) calc. for [C<sub>34</sub>H<sub>8</sub>F<sub>18</sub>N<sub>3</sub>O<sub>2</sub>Si]<sup>-</sup> [M]<sup>-</sup>, 860.0104; found 860.0108 (38%), deviation -0.5 ppm.



## 5.2.10.5 [pmpH][3d]

**GP** (NMR scale): Reaction was kept for 24 h at rt, yielding a colorless solid (37 mg, 91%).



$^1\text{H NMR}$  (600 MHz,  $\text{CD}_2\text{Cl}_2$ )  $\delta$  7.45 (m, 2H, *meta*- $\text{C}_{\text{Ph}}\text{H} / \text{H}^f$ ), 7.28 (m, 3H, *ortho*- $\text{C}_{\text{Ph}}\text{H} / \text{H}^f$  & *para*- $\text{C}_{\text{Ph}}\text{H} / \text{H}^b$ ), 4.58 (t,  $^1J_{\text{NH}} = 49$  Hz, 1H,  $\text{NH}$ ), 2.80 (d,  $J = 5.2$  Hz, 3H, pmp-N $\text{CH}_3$ ), 1.92 (d,  $J = 14.6$  Hz, 2H,  $\text{CH}_2$ ), 1.82 – 1.61 (m, 4H,  $\text{CH}_2$ ), 1.42 (s, 6H,  $\text{C}(\text{CH}_3)_2$ ), 1.36 (s, 6H,  $\text{C}(\text{CH}_3)_2$ ).

$^{13}\text{C NMR}$  [ $^{13}\text{C}$ ,  $^1\text{H}$ - $^{13}\text{C}$ -HSQC,  $^1\text{H}$ - $^{13}\text{C}$ -HMBC] (151 MHz,  $\text{CD}_2\text{Cl}_2$ )  $\delta$  131.8 ( $\text{C}_{\text{Ph}}$ ), 128.2 ( $\text{C}_{\text{Ph}}$ ), 128.1 ( $\text{C}_{\text{Ph}}$ ), 122.6 ( $\text{C}_{\text{Ph}}$ ), 112.5 ( $\text{C}^{\text{sp}}$ ), 101.6 ( $\text{C}^{\text{sp}}$ ), 67.1 (pmp  $\text{C}(\text{CH}_3)_2$ ), 38.6 (pmp  $\beta$ - $\text{C}$ ), 30.5 (pmp  $\text{CH}_3$ ), 30.3 (pmp N $\text{CH}_3$ ), 19.6 (pmp  $\text{CH}_3$ ), 15.4 (pmp  $\gamma$ - $\text{C}$ ).

$^{19}\text{F NMR}$  (565 MHz,  $\text{CD}_2\text{Cl}_2$ )  $\delta$  -147.2 (dd,  $^3J_{\text{FF}} = 23.3$ ,  $^4J_{\text{FF}} = 5.6$  Hz, 2F), -148.8 (m, 2F), -161.5 (t,  $^3J_{\text{FF}} = 21.5$  Hz, 2F), -166.3 (t,  $^3J_{\text{FF}} = 22.2$  Hz, 2F), -166.8 (t,  $^3J_{\text{FF}} = 19.5$  Hz, 2F), -169.92 (d,  $J = 21.3$  Hz, 2F), -171.78 (dt,  $^3J_{\text{FF}} = 21.3$  Hz,  $^4J_{\text{FF}} = 7.6$  Hz, 2F), -175.5 (td,  $^3J_{\text{FF}} = 21.4$  Hz,  $^4J_{\text{FF}} = 6.6$  Hz, 2F), -176.7 (td,  $^3J_{\text{FF}} = 21.6$  Hz,  $^4J_{\text{FF}} = 7.3$  Hz, 2F).

$^{29}\text{Si NMR}$  (119 MHz,  $\text{CD}_2\text{Cl}_2$ )  $\delta$  -108.4.

**HRMS ESI-** (in  $\text{CH}_2\text{Cl}_2$ ) ( $m/z$ ) calc. for  $[\text{C}_{32}\text{H}_5\text{F}_{18}\text{N}_2\text{O}_2\text{Si}]^- [\text{M}]^-$ , 818.9838; found 818.9840 (38%), deviation -0.2 ppm.

**5.2.10.6 [pmpH][3e]**

GP (NMR scale): Neat thiophene (0.4 mL) was used instead of  $\text{CD}_2\text{Cl}_2$  as solvent, resulting in a pale red to brown oil directly from the reaction mixture. Reaction was kept for 48 h at 80 °C, yielding a pale red, viscous oil (24 mg, 78%). Upon trituration with a spatula, a viscous solid was obtained at first, ultimately turning into a sticky, off-white powder.

**$^1\text{H}$  NMR** (400 MHz,  $\text{CD}_2\text{Cl}_2$ )  $\delta$  7.55 (dd,  $^3J_{\text{HH}} = 4.7$ ,  $^4J_{\text{HH}} = 1.0$  Hz, 1H, **H<sup>1</sup>**), 7.44 (dd,  $^3J_{\text{HH}} = 3.3$ ,  $^4J_{\text{HH}} = 1.1$  Hz, 1H, **H<sup>2</sup>**), 7.13 (dd,  $^3J_{\text{HH}} = 4.7$ ,  $J_{\text{HH}} = 3.4$  Hz, 1H, **H<sup>2</sup>**), 4.53 (br, 1H, **NH**), 2.83 (d,  $J = 5.8$  Hz, 3H, pmp-N**CH<sub>3</sub>**), 1.96 (d,  $J = 14.0$  Hz, 2H, **CH<sub>2</sub>**), 1.86 – 1.64 (m, 4H, **CH<sub>2</sub>**), 1.43 (s, 6H, **C(CH<sub>3</sub>)<sub>2</sub>**), 1.39 (s, 6H, **C(CH<sub>3</sub>)<sub>2</sub>**).

**$^{13}\text{C}$  NMR** [ $^{13}\text{C}$ ,  $^1\text{H}$ - $^{13}\text{C}$ -HSQC,  $^1\text{H}$ - $^{13}\text{C}$ -HMBC, DEPT-135] (101 MHz,  $\text{CD}_2\text{Cl}_2$ )  $\delta$  142.3 (**C<sup>4</sup>**), 137.3 (**C<sup>3</sup>**), 132.0 (**C<sup>2</sup>**), 128.4 (**C<sup>2</sup>**), 67.6 (pmp **C(CH<sub>3</sub>)<sub>2</sub>**), 39.1 (pmp  $\beta$ -**C**), 31.0 (pmp **CH<sub>3</sub>**), 30.7 (pmp **NCH<sub>3</sub>**), 20.0 (pmp **CH<sub>3</sub>**), 15.9 (pmp  $\gamma$ -**C**).

**$^{19}\text{F}$  NMR** (376 MHz,  $\text{CD}_2\text{Cl}_2$ )  $\delta$  -147.1 (dd,  $^3J_{\text{FF}} = 23.2$ ,  $^4J_{\text{FF}} = 5.9$  Hz, 2F), -148.9 (m, 2F), -162.0 (t,  $^3J_{\text{FF}} = 21.5$  Hz, 2F), -166.8 (t,  $^3J_{\text{FF}} = 22.3$  Hz, 2F), -167.1 (m, 2F), -170.1 (dt,  $^3J_{\text{FF}} = 21.5$  Hz,  $^4J_{\text{FF}} = 7.6$  Hz, 2F), -172.31 (dt,  $^3J_{\text{FF}} = 21.4$  Hz,  $^4J_{\text{FF}} = 7.9$  Hz, 2F), -175.9 (td,  $^3J_{\text{FF}} = 21.4$  Hz,  $^4J_{\text{FF}} = 7.0$  Hz, 2F), -177.2 (td,  $^3J_{\text{FF}} = 21.4$  Hz,  $^4J_{\text{FF}} = 7.5$  Hz, 2F).

**$^{29}\text{Si}$  NMR** (79 MHz,  $\text{CD}_2\text{Cl}_2$ )  $\delta$  -99.8.

**HRMS ESI<sup>-</sup>** (in  $\text{CH}_2\text{Cl}_2$ ) ( $m/z$ ) calc. for  $[\text{C}_{28}\text{H}_3\text{F}_{18}\text{N}_2\text{O}_2\text{SSi}]^-$   $[\text{M}]^-$ , 800.9403; found 800.9396 (100%), deviation 0.8 ppm.

### 5.2.10.7 Donor Induced Reversal of the Bond Cleavage

To a solution of [pmpH][**3a**] (11 mg) in CD<sub>2</sub>Cl<sub>2</sub> (0.45 mL) was added an equimolar amount of 1,3-Dimethyl-2-imidazolidinone (DMI) and the mixture was monitored using NMR spectroscopy. After 48 h at rt signals of N-methylindole in <sup>1</sup>H NMR spectra indicated a donor induced reversal of the bond cleavage (31%). Heating of the mixture to 60 °C accelerated the process and led to 91% conversion of the initial silicate after 40 h.<sup>dd</sup>

Apart from N-methylindole, **2**-DMI was identified as main product through comparison of <sup>19</sup>F NMR spectra. Minor unassigned signals (< 5%, assuming a structural relation to the **am<sup>F</sup>ph<sup>F</sup>** ligand system) are partially also found upon addition of DMI to unbound **2** and might correspond to a possible bis-adduct.

#### **2**-DMI

To a solution of unbound **2** (13 mg) in CD<sub>2</sub>Cl<sub>2</sub> was added 1 eq. DMI. NMR spectroscopy indicated adduct formation. The connectivity of the adduct was further confirmed by scXRD analysis of poor-quality crystals that formed upon gas diffusion of *n*-pentane into the reaction mixture. Yield was not determined.

<sup>1</sup>H NMR (600 MHz, CD<sub>2</sub>Cl<sub>2</sub>) δ 3.55 (br, 4H, **CH**<sub>2</sub>), 2.81 (s, 6H, **CH**<sub>3</sub>).

<sup>13</sup>C NMR (151 MHz, CD<sub>2</sub>Cl<sub>2</sub>) δ 45.9 (**CH**<sub>3</sub>), 31.4 (br, **CH**<sub>2</sub>).

CO signal was not detected.

<sup>19</sup>F NMR (565 MHz, CD<sub>2</sub>Cl<sub>2</sub>) δ -147.3 (br, 2F), -148.4 (br, 2F), -158.9 (t, <sup>3</sup>J<sub>FF</sub> = 21.5 Hz, 2F), -164.9 (br, 2F), -165.3 (br, 2F), -167.8 (dd, <sup>3</sup>J<sub>FF</sub>, <sup>4</sup>J<sub>FF</sub> = 21.1, 9.1 Hz, 2F), -170.0 (dd, <sup>3</sup>J<sub>FF</sub>, <sup>4</sup>J<sub>FF</sub> = 21.1, 9.1 Hz, 2F), -172.3 (td, <sup>3</sup>J<sub>FF</sub>, <sup>4</sup>J<sub>FF</sub> = 21.3, 5.4 Hz, 2F), -173.2 (td, <sup>3</sup>J<sub>FF</sub>, <sup>4</sup>J<sub>FF</sub> = 21.2, 5.8 Hz, 2F).

<sup>29</sup>Si NMR (119 MHz, CD<sub>2</sub>Cl<sub>2</sub>) δ -109.8.

---

<sup>dd</sup> Conversions determined through internal integration in <sup>1</sup>H NMR spectra.

### 5.2.11 KIE Determination for CH Cleavage of N-methylindole

For the determination of the kinetic isotope effect (KIE) N-methylindole was considered as a suitable substrate due to a fast and clean reaction and its regioselectivity (only reactivity in 3-position observed). 3-*deutero*-N-methylindole was prepared according to a literature known procedure (> 97% deuteration in 3-position).<sup>456</sup>

In a *J Young* type NMR tube, equimolar amounts of 3-*deutero*-N-methylindole and N-methylindole (1.0 eq., 80 μmol, each) were dissolved in CD<sub>2</sub>Cl<sub>2</sub> together with pmp (1.0 eq.) and hexamethylbenzene as internal standard (1.0 eq.). The mixture was analyzed by NMR spectroscopy. <sup>1</sup>H NMR experiments were conducted with a relaxation time of 60 s, to preclude misleading quantifications caused by incomplete integration data. Subsequently, **2** (1.0 eq.) was added and the reaction allowed to proceed for 12 h at rt. <sup>19</sup>F and <sup>29</sup>Si NMR spectroscopy confirmed full conversion of the FLP **2**/pmp. Assuming that the consumed substrate was fully converted to the respective silicate, a KIE (k<sub>H</sub>/k<sub>D</sub>) can be calculated from this data as shown below (uncertainty calculated assuming an integral error of 0.01 with *GAUSSIAN* error propagation).

#### Calculation of the KIE

When using an intermolecular experiment, commonly equimolar amounts of deuterated and protonated substrate are reacted and the KIE is calculated as a ratio of the yield derived from the protonated to the deuterated form.<sup>457</sup> The present experiment was planned accordingly, yet the exact ratio of protonated to deuterated form was determined using NMR integrals and the calculation therefore modified accordingly, using the yields referenced against the initial substrate (formula **I**).

$$\begin{aligned}
 \text{(I) } KIE = \frac{k_H}{k_D} &= \frac{[P_H]_{t>0}}{[S_H]_{t=0}} \bigg/ \frac{[P_D]_{t>0}}{[S_D]_{t=0}} = \frac{[P_H]_{t>0}}{[S_H]_{t=0}} \cdot \frac{[S_D]_{t=0}}{[P_D]_{t>0}} \\
 \text{(i) } [S_D]_{t=0} &= [S_{H+D}]_{t=0} - [S_H]_{t=0} \\
 \text{(ii) } [P_H]_{t>0} &= [S_H]_{t=0} - [S_H]_{t>0} \\
 \text{(iii) } [P_D]_{t>0} &= [P_{H+D}]_{t>0} - [P_H]_{t>0} = \\
 &= ([S_{H+D}]_{t=0} - [S_{H+D}]_{t>0}) - ([S_H]_{t=0} - [S_H]_{t>0}) \\
 \text{(II) } KIE &= \frac{[S_H]_{t=0} - [S_H]_{t>0}}{[S_H]_{t=0}} \cdot \frac{[S_{H+D}]_{t=0} - [S_H]_{t=0}}{([S_{H+D}]_{t=0} - [S_{H+D}]_{t>0}) - ([S_H]_{t=0} - [S_H]_{t>0})}
 \end{aligned}$$

Calibrating the spectra to the solvent signal and the integral for the internal standard at a constant value, the signals at 6.5 ppm, 7.2 ppm and 7.6 ppm were integrated, as all were judged sufficiently separated from neighboring resonances prior to and after the reaction proceeded. The resonance at 6.5 ppm represents the hydrogen involved in the cleavage process, the resonances at 7.2 ppm and 7.6 ppm both serve as estimation for the combined concentration of N-methylindole substrate (deuterated and protonated) and were averaged for the final KIE assessment. Relative values of the integrals are listed in Table 9.

Table 9. Resonances and integrals used for the assessment of the KIE. Signals were integrated in a range of  $\pm 0.1$  ppm when no neighboring signal was found in this range or otherwise to the maximal possible range.

	Integrated Signal [ppm]	Integral Value	Proportional To
t = 0	6.5 ( $H^B$ of substrate)	1.088	$[S_H]_{t=0}$
t = 12 h		0.378	$[S_H]_{t>0}$
t = 0	7.6 ( $H^A$ of substrate)	2.147	$[S_{H+D}]_{t=0}$
t = 12 h		1.240	$[S_{H+D}]_{t>0}$

The final KIE was calculated utilizing formula **II**. Instead of the molar concentrations, integral values of respective  $^1\text{H}$  NMR signals were utilized directly (Table 9), which are proportional to the molar concentrations. The latter might be derived through multiplication with the concentration of the internal standard.

Ultimately, a KIE of 3.5 can be assessed. It shall be noted that the present experiment is intended to give qualitative proof for a direct involvement of the C–H/D bond in the rate-determining step and does not serve as exact quantification of kinetic data. An assumed integral uncertainty of 0.01 propagates to an uncertainty of  $\pm 0.7$  of the final KIE (not considering used approximations and possible systematic errors).

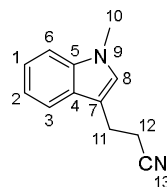
## 5.2.12 Catalytic Addition of N-heterocycles to Acrylonitrile

### 5.2.12.1 General Procedure

A *J. Young* type NMR tube was charged with 10 mol% **2** (10  $\mu$ mol), heteroarene (1.0 - 5.0 eq.) and  $\text{CD}_2\text{Cl}_2$  (0.45 mL). Cyclooctane (100  $\mu$ mol, 1 eq.) was added as internal standard for the determination of yields by internal integration. Acrylonitrile (1.0 - 3.0 eq.) was added, the tube capped, kept at rt under constant motion and the mixture was continuously monitored using  $^1\text{H}$  NMR spectroscopy. When the reaction had proceeded, aq. sat.  $\text{Na}_2\text{CO}_3$  solution was added, the phases separated, and the aqueous phase extracted with dichloromethane (x2). The combined organic phases were dried over  $\text{Na}_2\text{SO}_4$  and filtered over a short pad of silica, eluting with  $\text{CH}_2\text{Cl}_2$ . The solvent was removed under reduced pressure and the residue rigorously dried *in vacuo*.

### 5.2.12.2 3-(N-methylpyrrole-3-yl)-propionitrile (**4a**)

1.0 eq. N-methylindole, 3.0 eq. acrylonitrile. After 3 d at rt internal integration revealed >99% of product formation. Pale yellow viscous (87%).



$^1\text{H}$  NMR (200 MHz,  $\text{CD}_2\text{Cl}_2$ )  $\delta$  7.56 (d,  $J_{\text{HH}} = 7.7$  Hz, 1H), 7.34 (d,  $J = 8.1$  Hz, 1H), 7.24 (t,  $J_{\text{HH}} = 7.4$  Hz, 1H), 7.12 (t,  $J_{\text{HH}} = 7.3$  Hz, 1H), 7.02 (s, 1H), 3.76 (s, 3H), 3.12 (t,  $J_{\text{HH}} = 7.1$  Hz, 2H), 2.72 (t,  $J_{\text{HH}} = 7.1$  Hz, 2H).

$^1\text{H}$  NMR (600 MHz,  $\text{CDCl}_3$ )  $\delta$  7.56 (dd,  $J_{\text{HH}} = 7.9, 0.9$  Hz, 1H,  $\mathbf{H}^{\text{b}}$ ), 7.34 (dd,  $J_{\text{HH}} = 8.2, 0.9$  Hz, 1H,  $\mathbf{H}^{\text{c}}$ ), 7.28 (tt,  $J_{\text{HH}} = 9.0, 1.6$  Hz, 1H,  $\mathbf{H}^{\text{d}}$ ), 7.16 (tt,  $J_{\text{HH}} = 6.9, 1.2$  Hz, 1H,  $\mathbf{H}^{\text{e}}$ ), 7.01 (s, 1H,  $\mathbf{H}^{\text{f}}$ ), 3.78 (s, 3H,  $\mathbf{H}^{\text{g}}$ ), 3.13 (t,  $J_{\text{HH}} = 7.2$  Hz, 2H,  $\mathbf{H}^{\text{h}}$ ), 2.70 (t,  $J_{\text{HH}} = 7.2$  Hz, 2H,  $\mathbf{H}^{\text{i}}$ ).

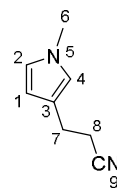
NMR data is consistent with the one found in literature.<sup>420</sup>

$^{13}\text{C}$  NMR [ $^{13}\text{C}$ ,  $^1\text{H}$ - $^{13}\text{C}$ -HSQC,  $^1\text{H}$ - $^{13}\text{C}$ -HMBC] (151 MHz,  $\text{CDCl}_3$ )  $\delta$  137.1 ( $\mathbf{C}^{\text{f}}$ ), 127.1 ( $\mathbf{C}^{\text{d}}$ ), 127.0 ( $\mathbf{C}^{\text{e}}$ ), 122.0 ( $\mathbf{C}^{\text{g}}$ ), 119.9 ( $\mathbf{C}^{\text{a}}$ ), 119.3 ( $\mathbf{C}^{\text{b}}$ ), 118.3 ( $\mathbf{C}^{\text{c}}$ ), 111.1 ( $\mathbf{C}^{\text{h}}$ ), 109.6 ( $\mathbf{C}^{\text{e}}$ ), 32.8 ( $\text{NCH}_3$ ,  $\mathbf{C}^{\text{g}}$ ), 21.7 ( $\mathbf{C}^{\text{h}}$ ), 19.0 ( $\mathbf{C}^{\text{i}}$ ).

GCMS EI+ (**B**) Retention time 14.5 min.  $m/z$  184.18 (26%)  $[\text{M}]^+$ , 144.14 (100%)  $[\text{M} - \text{CNCH}_2]^+$ .

### 5.2.12.3 3-(N-methylpyrrole-3-yl)-propionitrile (**4b**)

5.0 eq. N-methylpyrrole, 1.0 eq. acrylonitrile. After 14 h at rt internal integration revealed 86% of product formation. Pale yellow viscous (75%). Minor formation of **4b'** was observed (5% according to internal integration).



$^1\text{H NMR}$  (200 MHz,  $\text{CDCl}_3$ )  $\delta$  6.59 (t,  $J_{\text{HH}} = 2.3$  Hz, 1H), 6.08 (t,  $J_{\text{HH}} = 3.2$  Hz, 1H), 5.99 (m, 1H), 3.58 (s, 3H), 2.95 (t,  $J_{\text{HH}} = 7.5$  Hz, 3H), 2.65 (t,  $J_{\text{HH}} = 7.3$  Hz, 3H).

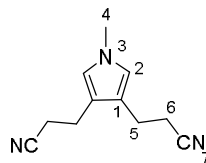
$^1\text{H NMR}$  (400 MHz,  $\text{CDCl}_3$ )  $\delta$  6.59 (d,  $J_{\text{HH}} = 4.4$  Hz, 1H,  $\text{H}^2$ ), 6.08 (d,  $J_{\text{HH}} = 6.3$  Hz, 1H,  $\text{H}^1$ ), 5.98 (ddd,  $J_{\text{HH}} = 2.6, 1.7, 0.9$  Hz, 1H,  $\text{H}^3$ ), 3.58 (s, 3H), 2.95 (td,  $J_{\text{HH}} = 7.6, 3.0$  Hz, 4H,  $\text{H}^7$ ), 2.65 (t,  $J_{\text{HH}} = 7.6$  Hz, 2H,  $\text{H}^8$ ).

$^{13}\text{C NMR}$  [ $^{13}\text{C}$ ,  $^1\text{H}$ - $^{13}\text{C}$ -HSQC,  $^1\text{H}$ - $^{13}\text{C}$ -HMBC] (101 MHz,  $\text{CDCl}_3$ )  $\delta$  129.0 ( $\text{C}^9$ ), 122.5 ( $\text{C}^2$ ), 119.3 ( $\text{C}^3$ ), 107.2 ( $\text{C}^1$ ), 106.6 ( $\text{C}^4$ ), 33.7 ( $\text{C}^6$ ), 22.7 ( $\text{C}^7$ ), 17.4 ( $\text{C}^8$ ).

GCMS EI+ (**B**) 11.5 min.  $m/z$  134.30 (24%)  $[\text{M}]^+$ , 94.25 (100%)  $[\text{M} - \text{CNCH}_2]^+$ .

### 5.2.12.4 3,3'-(N-methylpyrrole-3,4-diyl)-dipropionitrile (**4b'**)

1.0 eq. N-methylpyrrole, 3.0 eq. acrylonitrile. After 3 d at rt internal integration revealed 92% of product formation. Pale orange solid (80%).



$^1\text{H NMR}$  (200 MHz,  $\text{CD}_2\text{Cl}_2$ )  $\delta$  5.92 (s, 2H,  $\text{H}^2$ ), 3.43 (s, 3H,  $\text{H}^4$ ), 2.92 (t,  $J_{\text{HH}} = 7.2$  Hz, 4H,  $\text{H}^5$ ), 2.65 (t,  $J_{\text{HH}} = 7.0$  Hz, 4H,  $\text{H}^6$ ).

$^1\text{H NMR}$  [ $^{13}\text{C}$ ,  $^1\text{H}$ - $^{13}\text{C}$ -HSQC,  $^1\text{H}$ - $^{13}\text{C}$ -HMBC] (600 MHz,  $\text{CDCl}_3$ )  $\delta$  5.93 (s, 2H,  $\text{H}^2$ ), 3.46 (s, 3H,  $\text{H}^4$ ), 2.93 (t,  $J_{\text{HH}} = 7.5$  Hz, 4H,  $\text{H}^5$ ), 2.64 (t,  $J_{\text{HH}} = 7.5$  Hz, 4H,  $\text{H}^6$ ).

$^{13}\text{C NMR}$  (151 MHz,  $\text{CDCl}_3$ )  $\delta$  129.5 ( $\text{C}^1$ ), 119.2 ( $\text{C}^7$ ), 105.7 ( $\text{C}^2$ ), 30.4 ( $\text{C}^4$ ), 23.0 ( $\text{C}^5$ ), 17.2 ( $\text{C}^6$ ).

GCMS EI+ (**B**) 16.4 min.  $m/z$  187.18 (28%)  $[\text{M}]^+$ , 147.18 (90%)  $[\text{M} - \text{CNCH}_2]^+$ , 107.17 (100%)  $[\text{M} - \text{CNCH}_2 - \text{CN}]^+$ .

### 5.2.12.5 Reaction of [pmpH][**3a**] with Acrylonitrile

Reacting a solution of equimolar amounts [pmpH][**3a**] in  $\text{CD}_2\text{Cl}_2$  at rt revealed formation of 38% **4a** after 16 h (determined by internal  $^1\text{H}$  integration and GCMS measurements). Longer reactions times up to 14 d only revealed a minorly increased proportion of **4a**.

#### 5.2.12.6 Comparison Experiments with SiCl<sub>4</sub> and 1<sup>Cl</sup>

A *J. Young* type NMR tube was charged with N-methylpyrrole (21  $\mu\text{mol}$ ), equimolar amounts of silane (**2**, **1<sup>Cl</sup>**,<sup>255</sup> SiCl<sub>4</sub>) as well as pmp, and the compounds mixed in CD<sub>2</sub>Cl<sub>2</sub> (0.45 mL). The reaction mixtures were monitored using NMR spectroscopy. Conversions mentioned in the main manuscript were obtained through integration of <sup>1</sup>H NMR spectra after addition of hexamethylbenzene as internal standard.

### 5.2.13 Other Syntheses

#### 5.2.13.1 $1^{\text{Cl}}\text{-(sulfolane)}_2$

Perchlorocatechol (1.40 g, 2.0 eq.) was dissolved in a sulfolane/benzene mixture (28 mL, 97:3 V%).  $\text{SiCl}_4$  (0.39 mL, 3.39 mmol, 1.20 eq.) was added dropwise at rt, the mixture was allowed to stir for 15 min and then heated to 100 °C for 15 h. After cooling to rt, the formed colorless, crystalline solid (suitable for scXRD, details see section 7.6) was filtered and washed with benzene, dichloromethane, and *n*-pentane and the product was dried *in vacuo* (1.73 g, 81%).

$^1\text{H NMR}$  (600 MHz,  $\text{CD}_2\text{Cl}_2$ )  $\delta$  3.04 (m, 8H,  $\alpha\text{-CH}_2$ ), 2.20 (m, 8H,  $\beta\text{-CH}_2$ ).

$^{13}\text{C NMR}$  (151 MHz,  $\text{CD}_2\text{Cl}_2$ )  $\delta$  51.8 ( $\alpha\text{-CH}_2$ ), 23.2 ( $\beta\text{-CH}_2$ ).

$^{29}\text{Si NMR}$  spectroscopy was prevented by limited solubility in common deuterated organic solvents.

## 5.3 Computational Details

### 5.3.1 General Remarks

Unless stated otherwise, all computations were calculated using the *Orca* 4.1, 4.2 or 5.0 program package,<sup>458,459</sup> in part extended by the GFN-xTB methods provided in the corresponding software package.<sup>460-462</sup> As initial guess, VSEPR structures preoptimized with force-field methods in the *Avogadro*<sup>433</sup> software were used. In general, these starting structures were directly applied for the optimization. In some cases, which are specified, the starting structure was chosen as best conformation determined by the *Conformer Rotamer Ensemble Sampling Tool* (CREST),<sup>463</sup> using the GFN2-xTB method.<sup>461</sup>

The resolution-of-identity<sup>464</sup> and “chain of spheres”<sup>465</sup> approximation in the form of RIJCOSX was used in combination with matching auxiliary basis sets.<sup>466</sup> When applied, the *BECKE-JOHNSON* damping function<sup>467,468</sup> in conjunction with *GRIMME*’s semi-empirical dispersion correction<sup>469,470</sup> is denoted as *D3(BJ)*. The physically improved and more sophisticated successor model is denoted as *D4*.<sup>471</sup> Calculations incorporated the GFN2-xTB method (xTB2),<sup>461</sup> the composite schemes PBEh-3c<sup>472</sup> and r<sup>2</sup>SCAN-3c,<sup>473</sup> the PBE0,<sup>474,475</sup> PW6B95,<sup>476</sup> and DSD-BLYP<sup>477</sup> functionals, the basis sets def2-TZVPP,<sup>478,479</sup> def2-QZVPP,<sup>478,479</sup> aug-cc-pVQZ,<sup>480-485</sup> and cc-pVDZ.<sup>480-485</sup> Additionally, the DLPNO-CCSD(T)<sup>486-488</sup> method was utilized for obtaining single point energies. Solvation corrections incorporated the conductor-like polarizable continuum model (CPCM), the analytical linearized Poisson–Boltzmann model (ALPB)<sup>489</sup> or the *Universal Solvent Model* (SMD).<sup>490</sup> A concentration term of  $\Delta G_{\text{conc}} = RT \ln(24.5) = 7.9 \text{ kJ mol}^{-1}$  (298 K) for the solution Gibbs free energy was additionally considered, arising from a change of gas (1 atm) to solution phase (1 M).<sup>491</sup> Used combinations of schemes, functionals, basis sets, and solvation models are denoted respectively.

Thermodynamic data at 298 K were computed using the rigid-rotor harmonic oscillator (RRHO) approximation at the level of optimization.<sup>492</sup> Calculated structures have been confirmed as energetic minima on the potential energy surface by the analytical calculation of harmonic frequencies. Transition geometries were optimized toward a single negative Hessian matrix eigenvalue. It was ensured that the correct first-order saddle point on the potential energy surface was located by

animation of the imaginary frequency.<sup>434</sup> For the structures TS-[**1**<sup>3,5-Cm</sup>]<sub>2</sub><sup>‡</sup> and [**1**<sup>3,4,6-iPr</sup>]<sub>2</sub> one additional imaginary mode was encountered (value < 10 cm<sup>-1</sup>), which was respectively judged to be artificial after visualization. The artificial imaginary modes were treated as infinitesimal positive, and the respective Gibbs free energies thus manually corrected by -11.2 kJ mol<sup>-1</sup> per mode, according to *GRIMME*'s quasi-RRHO approach.<sup>492</sup>

For the computational study of the equilibrium of adduct formation between **1**<sup>CF<sub>3</sub></sup> and O(SiEt<sub>3</sub>)<sub>2</sub> the favored conformation was used as starting structure, which was determined with CREST.<sup>463</sup> The more reliable resulting final energies (Table A2) are better reflecting the corresponding experiment in comparison to the previously published data, which is still in qualitative agreement.

Computed cartesian coordinates are largely available free of charge in the supporting information of the respective publications.

Resulting energies, anion affinities, thermodynamic and kinetic data, as well as computed NMR resonances are summarized in section 7.3.

Computations were largely processed on the JUSTUS2 cluster, provided by the state of Baden-Württemberg through bwHPC and the German Research Foundation (DFG) through grant no INST 40/575-1 FUGG. The author kindly acknowledges this support.

### 5.3.2 Anion Affinities

Single point energies of optimized structures were obtained at the DLPNO-CCSD(T) level of theory in conjunction with suitable basis sets (methods are denoted along with the respective data in Table A3). Final anion affinities were determined according to the protocol proposed by *KROSSING*,<sup>33,89</sup> using an *isodesmic* reaction scheme against CCSD(T)/CBS anchor points.<sup>30,78</sup>

Solvation correction for the anion affinities was considered as suggested in literature.<sup>30,78</sup> To extract enthalpic contribution of solvation the following protocol was used. First, solvation free energies were obtained by COSMO-RS<sup>493</sup> in dichloromethane as implemented in ADF<sup>494</sup> based on BP86/TZP<sup>495</sup> single point energy calculations for the electrostatic solute-solvent interaction on the gas-phase

structures.<sup>496-499</sup> Then, COSMO-RS correction for enthalpies was achieved by calculating  $\Delta G$ -corrections at five different temperatures (278.15, 288.15, 298.15, 308.15, 318.15 K). A linear fit of satisfying  $\Delta G = \Delta H - T\Delta S$  plots of the obtained Gibbs free energy corrections against the temperature allowed to extract the corrections for  $\Delta H$ .

The anion affinity of  $\mathbf{1}^{\text{CF}_3}$  was computed in this work (Table A3). The displayed anion affinity in chapter 3.2 differs from this value but is shown as it utilized a higher optimization level. It was computed by *D. ROTH* in the course of his master's thesis.<sup>500</sup> For this, the structure was optimized at the PW6B95-D3(BJ)/def2-TZVPP level. The thermodynamic correction was obtained at the BP86-D3(BJ)/def2-SVP level of theory after re-optimization.

### 5.3.3 Calculation of NMR Resonances

Calculation of  $^{29}\text{Si}$  NMR resonances was conducted at the PBE0-D3(BJ)+SMD(*solvent*)/def2-TZVPP level of theory, as this combination was shown to be a reliable method.<sup>501</sup> Solvation effects were considered implicitly, using the *Universal Solvent Model* (SMD).<sup>490</sup> Resonances were referenced against tetramethylsilane, for which optimization and chemical shielding were calculated in the same manner.

### 5.3.4 Workflow for the Computational Analysis of FLP Ensembles

To generate a starting ensemble for computational analysis, the respective Lewis pairs were analyzed for conformers using the non-covalent interaction mode of the CREST program package. Solvation effects were accounted for dichloromethane implicitly with the ALPB method. The ensembles were then checked for duplicates using the root-mean-square-deviation approach (RMSD) with a cut-off of 0.8 Å, and double structures removed. The resulting structures (1396 for  $\mathbf{2}/\text{pmp}$ , 695 for  $\text{B}(\text{C}_6\text{F}_5)_3/\text{P}^t\text{Bu}_3$ ) were subsequently optimized at the r<sup>2</sup>SCAN-3c+CPCM( $\text{CH}_2\text{Cl}_2$ ) level. In case of imaginary modes, the structure was adjusted accordingly and reoptimized. This was done automated and iteratively. This resulted in ensembles consisting of 1392 ( $\mathbf{2}/\text{pmp}$ ) 695 ( $\text{B}(\text{C}_6\text{F}_5)_3/\text{P}^t\text{Bu}_3$ ) fully converged structures. In the case of  $\mathbf{2}/\text{pmp}$ , two structures were removed from further analysis as they were not

van-der-Waals adducts. The first was found to be a dative adduct, the second the iminium hydride ion pair [tmpCH<sub>2</sub>][H-2].

Based on those structures, the energetic quantification of secondary interactions was conducted. Lewis base and Lewis acid structures were extracted and single point calculations conducted on the PW6B95-D4+SMD(CH<sub>2</sub>Cl<sub>2</sub>)/def2-TZVPP level of theory. Then, orbital interactions were determined according to the ETS-NOCV approach,<sup>358</sup> as implemented in *Orca*. The results of these calculations further gave single-point energies for the final thermodynamic data (PW6B95-D4+SMD(CH<sub>2</sub>Cl<sub>2</sub>)/def2-TZVPP//r<sup>2</sup>SCAN-3c+CPCM(CH<sub>2</sub>Cl<sub>2</sub>)). Inter-fragment London Dispersion energies were obtained *via* the HFLD<sup>357</sup> method in conjunction with the cc-pVDZ basis set. The preorganization/deformation energies were determined by referencing the single-point energies from the fragments against the energy of the respective best conformer of Lewis acid/base, which was determined by the same workflow. The overall process is schematically illustrated in Figure 55.



Figure 55. Schematic illustration of the workflow used to derive the energies used for the evaluation of secondary interactions in FLP ensembles.



# 6

## REFERENCES

---

- 1 J. Barrault, Y. Pouilloux, J. M. Clacens, C. Vanhove, S. Bancquart, *Catal. Today* **2002**, *75*, 177-181.
- 2 H. Yamamoto, *Lewis acids in organic synthesis*, Wiley-VCH, Weinheim, **2002**.
- 3 A. Corma, H. García, *Chem. Rev.* **2003**, *103*, 4307-4366.
- 4 L. Greb, *Chem. Eur. J.* **2018**, *24*, 17881-17896.
- 5 G. C. Welch, R. R. S. Juan, J. D. Masuda, D. W. Stephan, *Science* **2006**, *314*, 1124-1126.
- 6 R. Maskey, M. Schädler, C. Legler, L. Greb, *Angew. Chem. Int. Ed.* **2018**, *57*, 1717-1720.
- 7 G. F. Rouelle, *Mém. Acad. R. Sci.* **1754**, 572-588.
- 8 W. B. Jensen, *J. Chem. Educ.* **2006**, *83*, 1130.
- 9 J. N. Brønsted, *Recl. Trav. Chim. Pays-Bas* **1923**, *42*, 718-728.
- 10 T. Lowry, *J. Soc. Chem. Ind.* **1923**, *42*, 43-51.
- 11 G. N. Lewis, *Valence and the Structure of Atoms and Molecules*, Chemical Catalog Company, New York, **1923**.
- 12 G. N. Lewis, *J. Franklin Inst.* **1938**, *226*, 293-313.
- 13 H. Yamamoto, *Lewis acid reagents: a practical approach*, Knovel, Norwich, NY, **2007**.
- 14 H. Yamamoto, K. Ishihara, *Acid catalysis in modern organic synthesis.*, Wiley-VCH, Weinheim, **2008**.
- 15 S. Kobayashi, K. Manabe, *Pure Appl. Chem.* **2000**, *72*, 1373-1380.
- 16 S. J. Lippard, J. M. Berg, *Principles of bioinorganic chemistry*, University Science Books, Mill Valley, CA, **1994**.
- 17 J. J. Badillo, N. V. Hanhan, A. K. Franz, *Curr. Opin. Drug Discov. Dev.* **2010**, *13*, 758-776.
- 18 S. Woodward, *Tetrahedron* **2002**, *58*, 1017-1050.
- 19 G. A. Olah, D. A. Klumpp, *Superelectrophiles and their chemistry*, Wiley-Interscience, Hoboken, **2008**.
- 20 P. Muller, *Pure Appl. Chem.* **1994**, *66*, 1077.
- 21 T. D. Coyle, H. D. Kaesz, F. G. A. Stone, *J. Am. Chem. Soc.* **1959**, *81*, 2989-2994.
- 22 B. D. Rowsell, R. J. Gillespie, G. L. Heard, *Inorg. Chem.* **1999**, *38*, 4659-4662.
- 23 R. G. Pearson, *J. Am. Chem. Soc.* **1963**, *85*, 3533-3539.
- 24 R. S. Drago, *Coord. Chem. Rev.* **1980**, *33*, 251-277.
- 25 R. S. Drago, *Pure Appl. Chem.* **1980**, *52*, 2261.
- 26 H. C. Brown, R. M. Adams, *J. Am. Chem. Soc.* **1942**, *64*, 2557-2563.
- 27 D. Himmel, S. K. Goll, I. Leito, I. Krossing, *Angew. Chem. Int. Ed.* **2010**, *49*, 6885-6888.
- 28 D. Himmel, V. Radtke, B. Butschke, I. Krossing, *Angew. Chem. Int. Ed.* **2018**, *57*, 4386-4411.
- 29 P. C. Maria, J. F. Gal, J. De Franceschi, E. Fargin, *J. Am. Chem. Soc.* **1987**, *109*, 483-492.
- 30 P. Erdmann, L. Greb, *ChemPhysChem* **2021**, *22*, 935-943.
- 31 C. Laurence, J. Graton, J.-F. Gal, *J. Chem. Educ.* **2011**, *88*, 1651-1657.
- 32 C. Laurence, J.-F. Gal, *Lewis basicity and affinity scales : data and measurement*, John Wiley & Sons, Chichester, West Sussex, U.K., **2010**.
- 33 H. Böhrer, N. Trapp, D. Himmel, M. Schleep, I. Krossing, *Dalton Trans.* **2015**, *44*, 7489-7499.
- 34 A. R. Jupp, T. C. Johnstone, D. W. Stephan, *Dalton Trans.* **2018**, *47*, 7029-7035.
- 35 R. G. Parr, L. v. Szentpály, S. Liu, *J. Am. Chem. Soc.* **1999**, *121*, 1922-1924.

## References

---

- 36 K. Mütter, P. Hrobárik, V. Hrobáriková, M. Kaupp, M. Oestreich, *Chem. Eur. J.* **2013**, *19*, 16579-16594.
- 37 A. E. Ashley, T. J. Herrington, G. G. Wildgoose, H. Zaher, A. L. Thompson, N. H. Rees, T. Krämer, D. O'Hare, *J. Am. Chem. Soc.* **2011**, *133*, 14727-14740.
- 38 P. Erdmann, L. Greb, *Angew. Chem. Int. Ed.* **2022**, *61*, e202114550.
- 39 M. A. Beckett, G. C. Strickland, J. R. Holland, K. Sukumar Varma, *Polymer* **1996**, *37*, 4629-4631.
- 40 U. Mayer, V. Gutmann, W. Gerger, *Monatsh. Chem.* **1975**, *106*, 1235-1257.
- 41 R. F. Childs, D. L. Mulholland, A. Nixon, *Can. J. Chem.* **1982**, *60*, 801-808.
- 42 G. J. P. Britovsek, J. Ugoletti, A. J. P. White, *Organometallics* **2005**, *24*, 1685-1691.
- 43 R. C. Neu, E. Y. Ouyang, S. J. Geier, X. Zhao, A. Ramos, D. W. Stephan, *Dalton Trans.* **2010**, *39*, 4285-4294.
- 44 R. J. Blagg, T. R. Simmons, G. R. Hatton, J. M. Courtney, E. L. Bennett, E. J. Lawrence, G. G. Wildgoose, *Dalton Trans.* **2016**, *45*, 6032-6043.
- 45 J. Ramler, C. Lichtenberg, *Chem. Eur. J.* **2020**, *26*, 10250-10258.
- 46 J. J. Jennings, B. W. Wigman, B. M. Armstrong, A. K. Franz, *J. Org. Chem.* **2019**, *84*, 15845-15853.
- 47 S. Kunzler, S. Rathjen, A. Merk, M. Schmidtman, T. Müller, *Chem. Eur. J.* **2019**, *25*, 15123-15130.
- 48 A. L. Liberman-Martin, R. G. Bergman, T. D. Tilley, *J. Am. Chem. Soc.* **2015**, *137*, 5328-5331.
- 49 S. Mummadi, D. Kenefake, R. Diaz, D. K. Unruh, C. Krempner, *Inorg. Chem.* **2017**, *56*, 10748-10759.
- 50 I. R. Beattie, T. Gilson, *J. Chem. Soc.* **1964**, 2292-2295.
- 51 K. F. Purcell, R. S. Drago, *J. Am. Chem. Soc.* **1966**, *88*, 919-924.
- 52 B. Swanson, D. F. Shriver, *Inorg. Chem.* **1970**, *9*, 1406-1416.
- 53 D. F. Shriver, B. Swanson, *Inorg. Chem.* **1971**, *10*, 1354-1365.
- 54 H. Knoezinger, H. Krietenbrink, *J. Chem. Soc., Faraday Trans. 1* **1975**, *71*, 2421-2430.
- 55 D. M. Byler, D. F. Shriver, *Inorg. Chem.* **1973**, *12*, 1412-1416.
- 56 B. v. Ahsen, B. Bley, S. Proemmel, R. Wartchow, H. Willner, F. Aubke, *Z. Anorg. Allg. Chem.* **1998**, *624*, 1225-1234.
- 57 C. S. Hanson, M. C. Psaltakis, J. J. Cortes, S. S. Siddiqi, J. J. Devery III, *J. Org. Chem.* **2020**, *85*, 820-832.
- 58 A. G. Pelmenschikov, R. A. van Santen, J. Janchen, E. Meijer, *J. Phys. Chem.* **1993**, *97*, 11071-11074.
- 59 T. Krahl, E. Kemnitz, *J. Fluorine Chem.* **2006**, *127*, 663-678.
- 60 C. P. Marshall, G. Scholz, T. Braun, E. Kemnitz, *Catal. Sci. Technol.* **2020**, *10*, 391-402.
- 61 B. Calvo, C. P. Marshall, T. Krahl, J. Kröhnert, A. Trunschke, G. Scholz, T. Braun, E. Kemnitz, *Dalton Trans.* **2018**.
- 62 H. Zhao, J. H. Reibenspies, F. P. Gabbai, *Dalton Trans.* **2013**, *42*, 608-610.
- 63 J. C. Haartz, D. H. McDaniel, *J. Am. Chem. Soc.* **1973**, *95*, 8562-8565.
- 64 M. K. Murphy, J. L. Beauchamp, *J. Am. Chem. Soc.* **1977**, *99*, 4992-4999.
- 65 M. K. Murphy, J. L. Beauchamp, *Inorg. Chem.* **1977**, *16*, 2437-2443.
- 66 J. W. Larson, T. B. McMahon, *J. Am. Chem. Soc.* **1985**, *107*, 766-773.
- 67 J. W. Larson, T. B. McMahon, *Inorg. Chem.* **1987**, *26*, 4018-4023.
- 68 H. D. B. Jenkins, H. K. Roobottom, J. Passmore, *Inorg. Chem.* **2003**, *42*, 2886-2893.
- 69 I. Krossing, I. Raabe, *Chem. Eur. J.* **2004**, *10*, 5017-5030.
- 70 M. Gonsior, I. Krossing, N. Mitzel, *Z. Anorg. Allg. Chem.* **2002**, *628*, 1821-1830.
- 71 T. E. Mallouk, G. L. Rosenthal, G. Mueller, R. Brusasco, N. Bartlett, *Inorg. Chem.* **1984**, *23*, 3167-3173.
- 72 A. P. Altshuller, *J. Am. Chem. Soc.* **1955**, *77*, 6187-6188.
- 73 L. Glasser, H. D. B. Jenkins, *Chem. Soc. Rev.* **2005**, *34*, 866-874.
- 74 C. G. Krespan, D. A. Dixon, *J. Fluorine Chem.* **1996**, *77*, 117-126.
- 75 M. Bursch, J. M. Mewes, A. Hansen, S. Grimme, *Angew. Chem. Int. Ed.* **2022**, *61*, e202205735.
- 76 M. O'Keeffe, *J. Am. Chem. Soc.* **1986**, *108*, 4341-4343.
- 77 K. O. Christe, D. A. Dixon, D. McLemore, W. W. Wilson, J. A. Sheehy, J. A. Boatz, *J. Fluorine Chem.* **2000**, *101*, 151-153.

- 78 P. Erdmann, J. Leitner, J. Schwarz, L. Greb, *ChemPhysChem* **2020**, *21*, 987-994.
- 79 N. F. Hall, J. B. Conant, *J. Am. Chem. Soc.* **1927**, *49*, 3047-3061.
- 80 S. Antoniotti, V. Dalla, E. Duñach, *Angew. Chem. Int. Ed.* **2010**, *49*, 7860-7888.
- 81 F. H. Westheimer, *Special Publication No. 8*, The Chemical Society, London, **1957**.
- 82 F. Grandinetti, G. Occhiucci, O. Ursini, G. de Petris, M. Speranza, *Int. J. Mass Spectrom. Ion Proc.* **1993**, *124*, 21-36.
- 83 F. Grandinetti, G. Occhiucci, M. E. Crestoni, S. Fornarini, M. Speranza, *Int. J. Mass Spectrom. Ion Proc.* **1993**, *127*, 137-146.
- 84 Y. Hayashi, J. J. Rohde, E. J. Corey, *J. Am. Chem. Soc.* **1996**, *118*, 5502-5503.
- 85 E. J. Corey, T. Shibata, T. W. Lee, *J. Am. Chem. Soc.* **2002**, *124*, 3808-3809.
- 86 K. Mahender Reddy, E. Bhimireddy, B. Thirupathi, S. Breitler, S. Yu, E. J. Corey, *J. Am. Chem. Soc.* **2016**, *138*, 2443-2453.
- 87 A. Hasegawa, K. Ishihara, H. Yamamoto, *Angew. Chem. Int. Ed.* **2003**, *42*, 5731-5733.
- 88 G. A. Olah, G. K. S. Prakash, J. Sommer, *Science* **1979**, *206*, 13-20.
- 89 L. O. Müller, D. Himmel, J. Stauffer, G. Steinfeld, J. Slattery, G. Santiso-Quiñones, V. Brecht, I. Krossing, *Angew. Chem. Int. Ed.* **2008**, *47*, 7659-7663.
- 90 W. E. Piers, T. Chivers, *Chem. Soc. Rev.* **1997**, *26*, 345-354.
- 91 G. Erker, *Dalton Trans.* **2005**, 1883-1890.
- 92 J. R. Lawson, R. L. Melen, *Inorg. Chem.* **2017**, *56*, 8627-8643.
- 93 R. W. Taft, F. G. Bordwell, *Acc. Chem. Res.* **1988**, *21*, 463-469.
- 94 L. M. Mihichuk, G. W. Driver, K. E. Johnson, *ChemPhysChem* **2011**, *12*, 1622-1632.
- 95 J. S. J. McCahill, G. C. Welch, D. W. Stephan, *Angew. Chem. Int. Ed.* **2007**, *46*, 4968-4971.
- 96 F.-G. Fontaine, D. W. Stephan, *Philos. Trans. R. Soc. A* **2017**, *375*, 20170004.
- 97 L. J. Hounjet, C. Bannwarth, C. N. Garon, C. B. Caputo, S. Grimme, D. W. Stephan, *Angew. Chem. Int. Ed.* **2013**, *52*, 7492-7495.
- 98 T. Mahdi, D. W. Stephan, *J. Am. Chem. Soc.* **2014**, *136*, 15809-15812.
- 99 H. C. Brown, H. I. Schlesinger, S. Z. Cardon, *J. Am. Chem. Soc.* **1942**, *64*, 325-329.
- 100 W. Tochtermann, *Angew. Chem. Int. Ed.* **1966**, *5*, 351-371.
- 101 W. Tochtermann, *Angew. Chem.* **1966**, *78*, 355-375.
- 102 D. W. Stephan, in *Frustrated Lewis Pairs I: Uncovering and Understanding*, Heidelberg, **2012**, 1-44.
- 103 G. C. Welch, D. W. Stephan, *J. Am. Chem. Soc.* **2007**, *129*, 1880-1881.
- 104 P. Spies, G. Erker, K. Kehr, K. Bergander, R. Fröhlich, S. Grimme, D. W. Stephan, *Chem. Commun.* **2007**, 5072-5074.
- 105 T. A. Rokob, A. Hamza, A. Stirling, T. Soos, I. Pápai, *Angew. Chem. Int. Ed.* **2008**, *47*, 2435-2438.
- 106 A. Hamza, A. Stirling, T. A. Rokob, I. Pápai, *Int. J. Quantum Chem.* **2009**, *109*, 2416-2425.
- 107 S. Grimme, H. Kruse, L. Goerigk, G. Erker, *Angew. Chem. Int. Ed.* **2010**, *49*, 1402-1405.
- 108 P. A. Chase, D. W. Stephan, *Angew. Chem. Int. Ed.* **2008**, *47*, 7433-7437.
- 109 D. Holschumacher, T. Bannenberg, C. G. Hrib, P. G. Jones, M. Tamm, *Angew. Chem. Int. Ed.* **2008**, *47*, 7428-7432.
- 110 C. F. Jiang, O. Blacque, H. Berke, *Organometallics* **2009**, *28*, 5233-5239.
- 111 C. F. Jiang, O. Blacque, T. Fox, H. Berke, *Organometallics* **2011**, *30*, 2117-2124.
- 112 V. Sumerin, F. Schulz, M. Nieger, M. Leskela, T. Repo, B. Rieger, *Angew. Chem. Int. Ed.* **2008**, *47*, 6001-6003.
- 113 S. J. Geier, D. W. Stephan, *J. Am. Chem. Soc.* **2009**, *131*, 3476-3477.
- 114 D. W. Stephan, G. Erker, *Angew. Chem. Int. Ed.* **2010**, *49*, 46-76.
- 115 P. A. Chase, G. C. Welch, T. Jurca, D. W. Stephan, *Angew. Chem. Int. Ed.* **2007**, *46*, 8050-8053.
- 116 P. Spies, S. Schwendemann, S. Lange, G. Kehr, R. Fröhlich, G. Erker, *Angew. Chem. Int. Ed.* **2008**, *47*, 7543-7546.
- 117 L. Greb, P. Oña-Burgos, B. Schirmer, S. Grimme, D. W. Stephan, J. Paradies, *Angew. Chem. Int. Ed.* **2012**, *51*, 10164-10168.
- 118 E. Otten, R. C. Neu, D. W. Stephan, *J. Am. Chem. Soc.* **2009**, *131*, 9918-9919.
- 119 R. C. Neu, E. Otten, A. Lough, D. W. Stephan, *Chem. Sci.* **2011**, *2*, 170-176.

- 120 A. J. P. Cardenas, B. J. Culotta, T. H. Warren, S. Grimme, A. Stute, R. Fröhlich, G. Kehr, G. Erker, *Angew. Chem.* **2011**, *123*, 7709-7713.
- 121 M. Sajid, A. Stute, A. J. P. Cardenas, B. J. Culotta, J. A. Hepperle, T. H. Warren, B. Schirmer, S. Grimme, A. Studer, C. G. Daniliuc, *J. Am. Chem. Soc.* **2012**, *134*, 10156-10168.
- 122 C. M. Mömning, E. Otten, G. Kehr, R. Fröhlich, S. Grimme, D. W. Stephan, G. Erker, *Angew. Chem. Int. Ed.* **2009**, *48*, 6643-6646.
- 123 I. Peuser, R. C. Neu, X. Zhao, M. Ulrich, B. Schirmer, J. A. Tannert, G. Kehr, R. Fröhlich, S. Grimme, G. Erker, *Chem. Eur. J.* **2011**, *17*, 9640-9650.
- 124 M. A. Dureen, D. W. Stephan, *J. Am. Chem. Soc.* **2010**, *132*, 13559-13568.
- 125 M. Sajid, A. Klose, B. Birkmann, L. Liang, B. Schirmer, T. Wiegand, H. Eckert, A. J. Lough, R. Froehlich, C. G. Daniliuc, *Chem. Sci.* **2013**, *4*, 213-219.
- 126 A. Adenot, N. von Wolff, G. Lefèvre, J. C. Berthet, P. Thuéry, T. Cantat, *Chem. Eur. J.* **2019**, *25*, 8118-8126.
- 127 J. S. McCahill, G. C. Welch, D. W. Stephan, *Angew. Chem. Int. Ed.* **2007**, *46*, 4968-4971.
- 128 M. A. Dureen, G. C. Welch, T. M. Gilbert, D. W. Stephan, *Inorg. Chem.* **2009**, *48*, 9910-9917.
- 129 M. A. Dureen, D. W. Stephan, *J. Am. Chem. Soc.* **2009**, *131*, 8396-8397.
- 130 C. Kreitner, S. J. Geier, L. J. Stanlake, C. B. Caputo, D. W. Stephan, *Dalton Trans.* **2011**, *40*, 6771-6777.
- 131 S. A. Weicker, D. W. Stephan, *Bull. Chem. Soc. Jpn.* **2015**, *88*, 1003-1016.
- 132 G. Ménard, D. W. Stephan, *Angew. Chem. Int. Ed.* **2012**, *51*, 8272-8275.
- 133 T. J. Herrington, B. J. Ward, L. R. Doyle, J. McDermott, A. J. P. White, P. A. Hunt, A. E. Ashley, *Chem. Commun.* **2014**, *50*, 12753-12756.
- 134 M. Reißmann, A. Schäfer, S. Jung, T. Müller, *Organometallics* **2013**, *32*, 6736-6744.
- 135 A. Schäfer, M. Reissmann, A. Schäfer, W. Saak, D. Haase, T. Müller, *Angew. Chem. Int. Ed.* **2011**, *50*, 12636-12638.
- 136 A. Schäfer, M. Reissmann, A. Schäfer, M. Schmidtman, T. Müller, *Chem. Eur. J.* **2014**, *20*, 9381-9386.
- 137 J. W. Runyon, O. Steinhof, H. V. R. Dias, J. C. Calabrese, W. J. Marshall, A. J. Arduengo, *Austr. J. Chem.* **2011**, *64*, 1165-1172.
- 138 E. R. Clark, M. J. Ingleson, *Angew. Chem. Int. Ed.* **2014**, *53*, 11306-11309.
- 139 E. R. Clark, M. J. Ingleson, *Organometallics* **2013**, *32*, 6712-6717.
- 140 A. Simonneau, R. Turrel, L. Vendier, M. Etienne, *Angew. Chem. Int. Ed.* **2017**, *56*, 12268-12272.
- 141 S. Arndt, M. Rudolph, A. S. K. Hashmi, *Gold Bull.* **2017**, *50*, 267-282.
- 142 S. R. Flynn, D. F. Wass, *ACS Catal.* **2013**, *3*, 2574-2581.
- 143 J. Lam, K. M. Szkop, E. Mosaferi, D. W. Stephan, *Chem. Soc. Rev.* **2019**, *48*, 3592-3612.
- 144 D. W. Stephan, *Science* **2016**, *354*, aaf7229.
- 145 D. W. Stephan, G. Erker, *Angew. Chem. Int. Ed.* **2015**, *54*, 6400-6441.
- 146 D. W. Stephan, G. Erker, *Chem. Sci.* **2014**, *5*, 2625-2641.
- 147 D. W. Stephan, *Acc. Chem. Res.* **2015**, *48*, 306-316.
- 148 D. W. Stephan, *J. Am. Chem. Soc.* **2015**, *137*, 10018-10032.
- 149 D. W. Stephan, *Chem* **2020**, *6*, 1520-1526.
- 150 C. Klein, in *Health Effects of Mineral Dusts*, De Gruyter, Berlin, Boston, **1993**, 7-60.
- 151 G. Busca, A. Gervasini, in *Advances in Catalysis*, Vol. 67, Academic Press, **2020**, 1-90.
- 152 S. E. Denmark, T. Wynn, *J. Am. Chem. Soc.* **2001**, *123*, 6199-6200.
- 153 S. E. Denmark, T. Wynn, G. L. Beutner, *J. Am. Chem. Soc.* **2002**, *124*, 13405-13407.
- 154 S. E. Denmark, G. L. Beutner, *J. Am. Chem. Soc.* **2003**, *125*, 7800-7801.
- 155 S. E. Denmark, G. L. Beutner, T. Wynn, M. D. Eastgate, *J. Am. Chem. Soc.* **2005**, *127*, 3774-3789.
- 156 A. V. Malkov, A. J. S. Liddon, P. Ramírez - López, L. Bendová, D. Haigh, P. Kočovský, *Angew. Chem. Int. Ed.* **2006**, *45*, 1432-1435.
- 157 S. E. Denmark, G. L. Beutner, *Angew. Chem. Int. Ed.* **2008**, *47*, 1560-1638.
- 158 R. Hrdina, F. Opekar, J. Roithová, M. Kotora, *Chem. Commun.* **2009**, 2314-2316.
- 159 A. G. Myers, S. E. Kephart, H. Chen, *J. Am. Chem. Soc.* **1992**, *114*, 7922-7923.
- 160 K. Matsumoto, K. Oshima, K. Utimoto, *J. Org. Chem.* **1994**, *59*, 7152-7155.

- 161 J. W. Kinnaird, P. Y. Ng, K. Kubota, X. Wang, J. L. Leighton, *J. Am. Chem. Soc.* **2002**, *124*, 7920-7921.
- 162 X. Zhang, K. N. Houk, J. L. Leighton, *Angew. Chem. Int. Ed.* **2005**, *44*, 938-941.
- 163 R. Hrdina, C. E. Müller, R. C. Wende, K. M. Lippert, M. Benassi, B. Spengler, P. R. Schreiner, *J. Am. Chem. Soc.* **2011**, *133*, 7624-7627.
- 164 W. A. Chalifoux, S. K. Reznik, J. L. Leighton, *Nature* **2012**, *487*, 86-89.
- 165 A. D. Dilman, S. L. Ioffe, *Chem. Rev.* **2003**, *103*, 733-772.
- 166 L. Ratjen, M. van Gemmeren, F. Pesciaioli, B. List, *Angew. Chem. Int. Ed.* **2014**, *53*, 8765-8769.
- 167 D. Höfler, M. v. Gemmeren, P. Wedemann, K. Kaupmees, I. Leito, M. Leutzsch, J. B. Lingnau, B. List, *Angew. Chem. Int. Ed.* **2017**, *56*, 1411-1415.
- 168 A. R. Bassindale, T. Stout, *Tetrahedron Lett.* **1985**, *26*, 3403-3406.
- 169 A. P. M. Robertson, J. N. Friedmann, H. A. Jenkins, N. Burford, *Chem. Commun.* **2014**, *50*, 7979-7981.
- 170 A. P. M. Robertson, S. S. Chitnis, S. Chhina, H. J. Cortes S, B. O. Patrick, H. A. Jenkins, N. Burford, *Can. J. Chem.* **2016**, *94*, 424-429.
- 171 T. Müller, in *Functional Molecular Silicon Compounds I: Regular Oxidation States*, Springer Cham, Switzerland, **2014**, 107-162.
- 172 H. F. T. Klare, M. Oestreich, *Dalton Trans.* **2010**, *39*, 9176-9184.
- 173 H. F. T. Klare, *ACS Catal.* **2017**, *7*, 6999-7002.
- 174 H. J. Frohn, M. Giessen, A. Klose, A. Lewin, V. V. Bardin, *J. Organomet. Chem.* **1996**, *506*, 155-164.
- 175 A. D. Dilman, V. V. Levin, A. A. Korlyukov, P. A. Belyakov, M. I. Struchkova, M. Y. Antipin, V. A. Tartakovskiy, *J. Organomet. Chem.* **2008**, *693*, 1005-1019.
- 176 S. Steinhauer, J. Bader, H.-G. Stammer, N. Ignat'ev, B. Hoge, *Angew. Chem. Int. Ed.* **2014**, *53*, 5206-5209.
- 177 S. Steinhauer, H. G. Stammer, B. Neumann, N. Ignat'ev, B. Hoge, *Angew. Chem. Int. Ed.* **2014**, *53*, 562-564.
- 178 D. Hartmann, M. Schädler, L. Greb, *Chem. Sci.* **2019**, *10*, 7379-7388.
- 179 L. Greb, *Synlett* **2023**, *34*, A-Q.
- 180 C. L. Frye, *J. Am. Chem. Soc.* **1964**, *86*, 3170-3171.
- 181 W. H. Stevenson, III, S. Wilson, J. C. Martin, W. B. Farnham, *J. Am. Chem. Soc.* **1985**, *107*, 6340-6352.
- 182 S. E. Denmark, R. T. Jacobs, G. Dai-Ho, S. Wilson, *Organometallics* **1990**, *9*, 3015-3019.
- 183 X. Zhang, K. N. Houk, J. L. Leighton, *Angew. Chem. Int. Ed.* **2005**, *44*, 938-941.
- 184 R. M. Guidry, R. S. Drago, *J. Am. Chem. Soc.* **1973**, *95*, 759-763.
- 185 H. Fleischer, *Eur. J. Inorg. Chem.* **2001**, *2001*, 393-404.
- 186 L. M. Sigmund, R. Maier, L. Greb, *Chem. Sci.* **2022**, *13*, 510-521.
- 187 A. Ben Saida, A. Chardon, A. Osi, N. Tumanov, J. Wouters, A. I. Adjieufack, B. Champagne, G. Berionni, *Angew. Chem. Int. Ed.* **2019**, *58*, 16889-16893.
- 188 F. Ebner, L. Greb, *Chem* **2021**, *7*, 2151-2159.
- 189 C. A. Ramsden, *Chem. Soc. Rev.* **1994**, *23*, 111-118.
- 190 E. Magnusson, *J. Am. Chem. Soc.* **1990**, *112*, 7940-7951.
- 191 D. Schomburg, R. Krebs, *Inorg. Chem.* **1984**, *23*, 1378-1381.
- 192 C. Chuit, R. J. Corriu, C. Reye, J. C. Young, *Chem. Rev.* **1993**, *93*, 1371-1448.
- 193 R. R. Holmes, *Chem. Rev.* **1990**, *90*, 17-31.
- 194 D. Roth, J. Stirn, D. W. Stephan, L. Greb, *J. Am. Chem. Soc.* **2021**, *143*, 15845-15851.
- 195 A. Hermannsdorfer, M. Driess, *Angew. Chem. Int. Ed.* **2021**, *60*, 13656-13660.
- 196 F. S. Tschernuth, T. Thorwart, L. Greb, F. Hanusch, S. Inoue, *Angew. Chem. Int. Ed.* **2021**, *60*, 25799-25803.
- 197 D. A. Dixon, T. Fukunaga, B. E. Smart, *J. Am. Chem. Soc.* **1986**, *108*, 4027-4031.
- 198 H. Reinsch, *Repert. Pharm.* **1839**, *68*, 49-58.
- 199 A. Rosenheim, O. Sorge, *Ber. Dtsch. Chem. Ges. A/B* **1920**, *53*, 932-939.
- 200 Q. Luo, L. Greb, *Eur. J. Inorg. Chem.* **2023**, *26*, e202300186.
- 201 R. Hess, R. Bach, H. Deuel, *Experientia* **1960**, *16*, 38-40.
- 202 A. Weiss, G. Reiff, A. Weiss, *Z. Anorg. Allg. Chem.* **1961**, *311*, 151-179.

## References

---

- 203 H. Bartels, *Helv. Chim. Acta* **1964**, *47*, 1605-1609.
- 204 D. W. Barnum, *Inorg. Chem.* **1970**, *9*, 1942-1943.
- 205 D. W. Barnum, *Inorg. Chem.* **1972**, *11*, 1424-1429.
- 206 W. Heinen, J. H. Oehler, in *Studies in Environmental Science, Vol. 3*, Elsevier, **1979**, 431-443.
- 207 I. Kostovic, Y. Kuchino, A. Macieira-Coelho, R. Rhoads, **2003**.
- 208 S. Bai, Y. Tsuji, Y. Okaue, T. Yokoyama, *Chem. Lett.* **2008**, *37*, 1168-1169.
- 209 J. C. Furgal, C. U. Lenora, *Phys. Sci. Rev.* **2020**, *5*, 20190024.
- 210 Y. N. M. Vol'nov, A., *Zh. Obshch. Khim.* **1943**, *13*, 213-216.
- 211 J. Zuckerman, *J. Chem. Soc.* **1962**, 873-876.
- 212 R. Schwarz, W. Kuchen, *Z. Anorg. Allg. Chem.* **1951**, *266*, 185-192.
- 213 H. Allcock, T. Nugent, L. Smeltz, *Synth. React. Inorg. Met.-Org. Chem.* **1972**, *2*, 97-104.
- 214 F. P. Boer, J. J. Flynn, J. W. Turley, *J. Am. Chem. Soc.* **1968**, *90*, 6973-6977.
- 215 J. J. Harland, R. O. Day, J. F. Vollano, A. C. Sau, R. R. Holmes, *J. Am. Chem. Soc.* **1981**, *103*, 5269-5270.
- 216 A. Boudin, G. Cerveau, C. Chuit, R. J. P. Corriu, C. Reye, *Angew. Chem. Int. Ed.* **1986**, *25*, 473-474.
- 217 C. M. Yoder, J. J. Zuckerman, *Inorg. Chem.* **1967**, *6*, 163-164.
- 218 M. Kira, K. Sato, H. Sakurai, *J. Org. Chem.* **1987**, *52*, 948-949.
- 219 V. Corce, L. M. Chamoreau, E. Derat, J. P. Goddard, C. Ollivier, L. Fensterbank, *Angew. Chem. Int. Ed.* **2015**, *54*, 11414-11418.
- 220 L. Chenneberg, C. Leveque, V. Corce, A. Baralle, J. P. Goddard, C. Ollivier, L. Fensterbank, *Synlett* **2016**, *27*, 731-735.
- 221 M. Jouffroy, D. N. Primer, G. A. Molander, *J. Am. Chem. Soc.* **2016**, *138*, 475-478.
- 222 C. Leveque, L. Chenneberg, V. Corce, J. P. Goddard, C. Ollivier, L. Fensterbank, *Org. Chem. Front.* **2016**, *3*, 462-465.
- 223 C. Leveque, L. Chenneberg, V. Corce, C. Ollivier, L. Fensterbank, *Chem. Commun.* **2016**, *52*, 9877-9880.
- 224 E. Levernier, K. Jaouadi, H. R. Zhang, V. Corce, A. Bernard, G. Gontard, C. Troufflard, L. Grimaud, E. Derat, C. Ollivier, L. Fensterbank, *Chem. Eur. J.* **2021**, *27*, 8782-8790.
- 225 S. Witzel, K. Sekine, M. Rudolph, A. S. K. Hashmi, *Chem. Commun.* **2018**, *54*, 13802-13804.
- 226 W. M. Seganish, P. DeShong, *Org. Lett.* **2004**, *6*, 4379-4381.
- 227 W. M. Seganish, P. DeShong, *J. Org. Chem.* **2004**, *69*, 1137-1143.
- 228 R. Maskey, H. Wadepohl, L. Greb, *Angew. Chem. Int. Ed.* **2019**, *58*, 3616-3619.
- 229 J. Roeser, D. Prill, M. J. Bojdys, P. Fayon, A. Trewin, A. N. Fitch, M. U. Schmidt, A. Thomas, *Nat. Chem.* **2017**, *9*, 977-982.
- 230 O. Yahiaoui, A. N. Fitch, F. Hoffmann, M. Fröba, A. Thomas, J. Roeser, *J. Am. Chem. Soc.* **2018**, *140*, 5330-5333.
- 231 D. Hartmann, T. Thorwart, R. Müller, J. Thusek, J. Schwabedissen, A. Mix, J. H. Lamm, B. Neumann, N. W. Mitzel, L. Greb, *J. Am. Chem. Soc.* **2021**, *143*, 18784-18793.
- 232 H. Meyer, G. Nagorsen, *Angew. Chem. Int. Ed.* **1979**, *18*, 551-553.
- 233 E.-U. Würthwein, P. von Ragué Schleyer, *Angew. Chem. Int. Ed.* **1979**, *18*, 553-554.
- 234 J. D. Dunitz, *Angew. Chem. Int. Ed.* **1980**, *19*, 1034-1034.
- 235 G. Nagorsen, H. Meyer, *Angew. Chem. Int. Ed.* **1980**, *19*, 1034-1034.
- 236 J. W. Bibber, C. L. Barnes, D. van der Helm, J. J. Zuckerman, *Angew. Chem. Int. Ed.* **1983**, *22*, 668-674.
- 237 D. Schomburg, *Angew. Chem. Int. Ed.* **1983**, *22*, 65-65.
- 238 W. Hönle, U. Dettlaff-Weglikowska, L. Walz, H. G. von Schnering, *Angew. Chem. Int. Ed.* **1989**, *28*, 623-624.
- 239 C. Y. Wong, J. D. Woollins, *Coord. Chem. Rev.* **1994**, *130*, 175-241.
- 240 U. Dettlaff-Weglikowska, E. Hey-Hawkins, H. G. v. Schnering, *Z. Naturforsch. B* **1991**, *46*, 609-614.
- 241 E. Hey-Hawkins, U. Dettlaff-Weglikowska, D. Thiery, H. G. Von Schnering, *Polyhedron* **1992**, *11*, 1789-1794.
- 242 F. E. Hahn, M. Keck, K. N. Raymond, *Inorg. Chem.* **1995**, *34*, 1402-1407.
- 243 P. Zanello, M. Corsini, *Coord. Chem. Rev.* **2006**, *250*, 2000-2022.

- 244 C. G. Pierpont, *Coord. Chem. Rev.* **2001**, *219*, 415-433.
- 245 D. L. J. Broere, R. Plessius, J. I. van der Vlugt, *Chem. Soc. Rev.* **2015**, *44*, 6886-6915.
- 246 R. Maskey, L. Greb, in *Encyclopedia of Inorganic and Bioinorganic Chemistry*, 1-15.
- 247 L. Greb, *Eur. J. Inorg. Chem.* **2022**, *2022*, e202100871.
- 248 A. Prokof'ev, T. Prokof'eva, N. Bubnov, S. Solodovnikov, I. Belostotskaya, V. Ershov, M. Kabachnik, *Bull. Acad. Sci. USSR, Div. Chem. Sci.* **1978**, *27*, 1726-1733.
- 249 A. I. Prokof'ev, T. I. Prokof'eva, I. S. Belostotskaya, N. N. Bubnov, S. P. Solodovnikov, V. V. Ershov, M. I. Kabachnik, *Tetrahedron* **1979**, *35*, 2471-2482.
- 250 A. Chekalov, A. Prokof'ev, N. Bubnov, S. Solodovnikov, A. Zhdanov, M. Kabachnik, *Bull. Acad. Sci. USSR, Div. Chem. Sci.* **1981**, *30*, 2064-2071.
- 251 A. K. Chekalov, A. I. Prokof'ev, N. N. Bubnov, S. P. Solodovnikov, A. A. Zhdanov, M. I. Kabachnik, *Bull. Acad. Sci. USSR, Div. Chem. Sci.* **1983**, *32*, 939-946.
- 252 R. Maskey, C. Bendel, J. Malzacher, L. Greb, *Chem. Eur. J.* **2020**, *26*, 17386-17389.
- 253 D. Hartmann, S. Braner, L. Greb, *Chem. Commun.* **2021**, *57*, 8572-8575.
- 254 D. Hartmann, T. Strunden, L. Greb, *Inorg. Chem.* **2022**, *61*, 15693-15698.
- 255 N. Ansmann, D. Hartmann, S. Sailer, P. Erdmann, R. Maskey, M. Schorpp, L. Greb, *Angew. Chem. Int. Ed.* **2022**, *61*, e202203947.
- 256 D. Hartmann, L. Greb, *Angew. Chem. Int. Ed.* **2020**, *59*, 22510-22513.
- 257 C.-M. Liu, E. Nordlander, D. Schmeh, R. Shoemaker, C. G. Pierpont, *Inorg. Chem.* **2004**, *43*, 2114-2124.
- 258 C. W. Lange, B. J. Conklin, C. G. Pierpont, *Inorg. Chem.* **1994**, *33*, 1276-1283.
- 259 G. A. Abakumov, N. N. Vavilina, Y. A. Kurskii, V. I. Nevodchikov, V. K. Cherkasov, A. S. Shavyrin, *Russ. Chem. Bull.* **2003**, *52*, 1847-1853.
- 260 I. Belostotskaya, N. Komissarova, E. Dzhuryan, V. Ershov, *Bull. Acad. Sci. USSR, Div. Chem. Sci.* **1972**, *21*, 1535-1536.
- 261 E. Torsueva, I. Belostotskaya, N. Komissarova, Y. A. Shlyapnikov, *Bull. Acad. Sci. USSR, Div. Chem. Sci.* **1976**, *25*, 1993-1996.
- 262 M. Bamberg, M. Bursch, A. Hansen, M. Brandl, G. Sentis, L. Kunze, M. Bolte, H.-W. Lerner, S. Grimme, M. Wagner, *J. Am. Chem. Soc.* **2021**, *143*, 10865-10871.
- 263 J. J. Adams, N. Arulsamy, B. P. Sullivan, D. M. Roddick, A. Neuberger, R. H. Schmehl, *Inorg. Chem.* **2015**, *54*, 11136-11149.
- 264 V. B. Vol'eva, T. I. Prokof'eva, I. S. Belostotskaya, N. L. Komissarova, D. B. Gorbunov, L. N. Kurkovskaya, *Russ. J. Org. Chem.* **2011**, *47*, 1310.
- 265 E. V. Ilyakina, O. G. Mishchenko, A. V. Piskunov, S. V. Maslennikov, I. V. Spirina, Y. A. Kurskii, A. V. Lado, *Russ. J. Gen. Chem.* **2009**, *79*, 724-727.
- 266 S. M. Kulikov, I. V. Kozhevnikov, M. N. Fomina, A. P. Krysin, *Bull. Acad. Sci. USSR, Div. Chem. Sci.* **1987**, *36*, 681-684.
- 267 I. A. Novikova, V. B. Vol'eva, N. L. Komissarova, I. S. Belostotskaya, V. V. Ershov, *Bull. Acad. Sci. USSR, Div. Chem. Sci.* **1981**, *30*, 1732-1735.
- 268 K. U. Ingold, *Can. J. Chem.* **1963**, *41*, 2807-2815.
- 269 R. N. Perutz, *Science* **2008**, *321*, 1168-1169.
- 270 C. Douvris, O. V. Ozerov, *Science* **2008**, *321*, 1188-1190.
- 271 V. J. Scott, R. Çelenligil-Çetin, O. V. Ozerov, *J. Am. Chem. Soc.* **2005**, *127*, 2852-2853.
- 272 J. R. Ludwig, P. M. Zimmerman, J. B. Gianino, C. S. Schindler, *Nature* **2016**, *533*, 374-379.
- 273 A. Djurovic, M. Vayer, Z. Li, R. Guillot, J.-P. Baltaze, V. Gandon, C. Bour, *Org. Lett.* **2019**, *21*, 8132-8137.
- 274 H. Albright, H. L. Vonesh, C. S. Schindler, *Org. Lett.* **2020**, *22*, 3155-3160.
- 275 A. J. Davis, R. B. Watson, D. J. Nasrallah, J. L. Gomez-Lopez, C. S. Schindler, *Nat. Catal.* **2020**, *3*, 787-796.
- 276 R. Wang, Y. Chen, M. Shu, W. Zhao, M. Tao, C. Du, X. Fu, A. Li, Z. Lin, *Chem. Eur. J.* **2020**, *26*, 1941-1946.
- 277 H. Albright, A. J. Davis, J. L. Gomez-Lopez, H. L. Vonesh, P. K. Quach, T. H. Lambert, C. S. Schindler, *Chem. Rev.* **2021**, *121*, 9359-9406.
- 278 S. R. Todtz, C. W. Schneider, T. Malakar, C. Anderson, H. Koska, P. M. Zimmerman, J. J. Devery III, *J. Am. Chem. Soc.* **2023**, *145*, 13069-13080.
- 279 D. Bergmann, J. Hinze, in *Electronegativity, Vol. 66*, Springer, Berlin, Heidelberg, **1987**, 145-190.

- 280 L. J. Saethre, N. Berrah, J. D. Bozek, K. J. Børve, T. X. Carroll, E. Kukkk, G. L. Gard, R. Winter, T. D. Thomas, *J. Am. Chem. Soc.* **2001**, *123*, 10729-10737.
- 281 D. H. McDaniel, H. C. Brown, *J. Org. Chem.* **1958**, *23*, 420-427.
- 282 G. K. S. Prakash, A. K. Yudin, *Chem. Rev.* **1997**, *97*, 757-786.
- 283 T. Furuya, A. S. Kamlet, T. Ritter, *Nature* **2011**, *473*, 470-477.
- 284 A. Studer, *Angew. Chem. Int. Ed.* **2012**, *51*, 8950-8958.
- 285 S. Barata-Vallejo, A. Postigo, *Coord. Chem. Rev.* **2013**, *257*, 3051-3069.
- 286 J. Charpentier, N. Fröh, A. Togni, *Chem. Rev.* **2015**, *115*, 650-682.
- 287 X. Liu, C. Xu, M. Wang, Q. Liu, *Chem. Rev.* **2015**, *115*, 683-730.
- 288 H. Xiao, Z. Zhang, Y. Fang, L. Zhu, C. Li, *Chem. Soc. Rev.* **2021**, *50*, 6308-6319.
- 289 T. Thorwart, Master thesis, Heidelberg University **2019**.
- 290 A. Kütt, V. Movchun, T. Rodima, T. Dansauer, E. B. Rusanov, I. Leito, I. Kaljurand, J. Koppel, V. Pihl, I. Koppel, G. Ovsjannikov, L. Toom, M. Mishima, M. Medebielle, E. Lork, G. V. Rösenthaller, I. A. Koppel, A. A. Kolomeitsev, *J. Org. Chem.* **2008**, *73*, 2607-2620.
- 291 R. Haiges, A. F. Baxter, N. R. Goetz, J. A. Axhausen, T. Soltner, A. Kornath, K. O. Christe, *Dalton Trans.* **2016**, *45*, 8494-8499.
- 292 I. M. Riddellstone, A. Kraft, J. Schaefer, I. Krossing, *Angew. Chem. Int. Ed.* **2018**, *57*, 13982-14024.
- 293 V. Gutmann, A. Scherhauser, *Monatsh. Chem.* **1968**, *99*, 335-339.
- 294 Y. Y. Lim, R. S. Drago, *Inorg. Chem.* **1972**, *11*, 202-&.
- 295 U. Tilstam, *Org. Process Res. Dev.* **2012**, *16*, 1273-1278.
- 296 P. D. Prince, M. J. Bearpark, G. S. McGrady, J. W. Steed, *Dalton Trans.* **2008**, 271-282.
- 297 A. Simonneau, M. Oestreich, *Nat. Chem.* **2015**, *7*, 816-822.
- 298 S. Rubinsztajn, J. Cella, in *Abstr. Pap. Am. Chem. Soc., Vol. 227*, Amer. Chem. Soc., 1155 16th ST, NW, Washington, DC 20036 USA, **2004**, pp. U452-U452.
- 299 D. J. Parks, J. M. Blackwell, W. E. Piers, *J. Org. Chem.* **2000**, *65*, 3090-3098.
- 300 D. Roth, H. Wadepohl, L. Greb, *Angew. Chem. Int. Ed.* **2020**.
- 301 J. Pahl, H. Elsen, A. Friedrich, S. Harder, *Chem. Commun.* **2018**, *54*, 7846-7849.
- 302 A. Wiesner, T. W. Gries, S. Steinhauer, H. Beckers, S. Riedel, *Angew. Chem. Int. Ed.* **2017**, *56*, 8263-8266.
- 303 I. M. Riddellstone, S. Keller, F. Kirschenmann, M. Schorpp, I. Krossing, *Eur. J. Inorg. Chem.* **2019**, 59-67.
- 304 H. A. van Kalker, F. L. van Delft, F. P. Rutjes, *ChemSusChem* **2013**, *6*, 1615-1624.
- 305 M. Schorpp, T. Heizmann, M. Schmucker, S. Rein, S. Weber, I. Krossing, *Angew. Chem. Int. Ed.* **2020**, *59*, 9453-9459.
- 306 A. Karton, S. Daon, J. M. L. Martin, *Chem. Phys. Lett.* **2011**, *510*, 165-178.
- 307 R. Panisch, M. Bolte, T. Müller, *J. Am. Chem. Soc.* **2006**, *128*, 9676-9682.
- 308 C. Douvris, E. S. Stoyanov, F. S. Tham, C. A. Reed, *Chem. Commun.* **2007**, 1145-1147.
- 309 C. Douvris, C. M. Nagaraja, C.-H. Chen, B. M. Foxman, O. V. Ozerov, *J. Am. Chem. Soc.* **2010**, *132*, 4946-4953.
- 310 T. Stahl, H. F. T. Klare, M. Oestreich, *ACS Catal.* **2013**, *3*, 1578-1587.
- 311 I. Mallov, A. J. Ruddy, H. Zhu, S. Grimme, D. W. Stephan, *Chem. Eur. J.* **2017**, *23*, 17692-17696.
- 312 A. Schäfer, W. Saak, D. Haase, T. Müller, *Angew. Chem. Int. Ed.* **2012**, *51*, 2981-2984.
- 313 B. Waerder, M. Pieper, L. A. Korte, T. A. Kinder, A. Mix, B. Neumann, H. G. Stammler, N. W. Mitzel, *Angew. Chem. Int. Ed.* **2015**, *54*, 13416-13419.
- 314 S. A. Weicker, D. W. Stephan, *Chem. Eur. J.* **2015**, *21*, 13027-13034.
- 315 N. von Wolff, G. Lefèvre, J. C. Berthet, P. Thuéry, T. Cantat, *ACS Catal.* **2016**, *6*, 4526-4535.
- 316 M. Kira, K. Sato, H. Sakurai, *Chem. Lett.* **1987**, *16*, 2243-2246.
- 317 P. Holtkamp, F. Friedrich, E. Stratmann, A. Mix, B. Neumann, H. G. Stammler, N. W. Mitzel, *Angew. Chem. Int. Ed.* **2019**, *58*, 5114-5118.
- 318 T. A. Kinder, R. Pior, S. Blomeyer, B. Neumann, H. G. Stammler, N. W. Mitzel, *Chem. Eur. J.* **2019**, *25*, 5899-5903.
- 319 D. J. Scott, N. A. Phillips, J. S. Sapsford, A. C. Deacy, M. J. Fuchter, A. E. Ashley, *Angew. Chem. Int. Ed.* **2016**, *55*, 14738-14742.
- 320 R. T. Cooper, J. S. Sapsford, R. C. Turnell-Ritson, D. H. Hyon, A. J. P. White, A. E. Ashley, *Philos. Trans. R. Soc. A* **2017**, *375*, 20170008.

- 321 J. S. Sapsford, D. Csokas, R. C. Turnell-Ritson, L. A. Parkin, A. D. Crawford, I. Pápai, A. E. Ashley, *ACS Catal.* **2021**, *11*, 9143-9150.
- 322 S. Das, S. Mondal, S. K. Pati, *Chem. Eur. J.* **2018**, *24*, 2575-2579.
- 323 T. vom Stein, M. Perez, R. Dobrovetsky, D. Winkelhaus, C. B. Caputo, D. W. Stephan, *Angew. Chem. Int. Ed.* **2015**, *54*, 10178-10182.
- 324 A. Kostenko, R. Dobrovetsky, *Eur. J. Org. Chem.* **2019**, *2019*, 318-322.
- 325 M. H. Holthausen, J. M. Bayne, I. Mallov, R. Dobrovetsky, D. W. Stephan, *J. Am. Chem. Soc.* **2015**, *137*, 7298-7301.
- 326 D. Chakraborty, E. Y. X. Chen, *Macromolecules* **2002**, *35*, 13-15.
- 327 A. J. V. Marwitz, J. L. Dutton, L. G. Mercier, W. E. Piers, *J. Am. Chem. Soc.* **2011**, *133*, 10026-10029.
- 328 W. A. Henderson Jr, C. Streuli, *J. Am. Chem. Soc.* **1960**, *82*, 5791-5794.
- 329 F. Medici, J. Maury, G. Lemiere, L. Fensterbank, *Chem. Eur. J.* **2019**, *25*, 9438-9442.
- 330 L. L. Zeonjuk, N. Vankova, A. Mavrandonakis, T. Heine, G. V. Roschenthaler, J. Eicher, *Chem. Eur. J.* **2013**, *19*, 17413-17424.
- 331 A. R. Jupp, *Dalton Trans.* **2022**, *51*, 10681-10689.
- 332 M. Heshmat, B. Ensing, *J. Phys. Chem. A* **2020**, *124*, 6399-6410.
- 333 L. Liu, L. L. Cao, Y. Shao, G. Menard, D. W. Stephan, *Chem* **2017**, *3*, 259-267.
- 334 L. J. C. van der Zee, S. Pahar, E. Richards, R. L. Melen, J. C. Slootweg, *Chem. Rev.* **2023**, *123*, 9653-9675.
- 335 B. Schirmer, S. Grimme, *Chem. Commun.* **2010**, *46*, 7942-7944.
- 336 D. M. Camaioni, B. Ginovska-Pangovska, G. K. Schenter, S. M. Kathmann, T. Autrey, *J. Phys. Chem. A* **2012**, *116*, 7228-7237.
- 337 T. A. Rokob, I. Bakó, A. Stirling, A. Hamza, I. Pápai, *J. Am. Chem. Soc.* **2013**, *135*, 4425-4437.
- 338 G. Skara, F. De Vleeschouwer, P. Geerlings, F. De Proft, B. Pinter, *Sci. Rep.* **2017**, *7*, 16024.
- 339 L. Liu, B. Lukose, B. Ensing, *J. Phys. Chem. C* **2017**, *121*, 2046-2051.
- 340 L. Liu, B. Lukose, P. Jaque, B. Ensing, *Green Energy Environ.* **2019**, *4*, 20-28.
- 341 G. Bistoni, A. A. Auer, F. Neese, *Chem. Eur. J.* **2017**, *23*, 865-873.
- 342 G. Skara, B. Pinter, J. Top, P. Geerlings, F. De Proft, F. De Vleeschouwer, *Chem. Eur. J.* **2015**, *21*, 5510-5519.
- 343 S. Gao, W. Wu, Y. Mo, *Int. J. Quantum Chem.* **2011**, *111*, 3761-3775.
- 344 L. Rocchigiani, G. Ciancaleoni, C. Zuccaccia, A. Macchioni, *J. Am. Chem. Soc.* **2014**, *136*, 112-115.
- 345 T. Wiegand, M. Siedow, O. Ekkert, J. Möbus, C. G. Daniliuc, G. Kehr, G. Erker, H. Eckert, *Solid State Nucl. Magn. Reson.* **2014**, *61-62*, 8-14.
- 346 L. R. Marques, R. A. Ando, *ChemPhysChem* **2023**, *24*, e202200715.
- 347 L. C. Brown, J. M. Hogg, M. Gilmore, L. Moura, S. Imberti, S. Gärtner, H. Q. N. Gunaratne, R. J. O'Donnell, N. Artioli, J. D. Holbrey, M. Swadźba-Kwaśny, *Chem. Commun.* **2018**, *54*, 8689-8692.
- 348 L. T. Littlewood A, Chen L, Barendt T, Jupp A., *ChemRxiv* **2023**, doi:10.26434/chemrxiv-22023-kqv26480, this content is a preprint and has not been peer-reviewed.
- 349 C. Bannwarth, A. Hansen, S. Grimme, *Isr. J. Chem.* **2015**, *55*, 235-242.
- 350 M. Becerra, M. Real-Enriquez, C. Espinosa-Gavilanes, C. H. Zambrano, R. Almeida, F. J. Torres, L. Rincón, *Theor. Chem. Acc.* **2016**, *135*, 77.
- 351 H. W. Kim, Y. M. Rhee, *Chem. Eur. J.* **2009**, *15*, 13348-13355.
- 352 M. Ullrich, A. J. Lough, D. W. Stephan, *Organometallics* **2010**, *29*, 3647-3654.
- 353 D. J. Scott, M. J. Fuchter, A. E. Ashley, *J. Am. Chem. Soc.* **2014**, *136*, 15813-15816.
- 354 D. Quinonero, C. Garau, C. Rotger, A. Frontera, P. Ballester, A. Costa, P. M. Deya, *Angew. Chem. Int. Ed.* **2002**, *41*, 3389-3392.
- 355 A. J. Neel, M. J. Hilton, M. S. Sigman, F. D. Toste, *Nature* **2017**, *543*, 637-646.
- 356 I. Alkorta, I. Rozas, J. Elguero, *J. Org. Chem.* **1997**, *62*, 4687-4691.
- 357 A. Altun, F. Neese, G. Bistoni, *J. Chem. Theory Comput.* **2019**, *15*, 5894-5907.
- 358 M. P. Mitoraj, A. Michalak, T. Ziegler, *J. Chem. Theory Comput.* **2009**, *5*, 962-975.
- 359 M. Heshmat, T. Privalov, *J. Phys. Chem. A* **2018**, *122*, 7202-7211.
- 360 I. Bakó, A. Stirling, S. Bálint, I. Pápai, *Dalton Trans.* **2012**, *41*, 9023-9025.
- 361 M. Pu, T. Privalov, *Isr. J. Chem.* **2015**, *55*, 179-195.

- 362 M. Pu, T. Privalov, *J. Chem. Phys.* **2013**, *138*.
- 363 M. Pu, T. Privalov, *ChemPhysChem* **2014**, *15*, 3714-3719.
- 364 M. Pu, T. Privalov, *ChemPhysChem* **2014**, *15*, 2936-2944.
- 365 F. London, *Z. Elektrochem.* **1929**, *35*, 552-555.
- 366 H. Pelzer, E. Wigner, *Z. Phys. Chem.* **1932**, *15B*, 445-471.
- 367 M. G. Evans, M. Polanyi, *Trans. Faraday Soc.* **1935**, *31*, 875-894.
- 368 D. H. Parker, R. B. Bernstein, *Annu. Rev. Phys. Chem.* **1989**, *40*, 561-595.
- 369 R. D. Levine, *Chem. Phys. Lett.* **1990**, *175*, 331-337.
- 370 M. Ben-Nun, R. D. Levine, *Int. Rev. Phys. Chem.* **1995**, *14*, 215-270.
- 371 A. Y. Houghton, T. Autrey, *J. Phys. Chem. A* **2017**, *121*, 8785-8790.
- 372 T. Özgün, K. Bergander, L. Liu, C. G. Daniliuc, S. Grimme, G. Kehr, G. Erker, *Chem. Eur. J.* **2016**, *22*, 11958-11961.
- 373 D. Yepes, P. Jaque, I. Fernández, *Chem. Eur. J.* **2016**, *22*, 18801-18809.
- 374 P. Sarkar, S. Das, S. K. Pati, *Inorg. Chem.* **2021**, *60*, 15180-15189.
- 375 A. Millanvois, C. Ollivier, L. Fensterbank, *Eur. J. Inorg. Chem.* **2022**, *2022*, e202101109.
- 376 S. Rendler, M. Oestreich, *Synthesis* **2005**, *11*, 1727-1747.
- 377 E. W. Colvin, *Chem. Soc. Rev.* **1978**, *7*, 15-64.
- 378 W. P. Weber, *Silicon Reagents for Organic Synthesis, Vol. 14*, Springer, Berlin, Heidelberg, **2012**.
- 379 R. J. Fessenden, J. S. Fessenden, *Adv. Drug Res.* **1967**, *4*, 95-132.
- 380 R. J. Fessenden, J. S. Fessenden, in *Adv. Organomet. Chem., Vol. 18*, Elsevier, **1980**, 275-299.
- 381 S. Gately, R. West, *Drug Dev. Res.* **2007**, *68*, 156-163.
- 382 M. W. Mutahi, T. Nittoli, L. X. Guo, S. M. Sieburth, *J. Am. Chem. Soc.* **2002**, *124*, 7363-7375.
- 383 R. Tacke, U. Wannagat, *Bioactive Organo-Silicon Compounds, Vol. 84*, Springer, Berlin, Heidelberg, **1979**.
- 384 N. Mizoshita, T. Tani, S. Inagaki, *Chem. Soc. Rev.* **2011**, *40*, 789-800.
- 385 M. Choi, H. S. Cho, R. Srivastava, C. Venkatesan, D. H. Choi, R. Ryoo, *Nat. Mater.* **2006**, *5*, 718-723.
- 386 C. Velasco-Santos, A. L. Martinez-Hernandez, M. Lozada-Cassou, A. Alvarez-Castillo, V. M. Castano, *Nanotechnology* **2002**, *13*, 495-498.
- 387 F. Wang, Z. Xie, H. Zhang, C. Y. Liu, Y. G. Zhang, *Adv. Funct. Mater.* **2011**, *21*, 1027-1031.
- 388 Z. L. Zhang, Y. H. Wang, W. F. Ren, Q. Q. Tan, Y. F. Chen, H. Li, Z. Y. Zhong, F. B. Su, *Angew. Chem. Int. Ed.* **2014**, *53*, 5165-5169.
- 389 C. Cheng, J. F. Hartwig, *Chem. Rev.* **2015**, *115*, 8946-8975.
- 390 S. C. Richter, M. Oestreich, *Trends Chem.* **2020**, *2*, 13-27.
- 391 H. Khatua, S. Das, S. Patra, B. Chattopadhyay, *Synthesis* **2023**, *55*, 3434-3453.
- 392 B. Neil, F. Lucien, L. Fensterbank, C. Chauvier, *ACS Catal.* **2021**, *11*, 13085-13090.
- 393 V. Iashin, K. Chernichenko, I. Pápai, T. Repo, *Angew. Chem. Int. Ed.* **2016**, *55*, 14146-14150.
- 394 C. M. Mömning, S. Frömel, G. Kehr, R. Fröhlich, S. Grimme, G. Erker, *J. Am. Chem. Soc.* **2009**, *131*, 12280-12289.
- 395 K. Chernichenko, Á. Madarász, I. Pápai, M. Nieger, M. Leskelä, T. Repo, *Nat. Chem.* **2013**, *5*, 718-723.
- 396 C. Jiang, O. Blacque, H. Berke, *Organometallics* **2010**, *29*, 125-133.
- 397 K. Chernichenko, M. Lindqvist, B. Kótai, M. Nieger, K. Sorochkina, I. Pápai, T. Repo, *J. Am. Chem. Soc.* **2016**, *138*, 4860-4868.
- 398 G. Ménard, D. W. Stephan, *Angew. Chem. Int. Ed.* **2012**, *51*, 4409-4412.
- 399 M.-A. Lègaré, M.-A. Courtemanche, É. Rochette, F.-G. Fontaine, *Science* **2015**, *349*, 513-516.
- 400 A. R. Jupp, D. W. Stephan, *Trends Chem.* **2019**, *1*, 35-48.
- 401 Q.-A. Chen, H. F. T. Klare, M. Oestreich, *J. Am. Chem. Soc.* **2016**, *138*, 7868-7871.
- 402 K. S. Lee, D. Katsoulis, J. Choi, *ACS Catal.* **2016**, *6*, 1493-1496.
- 403 B. Lu, J. R. Falck, *Angew. Chem. Int. Ed.* **2008**, *47*, 7508-7510.
- 404 D. Y. Wang, X. Y. Chen, J. J. Wong, L. Q. Jin, M. J. Li, Y. Zhao, K. N. Houk, Z. Z. Shi, *Nat. Commun.* **2021**, *12*, 524.
- 405 T. Tsuchimoto, M. Fujii, Y. Iketani, M. Sekine, *Adv. Synth. Catal.* **2012**, *354*, 2959-2964.
- 406 Y. H. Ma, S. J. Lou, G. Luo, Y. Luo, G. Zhan, M. Nishiura, Y. Luo, Z. M. Hou, *Angew. Chem. Int. Ed.* **2018**, *57*, 15222-15226.

- 407 K. Yamaguchi, Y. Wang, T. Oishi, Y. Kuroda, N. Mizuno, *Angew. Chem. Int. Ed.* **2013**, *52*, 5627-5630.
- 408 T. Baba, A. Kato, H. Yuasa, F. Toriyama, H. Handa, Y. Ono, *Catal. Today* **1998**, *44*, 271-276.
- 409 J. Ishikawa, M. Itoh, *J. Catal.* **1999**, *185*, 454-461.
- 410 J. Ishikawa, K. Inoue, M. Itoh, *J. Organomet. Chem.* **1998**, *552*, 303-311.
- 411 M. G. Voronkov, N. I. Ushakova, I. I. Tsykhanskaya, V. B. Pukhnarevich, *J. Organomet. Chem.* **1984**, *264*, 39-48.
- 412 A. A. Toutov, K. N. Betz, D. P. Schuman, W. B. Liu, A. Fedorov, B. M. Stoltz, R. H. Grubbs, *J. Am. Chem. Soc.* **2017**, *139*, 1668-1674.
- 413 A. A. Andreev, V. V. Konshin, N. V. Komarov, M. Rubin, C. Brouwer, V. Gevorgyan, *Org. Lett.* **2004**, *6*, 421-424.
- 414 R. Shimizu, T. Fuchikami, *Tetrahedron Lett.* **2000**, *41*, 907-910.
- 415 S. Bähr, M. Oestreich, *Angew. Chem. Int. Ed.* **2017**, *56*, 52-59.
- 416 R. R. Fraser, T. S. Mansour, S. Savard, *Can. J. Chem.* **1985**, *63*, 3505-3509.
- 417 G. R. Whittell, E. I. Balmont, A. P. M. Robertson, S. K. Patra, M. F. Haddow, I. Manners, *Eur. J. Inorg. Chem.* **2010**, 3967-3975.
- 418 P. Sarkar, S. Das, S. K. Pati, *Chem. Asian J.* **2022**, *17*, e202200148.
- 419 U. Frick, G. Simchen, *Synthesis* **1984**, *1984*, 929-930.
- 420 M. W. Majchrzak, G. Simchen, *Synthesis* **1986**, *1986*, 956-958.
- 421 L. T. An, J. P. Zou, L. L. Zhang, Y. Zhang, *Tetrahedron Lett.* **2007**, *48*, 4297-4300.
- 422 P. Chauhan, S. S. Chiemi, *RSC Adv.* **2012**, *2*, 6117-6134.
- 423 H. Firouzabadi, N. Iranpoor, F. Nowrouzi, *Chem. Commun.* **2005**, *6*, 789-791.
- 424 C. C. Lin, J. M. Hsu, M. N. V. Sastry, H. L. Fang, Z. J. Tu, J. T. Liu, C. F. Yao, *Tetrahedron* **2005**, *61*, 11751-11757.
- 425 Z. G. Li, Z. J. Shi, C. He, *J. Organomet. Chem.* **2005**, *690*, 5049-5054.
- 426 L. M. Hodges, J. Gonzalez, J. I. Koontz, W. H. Myers, W. D. Harman, *J. Org. Chem.* **1993**, *58*, 4788-4790.
- 427 N. Ansmann, T. Thorwart, L. Greb, *Angew. Chem. Int. Ed.* **2022**, *61*, e202210132.
- 428 R. Maskey, T. Thorwart, S. F. Ebel, A. Jovic, D. Hartmann, L. Greb, *Chem. Eur. J.* **2023**, *29*, e202300269.
- 429 D. Roth, T. Thorwart, C. Douglas, L. Greb, *Chem. Eur. J.* **2022**, *29*, e202203024.
- 430 I. J. Bruno, J. C. Cole, P. R. Edgington, M. Kessler, C. F. Macrae, P. McCabe, J. Pearson, R. Taylor, *Acta Crystallogr. B* **2002**, *58*, 389-397.
- 431 C. F. Macrae, P. R. Edgington, P. McCabe, E. Pidcock, G. P. Shields, R. Taylor, M. Towler, J. van de Streek, *J. Appl. Crystallogr.* **2006**, *39*, 453-457.
- 432 C. F. Macrae, I. Sovago, S. J. Cottrell, P. T. A. Galek, P. McCabe, E. Pidcock, M. Platings, G. P. Shields, J. S. Stevens, M. Towler, P. A. Wood, *J. Appl. Crystallogr.* **2020**, *53*, 226-235.
- 433 M. D. Hanwell, D. E. Curtis, D. C. Lonie, T. Vandermeersch, E. Zurek, G. R. Hutchison, *J. Cheminform.* **2012**, *4*, 17.
- 434 G. A. Andrienko, <https://www.chemcraftproq.com> **ChemCraft 1.8**.
- 435 R. Angnes, *GitHub repository* **2020**, doi:10.5281/zenodo.4065333.
- 436 O. V. Dolomanov, L. J. Bourhis, R. J. Gildea, J. A. K. Howard, H. Puschmann, *J. Appl. Crystallogr.* **2009**, *42*, 339-341.
- 437 P. van der Sluis, A. L. Spek, *Acta Crystallogr. A* **1990**, *46*, 194-201.
- 438 A. Spek, *Acta Crystallogr. C* **2015**, *71*, 9-18.
- 439 A. Spek, *J. Appl. Crystallogr.* **2003**, *36*, 7-13.
- 440 J. M. Schümann, J. P. Wagner, A. K. Eckhardt, H. Quanz, P. R. Schreiner, *J. Am. Chem. Soc.* **2021**, *143*, 41-45.
- 441 D. E. Wheeler, J. K. McCusker, *Inorg. Chem.* **1998**, *37*, 2296-2307.
- 442 S. H. Bertz, E. H. Fairchild, *Copper(I) Bromide*, in Encyclopedia of Reagents for Organic Synthesis.
- 443 L. Catti, K. Tiefenbacher, *Angew. Chem. Int. Ed.* **2018**, *57*, 14589-14592.
- 444 I. Krossing, *Chem. Eur. J.* **2001**, *7*, 490-502.
- 445 K. Garces, F. J. Fernandez-Alvarez, V. Polo, R. Lalrempuia, J. J. Perez-Torrente, L. A. Oro, *ChemCatChem* **2014**, *6*, 1691-1697.
- 446 Y. Misumi, Y. Ishii, M. Hidai, *Organometallics* **1995**, *14*, 1770-1775.

- 447 R. Kannan, S. Balasubramaniam, S. Kumar, R. Chammenahalli, E. D. Jemmis, A. Venugopal, *Chem. Eur. J.* **2020**, *26*, 12717-12721.
- 448 L. Monsigny, P. Thuery, J. C. Berthet, T. Cantat, *ACS Catal.* **2019**, *9*, 9025-9033.
- 449 R. Savela, R. Leino, *Synthesis* **2015**, *47*, 1749-1760.
- 450 M. Mehta, M. H. Holthausen, I. Mallov, M. Perez, Z. W. Qu, S. Grimme, D. W. Stephan, *Angew. Chem. Int. Ed.* **2015**, *54*, 8250-8254.
- 451 S.-H. Xiang, J. Xu, H.-Q. Yuan, P.-Q. Huang, *Synlett* **2010**, *2010*, 1829-1832.
- 452 L. S. Isaeva, G. I. Drogunova, A. S. Peregudov, E. I. Fedin, D. N. Kravtsov, *Metalloorg. Khim.* **1989**, *2*, 447-452.
- 453 S. Kronig, E. Theuergarten, D. Holschumacher, T. Bannenberg, C. G. Daniliuc, P. G. Jones, M. Tamm, *Inorg. Chem.* **2011**, *50*, 7344-7359.
- 454 K. Kikushima, M. Grellier, M. Ohashi, S. Ogoshi, *Angew. Chem. Int. Ed.* **2017**, *56*, 16191-16196.
- 455 P. Eisenberger, A. M. Bailey, C. M. Crudden, *J. Am. Chem. Soc.* **2012**, *134*, 17384-17387.
- 456 G. F. Riegel, S. R. Kass, *J. Org. Chem.* **2020**, *85*, 6017-6026.
- 457 E. M. Simmons, J. F. Hartwig, *Angew. Chem. Int. Ed.* **2012**, *51*, 3066-3072.
- 458 F. Neese, *Wiley Interdiscip. Rev. Comput. Mol. Sci.* **2012**, *2*, 73-78.
- 459 F. Neese, *Wiley Interdiscip. Rev. Comput. Mol. Sci.* **2018**, *8*, e1327.
- 460 S. Grimme, C. Bannwarth, P. Shushkov, *J. Chem. Theory Comput.* **2017**, *13*, 1989-2009.
- 461 C. Bannwarth, S. Ehlert, S. Grimme, *J. Chem. Theory Comput.* **2019**, *15*, 1652-1671.
- 462 C. Bannwarth, E. Caldeweyher, S. Ehlert, A. Hansen, P. Pracht, J. Seibert, S. Spicher, S. Grimme, *Wiley Interdiscip. Rev. Comput. Mol. Sci.* **2021**, *11*, e1493.
- 463 P. Pracht, F. Bohle, S. Grimme, *Phys. Chem. Chem. Phys.* **2020**, *22*, 7169-7192.
- 464 K. Eichkorn, O. Treutler, H. Ohm, M. Haser, R. Ahlrichs, *Chem. Phys. Lett.* **1995**, *242*, 652-660.
- 465 F. Neese, F. Wennmohs, A. Hansen, U. Becker, *Chem. Phys.* **2009**, *356*, 98-109.
- 466 K. Eichkorn, F. Weigend, O. Treutler, R. Ahlrichs, *Theor. Chem. Acc.* **1997**, *97*, 119-124.
- 467 A. D. Becke, E. R. Johnson, *J. Chem. Phys.* **2005**, *123*, 154101.
- 468 A. D. Becke, E. R. Johnson, *J. Chem. Phys.* **2005**, *122*, 154104.
- 469 S. Grimme, J. Antony, S. Ehrlich, H. Krieg, *J. Chem. Phys.* **2010**, *132*, 154104.
- 470 S. Grimme, S. Ehrlich, L. Goerigk, *J. Comput. Chem.* **2011**, *32*, 1456-1465.
- 471 E. Caldeweyher, S. Ehlert, A. Hansen, H. Neugebauer, S. Spicher, C. Bannwarth, S. Grimme, *J. Chem. Phys.* **2019**, *150*.
- 472 S. Grimme, J. G. Brandenburg, C. Bannwarth, A. Hansen, *J. Chem. Phys.* **2015**, *143*, 054107.
- 473 S. Grimme, A. Hansen, S. Ehlert, J.-M. Mewes, *J. Chem. Phys.* **2021**, *154*, 064103
- 474 J. P. Perdew, K. Burke, M. Ernzerhof, *Phys. Rev. Lett.* **1996**, *77*, 3865-3868.
- 475 C. Adamo, V. Barone, *J. Chem. Phys.* **1999**, *110*, 6158-6170.
- 476 Y. Zhao, D. G. Truhlar, *J. Phys. Chem. A* **2005**, *109*, 5656-5667.
- 477 S. Kozuch, D. Gruzman, J. M. Martin, *J. Phys. Chem. C* **2010**, *114*, 20801-20808.
- 478 A. Schäfer, C. Huber, R. Ahlrichs, *J. Chem. Phys.* **1994**, *100*, 5829-5835.
- 479 F. Weigend, R. Ahlrichs, *Phys. Chem. Chem. Phys.* **2005**, *7*, 3297-3305.
- 480 A. K. Wilson, D. E. Woon, K. A. Peterson, T. H. Dunning Jr., *J. Chem. Phys.* **1999**, *110*, 7667-7676.
- 481 N. B. Balabanov, K. A. Peterson, *J. Chem. Phys.* **2006**, *125*, 074110.
- 482 N. B. Balabanov, K. A. Peterson, *J. Chem. Phys.* **2005**, *123*, 064107.
- 483 D. E. Woon, T. H. Dunning Jr., *J. Chem. Phys.* **1993**, *98*, 1358-1371.
- 484 B. P. Prascher, D. E. Woon, K. A. Peterson, T. H. Dunning Jr., A. K. Wilson, *Theor. Chem. Acc.* **2011**, *128*, 69-82.
- 485 R. A. Kendall, T. H. Dunning Jr., R. J. Harrison, *J. Chem. Phys.* **1992**, *96*, 6796-6806.
- 486 F. Neese, A. Hansen, D. G. Liakos, *J. Chem. Phys.* **2009**, *131*, 064103.
- 487 C. Riplinger, F. Neese, *J. Chem. Phys.* **2013**, *138*, 034106.
- 488 C. Riplinger, B. Sandhoefer, A. Hansen, F. Neese, *J. Chem. Phys.* **2013**, *139*, 134101.
- 489 S. Ehlert, M. Stahn, S. Spicher, S. Grimme, *J. Chem. Theory Comput.* **2021**, *17*, 4250-4261.
- 490 A. V. Marenich, C. J. Cramer, D. G. Truhlar, *J. Phys. Chem. B* **2009**, *113*, 6378-6396.
- 491 C. J. Cramer, *Essentials of computational chemistry: theories and models*, John Wiley & Sons, **2013**.
- 492 S. Grimme, *Chem. Eur. J.* **2012**, *18*, 9955-9964.

- 
- 493 C. C. Pye, T. Ziegler, *Theor. Chem. Acc.* **1999**, *101*, 396-408.  
494 G. te Velde, F. M. Bickelhaupt, E. J. Baerends, C. Fonseca Guerra, S. J. A. van Gisbergen, J. G. Snijders, T. Ziegler, *J. Comput. Chem.* **2001**, *22*, 931-967.  
495 E. Van Lenthe, E. J. Baerends, *J. Comput. Chem.* **2003**, *24*, 1142-1156.  
496 F. Eckert, A. Klamt, *AIChE J.* **2002**, *48*, 369-385.  
497 A. Klamt, M. Diedenhofen, *J. Comput. Aided Mol. Des.* **2010**, *24*, 357-360.  
498 A. Klamt, *J. Phys. Chem.* **1995**, *99*, 2224-2235.  
499 A. Klamt, B. Mennucci, J. Tomasi, V. Barone, C. Curutchet, M. Orozco, F. J. Luque, *Acc. Chem. Res.* **2009**, *42*, 489-492.  
500 D. Roth, Master thesis, Heidelberg University **2019**.  
501 M. Bursch, T. Gasevic, J. B. Stückrath, S. Grimme, *Inorg. Chem.* **2021**, *60*, 272-285.  
502 A. M. Kelly-Rowley, V. M. Lynch, E. V. Anslyn, *J. Am. Chem. Soc.* **1995**, *117*, 3438-3447.  
503 S. Tshepelevitsh, A. Kütt, M. Lõkov, I. Kaljurand, J. Saame, A. Heering, P. G. Plieger, R. Vianello, I. Leito, *Eur. J. Org. Chem.* **2019**, *2019*, 6735-6748.  
504 H. K. Hall Jr., *J. Am. Chem. Soc.* **1957**, *79*, 5441-5444.  
505 E.-I. Rõõm, A. Kütt, I. Kaljurand, I. Koppel, I. Leito, I. A. Koppel, M. Mishima, K. Goto, Y. Miyahara, *Chem. Eur. J.* **2007**, *13*, 7631-7643.  
506 A. Streitwieser, Jr., D. M. E. Reuben, *J. Am. Chem. Soc.* **1971**, *93*, 1794-1795.  
507 F. G. Bordwell, *Acc. Chem. Res.* **1988**, *21*, 456-463.



# 7

## APPENDIX

---

### 7.1 List of Abbreviations

12c4	12-crown-4-ether	DA	donor affinity
18c6	18-crown-6-ether	DART	direct analysis in real time
2D	two-dimensional	DBU	1,8-diazabicyclo[5.4.0]undec-7-en
3c4e	three-center-four-electron	DCM	dichloromethane
9-BBN	9-borabicyclo(3.3.1)nonane	D <sub>e</sub>	dissociation energy
a.u.	atomic unit	DEPT	distortionless enhancement by polarization transfer
ADF	amsterdam density functional (software)	DFT	density functional theory
atm	atmosphere	Dim.	dimension
ATR	attenuated total reflection	diox	dioxolene
calc/calc.	calculated	DIPEA	N,N-di- <i>iso</i> -propyl-N-ethylamine
cat	catecholate	DLPNO	domain-based local pair natural orbital
CC	coupled cluster	DMA	dimethylacetamide
Cm	cumyl	DMF	dimethylformamide
cmp.	compare	DMSO	dimethylsulfoxide
COM	carbonyl-olefin-metathesis	DN	donor number
COSMO-RS	conductor-like screening model for real solvents	DTBP	2,6-di- <i>tert</i> -butylpyridine
CPCM	conductor-like polarizable continuum model	e.g.	<i>exempli gratia</i> (for example)
CREST	conformer-rotamer ensemble sampling tool (software)	EI	electron impact
		ELC	element-ligand-cooperativity

## Appendix

EPC	electrophilic phosphonium cation	HSAB	Pearson's principle of hard and soft acids and bases
EPR	electron paramagnetic resonance	Hz	Hertz
eq.	equivalent(s)	<i>i</i>	<i>iso</i>
ESI	electro-spray ionization	I	nuclear spin/intensity
Et	ethyl	IG	inverse gated
EF	electric field (model)	IR	infra red (refers to vibrational spectroscopy)
ET	electron transfer (model)	<sup>t</sup> Pr	<i>iso</i> -propyl
<i>et al.</i>	<i>et alii</i> (and others)	IUPAC	International Union of Pure and Applied Chemistry
ETS	extended transition state (scheme)	KIE	kinetic isotope effect
Fc	ferrocene	LA	Lewis acid
FIA	fluoride ion affinity	LB	Lewis base
FLP	frustrated Lewis pair	LP	lone-pair
FT	Fourier transformation	LUMO	lowest unoccupied molecular orbital
CI	configuration interaction	M	refers to the molecule of interest in MS data
GB	Gutmann-Beckett	m	mass
GCMS	gas chromatography mass spectrometry	MAS	magic angle spinning
GED	gas phase electron diffraction	Me	methyl
GEI	global electrophilicity index	Mes	mesityl
HF	Hartree–Fock	MS	mass spectrometry
HFLD	Hartree–Fock plus London dispersion (HFLD)	<i>n</i>	<i>normal</i>
HIA	hydride ion affinity	<sup>n</sup> Bu	<i>n</i> -butyl
HMBC	Heteronuclear Multiple Bond Correlation	NCI	non-covalent interaction
HMDS	bis(trimethylsilyl)amide / bis(trimethylsilyl)amine	NHC	N-heterocyclic carbene
HOMO	highest occupied molecular orbital	NIS	N-iodo-succinimide
HR	high resolution	NMR	nuclear magnetic resonance

NOCV	Natural Orbitals for Chemical Valence (theory)	SMD	solvation model density (universal solvent model)
<i>o</i>	ortho	S <sub>N</sub> Ar	nucleophilic aromatic substitution
oDCB	<i>ortho</i> -dichlorobenzene	sq	semiquinone
oDFB	<i>ortho</i> -difluorobenzene	<i>t</i>	<i>tert</i>
ORTEP	Oak Ridge thermal ellipsoid plot	<sup>t</sup> Bu/ <i>t</i> Bu	<i>tert</i> -butyl
<i>p</i>	para	THF	tetrahydrofuran
pmpp	1,2,2,6,6-pentamethylpiperidine	tmp	2,2,6,6-tetra-methylpiperidin-1-yl
ppm	parts per million	tmpH	2,2,6,6-tetra-methylpiperidine
q	quinone	TTP	tetratriflatopropenyl
r.a.	reducing agent	VSEPR	valence shell electron pair repulsion
RMSD	root-mean-square-deviation	WCA	weakly coordinating anion
RRHO	rigid-rotor-harmonic-oscillator	xs/xs.	excess
rt	room temperature	z	charge
scXRD	single crystal XRay diffraction		
SET	single electron transfer		

Abbreviations in the context of assignments for IR or NMR spectra are given in section 5.1.2. For a more concise explanation of the acronyms for computational methods it shall be referred to the respective citations.

---

## 7.2 List of Symbols and Constants

$\tilde{\nu}$	wavenumber [ $\text{cm}^{-1}$ ]
$\ddagger$	refers to transition state or assigned property
d	distance [ $\text{\AA}$ ]
E <sub>DEF</sub>	deformation or preorganization energy
E <sub>INT</sub>	interaction energy of preorganized fragments
E <sub>ORB</sub>	orbital interaction energy
G	Gibbs (free) energy/free enthalpy
H	enthalpy
<i>J</i>	NMR coupling constant
K	equilibrium constant
k <sub>B</sub>	Boltzmann constant
m/z	mass-to-charge ratio
pK <sub>a</sub>	negative common logarithm of the acid dissociation constant
R	universal gas constant
t	time [s, h, d]
T	temperature [ $^{\circ}\text{C}$ , K]
$\Delta$	difference
$\delta$	chemical shift [ppm]

## 7.3 Computational Data Tables and Figures

### 7.3.1 Thermodynamic Data

Table A1. Computed energies and thermodynamic data for the dimerization of **1<sup>3,6-tBu</sup>**, **1<sup>3,4,6-iPr</sup>**, **1<sup>3,5-Cm</sup>** and **1<sup>CF<sub>3</sub></sup>**. The derived  $\Delta G$  values are referenced against 2 equivalents of the respective monomers.

Compound	E <sup>OPT</sup> [H]	G <sup>OPT</sup> [H]	H <sup>OPT</sup> [H]	E <sup>SP</sup> [H]	G [kJ mol <sup>-1</sup> ]	$\Delta G$ [kJ mol <sup>-1</sup> ]
<b>1<sup>3,6-tBu</sup></b>	-1678.3346	-1677.7441	-1677.6512	-1680.5223	-4410653.7	<b>0.0</b>
TS-[ <b>1<sup>3,6-tBu</sup></b> ] <sub>2</sub> ‡	-3356.6703	-3355.4549	-3355.3020	-3361.0422	-8821218.1	<b>89.2</b>
[ <b>1<sup>3,6-tBu</sup></b> ] <sub>2</sub>	-3356.6860	-3355.4752	-3355.3172	-3361.0637	-8821286.5	<b>20.8</b>
<b>1<sup>3,4,6-iPr</sup></b>	-1756.7974	-1756.1537	-1756.0513	-1759.0875	-4616786.6	<b>0.0</b>
TS-[ <b>1<sup>3,4,6-iPr</sup></b> ] <sub>2</sub> ‡	-3513.5914	-3512.2695	-3512.0976	-3518.1673	-9233470.2	<b>103.0</b>
[ <b>1<sup>3,4,6-iPr</sup></b> ] <sub>2</sub>	-3513.6100	-3512.2914	-3512.1163	-3518.1777	-9233517.4	<b>55.8</b>
<b>1<sup>3,5-Cm</sup></b>	-2443.5766	-2442.7805	-2442.6625	-2446.9056	-6422253.0	<b>0.0</b>
TS-[ <b>1<sup>3,5-Cm</sup></b> ] <sub>2</sub> ‡	-4887.1676	-4885.5414	-4885.3393	-4893.8233	-12844467.7	<b>38.4</b>
[ <b>1<sup>3,5-Cm</sup></b> ] <sub>2</sub>	-4887.2103	-4885.5857	-4885.3802	-4893.8644	-12844568.8	
<b>1<sup>CF<sub>3</sub></sup></b>	-3741.7941	-3741.6364	-3741.5288	-3747.5683	-9838819.5	<b>0.0</b>
TS-[ <b>1<sup>CF<sub>3</sub></sup></b> ] <sub>2</sub> ‡	-7483.5664	-7483.2205	-7483.0350	-7495.1147	-19677509.0	<b>129.9</b>
[ <b>1<sup>CF<sub>3</sub></sup></b> ] <sub>2</sub>	-7483.6023	-7483.2579	-7483.0700	-7495.1516	-19677610.1	<b>28.9</b>

DSD-BLYP-D3(BJ)/def2-QZVPP+SMD(CH<sub>2</sub>Cl<sub>2</sub>)/PBEh-3c level of theory (*Orca 5.0*).

Table A2. Computed energies and thermodynamic data for the formation of **1<sup>CF<sub>3</sub></sup>-O(SiEt<sub>3</sub>)<sub>2</sub>**.

Compound	E <sup>OPT</sup> [H]	G <sup>OPT</sup> [H]	H <sup>OPT</sup> [H]	E <sup>SP</sup> [H]	G [kJ mol <sup>-1</sup> ]
<b>1<sup>CF<sub>3</sub></sup></b>	-1127,8234	-1127,4607	-1127,3859	-1128,9394	-2963070,7
O(SiEt <sub>3</sub> ) <sub>2</sub>	-4869,6485	-4869,0943	-4868,9414	-4876,5374	-12801886,7
<b>1<sup>CF<sub>3</sub></sup>-O(SiEt<sub>3</sub>)<sub>2</sub></b>	-3741,7935	-3741,6361	-3741,5280	-3747,5671	-9838817,2
<b>Thermodynamics</b>					<b><math>\Delta G</math></b>
<b>1<sup>CF<sub>3</sub></sup> + O(SiEt<sub>3</sub>)<sub>2</sub> → 1<sup>CF<sub>3</sub></sup>-O(SiEt<sub>3</sub>)<sub>2</sub></b>					<b>1.2</b>

DSD-BLYP-D3(BJ)/def2-QZVPP+SMD(CH<sub>2</sub>Cl<sub>2</sub>)/PBEh-3c level of theory (*Orca 5.0*). The preferred conformers were taken as starting structures as determined by *CREST*.

## Appendix

Table A3. Computed energies for the determination of *vacuum* fluoride and hydride ion affinities.

Compound	$E^{\text{OPT}}$ [H]	$H^{\text{OPT}}$ [H]	$E^{\text{SP}}$ [H]	$H_{\text{tot}}$ [kJ mol <sup>-1</sup> ]	FIA/HIA [kJ mol <sup>-1</sup> ]
MeSi <sub>3</sub> <sup>+</sup> [a]	-408.7706	-408.6530	-408.3655	-1071854.7	
Me <sub>3</sub> SiF <sup>[a]</sup>	-508.9244	-508.8018	-508.5046	-1334757.0	
MeSi <sub>3</sub> <sup>+</sup> [b]	-408.7706	-408.6530	-408.3665	-1071857.5	
Me <sub>3</sub> SiF <sup>[b]</sup>	-508.9244	-508.8018	-508.5079	-1334765.8	
Me <sub>3</sub> SiH <sup>[b]</sup>	-409.6509	-409.5238	-409.2547	-1074164.7	
MeSi <sub>3</sub> <sup>+</sup> [c]	-409.452919	-409.3386404	-408.3653909	-1071863.377	
Me <sub>3</sub> SiF <sup>[c]</sup>	-509.8061864	-509.686885	-508.5069251	-1334771.808	
Me <sub>3</sub> SiH <sup>[c]</sup>	-410.3370301	-410.2133899	-409.2537676	-1074171.232	
MeSi <sub>3</sub> <sup>+</sup> [d]	-408.7706172	-408.6530429	-408.3656672	-1071855.45	
Me <sub>3</sub> SiF <sup>[d]</sup>	-508.9244102	-508.8018929	-508.5071869	-1334777.01	
Me <sub>3</sub> SiH <sup>[d]</sup>	-409.6509401	-409.5239248	-409.2539535	-1074162.858	
<b>1</b> <sup>3,6-tBu</sup> [a]	-1680.5301	-1679.8646	-1679.2498	-4407123.6	
[F- <b>1</b> <sup>3,6-tBu</sup> ] <sup>-</sup> [a]	-1780.4803	-1779.8127	-1779.1771	-4669477.1	<b>403.7</b> (FIA)
[ <b>1</b> <sup>3,6-tBu</sup> ] <sup>•+</sup> [a]	-1680.2482	-1679.5847	-1678.9566	-4406358.9	
[F- <b>1</b> <sup>3,6-tBu</sup> ] <sup>•+</sup> [a]	-1780.3494	-1779.6812	-1779.0312	-4669092.2	<b>783.5</b> (FIA)
[F <sub>2</sub> - <b>1</b> <sup>3,6-tBu</sup> ] <sup>-</sup> [a]	-1880.2617	-1879.5910	-1878.9302	-4931370.8	<b>328.8</b> (FIA)
<b>1</b> <sup>CF<sub>3</sub></sup> [b]	-3746.9532	-3746.6937	-3745.3415	-9832713.5	
[F- <b>1</b> <sup>CF<sub>3</sub></sup> ] <sup>-</sup> [b]	-3846.9606	-3846.6980	-3845.3295	-10095224.1	<b>554.7</b> (FIA)
[H- <b>1</b> <sup>CF<sub>3</sub></sup> ] <sup>-</sup> [b]	-3747.6842	-3747.4170	-3746.0733	-9834614.9	<b>517.7</b> (HIA)
<b>1</b> <sup>CF<sub>3</sub></sup> [c]	-3754.5723	-3754.3205	-3745.3185	-9832673.4	
[F- <b>1</b> <sup>CF<sub>3</sub></sup> ] <sup>-</sup> [c]	-3854.7786	-3854.5234	-3845.3158	-10095207.4	<b>578.0</b> (FIA)
[H- <b>1</b> <sup>CF<sub>3</sub></sup> ] <sup>-</sup> [c]	-3755.3071	-3755.0475	-3746.0526	-9834580.3	<b>522.5</b> (HIA)
<b>2</b> <sup>[d]</sup>	-3259.3247	-3259.0637	-3257.6579	-8552296.1	
[F- <b>2</b> ] <sup>-</sup> [d]	-3359.3071	-3359.0442	-3357.6265	-8814758.9	<b>493.7</b> (FIA)
[H- <b>2</b> ] <sup>-</sup> [d]	-3260.0292	-3259.7610	-3258.3632	-8554129.0	<b>448.9</b> (HIA)

FIA/HIA =  $-\Delta H(\text{LA} + \text{Me}_3\text{SiY} \rightarrow \text{Me}_3\text{Si}^+ + \text{LA-Y}) - \text{anchor point}$

Anchor points: 952.5 kJ mol<sup>-1</sup> (FIA),<sup>78</sup> 923.5 kJ mol<sup>-1</sup> (HIA).<sup>30</sup>

[a] DLPNO-CCSD(T)/def2-QZVPP//PBE0-D3(BJ)/def2-TZVPP (*Orca 5.0*); [b] DLPNO-CCSD(T)/aug-cc-pVQZ//PBE0-D3(BJ)/def2-TZVPP (*Orca 5.0*); [c] DLPNO-CCSD(T)/aug-cc-pVQZ//PW6B95-D3(BJ)/def2-TZVPP//BP86/def2-SVP (*Orca 4.2*), derived by *D. ROTR*; [d] DLPNO-CCSD(T)/aug-cc-pVQZ//PBE0-D3(BJ)/def2-TZVPP (*Orca 4.2*).

Table A4. Solvation corrected ion affinities.

Compound	$\Delta H_{\text{solv}}(\text{CH}_2\text{Cl}_2)$ [kJ mol <sup>-1</sup> ]	System	FIA/HIA (CH <sub>2</sub> Cl <sub>2</sub> ) [kJ mol <sup>-1</sup> ]
F <sup>-</sup>	-333.9		
H <sup>-</sup>	-203.9		
<b>1</b> <sup>3,6-tBu</sup> [a]	-71.8		
[F- <b>1</b> <sup>3,6-tBu</sup> ] <sup>-</sup> [a]	-209.9	<b>1</b> <sup>3,6-tBu</sup> / [F- <b>1</b> <sup>3,6-tBu</sup> ] <sup>-</sup>	<b>201.9</b> (FIA)
[ <b>1</b> <sup>3,6-tBu</sup> ] <sup>•+</sup> [a]	-241.6		
[F- <b>1</b> <sup>3,6-tBu</sup> ] <sup>•</sup> [a]	-75.2	[ <b>1</b> <sup>3,6-tBu</sup> ] <sup>•+</sup> / [F- <b>1</b> <sup>3,6-tBu</sup> ] <sup>•</sup>	<b>277.2</b> (FIA)
[F <sub>2</sub> - <b>1</b> <sup>3,6-tBu</sup> ] <sup>•-</sup> [a]	-210.9	[F- <b>1</b> <sup>3,6-tBu</sup> ] <sup>•</sup> / [F <sub>2</sub> - <b>1</b> <sup>3,6-tBu</sup> ] <sup>•-</sup>	<b>124.6</b> (FIA)
<b>1</b> <sup>CF<sub>3</sub></sup> [b]	-68.6		
[F- <b>1</b> <sup>CF<sub>3</sub></sup> ] <sup>-</sup> [b]	-156.6	<b>1</b> <sup>CF<sub>3</sub></sup> / [F- <b>1</b> <sup>CF<sub>3</sub></sup> ] <sup>-</sup>	<b>302.8</b> (FIA)
[H- <b>1</b> <sup>CF<sub>3</sub></sup> ] <sup>-</sup> [b]	-154.7	<b>1</b> <sup>CF<sub>3</sub></sup> / [H- <b>1</b> <sup>CF<sub>3</sub></sup> ] <sup>-</sup>	<b>399.9</b> (HIA)
<b>2</b> [d]	-64.7		
[F- <b>2</b> ] <sup>-</sup> [d]	-162.8	<b>2</b> / [F- <b>2</b> ] <sup>-</sup>	<b>251.8</b> (FIA)
[H- <b>2</b> ] <sup>-</sup> [d]	-158.9	<b>2</b> / [H- <b>2</b> ] <sup>-</sup>	<b>339.2</b> (HIA)

[a]-[d] refer to the derived gas phase values, shown in Table A3.

## Appendix

Table A5. Computed energies for the calculation of thermodynamics and kinetics for adduct formation, side reactivities and cooperative dihydrogen cleavage between **2** and different Lewis bases.

Compound	$E^{OPT}$ [a.u.]	$G^{OPT}$ [a.u.]	$H^{OPT}$ [a.u.]	$E^{SP}$ [a.u.]	$G$ [kJ mol <sup>-1</sup> ]
H <sub>2</sub>	-1.1687	-1.1701	-1.1553	-1.1723	-3073.7
[H-2] <sup>-</sup>	-3260.0292	-3259.8663	-3259.7609	-3257.5135	-8552166.8
<b>2</b>	-3259.3246	-3259.1694	-3259.0636	-3256.7757	-8550250.0
P <sup>t</sup> Bu <sub>3</sub>	-814.3881	-814.0597	-814.0000	-813.5781	-2135179.4
[HP <sup>t</sup> Bu <sub>3</sub> ] <sup>+</sup>	-814.7931	-814.4540	-814.3935	-814.0446	-2136376.1
<b>Thermodynamics</b>					<b>ΔG</b>
P <sup>t</sup> Bu <sub>3</sub> + <b>2</b> → 2-P <sup>t</sup> Bu <sub>3</sub>					-20.7
<b>2</b> + H <sub>2</sub> + P <sup>t</sup> Bu <sub>3</sub> → [H-2] <sup>-</sup> + [HP <sup>t</sup> Bu <sub>3</sub> ] <sup>+</sup>					-39.8
2-P <sup>t</sup> Bu <sub>3</sub> + H <sub>2</sub> → [H-2] <sup>-</sup> + [H P <sup>t</sup> Bu <sub>3</sub> ] <sup>+</sup>					-19.1
tmpH	-408.8405	-408.6046	-408.5580	-408.4391	-1071729.7
[tmpH <sub>2</sub> ] <sup>+</sup>	-409.2334	-408.9825	-408.9356	-408.9087	-1072923.2
<b>2</b> -tmp	-3668.2001	-3667.7777	-3667.6521	-3665.2551	-9622011.2
<b>Thermodynamics</b>					<b>ΔG</b>
<b>2</b> + tmpH → <b>2</b> -tmpH					-31.5
<b>2</b> + H <sub>2</sub> + tmpH → [H-2] <sup>-</sup> + [tmpH <sub>2</sub> ] <sup>+</sup>					-36.6
<b>2</b> -tmpH + H <sub>2</sub> → [H-2] <sup>-</sup> + [tmpH <sub>2</sub> ] <sup>+</sup>					-5.1
DTBP	-562.3565	-562.0826	-562.0267	-561.7891	-1474250.5
[DTBP-H] <sup>+</sup>	-562.7483	-562.4607	-562.4041	-562.2466	-1475415.5
<b>Thermodynamics</b>					<b>ΔG</b>
<b>2</b> + H <sub>2</sub> + DTBP → [H-2] <sup>-</sup> + [DTBPH] <sup>+</sup>					-8.1
DIPEA	-370.7320	-370.5048	-370.4566	-370.3711	-971805.0
[H-DIPEA] <sup>+</sup>	-371.1268	-370.8837	-370.8356	-370.8440	-973004.9
<b>2</b> -DIPEA	-3630.0807	-3629.6657	-3629.5394	-3627.1788	-9522061.4
<sup>t</sup> Pr <sub>2</sub> N-CH=CH <sub>2</sub>	-369.5154	-369.3110	-369.2637	-369.1536	-968668.3
[ <sup>t</sup> Pr <sub>2</sub> N <sup>+</sup> =CH-CH <sub>2</sub> -1 <sup>-</sup> ]	-3628.8837	-3628.4959	-3628.3676	-3625.9794	-9518983.7
[ <sup>t</sup> PrEtN <sup>+</sup> =CMe-CH <sub>2</sub> -1 <sup>-</sup> ]	-3628.8912	-3628.5025	-3628.3751	-3625.9867	-9519000.6
<b>Thermodynamics</b>					<b>ΔG</b>
<b>2</b> + DIPEA → <b>2</b> -DIPEA					-6.5
<b>2</b> + H <sub>2</sub> + DIPEA → [H-2] <sup>-</sup> + [H-DIPEA] <sup>+</sup>					-43.0
<b>2</b> -DIPEA + H <sub>2</sub> → [H-2] <sup>-</sup> + [H-DIPEA] <sup>+</sup>					-36.6
[ <sup>t</sup> PrEtN <sup>+</sup> =CMe-CH <sub>2</sub> -2 <sup>-</sup> ] → [ <sup>t</sup> Pr <sub>2</sub> N <sup>+</sup> =CH-CH <sub>2</sub> -2 <sup>-</sup> ]					16.9
<b>2</b> -DIPEA → 0.5 [H-2] <sup>-</sup> + 0.5 [DIPEA-H] <sup>+</sup> + 0.5 [ <sup>t</sup> PrEtN <sup>+</sup> =CMe-CH <sub>2</sub> -2 <sup>-</sup> ]					-24.7
[ <sup>t</sup> PrEtN <sup>+</sup> =CMe-CH <sub>2</sub> -1 <sup>-</sup> ] + 2 H <sub>2</sub> → [H-2] <sup>-</sup> + [DIPEA-H] <sup>+</sup>					-23.7
NHC <sup>t</sup> Bu	-540.2633	-540.0065	-539.9520	-539.7422	-1416411.1
[NHC <sup>t</sup> BuH] <sup>+</sup>	-540.7084	-540.4375	-540.3830	-540.2460	-1417696.7
<b>2</b> -NHC <sup>t</sup> Bu	-3799.6395	-3799.1925	-3799.0627	-3796.5662	-9966703.8
<b>2</b> - <sup>a</sup> NHC <sup>t</sup> Bu	-3799.6602	-3799.2175	-3799.0842	-3796.5934	-9966786.5
<b>Thermodynamics</b>					<b>ΔG</b>
<b>2</b> + NHC <sup>t</sup> Bu → <b>2</b> -NHC <sup>t</sup> Bu					-42.7
<b>2</b> -NHC <sup>t</sup> Bu + H <sub>2</sub> → [H-2] <sup>-</sup> + [NHC <sup>t</sup> BuH] <sup>+</sup>					-86.0
<b>2</b> + NHC <sup>t</sup> Bu → <b>2</b> - <sup>a</sup> NHC <sup>t</sup> Bu					-125.4
<b>2</b> - <sup>a</sup> NHC <sup>t</sup> Bu + H <sub>2</sub> → [H-2] <sup>-</sup> + [NHC <sup>t</sup> BuH] <sup>+</sup>					-3.4

pmp	-448.095307	-447.831726	-447.782915	-447.6534	-1174614.1
[pmpH] <sup>+</sup>	-448.50225	-448.224124	-448.174685	-448.1345	-1175839.2
2-pmp	-3707.44206	-3706.99027	-3706.86404	-3704.458	-9724860.3
[2⋯⋯pmp] <sup>VDW</sup>	-3707.44803	-3707.00438	-3706.87273	-3704.455	-9724873.6
[pmpH][H-2]	-3708.64506	-3708.17942	-3708.04636	-3705.669	-9728003.5
TS <sup>‡</sup> [2--H-H--pmp] <sup>‡</sup>	-3708.60579	-3708.14825	-3708.01664	-3705.609	-9727867.9
<b>Thermodynamics</b>					<b>ΔG</b>
2 + pmp → 2-pmp					3.8
2 + H <sub>2</sub> + pmp → [H-2] <sup>-</sup> + [pmpH] <sup>+</sup>					-68.3
2 + pmp → [2⋯⋯pmp] <sup>VDW</sup>					-9.5
[2⋯⋯pmp] <sup>VDW</sup> + H <sub>2</sub> → [pmpH][H-2]					-56.2
[H-2] <sup>-</sup> + [pmpH] <sup>+</sup> → [pmpH][H-2]					2.6
<b>Kinetics</b>					<b>ΔG</b>
[2⋯⋯pmp] <sup>VDW</sup> + H <sub>2</sub> → TS <sup>‡</sup>					79.4
[tmpCH <sub>2</sub> ] <sup>+</sup>	-447.273231	-447.018751	-446.970903	-446.9036	-1172669.4
[tmpCH <sub>2</sub> <sup>+</sup> --H-H--pmp] <sup>‡</sup>	-896.560651	-896.008148	-895.930415	-895.7253	-2350268.5
<b>Thermodynamics</b>					<b>ΔG</b>
2 + pmp → [H-2] <sup>-</sup> + [tmpCH <sub>2</sub> ] <sup>+</sup>					27.8
[tmpCH <sub>2</sub> ] <sup>+</sup> + H <sub>2</sub> → [pmpH] <sup>+</sup>					-96.1
<b>Kinetics</b>					<b>ΔG</b>
[tmpCH <sub>2</sub> ] <sup>+</sup> + pmp + H <sub>2</sub> → TS <sup>‡</sup>					88.7

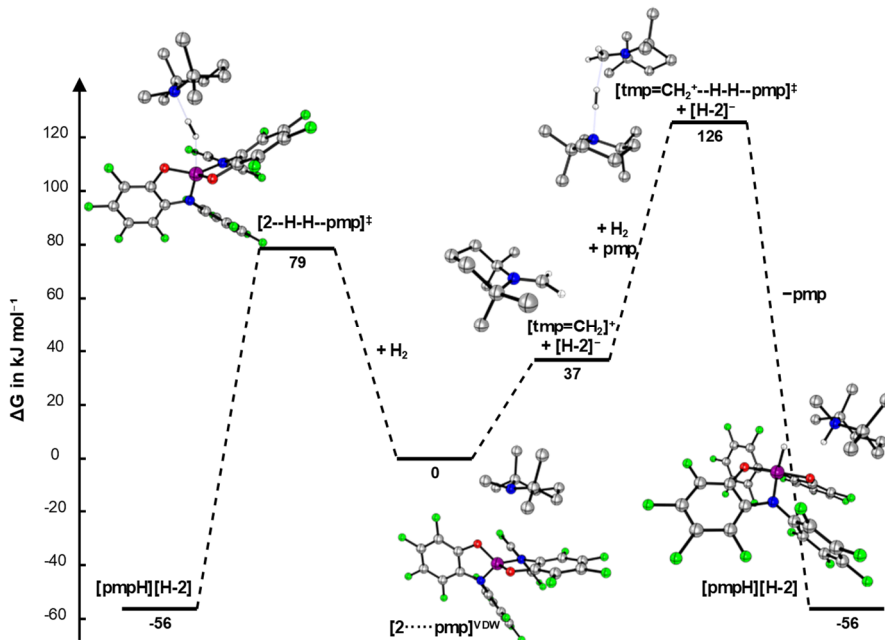


Figure A1. Free energy profile for the direct cooperative dihydrogen cleavage by 2/pmp, and an indirect pathway with the iminium ion [tmpCH<sub>2</sub>]<sup>+</sup> as the active species. In the displayed structures sp<sup>3</sup>-carbon bound hydrogen atoms are omitted for clarity.

## Appendix

Table A6. Computed energies for the calculation of thermodynamics and kinetics for the cooperative CH bond cleavage.

Compound	E <sup>OPT</sup> [a.u.]	G <sup>OPT</sup> [a.u.]	H <sup>OPT</sup> [a.u.]	E <sup>SP</sup> [a.u.]	G [kJ mol <sup>-1</sup> ]
<b>2</b>	-3259.3246	-3259.1694	-3259.0636	-3256.7757	-8550250.0
pmp	-448.0953	-447.8317	-447.7829	-447.6534	-1174614.1
[pmpH] <sup>+</sup>	-448.5023	-448.2241	-448.1747	-448.1345	-1175839.2
[2 $\cdots$ pmp] <sup>VDW</sup>	-3707.4480	-3707.0044	-3706.8727	-3704.4546	-9724873.6
N-methylindole	-402.8151	-402.6894	-402.6480	-402.4032	-1056171.5
[3a] <sup>-</sup> / [2-C <sub>9</sub> H <sub>5</sub> NCH <sub>3</sub> <sup>C3-pos.</sup> ] <sup>-</sup>	-3661.6797	-3661.3855	-3661.2624	-3658.7465	-9605259.5
2 $\cdots$ C <sub>9</sub> H <sub>6</sub> NCH <sub>3</sub> <sup>C3-pos.</sup> ( <b>INT-3a</b> )	-3662.1568	-3661.8479	-3661.7263	-3659.1977	-9606405.5
[TS-3a-FLP <sup>C2-pos.</sup> ] <sup>‡</sup>	-4110.2442	-4109.6491	-4109.5033	-4106.8349	-10780925.6
[TS-3a-FLP <sup>C3-pos.</sup> ] <sup>‡</sup>	-4110.2632	-4109.6663	-4109.5219	-4106.8595	-10780985.6
<b>Thermodynamics</b>					<b><math>\Delta</math>G</b>
[2 $\cdots$ pmp] <sup>VDW</sup> + N-methylindole $\rightarrow$ [3a] <sup>-</sup> + [pmpH] <sup>+</sup>					-53.6
[2 $\cdots$ pmp] <sup>VDW</sup> + N-methylindole $\rightarrow$ 2 $\cdots$ C <sub>9</sub> H <sub>6</sub> NCH <sub>3</sub> <sup>C3-pos.</sup> + pmp					25.5
<b>Kinetics</b>					<b><math>\Delta</math>G</b>
[2 $\cdots$ pmp] <sup>VDW</sup> + N-methylindole $\rightarrow$ [TS-3a-FLP <sup>C2-pos.</sup> ] <sup>‡</sup>					119.5
[2 $\cdots$ pmp] <sup>VDW</sup> + N-methylindole $\rightarrow$ [TS-3a-FLP <sup>C3-pos.</sup> ] <sup>‡</sup>					59.5
N-methylpyrrole	-249.2839	-249.2019	-249.1666	-249.0409	-653633.8
[3b] <sup>-</sup> / [2-C <sub>4</sub> H <sub>3</sub> NCH <sub>3</sub> <sup>C3-pos.</sup> ] <sup>-</sup>	-3508.1445	-3507.8959	-3507.7772	-3505.3821	-9202721.0
2 $\cdots$ C <sub>4</sub> H <sub>4</sub> NCH <sub>3</sub> <sup>C3-pos.</sup> ( <b>INT-3b</b> )	-3508.6232	-3508.3608	-3508.2425	-3505.8287	-9203856.9
[TS-3b-FLP <sup>C2-pos.</sup> ] <sup>‡</sup>	-3956.7192	-3956.1688	-3956.0278	-3953.4817	-10378413.8
[TS-3b-FLP <sup>C3-pos.</sup> ] <sup>‡</sup>	-3956.7252	-3956.1755	-3956.0343	-3953.4891	-10378435.3
[TS-3b-ELC-O <sup>C2-pos.</sup> ] <sup>‡</sup>	-3508.5774	-3508.3192	-3508.2022	-3505.7758	-9203729.1
[TS-3b-ELC-O <sup>C3-pos.</sup> ] <sup>‡</sup>	-3508.5765	-3508.3190	-3508.2016	-3505.7769	-9203733.8
[TS-3b-ELC-N <sup>C2-pos.</sup> ] <sup>‡</sup>	-3508.5760	-3508.3188	-3508.2008	-3505.7739	-9203727.0
[TS-3b-ELC-N <sup>C3-pos.</sup> ] <sup>‡</sup>	-3508.5749	-3508.3183	-3508.2000	-3505.7750	-9203731.4
<b>Thermodynamics</b>					<b><math>\Delta</math>G</b>
[2 $\cdots$ pmp] <sup>VDW</sup> + N-methylpyrrole $\rightarrow$ [3b] <sup>-</sup> + [pmpH] <sup>+</sup>					-52.8
[2 $\cdots$ pmp] <sup>VDW</sup> + N-methylpyrrole $\rightarrow$ 2 $\cdots$ C <sub>4</sub> H <sub>4</sub> NCH <sub>3</sub> <sup>C3-pos.</sup> + pmp					36.4
<b>Kinetics (FLP)</b>					<b><math>\Delta</math>G</b>
[2 $\cdots$ pmp] <sup>VDW</sup> + N-methylpyrrole $\rightarrow$ [TS-3b-FLP <sup>C2-pos.</sup> ] <sup>‡</sup>					93.6
[2 $\cdots$ pmp] <sup>VDW</sup> + N-methylpyrrole $\rightarrow$ [TS-3b-FLP <sup>C3-pos.</sup> ] <sup>‡</sup>					72.1
<b>Kinetics (ELC)</b>					<b><math>\Delta</math>G</b>
[2 $\cdots$ pmp] <sup>VDW</sup> + N-methylpyrrole $\rightarrow$ [TS-3b-ELC-O <sup>C2-pos.</sup> ] <sup>‡</sup> + pmp					164.2
[2 $\cdots$ pmp] <sup>VDW</sup> + N-methylpyrrole $\rightarrow$ [TS-3b-ELC-O <sup>C3-pos.</sup> ] <sup>‡</sup> + pmp					159.6
[2 $\cdots$ pmp] <sup>VDW</sup> + N-methylpyrrole $\rightarrow$ [TS-3b-ELC-N <sup>C2-pos.</sup> ] <sup>‡</sup> + pmp					166.3
[2 $\cdots$ pmp] <sup>VDW</sup> + N-methylpyrrole $\rightarrow$ [TS-3b-ELC-N <sup>C3-pos.</sup> ] <sup>‡</sup> + pmp					162.0
thiophene	-552.7634	-552.7235	-552.6913	-552.2663	-1449862.5
[3e] <sup>-</sup> / [2-C <sub>4</sub> H <sub>3</sub> SC <sup>2-pos.</sup> ] <sup>-</sup>	-3811.6307	-3811.4236	-3811.3084	-3808.6127	-9998961.6
[2-C <sub>4</sub> H <sub>3</sub> SC <sup>3-pos.</sup> ] <sup>-</sup>	-3811.6267	-3811.4202	-3811.3044	-3808.6076	-9998950.3
[TS-3e-FLP <sup>C2-pos.</sup> ] <sup>‡</sup>	-4260.1957	-4259.6898	-4259.5504	-4256.7027	-11174637.7
[TS-3e-FLP <sup>C3-pos.</sup> ] <sup>‡</sup>	-4260.1879	-4259.6807	-4259.5425	-4256.6951	-11174614.2
<b>Thermodynamics</b>					<b><math>\Delta</math>G</b>
[2 $\cdots$ pmp] <sup>VDW</sup> + thiophene $\rightarrow$ [3e] <sup>-</sup> + [pmpH] <sup>+</sup>					-64.7
[2 $\cdots$ pmp] <sup>VDW</sup> + thiophene $\rightarrow$ [2-C <sub>4</sub> H <sub>3</sub> SC <sup>3-pos.</sup> ] <sup>-</sup> + [pmpH] <sup>+</sup>					-53.4
<b>Kinetics (FLP)</b>					<b><math>\Delta</math>G</b>
[2 $\cdots$ pmp] <sup>VDW</sup> + thiophene $\rightarrow$ [TS-3e-FLP <sup>C2-pos.</sup> ] <sup>‡</sup>					98.4
[2 $\cdots$ pmp] <sup>VDW</sup> + thiophene $\rightarrow$ [TS-3e-FLP <sup>C3-pos.</sup> ] <sup>‡</sup>					121.9
phenylacetylene (PhCCH)	-308.1402	-308.0605	-308.0228	-307.8239	-807974.5

## Computational Data Tables and Figures

$[3d]^- / [2-CCPh]^-$	-3567.0122	-3566.7658	-3566.6437	-3564.1757	-9357089.0
$2-PhCCH$	-3567.4713	-3567.2112	-3567.0912	-3564.5982	-9358162.4
<b>Thermodynamics</b>					<b><math>\Delta G</math></b>
$[2\cdots pmp]^{VDW} + PhCCH \rightarrow [3d]^- + [pmpH]^+$					-80.1
$[2\cdots pmp]^{VDW} + PhCCH \rightarrow [2-PhCCH]^- + [pmpH]^+$					71.7
$SiCl_4$	-2129.8583	-2129.8835	-2129.8435	-2128.1797	-5587594.6
$pmp-SiCl_4$	-2577.9019	-2577.6350	-2577.5706	-2575.7864	-6762019.1
$[TS-N-methylpyrrole-pmp-SiCl_4]^\ddagger$	-2827.2050	-2826.8399	-2826.7603	-2824.8439	-7415661.8
<b>Thermodynamics</b>					<b><math>\Delta G</math></b>
$SiCl_4 + pmp \rightarrow pmp-SiCl_4$					189.6
<b>Kinetics</b>					<b><math>\Delta G</math></b>
$SiCl_4 + pmp + N-methylpyrrole \rightarrow [TS-N-methylpyrrole-pmp-SiCl_4]^\ddagger$					180.7
$1^{Cl}$	-4727.7242	-4727.6717	-4727.5971	-4723.9832	-12402672.9
$pmp-1^{Cl}$	-5175.8413	-5175.4947	-5175.3970	-5171.6652	-13577290.3
$[TS-N-methylpyrrole-pmp-1^{Cl}]^\ddagger$	-5425.1240	-5424.6786	-5424.5665	-5420.6961	-14230861.4
$[1^{Cl}\cdots pmp]^{VDW}$	-5175.8359	-5175.4953	-5175.3940	-5171.6494	-13577264.5
$1^{Cl}\cdots C_4H_4NCH_3$	-4977.0220	-4976.8625	-4976.7750	-4973.0387	-13056287.3
$[1^{Cl}-C_4H_4NCH_3^{C3-pos}]^-$	-4976.5412	-4976.3951	-4976.3069	-4972.5914	-13055148.4
$[1^{Cl}-C_4H_4NCH_3^{C2-pos}]^-$	-4976.5429	-4976.3966	-4976.3086	-4972.5895	-13055142.6
<b>Thermodynamics<sup>§</sup></b>					<b><math>\Delta G</math></b>
$1^{Cl} + pmp \rightarrow pmp-1^{Cl}$					-3.3
$1^{Cl} + pmp \rightarrow [1^{Cl}\cdots pmp]^{VDW}$					22.5
$1^{Cl} + N-methylpyrrole \rightarrow 1^{Cl}\cdots C_4H_4NCH_3$					19.5
$1^{Cl} + N-methylpyrrole + pmp \rightarrow [pmpH]^+ + [1^{Cl}-C_4H_4NCH_3^{C2-pos}]^-$					-61.0
$1^{Cl} + N-methylpyrrole + pmp \rightarrow [pmpH]^+ + [1^{Cl}-C_4H_4NCH_3^{C3-pos}]^-$					-66.8
<b>Kinetics<sup>§</sup></b>					<b><math>\Delta G</math></b>
$1^{Cl} + N-methylpyrrole + pmp \rightarrow [TS-N-methylpyrrole-pmp-1^{Cl}]^\ddagger$					62.7

<sup>§</sup> Energies derived are calculated using the monomeric  $1^{Cl}$  structure due to computational ease. It shall be noted that the donor-free form is not monomeric and undergoes oligomerization (cmp. Table A7 and Table A8).

## Appendix

Table A7. Computed energies for the assessment of thermodynamic data for the oligomerization of  $\mathbf{1}^{\text{Cl}}$ . Linear mode, cyclic modes A and B refer to Figure 10 in the main text.

n	E [H]	G [H]	H [H]	G [kJ mol <sup>-1</sup> ]
<b>Linear Mode</b>				
1	-80.3410	-80.2966	-80.2193	0.0
2	-160.7063	-160.5928	-160.4622	0.5
3	-241.0962	-240.9098	-240.7293	-17.5
4	-321.4915	-321.2302	-321.0015	-28.7
5	-401.8684	-401.5349	-401.2559	-27.2
6	-482.2427	-481.8365	-481.5076	-24.9
7	-562.6361	-562.1593	-561.7785	-31.2
8	-643.0138	-642.4625	-642.0334	-29.4
9	-723.4161	-722.7935	-722.3130	-36.2
10	-803.7736	-803.0794	-802.5474	-29.8
11	-884.1712	-883.4035	-882.8219	-33.6
<b>Cyclic A</b>				
2	-160.6595	-160.5439	-160.4169	64.8
3	-241.0876	-240.9011	-240.7203	-9.9
4	-321.4742	-321.2134	-320.9833	-17.7
5	-401.8302	-401.4963	-401.2168	-7.0
6	-482.2017	-481.7956	-481.4652	-7.0
7	-562.5796	-562.0986	-561.7199	-8.4
8	-642.9456	-642.3924	-641.9632	-6.4
9	-723.3486	-722.7204	-722.2424	-14.8
10	-803.7081	-803.0074	-802.4794	-10.8
<b>Cyclic B</b>				
2	-160.6595	-160.5439	-160.4169	64.8
3	-241.0854	-240.8944	-240.7191	-4.0
4	-321.4200	-321.1576	-320.9318	18.9
5	-401.8614	-401.5295	-401.2502	-24.4
6	-482.2670	-481.8600	-481.5326	-35.2
7	-562.6396	-562.1594	-561.7830	-31.2
8	-643.0347	-642.4805	-642.0550	-35.3
9	-723.4161	-722.7910	-722.3139	-35.4
10	-803.7674	-803.0718	-802.5426	-27.8
11	-884.1958	-883.4236	-882.8486	-38.4

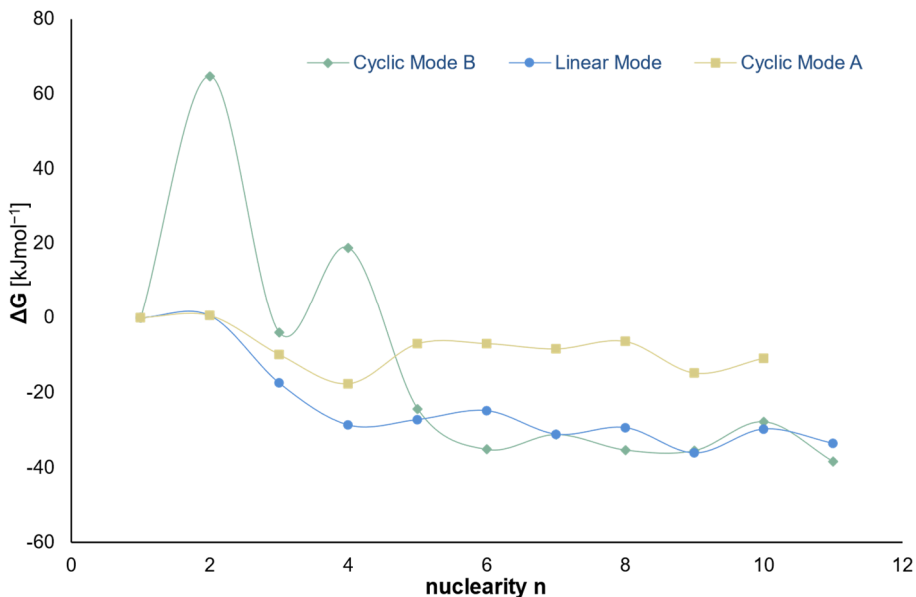


Figure A2. Depiction of the Gibbs free energy change of  $1^{Cl}$  upon oligomerization. Linear mode, cyclic modes A and B refer to the illustrations in Figure 10.

Table A8. Computed energies for the assessment of a reliable oligomerization energy of  $1^{Cl}$  based on the GFN2-xTB data.

n	$E^{xtB2}$ [H]	$G^{xtB2}$ [H]	$H^{xtB2}$ [H]	$E^{SP}$ [H]	$G^{total}$ [kJ mol <sup>-1</sup> ]
1	-80.3410	-80.2966	-80.2193	-4733.9361	-4733.9
6	-482.2699	-481.8631	-481.5355	-28403.7996	-28403.4
$1^{Cl} \rightarrow 1/6 [1^{Cl}]_6$ (cyclic B)					-25.0

The respective structures have been optimized at the PBEh-3c+CPCM(CH<sub>2</sub>Cl<sub>2</sub>) level of theory. Final single point energies were then obtained at the PW6B95-D3(BJ)+SMD(CH<sub>2</sub>Cl<sub>2</sub>)/def2-TZVPP level. Computation of the thermodynamic corrections was done at the GFN2-xTB+ALPB(CH<sub>2</sub>Cl<sub>2</sub>) level after re-optimization of the PBEh-3c structures.

## 7.3.2 Computed NMR Resonances

Table A9. Computed data for the calculation of  $^{29}\text{Si}$  NMR resonances.

Compound	Isotropic Shielding	Solvent	Resonance $\delta$ [ppm]
$\text{Si}(\text{CH}_3)_4$ [a]	332.45	$\text{CH}_2\text{Cl}_2$	0.0
$\text{Si}(\text{CH}_3)_4$ [b]	332.13	$\text{CH}_2\text{Cl}_2$	0.0
$\text{Si}(\text{CH}_3)_4$ [b]	332.12	$\text{CH}_3\text{CN}$	0.0
$\text{Si}(\text{CH}_3)_4$ [c]	332.63	$\text{CH}_2\text{Cl}_2$	0.0
$\text{Si}(\text{CH}_3)_4$ [c]	332.64	THF	0.0
$\text{Si}(\text{CH}_3)_4$ [c]	332.69	toluene	0.0
<b>1</b> $3,4,6\text{-iPr}$ [a]	371.22	$\text{CH}_2\text{Cl}_2$	-38.8
[ <b>1</b> $3,4,6\text{-iPr}$ ] <sub>2</sub> [a]	405.15	$\text{CH}_2\text{Cl}_2$	-72.7
	398.58		-66.1
<b>1</b> $3,5\text{-Cm}$ [a]	371.37	$\text{CH}_2\text{Cl}_2$	-38.9
[ <b>1</b> $3,5\text{-Cm}$ ] <sub>2</sub> [b]	401.29	$\text{CH}_2\text{Cl}_2$	-69.2
	406.39		-74.3
<b>1</b> $3,6\text{-tBu}$ [a]	371.37	$\text{CH}_2\text{Cl}_2$	-38.9
[ <b>1</b> $3,6\text{-tBu}$ ] <sub>2</sub> [a]	410.92	$\text{CH}_2\text{Cl}_2$	-78.5
	410.39		-77.9
<b>1</b> $\text{CF}_3$ [b]	374.93	$\text{CH}_2\text{Cl}_2$	-42.8
<b>1</b> $\text{CF}_3\text{-}(\text{OCPh}_2)$ [b]	436.15	$\text{CH}_2\text{Cl}_2$	-104.0
[Cl- <b>1</b> $\text{CF}_3$ ]- [b]	416.98	$\text{CH}_3\text{CN}$	-84.9
	433.95		-101.8
<b>1</b> $\text{CF}_3\text{-O}(\text{SiEt}_3)_2$ [b]	273.54	$\text{CH}_2\text{Cl}_2$	58.6
	274.70		57.4
( $\text{Et}_3\text{Si}$ ) <sub>2</sub> O [b]	327.58	$\text{CH}_2\text{Cl}_2$	4.6
	333.51		-1.4
<b>2</b> [c]	374.27	$\text{CH}_2\text{Cl}_2$	-41.6
[tmpCO <sub>2</sub> - <b>2</b> ]- [a][z]	484.78	$\text{CH}_2\text{Cl}_2$	-152.3
[H- <b>2</b> ]- [c]	430.90	$\text{CH}_2\text{Cl}_2$	-98.3
[H- <b>2</b> ]- [c]	430.81	THF	-98.2
[H- <b>2</b> ]- [c]	430.53	toluene	-97.8
[Cl- <b>2</b> ]- [c]	429.91	$\text{CH}_2\text{Cl}_2$	-97.3
[ <sup>i</sup> Pr <sub>2</sub> N <sup>+</sup> =CH-CH <sub>2</sub> - <b>2</b> ]- [c]	434.75	toluene	-102.1
[ <sup>i</sup> PrEtN <sup>+</sup> =CMe-CH <sub>2</sub> - <b>2</b> ]- [c]	432.97	toluene	-100.3

Calculation of the NMR resonances at the PBE0-D3(BJ)+SMD(solvent)/def2-TZVPP level of theory. Optimization level: [a] PBEh-3c (*Orca 5.0*) [b] Opt. PBEh-3c (*Orca 4.2*) [c] PBE0-D3(BJ)/def2-TZVPP (*Orca 5.0*) [z] starting structure was determined by *CREST*.

## 7.4 Cyclic Voltammetry Experiments

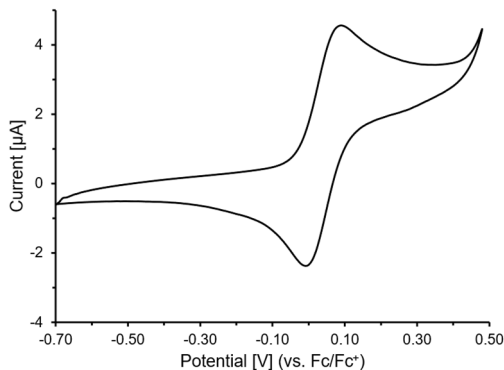


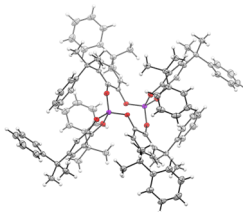
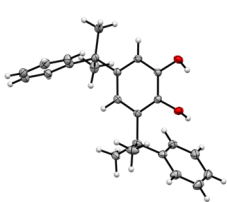
Figure A3. Cyclic voltammogram of **1,3,6-tBu** in dichloromethane with  $[N^tBu_4][PF_6]$  at 50 mV/s.

## 7.5 $pK_a$ -Comparison for pmp and CH Substrates

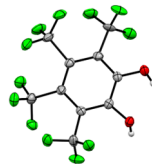
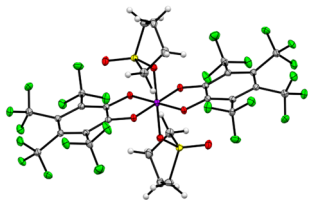
Table A10. Collected  $pK_a$  data for substrates, pmp, and related N-methylpiperidine in different solvents.

Compound	$pK_a$ (H <sub>2</sub> O)	$pK_a$ (DMSO)	$pK_a$ (CH <sub>3</sub> CN)	$pK_a$ (THF)
pentamethylpiperidine (pmp) (protonated)			18.2 <sup>502</sup>	
N-methylpiperidine (protonated)	10.1 <sup>503,504</sup>	8.4 ( $\pm 1.2$ ) <sup>503</sup>	18.2 <sup>503,505</sup>	12.9 <sup>503,505</sup>
N-methylindole				38.1 <sup>416</sup> (C <sup>2</sup> -H)
N-methylpyrrole				39.5 <sup>416</sup> (C <sup>2</sup> -H)
thiophene				33.0 <sup>416</sup> (C <sup>2</sup> -H)
phenylacetylene	23.2 <sup>506</sup>	28.7 <sup>507</sup>		

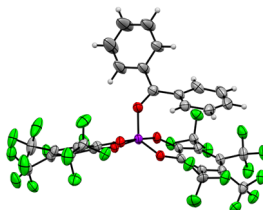
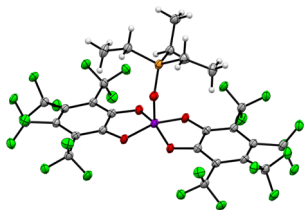
## 7.6 Crystallographic Data



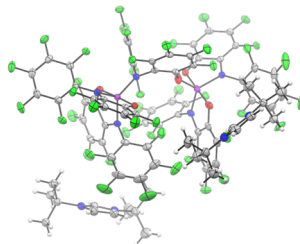
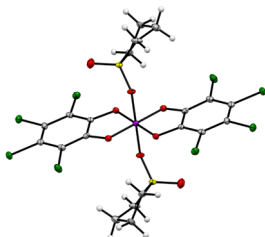
Compound	H <sub>2</sub> cat <sup>3,5</sup> -Cm	[1,3,5-Cm] <sub>2</sub>
CCDC number	2095074	2095075
Empirical formula	C <sub>24</sub> H <sub>26</sub> O <sub>2</sub>	C <sub>96</sub> H <sub>96</sub> O <sub>8</sub> Si <sub>2</sub>
Formula weight	346.45	1433.90
Temperature [K]	100(2)	100(2)
Crystal system	monoclinic	triclinic
Space group (number)	<i>C</i> 2/ <i>c</i> (15)	<i>P</i> $\bar{1}$ (2)
<i>a</i> [Å]	23.2891(17)	10.220(4)
<i>b</i> [Å]	12.5097(7)	12.745(5)
<i>c</i> [Å]	13.4666(8)	17.522(10)
$\alpha$ [°]	90	110.193(16)
$\beta$ [°]	98.109(3)	95.634(14)
$\gamma$ [°]	90	100.919(7)
Volume [Å <sup>3</sup> ]	3884.1(4)	2069.8(16)
<i>Z</i>	8	1
$\rho_{\text{calc}}$ [gcm <sup>-3</sup> ]	1.185	1.150
$\mu$ [mm <sup>-1</sup> ]	0.074	0.099
<i>F</i> (000)	1488	764
Crystal size [mm <sup>3</sup> ]	0.346×0.252×0.111	0.175×0.145×0.097
Crystal color	colorless	colorless
Crystal shape	block	block
Radiation	MoK $\alpha$ ( $\lambda$ =0.71073 Å)	MoK $\alpha$ ( $\lambda$ =0.71073 Å)
2 $\theta$ range [°]	4.64 to 62.15 (0.69 Å)	4.12 to 50.00 (0.84 Å)
	-33 ≤ <i>h</i> ≤ 33	-12 ≤ <i>h</i> ≤ 12
Index ranges	-17 ≤ <i>k</i> ≤ 18	-15 ≤ <i>k</i> ≤ 15
	-19 ≤ <i>l</i> ≤ 19	-20 ≤ <i>l</i> ≤ 20
Reflections collected	50491	93269
	6209	7273
Independent reflections	<i>R</i> <sub>int</sub> = 0.0504	<i>R</i> <sub>int</sub> = 0.0941
	<i>R</i> <sub>sigma</sub> = 0.0297	<i>R</i> <sub>sigma</sub> = 0.0436
Completeness to $\vartheta = 25.242^\circ$	99.7 %	99.8 %
Data / Restraints / Parameters	6209/84/243	7273/968/486
Goodness-of-fit on <i>F</i> <sup>2</sup>	1.182	1.071
Final <i>R</i> indexes	<i>R</i> <sub>1</sub> = 0.0656	<i>R</i> <sub>1</sub> = 0.0426
[ <i>I</i> ≥2 $\sigma$ ( <i>I</i> )]	w <i>R</i> <sub>2</sub> = 0.1525	w <i>R</i> <sub>2</sub> = 0.0932
Final <i>R</i> indexes	<i>R</i> <sub>1</sub> = 0.0738	<i>R</i> <sub>1</sub> = 0.0555
[all data]	w <i>R</i> <sub>2</sub> = 0.1563	w <i>R</i> <sub>2</sub> = 0.1012
Largest peak/hole [eÅ <sup>-3</sup> ]	0.45/-0.23	0.26/-0.27



Compound	1 <sup>CF<sub>3</sub></sup> -(sulfolane) <sub>2</sub>	H <sub>2</sub> cat <sup>CF<sub>3</sub></sup> -(sulfolane)
CCDC number	2070467	2070469
Empirical formula	C <sub>34</sub> H <sub>22</sub> F <sub>24</sub> O <sub>8</sub> S <sub>2</sub> Si	C <sub>14</sub> H <sub>10</sub> Cl <sub>0</sub> F <sub>12</sub> O <sub>4</sub> S
Formula weight	1106.72	502.28
Temperature [K]	100	100(2)
Crystal system	triclinic	monoclinic
Space group (number)	$P\bar{1}$ (2)	$C2/c$ (15)
<i>a</i> [Å]	9.5386(12)	18.1928(11)
<i>b</i> [Å]	9.8566(18)	19.8514(10)
<i>c</i> [Å]	11.7258(17)	20.0516(11)
$\alpha$ [°]	85.560(6)	90
$\beta$ [°]	68.090(4)	107.826(2)
$\gamma$ [°]	69.683(6)	90
Volume [Å <sup>3</sup> ]	957.5(3)	6894.0(7)
<i>Z</i>	1	16
$\rho_{\text{calc}}$ [gcm <sup>-3</sup> ]	1.919	1.936
$\mu$ [mm <sup>-1</sup> ]	0.342	0.336
<i>F</i> (000)	552	4000
Crystal size [mm <sup>3</sup> ]	0.12×0.103×0.094	0.32×0.18×0.08
Crystal color	colorless	colorless
Crystal shape	irregular	plate
Radiation	MoK $\alpha$ ( $\lambda$ =0.71073 Å)	MoK $\alpha$ ( $\lambda$ =0.71073 Å)
2 $\theta$ range [°]	4.41 to 54.25 (0.78 Å)	4.10 to 54.27 (0.78 Å)
	-12 ≤ <i>h</i> ≤ 12	-23 ≤ <i>h</i> ≤ 22
Index ranges	-12 ≤ <i>k</i> ≤ 12	0 ≤ <i>k</i> ≤ 25
	-15 ≤ <i>l</i> ≤ 15	0 ≤ <i>l</i> ≤ 25
Reflections collected	45166	7630
	4230	7630
Independent reflections	$R_{\text{int}} = 0.0523$ $R_{\text{sigma}} = 0.0232$	$R_{\text{int}} = 0.0468$ $R_{\text{sigma}} = 0.0119$
Completeness to $\vartheta = 25.242^\circ$	99.9 %	100.0 %
Data / Restraints / Parameters	4230/0/313	7630/163/850
Goodness-of-fit on $F^2$	1.040	1.052
Final <i>R</i> indexes	$R_1 = 0.0275$	$R_1 = 0.0345$
[ $I \geq 2\sigma(I)$ ]	$wR_2 = 0.0642$	$wR_2 = 0.0891$
Final <i>R</i> indexes	$R_1 = 0.0381$	$R_1 = 0.0389$
[all data]	$wR_2 = 0.0683$	$wR_2 = 0.0929$
Largest peak/hole [eÅ <sup>-3</sup> ]	0.37/-0.41	0.45/-0.39

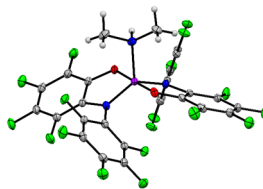
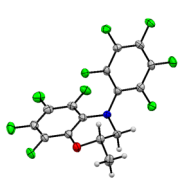


Compound	1 <sup>CF<sub>3z</sub></sup> (OPEt <sub>3</sub> )	1 <sup>CF<sub>3z</sub></sup> (OCPH <sub>2</sub> )·C <sub>6</sub> H <sub>6</sub>
CCDC number	2070466	2070468
Empirical formula	C <sub>26</sub> H <sub>15</sub> F <sub>24</sub> O <sub>5</sub> PSi	C <sub>42</sub> H <sub>19</sub> F <sub>24</sub> O <sub>5</sub> Si
Formula weight	922.44	1087.66
Temperature [K]	100.0	101(2)
Crystal system	triclinic	triclinic
Space group (number)	<i>P</i> $\bar{1}$ (2)	<i>P</i> $\bar{1}$ (2)
<i>a</i> [Å]	10.9648(10)	12.0751(15)
<i>b</i> [Å]	11.6048(10)	13.7369(17)
<i>c</i> [Å]	14.5292(12)	14.1223(16)
$\alpha$ [°]	110.008(3)	86.848(4)
$\beta$ [°]	107.408(3)	88.870(4)
$\gamma$ [°]	97.525(4)	65.183(4)
Volume [Å <sup>3</sup> ]	1600.5(2)	2123.0(4)
<i>Z</i>	2	2
$\rho_{\text{calc}}$ [gcm <sup>-3</sup> ]	1.914	1.701
$\mu$ [mm <sup>-1</sup> ]	0.303	0.208
<i>F</i> (000)	912	1082
Crystal size [mm <sup>3</sup> ]	0.115×0.095×0.086	0.240×0.120×0.100
Crystal color	colorless	yellow
Crystal shape	block	block
Radiation	MoK $\alpha$ ( $\lambda=0.71073$ Å)	MoK $\alpha$ ( $\lambda=0.71073$ Å)
2 $\theta$ range [°]	3.87 to 52.99 (0.80 Å)	4.47 to 56.56 (0.75 Å)
	-13 ≤ <i>h</i> ≤ 13	-16 ≤ <i>h</i> ≤ 16
Index ranges	-14 ≤ <i>k</i> ≤ 14	-18 ≤ <i>k</i> ≤ 18
	-18 ≤ <i>l</i> ≤ 18	-18 ≤ <i>l</i> ≤ 18
Reflections collected	50414	48697
	6582	10511
Independent reflections	<i>R</i> <sub>int</sub> = 0.0780	<i>R</i> <sub>int</sub> = 0.0762
	<i>R</i> <sub>sigma</sub> = 0.0413	<i>R</i> <sub>sigma</sub> = 0.0609
Completeness to	99.9 %	99.8 %
$\vartheta = 25.242^\circ$		
Data / Restraints / Parameters	6582/0/517	10511/3419/1108
Goodness-of-fit on <i>F</i> <sup>2</sup>	1.039	1.030
Final <i>R</i> indexes	<i>R</i> <sub>1</sub> = 0.0372	<i>R</i> <sub>1</sub> = 0.0607
[ <i>I</i> ≥2 $\sigma$ ( <i>I</i> )]	w <i>R</i> <sub>2</sub> = 0.0867	w <i>R</i> <sub>2</sub> = 0.1572
Final <i>R</i> indexes	<i>R</i> <sub>1</sub> = 0.0593	<i>R</i> <sub>1</sub> = 0.0982
[all data]	w <i>R</i> <sub>2</sub> = 0.0952	w <i>R</i> <sub>2</sub> = 0.1813
Largest peak/hole [eÅ <sup>-3</sup> ]	0.31/-0.38	0.72/-0.38

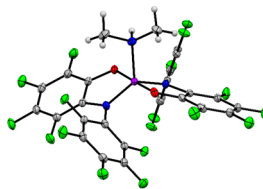
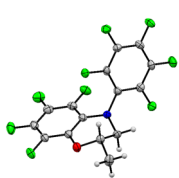


Compound	1 <sup>Cl</sup> -(sulfolane) <sub>2</sub>	[HNHC <sup>tBu</sup> ] <sub>2</sub> [Si <sub>2</sub> am <sup>F</sup> ph <sup>F</sup> <sub>5</sub> ]
CCDC number	2070464	-
Empirical formula	C <sub>20</sub> H <sub>16</sub> Cl <sub>8</sub> O <sub>8</sub> S <sub>2</sub> Si	C <sub>82</sub> H <sub>42</sub> F <sub>45</sub> N <sub>9</sub> O <sub>5</sub> Si <sub>2</sub>
Formula weight	760.14	2144.42
Temperature [K]	100.0	100.00
Crystal system	triclinic	triclinic
Space group (number)	<i>P</i> $\bar{1}$ (2)	<i>P</i> $\bar{1}$ (2)
<i>a</i> [Å]	7.2278(6)	15.925(2)
<i>b</i> [Å]	9.2581(7)	16.647(2)
<i>c</i> [Å]	11.5754(9)	16.716(3)
$\alpha$ [°]	103.618(3)	83.829(6)
$\beta$ [°]	105.853(3)	80.842(6)
$\gamma$ [°]	105.889(3)	87.238(5)
Volume [Å <sup>3</sup> ]	675.16(9)	4347.5(11)
<i>Z</i>	1	2
$\rho_{\text{calc}}$ [gcm <sup>-3</sup> ]	1.870	1.638
$\mu$ [mm <sup>-1</sup> ]	1.081	0.195
<i>F</i> (000)	382	2140
Crystal size [mm <sup>3</sup> ]	0.103×0.088×0.065	0.434×0.129×0.106
Crystal color	colorless	colorless
Crystal shape	irregular	plate
Radiation	MoK $\alpha$ ( $\lambda$ =0.71073 Å)	MoK $\alpha$ ( $\lambda$ =0.71073 Å)
2 $\theta$ range [°]	3.88 to 55.05 (0.77 Å)	3.86 to 50.00 (0.84 Å)
	-9 ≤ <i>h</i> ≤ 9	-18 ≤ <i>h</i> ≤ 18
Index ranges	-12 ≤ <i>k</i> ≤ 12	-19 ≤ <i>k</i> ≤ 19
	-15 ≤ <i>l</i> ≤ 15	-19 ≤ <i>l</i> ≤ 19
Reflections collected	21585	227858
	3103	15300
Independent reflections	<i>R</i> <sub>int</sub> = 0.0701	<i>R</i> <sub>int</sub> = 0.0727
	<i>R</i> <sub>sigma</sub> = 0.0407	<i>R</i> <sub>sigma</sub> = 0.0297
Completeness to	99.9 %	99.9 %
$\theta$ = 25.242°		
Data / Restraints / Parameters	3103/0/178	15300/0/1300
Goodness-of-fit on <i>F</i> <sup>2</sup>	1.125	1.048
Final <i>R</i> indexes	<i>R</i> <sub>1</sub> = 0.0446	<i>R</i> <sub>1</sub> = 0.0466
[ <i>I</i> ≥ 2 $\sigma$ ( <i>I</i> )]	w <i>R</i> <sub>2</sub> = 0.1006	w <i>R</i> <sub>2</sub> = 0.1226
Final <i>R</i> indexes	<i>R</i> <sub>1</sub> = 0.0561	<i>R</i> <sub>1</sub> = 0.0540
[all data]	w <i>R</i> <sub>2</sub> = 0.1059	w <i>R</i> <sub>2</sub> = 0.1299
Largest peak/hole [eÅ <sup>-3</sup> ]	0.52/-0.44	0.56/-0.41

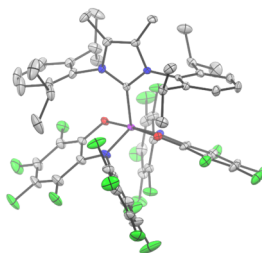
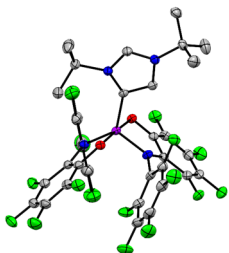
Appendix



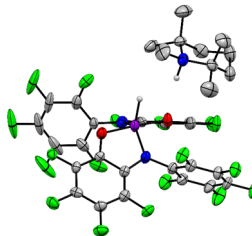
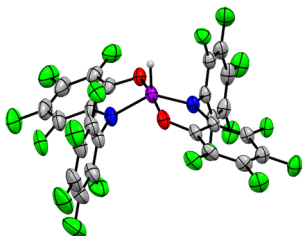
Compound	am <sup>F</sup> ph <sup>F</sup> C <sub>3</sub> H <sub>6</sub>	2-HNMe <sub>2</sub>
CCDC number	2181650	2181653
Empirical formula	C <sub>15</sub> H <sub>6</sub> F <sub>9</sub> NO	C <sub>26</sub> H <sub>7</sub> F <sub>18</sub> N <sub>3</sub> O <sub>2</sub> Si
Formula weight	387.21	763.44
Temperature [K]	100.00	100(2)
Crystal system	triclinic	monoclinic
Space group (number)	$P\bar{1}$ (2)	$C2/c$ (15)
<i>a</i> [Å]	9.859(3)	19.973(6)
<i>b</i> [Å]	10.807(3)	15.632(7)
<i>c</i> [Å]	13.981(4)	18.268(5)
$\alpha$ [°]	75.839(11)	90
$\beta$ [°]	81.301(10)	110.692(8)
$\gamma$ [°]	80.229(10)	90
Volume [Å <sup>3</sup> ]	1414.1(7)	5336(3)
<i>Z</i>	4	8
$\rho_{\text{calc}}$ [gcm <sup>-3</sup> ]	1.819	1.901
$\mu$ [mm <sup>-1</sup> ]	0.196	0.250
<i>F</i> (000)	768	3008
Crystal size [mm <sup>3</sup> ]	0.336×0.279×0.126	0.318×0.158×0.149
Crystal color	colorless	colorless
Crystal shape	block	block
Radiation	MoK $\alpha$ ( $\lambda=0.71073$ Å)	MoK $\alpha$ ( $\lambda=0.71073$ Å)
2 $\theta$ range [°]	3.92 to 54.18 (0.78 Å)	3.68 to 57.40 (0.74 Å)
Index ranges	-12 ≤ <i>h</i> ≤ 12 -13 ≤ <i>k</i> ≤ 13 0 ≤ <i>l</i> ≤ 17	-26 ≤ <i>h</i> ≤ 26 -21 ≤ <i>k</i> ≤ 21 -24 ≤ <i>l</i> ≤ 24
Reflections collected	6205	180286
Independent reflections	6205 $R_{\text{int}} = 0.0568$ $R_{\text{sigma}} = 0.0241$	6877 $R_{\text{int}} = 0.0518$ $R_{\text{sigma}} = 0.0153$
Completeness to $\theta = 25.242^\circ$	99.7 %	99.9 %
Data / Restraints / Parameters	6205/19/523	6877/1213/477
Goodness-of-fit on $F^2$	1.100	1.060
Final <i>R</i> indexes	$R_1 = 0.0461$	$R_1 = 0.0316$
[ $I \geq 2\sigma(I)$ ]	$wR_2 = 0.1211$	$wR_2 = 0.0850$
Final <i>R</i> indexes	$R_1 = 0.0521$	$R_1 = 0.0348$
[all data]	$wR_2 = 0.1240$	$wR_2 = 0.0882$
Largest peak/hole [eÅ <sup>-3</sup> ]	0.41/-0.33	0.41/-0.35



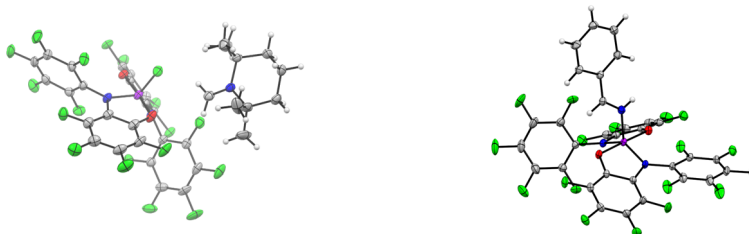
Compound	2-(CH <sub>2</sub> Cl <sub>2</sub> )	2-(OPtEt <sub>3</sub> )
CCDC number	2181652	2181651
Empirical formula	C <sub>25</sub> H <sub>2</sub> Cl <sub>2</sub> F <sub>18</sub> N <sub>2</sub> O <sub>2</sub> Si	C <sub>30</sub> H <sub>15</sub> F <sub>18</sub> N <sub>2</sub> O <sub>3</sub> PSi
Formula weight	803.28	852.50
Temperature [K]	100.0	100.00
Crystal system	monoclinic	monoclinic
Space group (number)	<i>P2<sub>1</sub>/n</i> (13)	<i>P2<sub>1</sub>/n</i> (14)
<i>a</i> [Å]	13.2428(12)	10.260(4)
<i>b</i> [Å]	7.6170(8)	17.927(7)
<i>c</i> [Å]	13.3053(13)	17.529(7)
$\alpha$ [°]	90	90
$\beta$ [°]	95.228(4)	100.412(14)
$\gamma$ [°]	90	90
Volume [Å <sup>3</sup> ]	1336.5(2)	3171(2)
<i>Z</i>	2	4
$\rho_{\text{calc}}$ [gcm <sup>-3</sup> ]	1.996	1.786
$\mu$ [mm <sup>-1</sup> ]	0.447	0.270
<i>F</i> (000)	784	1696
Crystal size [mm <sup>3</sup> ]	0.185×0.133×0.099	0.251×0.209×0.066
Crystal color	colorless	colorless
Crystal shape	block	plate
Radiation	MoK $\alpha$ ( $\lambda$ =0.71073 Å)	MoK $\alpha$ ( $\lambda$ =0.71073 Å)
2 $\theta$ range [°]	4.15 to 55.99 (0.76 Å)	3.28 to 50.00 (0.84 Å)
Index ranges	-17 ≤ <i>h</i> ≤ 17	-12 ≤ <i>h</i> ≤ 12
	-10 ≤ <i>k</i> ≤ 10	-17 ≤ <i>k</i> ≤ 21
	-17 ≤ <i>l</i> ≤ 17	-20 ≤ <i>l</i> ≤ 18
Reflections collected	49135	11633
	3225	4752
Independent reflections	<i>R</i> <sub>int</sub> = 0.0558	<i>R</i> <sub>int</sub> = 0.0793
	<i>R</i> <sub>sigma</sub> = 0.0239	<i>R</i> <sub>sigma</sub> = 0.1105
Completeness to	100.0 %	85.1 %
$\vartheta$ = 25.242°		
Data / Restraints / Parameters	3225/0/227	4752/144/499
Goodness-of-fit on <i>F</i> <sup>2</sup>	1.075	1.155
Final <i>R</i> indexes	<i>R</i> <sub>1</sub> = 0.0383	<i>R</i> <sub>1</sub> = 0.1268
[ <i>I</i> ≥2 $\sigma$ ( <i>I</i> )]	<i>wR</i> <sub>2</sub> = 0.1115	<i>wR</i> <sub>2</sub> = 0.2840
Final <i>R</i> indexes	<i>R</i> <sub>1</sub> = 0.0426	<i>R</i> <sub>1</sub> = 0.1664
[all data]	<i>wR</i> <sub>2</sub> = 0.1155	<i>wR</i> <sub>2</sub> = 0.3261
Largest peak/hole [eÅ <sup>-3</sup> ]	0.37/-0.90	1.07/-1.84



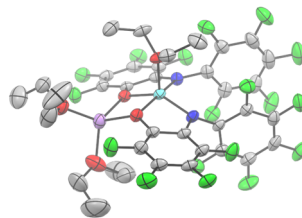
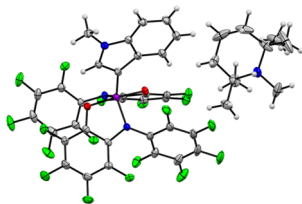
Compound	2-aNHC <sup>t</sup> Bu	2-NHCDipp.Me
CCDC number	2181654	-
Empirical formula	C <sub>35</sub> H <sub>20</sub> F <sub>18</sub> N <sub>4</sub> O <sub>2</sub> Si	C <sub>54</sub> H <sub>42</sub> Cl <sub>2</sub> F <sub>18</sub> N <sub>4</sub> O <sub>2</sub> Si
Formula weight	898.64	1219.90
Temperature [K]	100.00	100.00
Crystal system	monoclinic	monoclinic
Space group (number)	<i>P</i> 2 <sub>1</sub> / <i>c</i> (14)	<i>P</i> 2 <sub>1</sub> / <i>c</i> (14)
<i>a</i> [Å]	17.9305(15)	16.6552(10)
<i>b</i> [Å]	10.3399(7)	13.0303(8)
<i>c</i> [Å]	19.2867(14)	24.2589(16)
$\alpha$ [°]	90	90
$\beta$ [°]	105.741(2)	91.090(2)
$\gamma$ [°]	90	90
Volume [Å <sup>3</sup> ]	3441.6(4)	5263.8(6)
<i>Z</i>	4	4
$\rho_{\text{calc}}$ [gcm <sup>-3</sup> ]	1.734	1.539
$\mu$ [mm <sup>-1</sup> ]	0.209	0.257
<i>F</i> (000)	1800	2480
Crystal size [mm <sup>3</sup> ]	0.145×0.14×0.111	0.199×0.174×0.154
Crystal color	colorless	colorless
Crystal shape	block	block
Radiation	MoK $\alpha$ ( $\lambda$ =0.71073 Å)	MoK $\alpha$ ( $\lambda$ =0.71073 Å)
2 $\theta$ range [°]	4.39 to 55.08 (0.77 Å)	3.97 to 57.33 (0.74 Å)
	-23 ≤ <i>h</i> ≤ 23	-22 ≤ <i>h</i> ≤ 22
Index ranges	-13 ≤ <i>k</i> ≤ 13	-17 ≤ <i>k</i> ≤ 17
	-25 ≤ <i>l</i> ≤ 25	-32 ≤ <i>l</i> ≤ 32
Reflections collected	156533	129922
	7932	13397
Independent reflections	<i>R</i> <sub>int</sub> = 0.0918	<i>R</i> <sub>int</sub> = 0.0693
	<i>R</i> <sub>sigma</sub> = 0.0306	<i>R</i> <sub>sigma</sub> = 0.0326
Completeness to $\vartheta = 25.242^\circ$	100.0 %	100.0 %
Data / Restraints / Parameters	7932/0/547	13397/81/781
Goodness-of-fit on <i>F</i> <sup>2</sup>	1.045	1.189
Final <i>R</i> indexes	<i>R</i> <sub>1</sub> = 0.0452	<i>R</i> <sub>1</sub> = 0.0683
[ <i>I</i> ≥2 $\sigma$ ( <i>I</i> )]	w <i>R</i> <sub>2</sub> = 0.1066	w <i>R</i> <sub>2</sub> = 0.1365
Final <i>R</i> indexes	<i>R</i> <sub>1</sub> = 0.0592	<i>R</i> <sub>1</sub> = 0.0805
[all data]	w <i>R</i> <sub>2</sub> = 0.1195	w <i>R</i> <sub>2</sub> = 0.1412
Largest peak/hole [eÅ <sup>-3</sup> ]	0.91/-0.40	0.41/-0.40



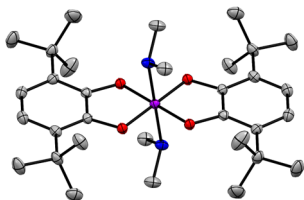
Compound	[Li@12c4][H-2]	[pmpH][H(F)-2]
CCDC number	2181656	2181655
Empirical formula	C <sub>42.50</sub> H <sub>39</sub> F <sub>18</sub> LiN <sub>2</sub> O <sub>10</sub> Si	C <sub>34</sub> H <sub>22.66</sub> F <sub>18.34</sub> N <sub>3</sub> O <sub>2</sub> Si
Formula weight	1114.78	881.83
Temperature [K]	100(2)	100.00
Crystal system	triclinic	monoclinic
Space group (number)	$P\bar{1}$ (2)	$C2/c$ (15)
<i>a</i> [Å]	10.7473(5)	26.099(2)
<i>b</i> [Å]	12.4855(5)	15.3278(13)
<i>c</i> [Å]	19.9055(9)	18.8297(13)
$\alpha$ [°]	76.609(2)	90
$\beta$ [°]	77.777(2)	112.160(3)
$\gamma$ [°]	74.887(2)	90
Volume [Å <sup>3</sup> ]	2475.76(19)	6976.2(10)
<i>Z</i>	2	8
$\rho_{\text{calc}}$ [gcm <sup>-3</sup> ]	1.495	1.679
$\mu$ [mm <sup>-1</sup> ]	0.171	0.205
<i>F</i> (000)	1134	3542
Crystal size [mm <sup>3</sup> ]	0.202×0.186×0.145	0.178×0.145×0.088
Crystal color	colorless	colorless
Crystal shape	block	block
Radiation	MoK $\alpha$ ( $\lambda=0.71073$ Å)	MoK $\alpha$ ( $\lambda=0.71073$ Å)
2 $\theta$ range [°]	3.69 to 57.65 (0.74 Å)	4.28 to 57.55 (0.74 Å)
	-14 ≤ <i>h</i> ≤ 14	-35 ≤ <i>h</i> ≤ 35
Index ranges	-16 ≤ <i>k</i> ≤ 16	-20 ≤ <i>k</i> ≤ 20
	-26 ≤ <i>l</i> ≤ 26	-23 ≤ <i>l</i> ≤ 25
Reflections collected	115223	129999
	12861	9073
Independent reflections	$R_{\text{int}} = 0.0563$	$R_{\text{int}} = 0.0488$
	$R_{\text{sigma}} = 0.0306$	$R_{\text{sigma}} = 0.0210$
Completeness to $\theta = 25.242^\circ$	99.9 %	100.0 %
Data / Restraints / Parameters	12861/1725/897	9073/1517/642
Goodness-of-fit on $F^2$	1.040	1.058
Final <i>R</i> indexes	$R_1 = 0.0490$	$R_1 = 0.0482$
[ $2\sigma(I)$ ]	$wR_2 = 0.1219$	$wR_2 = 0.1284$
Final <i>R</i> indexes	$R_1 = 0.0748$	$R_1 = 0.0605$
[all data]	$wR_2 = 0.1387$	$wR_2 = 0.1383$
Largest peak/hole [eÅ <sup>-3</sup> ]	0.30/-0.33	0.88/-0.65



Compound	[tmpCH <sub>2</sub> ][F-2]	2-HN=CHPh
CCDC number	-	-
Empirical formula	C <sub>34</sub> H <sub>20</sub> F <sub>19</sub> N <sub>3</sub> O <sub>2</sub> Si	C <sub>31</sub> H <sub>7</sub> F <sub>18</sub> N <sub>3</sub> O <sub>2</sub> Si
Formula weight	891.62	823.49
Temperature [K]	100.00	100(2)
Crystal system	monoclinic	triclinic
Space group (number)	<i>P</i> 2 <sub>1</sub> / <i>n</i> (14)	<i>P</i> $\bar{1}$ (2)
<i>a</i> [Å]	11.4801(11)	8.7667(10)
<i>b</i> [Å]	12.0655(10)	11.7053(14)
<i>c</i> [Å]	49.690(5)	15.1113(16)
$\alpha$ [°]	90	85.435(4)
$\beta$ [°]	91.772(3)	76.852(4)
$\gamma$ [°]	90	79.512(5)
Volume [Å <sup>3</sup> ]	6879.5(11)	1483.6(3)
<i>Z</i>	8	2
$\rho_{\text{calc}}$ [gcm <sup>-3</sup> ]	1.722	1.843
$\mu$ [mm <sup>-1</sup> ]	0.211	0.232
<i>F</i> (000)	3568	812
Crystal size [mm <sup>3</sup> ]	0.451×0.376×0.274	0.390×0.224×0.108
Crystal color	colorless	orange
Crystal shape	block	block
Radiation	MoK $\alpha$ ( $\lambda$ =0.71073 Å)	MoK $\alpha$ ( $\lambda$ =0.71073 Å)
2 $\theta$ range [°]	3.62 to 53.48 (0.79 Å)	4.41 to 61.22 (0.70 Å)
	-14 ≤ <i>h</i> ≤ 14	-12 ≤ <i>h</i> ≤ 12
Index ranges	-15 ≤ <i>k</i> ≤ 15	-16 ≤ <i>k</i> ≤ 16
	-57 ≤ <i>l</i> ≤ 62	-21 ≤ <i>l</i> ≤ 21
Reflections collected	231242	99765
	14593	9115
Independent reflections	<i>R</i> <sub>int</sub> = 0.0375	<i>R</i> <sub>int</sub> = 0.0580
	<i>R</i> <sub>sigma</sub> = 0.0168	<i>R</i> <sub>sigma</sub> = 0.0294
Completeness to $\vartheta = 25.242^\circ$	100.0 %	99.6 %
Data / Restraints / Parameters	14593/0/1071	9115/363/563
Goodness-of-fit on <i>F</i> <sup>2</sup>	1.114	1.124
Final <i>R</i> indexes	<i>R</i> <sub>1</sub> = 0.0428	<i>R</i> <sub>1</sub> = 0.0450
[ <i>I</i> ≥2 $\sigma$ ( <i>I</i> )]	<i>wR</i> <sub>2</sub> = 0.1029	<i>wR</i> <sub>2</sub> = 0.1182
Final <i>R</i> indexes	<i>R</i> <sub>1</sub> = 0.0444	<i>R</i> <sub>1</sub> = 0.0491
[all data]	<i>wR</i> <sub>2</sub> = 0.1039	<i>wR</i> <sub>2</sub> = 0.1215
Largest peak/hole [eÅ <sup>-3</sup> ]	0.43/-0.40	0.50/-0.45



Compound	[pmpH][3a]	[Li(OEt <sub>2</sub> )] [Et <sub>2</sub> O-Al(am <sup>F</sup> ph <sup>F</sup> ) <sub>2</sub> ]
CCDC number	2279861	-
Empirical formula	C <sub>43</sub> H <sub>30</sub> F <sub>18</sub> N <sub>4</sub> O <sub>2</sub> Si	C <sub>36</sub> H <sub>30</sub> AlF <sub>18</sub> LiN <sub>2</sub> O <sub>5</sub>
Formula weight	1004.80	946.54
Temperature [K]	100.00	150.00
Crystal system	monoclinic	monoclinic
Space group (number)	<i>P</i> 2 <sub>1</sub> / <i>c</i> (14)	<i>P</i> 2 <sub>1</sub> / <i>c</i> (14)
<i>a</i> [Å]	19.1013(6)	10.5026(7)
<i>b</i> [Å]	11.5155(3)	17.3648(10)
<i>c</i> [Å]	19.3079(6)	21.7660(15)
α [°]	90	90
β [°]	105.8930(10)	92.868(3)
γ [°]	90	90
Volume [Å <sup>3</sup> ]	4084.6(2)	3964.6(4)
<i>Z</i>	4	4
ρ <sub>calc</sub> [gcm <sup>-3</sup> ]	1.634	1.586
μ [mm <sup>-1</sup> ]	0.185	0.181
<i>F</i> (000)	2032	1912
Crystal size [mm <sup>3</sup> ]	0.412×0.383×0.295	0.348×0.322×0.246
Crystal color	colorless	colorless
Crystal shape	block	block
Radiation	MoK <sub>α</sub> (λ=0.71073 Å)	MoK <sub>α</sub> (λ=0.71073 Å)
2θ range [°]	4.17 to 56.71 (0.75 Å)	3.88 to 58.26 (0.73 Å)
	-25 ≤ <i>h</i> ≤ 25	-14 ≤ <i>h</i> ≤ 14
Index ranges	-15 ≤ <i>k</i> ≤ 15	-23 ≤ <i>k</i> ≤ 23
	-25 ≤ <i>l</i> ≤ 25	-29 ≤ <i>l</i> ≤ 29
Reflections collected	106718	272968
	10124	10681
Independent reflections	<i>R</i> <sub>int</sub> = 0.0412	<i>R</i> <sub>int</sub> = 0.0608
	<i>R</i> <sub>sigma</sub> = 0.0198	<i>R</i> <sub>sigma</sub> = 0.0196
Completeness to	99.1 %	100.0 %
ϑ = 25.242°		
Data / Restraints / Parameters	10124/0/619	10681/278/728
Goodness-of-fit on <i>F</i> <sup>2</sup>	1.027	1.037
Final <i>R</i> indexes	<i>R</i> <sub>1</sub> = 0.0425	<i>R</i> <sub>1</sub> = 0.0455
[ <i>I</i> ≥ 2σ( <i>I</i> )]	w <i>R</i> <sub>2</sub> = 0.1074	w <i>R</i> <sub>2</sub> = 0.1289
Final <i>R</i> indexes	<i>R</i> <sub>1</sub> = 0.0456	<i>R</i> <sub>1</sub> = 0.0531
[all data]	w <i>R</i> <sub>2</sub> = 0.1099	w <i>R</i> <sub>2</sub> = 0.1370
Largest peak/hole [eÅ <sup>-3</sup> ]	0.86/-0.62	0.56/-0.70



Compound	1 <sup>3,6-tBu</sup> -(HNMe <sub>2</sub> ) <sub>2</sub> • CH <sub>3</sub> CN
CCDC number	-
Empirical formula	C <sub>34</sub> H <sub>57</sub> N <sub>3</sub> O <sub>4</sub> Si
Formula weight	599.91
Temperature [K]	100(2)
Crystal system	tetragonal
Space group (number)	<i>I</i> 4 <sub>1</sub> / <i>a</i> (88)
<i>a</i> [Å]	20.8185(9)
<i>b</i> [Å]	20.8185(9)
<i>c</i> [Å]	16.9756(10)
$\alpha$ [°]	90
$\beta$ [°]	90
$\gamma$ [°]	90
Volume [Å <sup>3</sup> ]	7357.4(8)
<i>Z</i>	8
$\rho_{\text{calc}}$ [gcm <sup>-3</sup> ]	1.083
$\mu$ [mm <sup>-1</sup> ]	0.101
<i>F</i> (000)	2624
Crystal size [mm <sup>3</sup> ]	0.183×0.157×0.119
Crystal color	colourless
Crystal shape	block
Radiation	MoK $\alpha$ ( $\lambda$ =0.71073 Å)
2 $\theta$ range [°]	3.91 to 54.24 (0.78 Å)
	-26 ≤ <i>h</i> ≤ 26
Index ranges	-26 ≤ <i>k</i> ≤ 26
	-21 ≤ <i>l</i> ≤ 21
Reflections collected	176958
	4076
Independent reflections	$R_{\text{int}} = 0.0671$
	$R_{\text{sigma}} = 0.0155$
Completeness to	100.0 %
$\vartheta = 25.242^\circ$	
Data / Restraints / Parameters	4076/0/205
Goodness-of-fit on <i>F</i> <sup>2</sup>	0.7144/0.7455
	(multi-scan)
Final <i>R</i> indexes	1.060
[ $I \geq 2\sigma(I)$ ]	
Final <i>R</i> indexes	$R_1 = 0.0342$
[all data]	$wR_2 = 0.0909$
	$R_1 = 0.0404$
Largest peak/hole [eÅ <sup>-3</sup> ]	$wR_2 = 0.0966$

# DANKSAGUNG

---

An dieser Stelle möchte ich mich bei allen bedanken die in irgendeiner Form zum Gelingen dieser Arbeit beigetragen haben. Zunächst gilt mein Dank den Personen, die in primärer Relation dazu stehen.

Zuallererst danke ich daher Prof. Dr. Lutz Greb für die Möglichkeit zur Anfertigung dieser Arbeit. Lieber Lutz, vielen Dank auch für dein großes Interesse an meinen Experimenten, für dein kontinuierliches Vertrauen in mich, und für einen stets verständnisvollen Umgang auch in wackligeren Zeiten. Es hat Spaß gemacht dich in deinem Werdegang zu begleiten!

Prof. Dr. Dr. Hans-Jörg Himmel möchte ich nicht nur für die Übernahme des Koreferats danken, sondern auch für zahlreiche Anregungen zu Experimenten im Rahmen von Seminarvorträgen, die unkomplizierte Eingliederung in seinen Arbeitskreis sowie die Bereitstellung von experimenteller Infrastruktur, speziell zu Beginn dieser Arbeit.

Vielen Dank an Christoph Bendel, Nils Ansmann, Lennart Stoess, und vor allem Rezisha Maskey für das Korrekturlesen von Teilen dieser Arbeit.

Den Mitarbeiterinnen und Mitarbeitern aller Einrichtungen der chemischen Institute wird für schnellen und zuverlässigen Service gedankt.

Ein herzliches Dankeschön auch an meine Praktikantinnen und Praktikanten, Senta Kohl, Rosa Müller, Lotta Tölke, sowie Lukas Lehr. Ihr habt in verschiedensten Formen meine Arbeit bereichert.

Selbstverständlich gibt es zahlreiche Personen denen ich im Zusammenhang dieser Arbeit, und damit untrennbar auch im Kontext meiner Studienzeit und meinem Leben hier, danken möchte. In erster Linie zählen dazu das gesamte Kollegium der Arbeitskreise Greb und Himmel, ehemalige Kommilitoninnen und Kommilitonen, natürlich aber auch Familie und Freunde. Um allerdings den Rahmen dieser Arbeit zu wahren, soll an dieser Stelle ein generischer Dank ausgesprochen sowie auf eine beiliegende Erweiterung zu einer persönlichen Danksagung verwiesen werden.

Für den wichtigsten Beitrag möchte ich lediglich noch kurz, aber nachdrücklich meinen Eltern, Claudia und Vitus, danken – dafür, dass ihr mir das alles erst ermöglicht habt.



# EIDESSTÄTTLICHE VERSICHERUNG

GESAMTFAKULTÄT FÜR MATHEMATIK, INGENIEUR-  
UND NATURWISSENSCHAFTEN  
COMBINED FACULTY OF MATHEMATICS, ENGINEERING  
AND NATURAL SCIENCES

RUPRECHT-KARLS-  
UNIVERSITÄT  
HEIDELBERG



**Eidesstattliche Versicherung gemäß § 8 der Promotionsordnung für die Gesamtfakultät für Mathematik, Ingenieur- und Naturwissenschaften der Universität Heidelberg / Sworn Affidavit according to § 8 of the doctoral degree regulations of the Combined Faculty of Mathematics, Engineering and Natural Sciences at Heidelberg University**

1. Bei der eingereichten Dissertation zu dem Thema / *The thesis I have submitted entitled*

**Modulation of Silicon's Lewis Acidity – Enhanced Reactivity through Ligand Design** .....

.....  
handelt es sich um meine eigenständig erbrachte Leistung / *is my own work*.

2. Ich habe nur die angegebenen Quellen und Hilfsmittel benutzt und mich keiner unzulässigen Hilfe Dritter bedient. Insbesondere habe ich wörtlich oder sinngemäß aus anderen Werken übernommene Inhalte als solche kenntlich gemacht. / *I have only used the sources indicated and have not made unauthorised use of services of a third party. Where the work of others has been quoted or reproduced, the source is always given.*

3. Die Arbeit oder Teile davon habe ich ~~wie folgt~~ bislang nicht<sup>1)</sup> an einer Hochschule des In- oder Auslands als Bestandteil einer Prüfungs- oder Qualifikationsleistung vorgelegt. / *I have not yet/have already<sup>1)</sup> presented this thesis or parts thereof to a university as part of an examination or degree.*

Titel der Arbeit / *Title of the thesis:* .....

Hochschule und Jahr / *University and year:* .....

Art der Prüfungs- oder Qualifikationsleistung / *Type of examination or degree:* .....

4. Die Richtigkeit der vorstehenden Erklärungen bestätige ich. / *I confirm that the declarations made above are correct.*

5. Die Bedeutung der eidesstattlichen Versicherung und die strafrechtlichen Folgen einer unrichtigen oder unvollständigen eidesstattlichen Versicherung sind mir bekannt. / *I am aware of the importance of a sworn affidavit and the criminal prosecution in case of a false or incomplete affidavit.*

Ich versichere an Eides statt, dass ich nach bestem Wissen die reine Wahrheit erklärt und nichts verschwiegen habe. / *I affirm that the above is the absolute truth to the best of my knowledge and that I have not concealed anything.*

.....  
Ort und Datum / *Place and date*

.....  
Unterschrift / *Signature*

<sup>1)</sup> Nicht Zutreffendes streichen. Bei Bejahung sind anzugeben; der Titel der andernorts vorgelegten Arbeit, die Hochschule, das Jahr der Vorlage und die Art der Prüfungs- oder Qualifikationsleistung. / *Please cross out what is not applicable. If applicable, please provide: the title of the thesis that was presented elsewhere, the name of the university, the year of presentation and the type of examination or degree.*

The German text is legally binding.

